UNIVERSITY OF CAPE TOWN

DEPARTMENT OF MECHANICAL ENGINEERING

AN IN-SHOE GAIT ANALYSIS DEVICE TO MEASURE THE MAXIMUM SHEAR STRESSES AT THE FIRST METATARSAL HEAD

MICHAEL PAUL CLARKE

Submitted to the University of Cape Town in fulfilment of the requirements for Degree of Master of Science.

September 1996

DECLARATION

I declare that this thesis is essentially my own work. Work which is not my own is accordingly accredited with a reference.

Signed : Signed by candidate

Michael Paul Clarke

Date : 9.10.96

ACKNOWLEDGEMENTS

I would like to take the opportunity to thank the following people :

Professor Gerald Nurick, my supervisor, without whose genuine support and understanding this thesis would not have been possible.

Mr Julian Mayer, without whose genius and precision the new sensor would not have been made.

Mr Hellmut Bowles, for the many informal conversations relating to the stress analysis and finite element model of the new sensor.

Mr Hennie Mulder, of URESIL Products, for the supplying the insole material for the new instrumented insole and the diabetic shoe. Also for the advice he gave me as a podiatrist.

Mr Steve Williams, of ADIDAS shoes, for the use of the *footscan* pressure mat. Also for the advice he gave me on the design and function of running shoes.

My close friends, Emmy, Ken, Victor, Febe and all those that I have not mentioned, for keeping me motivated and giving me the advice when I needed it. Good luck.

Tasha, who will always be known for her affliction with the boyz, for proof reading my thesis when I'm sure she could easily have been doing other things. Thanx.

To those who are always with me in spirit. You will never be forgotten. There is a Valley where rests a beautiful part of Nature.

My "honeybunny" - Julia, whose continual upliftment, sincerity and love prevented me from being dropped from the bunch and having to go it alone in the abyss. It takes a Gemini to understand a Gemini - your such a Gem.

To my parents for hanging in with me through my years of academia. Hakuna Matata !

ABSTRACT

Recent research indicates that the shear stresses acting on a diabetic's foot are one of the major mechanical contributors to the high incidence of ulceration experienced by these patients. These stresses together with direct pressure are thought to have an effect on blood flow occlusion elsewhere in the body. The reduced blood flow may relate in moderation to reduced tissue tolerance or repair capability or even in more severe cases to cell death. Repeated vascular occlusion in a normal person would produce a minor blister or a swollen area, but with a diabetic patient it has the ability to create large incisions and ulcers. This is because diabetic patients are unable to redistribute the load on their feet due to the lack of sensation in their lower extremities. This results in diabetes being the number one cause of all lower limb amputations and accounting for 50 to 70 % of all non-traumatic amputations in the U.S. In the same country, it accounts for $200 million a year in treatment costs directly related to diabetic foot infections. Quantifying the magnitude and duration of these shear stresses therefore has the potential to play a crucial role in assisting podiatrists and clinicians in their diagnosis and treatment of these patients. However these stresses have not been widely evaluated due to lack of suitable instrumentation for their measurement.

A technique which has proven to be the most successful in measuring these stresses involves placing a discrete transducer inside a customised insole and fitting it to a patient's shoe. This report sets out to design a similar technique but with the use of a differently designed transducer. The validity of and confidence in the proposed transducer was established by assessing and comparing the results of the transducer under a series of controlled tests with the results of other transducers presented in the literature. To allow an accurate assessment of the transducer to be made, the tests which were performed on the transducer were controlled and conducted at a fixed walking speed.

The first stage in the design process involved selecting the anatomical site for the transducer. The first metatarsal head was selected because the maximum vertical and maximum shear stresses have been shown to occur simultaneously in this region. The significance of this similarity is that it allows pressure sensing devices to locate the shear transducer.

The computational theory used was based on the assumptions and equations of two dimensional plane strain for linear elastic isotropic homogeneous materials. The transducer is based on the principle that a shear angle is induced on a plane when a shear stress is applied to a plane continuous and orthogonal to it. This principle was adapted into the design of the transducer in the form of a square block of material, whose two orthogonal lateral surfaces were used to measure the shear stress applied to its top surface. The design of the transducer consists of a block of material, two laterally positioned rectangular strain rosettes and a circular base.

The first series of tests conducted on the transducer were intended to verify and establish its material properties and characteristics. A model of the transducer was then constructed using the finite element package ABAQUS. Two Shape Factors - one for calibration purposes and the other for in-shoe testing - were generated for the transducer to allow for the effects of the geometrical inconsistencies present in its design to be accounted for. Without these Shape Factors the equations and assumptions of linear elasticity would not have been appropriate.

A series of controlled pilot and analysis tests were then performed using the custom designed insole and transducer fitted to a diabetic shoe. The diabetic shoe was worn by a subject who performed the tests on a treadmill at a laboratory in the Sports Institute of South Africa.

The repeatability, timing, direction and magnitudes of the shear profiles obtained were found to compare well with the literature. It was concluded that the transducer is able to measure the maximum shear stresses acting at the first metatarsal head under controlled conditions. It is recommended that the effects of temperature on the material properties of the transducer be accounted for and a software package developed to present the transducer's data in a format which is immediately available for inspection.

TABLE OF CONTENTS

LIST OF ILLUSTRATIONS

Figures **Page**

Figures **Page**

Figures **Page**

Figures **Page**

Tables **Page**

Tables **Page**

GLOSSARY

Abductory twist	Inward movement of the forefoot relative to the heel during the push-off phase of the gait cycle.
Amino acids	Together form the basis and structure of all proteins. A protein is a polymer of amino acids.
A priori	Based on theory instead of experience.
Articulation point	Point of attachment.
CHS	Cross Head Speed of the tensile testing machine.
COP	Centre Of Pressure. Relates to the position of resultant pressure acting on the sole of the foot during gait.
Diabetic neuropathy	Neuroligically related disorder effecting diabetics.
Dorsal surface of foot	Top surface of the foot.
FEM	Finite Element Method
Gait cycle	Single sequence of one limb from initial heel contact to second heel strike.
MTH 1	First metatarsal head of the foot.
Occlusion	Blockage of blood flow
Plantar surface	Bottom surface or sole of the foot.
Prominences	Projecting or noticeable bony areas of the foot.
Proteins	Major structural component of cells. Mediating every metabolic process within the cell.
PVA	Polyvinylacetate. (Type of polymer.)

UHI-PMMA	Ultra High Impact Polymethylmethacrylate. (Type of amorphous polymer.)
Radiographic	Study of gait using X-rays.
R-Value	Reliability coefficient
Tibia	Larger of the two bones between the knee and ankle.

One of the side effects of diabetes mellitus is a loss of sensation in the feet and a poor blood supply to their lower extremities. This results in a diabetic's foot becoming sensitive to the repeated stresses developed during gait. As diabetics loose sensation in their feet, they do not adjust their gait patterns to relieve the affected areas from the abnormally high levels of stress which they are experiencing. As a result, diabetics generally only receive treatment for their injury when it has become very serious. Often the only means of treatment is to amputate the infected foot.

The most appropriate means of treatment is regarded as regular consultation with a clinician. Possible areas of high stress might then be predicted and treated before becoming harmful. The scope therefore exists for the development of in-shoe gait analysis devices which measure the maximum shear stresses on the plantar surface of the foot during gait.

There are presently two types of in-shoe stress measurement techniques. One technique uses a matrix of pressure sensitive sensors in the form of an insole. The other uses discrete sensors at selected anatomical locations to specifically measure shear stresses. Considerable success has been achieved with pressure sensitive matrix devices, yet the design and progression of discrete sensors have been limited. This has been attributed largely to the complexity required in the design of the sensor and the environment into which the sensor is placed.

There are two means of locating discrete sensors inside the shoe. Each sensor may be attached directly to the sole of the foot. Alternatively, an insole is used to mount the sensor at the required location. This is the preferred method. The insole, which is made of two different density materials, provides stability and protection for the sensor. The higher density material is used in the region surrounding the sensor and the lower density material makes up the rest of the insole.

The discrete sensor is designed to measure the two orthogonal shear components which the foot experiences during gait. The components are referred to as the anterior-posterior and the medial-lateral shear stresses. The former acts in the forward-back direction and the latter in the inside-outside direction of the leg. The vertical component acts perpendicular to the plantar surface.

The objectives of this thesis are :

1. To perform an extensive literature survey to acquire information which will assist in the understanding of the anatomy of the foot, its behavior during gait, the environment into which the sensor is to be placed and the design of discrete transducers which have previously been used. The limitations, advantages and findings of the studies reviewed are intended to provide the guidelines for the design and analysis of a new instrumented in-shoe device.

2. To locate a position on the plantar surface for the new sensor.

3. To design a sensor which functions according to the principles of plane strain linear elasticity. The sensor is required to measure the two maximum orthogonal shear stresses which occur at a selected anatomical site on the plantar surface during gait.

4. To select a material to function as the sensor. The material is to behave in a linear, isotropic, homogeneous manner.

5. To develop a computational model of the sensor using the Finite Element Method (FEM) provided by ABAQUS. The FEM model is intended to account for the geometrical discontinuities of the sensor. This will allow the equations of small displacement linear two dimensional plane strain to be used in the design of the sensor. Without the FEM model, the equations of linear elasticity cannot be used as they are only valid when the elements of a material are continuous with one another.

6. To develop a means of verifying the theory used in the design of the sensor. The same technique is intended to assess the performance of the sensor as it is not possible to calibrate the sensor inside the shoe.

7. To design and construct the insole in which the new sensor is positioned.

8. To perform a series of controlled tests on the new instrumented insole in a laboratory. Controlling the tests will allow the results obtained from the sensor to be directly compared with the literature. The correlation between the results of the new sensor and the literature provides the means for assessing its performance, as well as validating the design and theory used to construct it.

9. To comment on and compare the results of the new instrumented insole to the results presented in the literature.

The thesis begins in Chapter 2 with an overview of the research which has been applied to the science of gait analysis. Chapter 3 covers the design protocol which is adopted in the design of the new in-shoe sensor. Chapter 4 presents the results of the controlled tests performed on the sensor. It also analyses the performance and validity of the new in-shoe gait analysis device. Appropriate conclusions based on the performance, findings and results of the new in-shoe sensor are drawn in Chapter 5 and recommendations for the possible improvement or further development of the new gait analysis device are made Chapter 6.

CHAPTER 2

LITERATURE REVIEW

2.1 INTRODUCTION

The literature review provides the guidelines for the design of a new instrumented in - shoe gait analysis device which measures the shear stresses occurring at the first metatarsal head of the foot during the stance phase of the gait cycle.

The different techniques which are used to quantify the parameters that define gait are investigated. The findings, limitations and advantages of the studies which have been devoted to the study of gait, assist in developing the design criteria for the new instrumented in - shoe gait analysis device.

2.1.1 GAIT ANALYSIS

The gait cycle forms the basis for any research which relates to quantifying the forces experienced by the foot during locomotion[1]. In most cases, gait dysfunctions are multifactorial in origin. Appropriate intervention requires a clear understanding of normal locomotion, the biomechanics of gait and the underlying pathophysiology of gait deviations.

In the literature, the various factors which influence the gait cycle are described using either a qualitative observation technique or a quantitative evaluation technique[2,3]. The former is dependent on the experience of the clinician and relies on the clinician's judgment to make an accurate visual diagnosis. This type of analysis does not provide quantitative information and has many limitations due to the speed and complexity of human locomotion. This is further complicated by the gait deviations and compensations present in pathological gait.

A more scientific approach is the quantitative evaluation technique, where gait is studied through the collection of a wide range of information in the laboratory. The quantitative variables which can be recorded are grouped into two categories. These are kinematics (motion analysis) and kinetics (force analysis)[2].

The assessment of comparable and objective parameters has the distinct advantage of being an objective comparison of therapy results, an investigator independent long - term control and the creator of an objective data base[2]. The design, the methods, the results, the conclusions and the recommendations of the various kinematic and kinetic techniques used to obtain these quantitative variables, form the basis and background of the information needed to implement a technique that will be able to determine the shear stresses under the first metatarsal head of the feet during gait. Each technique has its own advantages and disadvantages depending on the particular type of application in which it is used. The application is defined by the type of pathology or condition which is being investigated.

2.1.2 PATHOLOGICAL GAIT

With each application, the primary objective is to evaluate the dynamic basis for an observed gait deviation. Pathological gait can result from a variety of clinical conditions.

There are three major categories of etiologies[1] :

1. ***Structural*** (musculoskeletal deformities)

2. ***Joint and soft tissue pathology*** (arthritis, soft tissue contractures)

3. ***Neurological disorders*** (pathology of the peripheral or central nervous system)

Each technique allows an objective assessment of the impact of various treatment interventions. They also develop objective selection criteria for different management options before and after therapeutic intervention.

Examples of such interventions could include the following :

- ***Structural*** : The use of a walking aid or the realignment of a prosthesis.
- ***Joint and soft tissue pathology*** : The application or modification of an orthotic or a special shoe. The correct design or use of running shoe.
- ***Neurological*** : Nerve or local pharmacological intervention.

2.1.3 GAIT ANALYSIS ASSOCIATED WITH JOINT AND SOFT TISSUE PATHOLOGY

As a result of the unprecedented growth of human physical activity in recent years the most common application of gait analysis, has been in the field of joint and soft tissue pathology. Particular attention has been focused on shoe research and development[4]. The main focus has been on the connection between physical activities and the occurrence of injuries and/or the influence of footwear on the movement and load characteristics of the foot[5]. The research in this field has provided a wealth of important information which has been applied to many other studies related to gait analysis. An understanding of the research that has been put into the design and function of running shoes therefore provides an important insight into the factors, be they for performance enhancement or rehabilitation purposes, which can influence and manipulate the load distributions experienced by different types of feet during pathological gait.

2.1.4 GAIT ANALYSIS ASSOCIATED WITH PERIPHERAL NEUROPATHY

The symptoms and signs of peripheral neuropathy associated with diabetic patients provides the motivation for the design of the in - shoe gait analysis device developed in this thesis.

Diabetics loose proprioreception (sensation) in their feet. As a result, they can injure their feet without even being aware of the injury. This loss of sensation results in the formation of large painless ulcers or long incisions which, unless correctly treated, can become infected and even lead to an amputation of the foot.

Repetitive mechanical stress on the bony prominences of the foot of a patient who has lost his/her protective sensation, is one of the most common causes of ulceration[3]. A major reason why diabetic feet ulcerate is that the decreased sensation interferes with the person's ability to limp when normally painful stimuli occur[6].

The statistics relating to diabetics are alarming:

- In the U.S. $200,000,000 a year is spent on direct hospital costs for diabetic foot infections[7].
- There are 600,000 new cases of diabetes each year in the U.S.[8].
- Amputations in the diabetic patient account for 50 % to 70 % of all non-traumatic amputations[9] which amounts to 35,000 major diabetic related amputations being performed each year in the U.S[10].
- Diabetes is the number one medical cause of lower limb amputations[11].
- 20% of patients who have any part of their foot amputated can die within 2 years[12] as a result of the complications associated with the trauma on their feet.

It is estimated that more than 50% of the amputations within the diabetic population could be prevented by adequate foot care[13]. To reduce the risk of amputation, podiatrists and clinicians use their qualitative skills together with the appropriate type of quantitative technology to measure the stresses at particular points on the plantar surface of the foot at particular times in the gait cycle.

Abnormally high pressures have been measured under the feet of patients with diabetic neuropathy[14,15]. These clinical studies established a clear relationship between areas of high direct pressure such as the plantar metatarsal heads and ulcer formation in diabetic neuropathy.

The mechanical stresses that are experienced under the plantar surface can result from two factors : direct pressure normal to the surface and shear stresses parallel to the surface. Shear stress is thought to be contributory to the damage process leading to ulceration[16]. Bennett[17] reported that at a sufficiently high level of shear stress (roughly 1Kpa or 0.145PSI) the pressure necessary to produce vascular occlusion of the microcirculation was half that required when little shear was present. Pollard and LeQuesne[18] showed that sites of healed ulcers correspond with the area of greatest horizontal shear stress and confirmed that the vertical force was also maximal in this region.

Tappin and Robertson[19] investigated the relative timing of the shear forces and vertical forces under the foot and found that at two sites (the first metatarsal head and the fourth/fifth metatarsal heads) the mean vertical and shear peaks lie within two standard errors of one another, indicating that the maximum shear force and the maximum vertical force are occurring at the same time. Therefore intermittent occlusion of the blood supply to the skin may occur. The results show that in normal subjects the shear and vertical forces acting at certain sites under the forefoot occur simultaneously and can be of sufficient magnitude to cause intermittent occlusion of the blood flow to the skin[19].

The combined effect of the shear and vertical forces is thought to be a contributory factor in neuropathic plantar ulceration. It has also been shown to have a cumulative effect with direct pressure on blood flow occlusion elsewhere in the body[20]. Reduced blood flow reduces the tissue's tolerance and repair capability. The contribution of plantar shear stress to ulcer formation has, however, not been widely evaluated due to lack of suitable instrumentation for its measurement[19].

2.2 INTERNAL AND EXTERNAL FACTORS ASSOCIATED WITH GAIT ANALYSIS

An understanding of the anatomical structures that are either directly or indirectly involved during the gait cycle is necessary to any understanding of the external parameters that might effect the cycle. Any form of pathology that is related to gait can present itself almost anywhere on the human body. Typically the lower extremities account for 79% of all injuries that occur during running. Of these injuries the knee region accounts for 25%, the leg 32%, the ankle joint complex 15% and the foot 7% of all injuries diagnosed during running[5].

As the feet are the first contact points which the body experiences during gait all the loads which are transmitted through the body initially have to travel through the feet. How these loads are transmitted by the feet is important to an understanding of the quantitative results which are measured. This is because the foot has its own complex means of adjusting to the loads that it experiences. S*ection 2.2.1* is concerned with understanding the basic anatomy and biomechanics of the feet. The anatomical terms used are also defined in *section 2.2.1.*

2.2.1 BASIC ANATOMY AND BIOMECHANICS OF THE FOOT

The foot is a complex part of the human anatomy consisting of 26 bones and allowing movement in six different directions. Its complexity often leads to responses that are confusing unless one has an understanding of how it behaves under stress[21].

2.2.2 THE STRUCTURE OF THE FOOT

The heel or rearfoot is made up of the calcaneus and talus. The talus articulates with the tibia and the fibula at the ankle joint complex. The name of the joint at the articulation point of the tibia and talus is the talocrural joint. The articulation point of the calcaneus and talus is the subtalar joint. The joint complex is shown in *figure2.1.* The midfoot is comprised of the navicular, cuboid and cuneiforms which together with the metatarsals form the arch of the foot.

The metatarsals are numbered one through five, such that metatarsal one is connected to the phalanges of the big toe and metatarsal five to the phalanges of the little toe. The phalanges form the forefoot. The sole of the foot is known as the plantar surface of the foot and the top surface the dorsal surface of the foot[21]. The structure and terms used to define the foot are shown in *figure 2.2*.

2.2.3 TERMS USED TO DEFINE THE FOOT

- **Anterior / Posterior:**

  This is the axis from the center of the calcaneus to the contact point of the second and third phalanges, parallel to the plantar surface of the foot. An advancement from the rearfoot to the forefoot is movement in an anterior direction. The most posterior point of the foot is the tip of the calcaneus and the most anterior point is either the big toe or the third phalange of the second metatarsal[21]. Therefore any structure that is closer to forefoot than another anatomical structure is regarded as being anterior to the forefoot and any anatomical structure that is closer to the tip of the calcaneus than another structure is regarded as being posterior to it.

- **Medial / Lateral:**

  This is the axis from the inside to the outside of the foot, parallel to the plantar surface of the foot. The big toe is regarded as being medial and the little toe as being lateral[21].

- **Inferior / Superior:**

  The axis from the plantar to dorsal surface of the foot perpendicular to the plantar surface of the foot[21] is known as the inferior superior axis.

2.2.4 GENERAL MOVEMENT DESCRIPTION

Clinical : Relates to arbitrarily defined axes or coordinate systems. Clinical movement descriptions are torsion, abduction and adduction, inversion and eversion and plantarflexion/dorsiflexion[5].

Functional : Relates to movement of actual joint axes which are related to actual anatomical functions. It is however at times difficult to quantify functional movements clinical movement descriptions are therefore introduced. A functional movement description is pronation and supination[5].

1. ***Plantar - Dorsiflexion*:** Rotation of the foot around a medial - lateral axis of the foot. This movement occurs primarily at the talocrural joint.

2. ***Abduction - Adduction*:** Rotation of the foot around an inferior - superior axis of the foot. Abduction is movement away from the midline of the body and adduction is movement towards the midline of the body. This general movement occurs throughout all the joints of the foot.

3. ***Inversion - Eversion*:** Rotation of the foot around an anterior - posterior axis of the foot. This movement occurs primarily at the sub - talar joint.

4. ***Pronation - Supination*:** Rotation of the foot around the sub - talar axis. It is a combination of the clinical movement descriptions presented above. Pronation is a combination of dorsiflexion, abduction and eversion while supination is a combination of plantarflexion, adduction and inversion.

5. ***Torsion*:** Rotation of the forefoot with respect to the rearfoot around the anterior - posterior axis of the foot.

Pronation and supination are the two most important parameters which are used to detect irregularities in gait patterns. A considerable amount of research has gone into establishing the effects of shoes on these two parameters. This is shown in *section2.5* and *section2.6.*

2.2.5 THE BIOMECHANICAL STRUCTURE OF THE FOOT

Lower limb mechanics of injured runners are associated to two types of feet, namely the clunk foot and the hypermobile foot[4]. The clunk foot is a rigid, stable, immobile, high arched structure which lacks adequate cushioning properties. The hypermobile foot has cushioning properties because of its ability to pronate, but is unstable as a result. It is the excessive inward rotation (pronation) which causes the most common injuries.

These two cases are regarded as the two extremes and as such show that shoes need to be designed either for shock absorption or for motion control[4]. As each condition has quite different characteristics, their requirements in shoe design are mutually exclusive. Research aimed at assisting in the treatment of these two types of feet is presented in *section2.5* and *section2.6.*

2.3 NORMAL LOCOMOTION - THE GAIT CYCLE

An understanding of the gait cycle is important for a number of reasons :

- It allows pathological gait to be correlated to the normal gait cycle to ascertain the causes and effects of any abnormality[3].
- It shows the sequence and relative timing of events which occur during gait[19].
- It defines the terms which are necessary for any assessment of human locomotion[22].

A single sequence of functions by one lower limb is called the gait cycle. The gait cycle has two basic components: the stance phase during which the foot is in contact with the ground, and the swing phase during which the foot is the air for limb advancement. The convention is to describe the cycle in terms of a percentage, rather than the time elapsed, as it has been observed that the events occur in a remarkably similar sequence and are independent of time, thus allowing normalization of the data for multiple subjects[22]. Footstrike is designated as 0%, toe off as 62% and second foot strike as 100% as shown in *figure2.3.* The stance phase makes up 62% of the cycle while the remaining 38 % consists of the swing phase[1].

Tappin and Robertson[19] compare the timing of the values of the shear forces in the horizontal plane with the vertical forces under the forefoot. The comparisons are made as a percentage of the stance phase of the gait cycle and are therefore not influenced by the velocity of walking. The results from the study show that the forefoot is initially subjected to shear under the lateral metatarsal heads at 10% of the stance time, thereafter as a result of sub-talar joint pronation, the shear force is transferred across to the medial metatarsal heads at 15% of the stance time and finally to the big toe at 28% of the stance time.

The peak shear forces occur laterally in the forefoot region at 58% of the stance phase, medially at 68% of the stance phase and at the big toe at 73% of the stance phase. Shear at push-off ends at 86% laterally before medially at 89%. Shear ends at the big toe ends at 94% of the stance phase. Shearing forces occur between 73% and 80% of the stance phase[19]. The fact that the shear forces end sooner than the vertical forces is an indication that at push-off, the final motion is an elevation rather than a motion in the forward direction. The important findings from this study are the times at which the shear stresses occur during the stance phase and that the shear and vertical forces acting under the forefoot in the first, fourth and fifth metatarsal heads, occur simultaneously.

2.4 HISTORICAL DEVELOPMENT OF GAIT ANALYSIS

Interest in the actual patterns of human motion goes back to prehistoric times, as is depicted in remnants of cave drawings, statues and paintings. Such replications were however, subjective impressions of the artist. It was not until the early part of the nineteenth century that the first quantitative study of human locomotion was made by Marey, a French physiologist in 1885[23]. He used a photographic "gun" to record displacements in human gait and chronophotographic equipment to create a stick diagram of a runner. During this same period Muybridge[23] sequentially triggered 24 cameras to record the patterns of a running man in the United States.

The advent of photography produced numerous detailed studies, such as those performed by the Weber[24] brothers, of the movements that occur during human locomotion. Modern systems now involve the use of high speed video or film recording or specialized optoelectronics apparatus in which active optical sources attached to the subject serve as markers. A modern example is biostereometrics, which uses two high-speed videos and active optical sources attached to a subject to create three dimensional images of specific gait movements[25]. Other modern kinematic techniques involve the use of accelerometers[26] and electrogoniometers[27].

The term used for the description of human movement is kinematics. Kinematics are not concerned with the forces, either internal or external, which cause the movement, but rather with the details of the movement itself[23]. In the field of kinematic analysis, human movement is described using a reference system which can either be *absolute*-which is movement described relative to the ground or *relative*-which is movement described relative to another anatomical structure. Parameters that are involved in a kinematic analysis are anthropometric data (anatomical dimensions), angle changes (goniometers), displacement changes, velocity changes and acceleration changes (accelerometers).

The first attempt to quantify the kinetics experienced during gait was made by Braune and Fisher[28] in 1900 who calculated the ground reaction forces based on the kinematics of a movement with an assumed mass distribution of the human body. In 1920 Amar[29] made the first attempt to measure the two components of the ground reaction forces during running. In 1934 Elftman[30] successfully advanced plantar stress measurement from static footprint analysis to the instantaneous recording of vertical plantar stress by using a rubber mat with a surface of rubber pyramids whose deformations were recorded cinematographically. In 1978 Miller[31] used a force plate to present data which indicated the vertical forces for a single subject during a "slow jog". Using a force platform, Cavanagh and LaFortune[32] measured the three components of the ground reaction forces of 17 subjects in 1980. This study introduced the concept of Center Of Pressure (COP). The COP is considered to be the point of application of the resultant force on the plantar surface of the foot at any time in the stance phase.

Two methodologies are available for the modern measurement of ground reaction forces. Pressure platforms measure only the vertical components (e.g. EMED-SF which use the capacitive method)[33-35]. Force platforms (e.g. Kistler which use piezoelectric technology and AMTI which use strain gauge theory)[26,36] measure the resultant three dimensional ground reaction force and the point of application of this force. Recently measurements have been made using instrumented insoles which are placed inside the shoe (e.g. EMED-PEDAR and FSCAN)[16,37,38,39].

The first attempts to use foot-mounted pressure transducers were made by Schwartz and Heath in 1932[40]. In 1947 they developed small, discrete stress transducers[41]. In 1976 Spolek and Lippert[42] developed an instrumented shoe with two load cells which was based on strain gauge principles and beam theory. One cell was positioned under the heel and the other under the forefoot of the shoe. The components of foot-to-ground forces and moments were measured with the use of goniometers which simultaneously monitored the position of the lower leg. The forces measured were transformed into three orthogonal components relative to the ground. Modern-day techniques involve various different methodologies. These include the capacitive principle[37], the piezoelectric principle[39], the magneto-resistive principle[16], the semi-conductor strain gauge theory[17] and the force-sensing resistor ink theory as developed by Tekscan (Tekscan, Inc., Boston, MA).

The various techniques which have been developed to analyze gait are presented in *section2.5*, *section2.6* and *section2.7*.

2.5 AN ASSESSMENT OF THE KINEMATIC TECHNIQUES USED TO QUANTIFY THE PARAMETERS DEFINING GAIT

There are two measurement techniques used in the kinematic analyses of human gait. They are *direct measurement* and *image measurement*[23]. The former primarily uses goniometers and accelerometers while the latter uses cinematography, television or optoelectric techniques.

2.5.1 DIRECT MEASUREMENT TECHNIQUES :

2.5.1.1 GONIOMETERS

Methodology :

A goniometer is an electrical tri-planar potentiometer that can be attached to an anatomical structure to measure its joint angles. A constant voltage is applied across the outside terminals and as the angle changes, the voltage across the terminals changes linearly.

It was used by Spolek and Lippert[42] to measure the angle changes of the foot relative to the ground at specific locations during gait. Smart and Robertson[27] used a tri-planar electrogoniometer to study the effects of corrective orthotic devices on selected parameters of running gait *(figure 2.4)*. They investigated the angular displacements occurring at the left ankle during running.

Findings :

The findings of Smart and Robertson[27] were that corrective running orthotics significantly reduce the amount of support phase eversion. This can be clinically interpreted as a reduction in foot pronation. The study also reflected an inherent error between trial calibrations as a result of movement of the goniometer caused by the impact forces experienced during running.

Advantages / Benefits :

- A goniometer is inexpensive[23].
- Output signal is available immediately for recording or conversion into a computer[23].

Disadvantages / Limitations :

- Relative angular data is given as opposed to absolute angles[23].
- It can require an excessive amount of time to fit and align[27].

- If a large number of goniometers are fitted, movement can be encumbered by the straps and cables[23].
- Slippage and movement introduces error[27].
- More complex goniometers are required for joints which do not move as hinge joints (e.g. the ankle joint complex)[23].

2.5.1.2 ACCELEROMETERS

Methodology :

Accelerometers are typically used in gait analysis to measure the accelerations occurring on the tibia[26]. The accelerations experienced by the tibia are used to infer what ground reaction accelerations the foot is experiencing during gait. The research using accelerometers focused primarily on evaluating the effects of varying shoe designs. The accelerometers are either strapped to skin of the tibia[43] or fastened into the bone of the tibia[44] *(figure 2.5.)*. A considerable amount of research was done to check the validity of using accelerometers in gait analysis.

Findings :

In a study by Valiant, McMahon and Frederick[43] evaluating the cushioning properties of athletic shoes, it was found that a low mass and high strap tension are desirable for an adequate transducer frequency response. This suggests that the soft tissue between the accelerometer and the tibia may be modeled as a reinforced elastic sheet. When loaded in either direction the sheet results in more tensile elements becoming taut, thereby increasing both stiffness and damping.

These factors were highlighted when the results were compared with data obtained simultaneously using a force plate. The accelerometer measurements were found to overestimate the accelerations by as much 20% to 30%. It showed that a stiff attachment for accelerometers is required for accurate measurements. In a study by Henning and LaFortune[44] a comparison was made between bone mounted and skin mounted accelerometers. It was found that the amplitudes from the skin mounted accelerometers were two times higher than those mounted in the bone.

In the same study an evaluation was made between the correlation of ground reaction forces and tibial acceleration measurements. The axial acceleration experienced by the bone is determined by gravitation, the impact forces and the centrifugal forces due to the rotation of the tibia during gait. The method adopted included accelerometers, a force plate and cinematography techniques which allowed the centrifugal forces to be accounted for. These forces cannot be accounted for when accelerometers are used in isolation. The study showed that the accelerations in the anterior-posterior direction are higher than the axial accelerations as a result of the centrifugal forces.

Hennig and LaFortune's study highlighted three important considerations. The first was that the acceleration in the anterior-posterior direction is greater than the axial acceleration. Secondly, tibial and ankle joint angular motion and gravity contribute to axial acceleration during gait. Thirdly, unless intricate and complicated equipment is used, it is not possible to correlate the accelerations measured at the tibia to the axial accelerations at the ground. These findings indicate that care needs to be taken when inferring ground impact magnitudes from tibia attached accelerometer measurements.

Advantages / Benefits :

- An output signal is available immediately for recording or conversion using a computer[23].
- The use of accelerometers is well documented.
- The availability of many different designs.

Disadvantages / Limitations :

- The acceleration signal is a relative measurement whereas the limb moves in an absolute direction[23].
- In order for the accelerometer to produce accurate measurements it has to be inserted into the bone of the tibia[44]. This is an unpopular technique.

- A considerable amount of equipment (accelerometers, force plate, video/cameras) is required in order to correctly represent the ground reactions occurring during gait[44].

- It is not possible to isolate the accelerations at particular points on the plantar surface of the foot[23].

2.5.2 IMAGING MEASUREMENT TECHNIQUES

Many types of imaging techniques may be used to quantify gait's defining parameters. Two of the most popular techniques are reviewed below.

2.5.2.1 VIDEO AND CINEMATOGRAPHY TECHNIQUES

Methodology :

Kinematic techniques monitor angle changes which occur between markers positioned at specific points on the lower limb[45-48]. The angle changes are then translated into displacements which with a given time frame can be translated into velocity. This can also be translated into acceleration. The most common method of establishing an absolute reference frame is to move a mechanical x - y - z coordinate system until a pointer lies on the center of the desired landmark. All movement is then referenced to this anatomical datum.

Movement of the camera, imperfect alignment of the film in the sprockets, human errors in determining the center of a body marker and the precision of the analog-to-digital conversion all result in raw data that is imperfect. Such data is described as having noise or additional artifact data. Calculation of the angles measured by the video cameras requires that this raw data be smoothed by means of a harmonic (or frequency) analysis.

Harmonic analysis is based on a signal's frequency content. Spectral plots are plots that show the amplitude or power of each frequency component plotted against frequency. The mathematical process to accomplish this is called a Fourier transformation. The Fourier transformation of non periodic signals is defined by its lowest frequency, the fundamental frequency, and frequencies incrementally higher called harmonics. Any periodic signal can be broken down into its harmonic components. The sum of the amplitudes of these harmonics is called a Fourier series.

At a normal walking speed of 120 steps /min (2 Hz), harmonics at 2Hz, 4Hz and so on would be expected[23]. Normal walking analyzed by Winter et al[23] showed that 99.7% of the signal power is contained in the lower seven harmonics. Above the seventh harmonic there is still some signal power, but it has the characteristics of noise. Usually the random noise is of a high frequency. The presence of the higher-frequency noise is of considerable importance when trying to calculate velocities and accelerations from displacement data. The relative amplitude of the signal changes increases with each differentiation of increasing frequency. The first derivative velocity, increases amplitude proportional to frequency while the second derivative increases amplitude proportional to $(\text{frequency})^2$.

Assuming that the amplitude of the first three harmonics of a signal are equal, the first derivative for all three harmonics increases linearly while the first derivative of the third harmonic increases by three times and the second derivative by nine times. This means that even a small error in the displacement measurements will amount to considerable errors in the velocity amplitudes and even more errors in the acceleration amplitudes. The problem can be resolved by smoothing or filtering the raw data.

The first of the raw data smoothing techniques is curve fitting. The basic assumption is that the original signal has a predetermined shape which can be smoothed by fitting a best fit curve to the raw data. Various curve fitting techniques include using a certain order polynomial, a linear regression or a cubic spline.

Digital filtering is achieved by analyzing the frequency spectrum of both the signal and the noise. The objective is to select a cut-off frequency or frequency band which will allow the maximum amount of actual data to be measured while eliminating as much of the noise as possible. Essentially it serves the purpose of a filter which can be either a low pass, band pass or high pass filter. The order of a filter determines the sharpness of the cutoff. The higher the order the sharper the cutoff. A fourth order Butterworth-type low pass filter with a cutoff frequency of 6 Hz is the most commonly used filter in gait analysis[23].

A final consideration is the sampling frequency. The sampling theorem states that the process signal must be sampled at a frequency at least twice as high as the highest frequency present in the signal itself. If the signal is sampled to low, aliasing errors are encountered. These result in false frequencies which are not present in the original data. For normal and pathological gait studies, kinetic and energy analyses can be done with negligible error using a sampling frequency of 24 Hz[23].

Findings :

Kinematic studies which have been done on feet are primarily concerned with the movement of bare feet or the effect of shoes on the movement of the feet inside the shoe[45-48]. The markers are positioned at specific points to determine the absolute angular displacements which occur at these points. These results, depending on the particular analysis being undertaken, are then interpreted clinically. An illustration where Nigg et al[45] placed markers on the lower leg and foot to examine the effects of various insoles is shown in *figure2.6*. They used two video cameras and a force plate in their research. The main variables which are shown in *figure2.6* are described below.

γ = Initial rearfoot angle and $\theta\ \gamma$ is the total shoe pronation

β = Initial Achilles tendon angle and $\theta\ \beta$ is the total joint pronation

α = Initial lower leg angle (all initial variables are determined from the last film frame before ground contact)

δ = Initial sole angle

η = Initial tibia angle

ε = Initial knee angle

The study by Nigg et al[45] found that the various insoles investigated have no significant effect on the mean vertical impact force or the time at which it occurred. It also found that the regular insole which is the hardest and thinnest insole, describes the least pronation. It is postulated by Nigg et al[45] that the reason for this is the lower position of the heel in the shoe with the regular insole. By raising the heel, the axis of rotation of the subtalar joint moves further away from the ground. As a result, the moment arm of the ground reaction force about a vertical axis through the subtalar joint increases which increases the moment about this axis. The increased moment results in a greater ground reaction force being applied to the ankle. Although Nigg et al's[45] hypothesis is conceivable, a better explanation is given by Luethi et al[46].

Luethi et al[46] found that harder shoes can result in lower impact forces than shoes with softer soles as a result of a change in foot movement during impact. They hypothesize that the greater amounts of initial pronatory movement are as result of the leverage of the ground reaction force with respect to the subtalar joint axis. A shoe with a stiff sole increases the lever of the impact force and thus produces a greater moment about the joint. This increased moment results in greater joint motion and simultaneously lowers the ground reaction forces[46]. The results from the study by Luethi et al[46] are presented in *figure2.7*.

The studies by Nigg et al[45] and Luethi et al[46] show that the mechanisms of the foot are such that it has the ability to dissipate load through movement of its joints. This is shown in a study by Stacoff et al[47] who examined rearfoot motion and its effect on the design of running shoes. They found that the most torsion occurs during barefoot running which indicates again that the foot uses motion to dissipate the ground impact loads during the gait cycle. These studies therefore illustrate the importance of having an understanding of the various anatomical mechanisms of the foot when designing any device which measures either its movement or the forces it transmits to the ground.

Stussi et al[48] questioned the validity of using markers on the shoe to evaluate the effect of shoes on the motion of the foot. Their study investigated the movement of the heel within a running shoe by placing markers on the heel of the shoe and on the heel of the foot. The markers were visible through windows in the heel of the shoe. *Figure2.8* shows a schematic of the test procedure. The angle between a line joining the two markers on the Achilles tendon and the line joining the markers on the heel of the shoe was called the shoe angle(βs) and the line joining the markers on the heel of the foot was called the foot angle(βf). The datum was taken from the angle of the line joining the Achilles markers at touchdown. A shift of almost 10 degrees between the heel-pronation and the shoe pronation was found. This was accounted for by the fact that the datum which was made in a weight bearing condition at touchdown is different to a datum that is made in a non weight bearing condition.

The study showed that the heel of the foot inside the shoe, under load in a standing position, is initially pronated. This initial pronation cannot be detected from inspection of the markers on the heel of the shoe. The finding casts doubt on the validity of using markers on the heel of the shoe to infer how the foot is responding to load because there is movement of the foot inside the shoe during the stance and swing phase. It also casts doubt on the correct manner in which to establish a datum from which all the angles are eventually calculated.

Advantages / Benefits :

- Uncomplicated to attach markers[23,46].
- Instant replay with the capability to convert data immediately[47].
- Relatively inexpensive equipment required[23].

Disadvantages / Limitations :

- The effect of projection errors as a result of having a two-dimensional rather than a three-dimensional analysis. It is evident that two -dimensional angles in one plane are influenced by rotations in another plane[25].

- Errors due to movement of the markers on the skin surface. This results in a misrepresentation of the bone and joint movements[23].

- Errors due to movement of the foot inside the shoe. This has an effect on establishing a reference datum from which all the kinematic measurements are made[48].

- Errors due to digitization of angular data. Any noise that is present in the initial kinematic data which has not been correctly removed, will greatly attenuate the overall error of the experiment[23].

- Unable to evaluate the loads at particular points on the plantar surface of the foot[23].

2.6 AN ASSESSMENT OF THE KINETIC TECHNIQUES USED TO QUANTIFY THE PARAMETERS DEFINING GAIT

Two main techniques are used when attempting to quantify the forces which are transmitted through the feet during gait. The first technique uses force sensitive plates. These are either specially designed mats which provide quantitative information about the three components of force acting at a particular point on the plate (e.g. Kistler force plate[32]) or they are pressure plates[33-35] which indicate the pressure at particular points on the foot during the stance phase.

The second technique involves specifically designed apparatus which simulates the loads experienced by the feet during gait (e.g. a pendulum with a force transducer striking the heel of the foot[36]). This second technique is limited by the fact that it does not simulate the loads experienced by the feet during gait (i.e. inertial effects and centrifugal effects) which are of crucial importance as shown in *section2.5.1*. This thesis will therefore only examine the technique which uses force sensitive plates.

2.6.1 PRESSURE PLATES

Methodology :

Pressure plates are unidirectional force transducers which measure the normal vertical forces over specific areas. Such devices work on the principle that an electrical signal can be calibrated to be proportional to an applied force. There are many ways to convert a force into an electrical signal. The various techniques use resistive technology (e.g.Musgrave systems), optical methods (e.g.Pedobarograph) and capacitive methods (e.g.EMED systems). The experimental technique usually follows the following protocol :

- Familiarization period - so that the individual strikes the platform at the correct cadence and with a natural uniform gait pattern.
- The subject then walks or runs on a set walkway and strikes the platform once with the selected foot.
- Measurements are taken and analyzed.

The various methods which are used to determine the pressures on the feet during gait are presented below.

2.6.1.1 RESISTIVE METHODS

These sensors either use resistive foams or are based on the carbon microphone principle. The latter technique involves using a semi-conductive ink (carbon) which is applied between two layers of plastic mylar and covered with a conductive silver-based ink[2]. When pressure is applied, the contact area between the semi-conducting carbon and the conducting silver is increased simultaneously decreasing the resistance. A limitation is that the resistance at zero load is infinite. This makes the calibration very difficult. Another limitation is that the semi-conducting carbon may change its shape due to shear forces over time. The changes alter the assignment of pressure to a certain resistance.

2.6.1.2 OPTICAL METHODS

These methods measure pressure by filming the underside of a lighted glass plate across which a person walks. The top of the glass plate is covered by a thin sheet of opaque reflective plastic. The amount of light escaping from the glass which is seen by the camera varies according to the pressure at each point. These gray scale images are then converted to pressure values. A limitation is the inability to calibrate the entire plate or calibrate each single sensor. It is therefore difficult to relate gray scale values to absolute pressure values. The Podotrack System is a commercially available system which has been developed using the pedobarographic technique. This technique uses a reference card calibrated to relate different shades of gray to footprint pressures left on a specially treated piece of carbon paper[2].

2.6.1.3 CAPACITIVE METHODS

The capacitive method utilizes the phenomena that when the distance between two plates separated by a dielectric material changes, there is a corresponding change in the capacitance of the sensor[2,23]. The quality of a capacitive sensor depends on the material and shape of the dielectric used. The advantage of capacitive sensors is their simple calibration. Even for large sensor numbers (platforms containing up to 4096 sensors), each sensor can be calibrated individually[49]. An example of a commercially available system which uses capacitive technology is a pressure platform (EMED-SF) developed by Novel GMBH of Munich, Germany. The EMED-SF offers numerous features, one of which includes being able to mask a sensor or a group of sensors and do an analysis of the parameters involved which quantify the pressures at a particular point on the sole of the foot. *Figure2.9* gives an illustration of the various windows which are available on the software provided by Novel GMBH.

2.6.1.4 THE CONCEPT OF CENTER OF PRESSURE - (COP)

The COP is the position of the resultant force at a particular point in time during the stance phase[32]. On a pressure plate supported on it's four corners, the location of the COP is calculated from the proportion of the overall force which is distributed in each of the four support bases. The path of COP is used as a means of clinically determining the overall movement of the foot during the stance phase. An example of rearfoot and midfoot strikers using the COP concept is illustrated in *figure 2.10.* A shift too far medially or laterally of the COP is indicative of some abnormal gait condition.

One of the limitations of the COP concept is shown in *figure 2.10* where the COP is seen to fall outside the borderline of the shoe[33]. One reason for this could be that placement of the foot is preceded by a scuffling phase when forces greater than threshold exist between the foot and the floor but final placement has not yet been made. A second cause could be the "abductory twist" which occurs at the time when the pressure distribution is centered in the forefoot. The twist describes the small medial movement of the heel.

Another limitation of the COP concept is the phenomena which occurs at mid stance where pressure is distributed over the rear and forefoot. The COP concept places the COP in the center of the foot where there is little or no pressure regardless of the load on the foot. Research is ongoing as to whether the technique of COP measurement has the required sensitivity to distinguish subtle changes in pressure distribution which may seriously affect the well-being of the runner[32].

Findings :

Bennett et al[35] determined the pressures beneath the big toe, the metatarsal heads and the heel in healthy adults walking at 100 steps/min using the Musgrave force platform system. They found the average maximum pressures at selected anatomical locations on the plantar surface of the foot. The results from the study are presented in *Table2.1.*

Anatomical location	**Mean Pressure**	**Standard Deviation**
	(kPa)	**(kPa)**
Second to fourth metatarsal heads	420	100
Big Toe	350	110
First metatarsal head	310	90
Fifth metatarsal head	230	100

Table 2.1 Peak pressures measured in the forefoot region by Bennett et al [35]

The order of mean peak pressure of each plantar structure from highest to lowest was the second, third, fourth metatarsal heads (considered collectively), then the big toe, followed by the first metatarsal head.

In a study by Henning et al[50] the pressures under the right foot were recorded during barefoot walking at a slow walking speed of approximately 1 m/sec with the capacitive pressure distribution platform developed by Novel GMBH. The necessity to target the small area of the platform (200mm*340 mm) during walking at a prescribed gait velocity was found to cause a disturbed gait pattern. Clarke[51] showed that an increase in gait speed from 1.33m/sec to 1.79m/sec created an increase in the peak pressure values across all foot regions of only 7.2%. Patients were therefore asked to walk at their own comfortable walking speed. The average mass of the 111 adults tested was 70Kg with a standard deviation of ±11.8Kg. The study protocol used five dynamic recordings of each foot. According to Hughes et al[49], averaging five trials for each subject achieves a high coefficient of reliability for peak pressure (R=0.94). The results of the study by Henning et al[50] are presented in *Table2.2.*

Anatomical location	Mean peak pressure
	(kPa)
Second, third and fourth metatarsal	380
Big toe	416
First metatarsal	314
Fifth metatarsal	216

Table 2.2 Peak pressures in the forefoot region measured by Henning et al [50]

Advantages / Benefits :

- Pressure plates provide a quantitative means of assessing the vertical forces acting at specific points on the sole of the foot during gait without shoes and specific points on the sole of the shoe when shoes are worn.[33-35]
- The results are easy to interpret and use and in the case of the capacitive method, easy to calibrate.[48]

Disadvantages / Limitations :

- The use of the COP concept is not entirely indicative of the movement of the center of pressure on the plantar surface of the foot during gait.[33]
- Consecutive steps are not possible with pressure plate analysis.[23]
- The shoe-foot interface cannot be measured. Only the foot-ground or shoe-ground interfaces can be measured. The effect of the shoe is to distribute the pressure over a wider area such that measurements between the shoe and the ground do not give a clear indication of the pressure being experienced by the various regions of the foot.[33]

- Pressure plates represent the entire bodies center of gravity. This has an effect on the readings which are measured by the pressure plate. For example, when standing on the force plate, a movement of the arm produces a pressure on the pressure plate. It is therefore fair to assume that the loads which are measured using a pressure plate do not all result from foot contact with the ground[35].

2.6.2 MULTIDIRECTIONAL FORCE PLATE

Methodology :

In order to measure forces in two or more directions it is necessary to use a bi- or tri-directional force transducer. Such a device consists of two or more force transducers mounted at right angles to each other. These plates are able to measure forces in the vertical direction and in the two shear directions. These three directions are commonly called the vertical, medial-lateral and anterior-posterior components of the applied force.

2.6.2.1 THE PIEZOELECTRIC METHOD

This method, which utilizes the piezoelectric characteristics of quartz, is the most accurate method of measuring dynamic forces. It has a low hysteresis response, behaves linearly and is highly sensitive. The signal of quartz is time-dependent (drift), and as such problems are encountered when measurements are taken over long periods of time. As the contact time in gait analysis is typically below 1 sec, this problem is rarely encountered[2].

2.6.2.2 THE STRAIN GAUGE METHOD

The advantage of this technology is its time-independence. The disadvantages are the large amount of deformation required, it's high inertia forces and it's limited range and speed[2].

Findings :

The most comprehensive research done using a force platform was done by Cavanagh and LaFortune[32]. The ground reaction forces of 17 subjects were analyzed while running at 4.5m/sec. Although this study was done using running subjects, it serves to illustrate the forces which occur during running. It also illustrates the type of data which is available using force platforms and the method which is used to smooth the raw data. The data which is presented using force platforms, is presented as the resultant force acting over the area of the foot which is in contact with the force plate at a particular time. It is usually expressed as a percentage of the subject's body weight (BW).

The method used to normalize the different subjects in this study[32] is to either dilate or compress the data to the mean contact time, average the peaks for each particular curve and then fit the best fit curve between the averaged peaks, thereby producing one normalized curve. The mean force-time curves representing the mediolateral, anteroposterior and vertical components for the contact phase are presented in *figure2.11*. The mean peak to peak force components were 3BW, 1BW and 0.3BW in the vertical, anteroposterior and mediolateral directions respectively. The transition from braking to propulsion occurred at approximately 48% of the total support time. The point of maximum braking occurred at 22% of the stance phase while the point of maximum propulsion occurred at 70% of the stance phase.

Advantages / Benefits :

- Measures the three components of the resultant force acting on the plantar surface of the foot[32].

Disadvantages / Limitations :

- As with pressure plates, force plates only allow a single step analysis and can result in a subject adopting an abnormal gait pattern in attempting to strike a platform at a specific cadence[16].

- Presents no information of the response of the foot inside the shoe during loading[52].

- Unable to present information at specific points on the plantar surface of the foot. Only a resultant force is presented. This is shown by Gross et al[53] who placed a marble inside a shoe beneath the first metatarsal. The subject first walked across the pressure platform and a force plate without the marble and then repeated the procedure with the marble inside the shoe. Pressure analysis indicated a much increased pressure in the area of the marble yet the COP paths produced from the force plate data were nearly identical.

- Force platforms are sensitive pieces of equipment and as such require a stable environment in which to operate (i.e. solid foundations)[23].

2.7 AN ASSESSMENT OF THE METHODS USED FOR IN - SHOE STRESS MEASUREMENT

There are two types of in-shoe stress measurement devices. The one type uses *discrete transducers* and the other *matrix transducers*[52].

2.7.1 DISCRETE DEVICES

Methodology :

These are devices which are positioned at selected anatomical points on the plantar surface of the foot. There are two ways of establishing contact of the sensor with the foot. The first method is to attach the sensor directly onto the sole of the foot [54-55] or to the surface of the insole which is in contact with the plantar surface of foot[53]. The second method is to recess the sensor inside a specially designed insole which houses the sensor[16].

Sensors may be placed by using a qualitative technique (e.g. palpation of the bony prominences) to locate the points of maximum pressure in a static environment[53-55] or by using a quantitative method (e.g. pressure plate, force plate) to locate the areas maximum pressure on the plantar surface during dynamic conditions.[16]

Discrete sensors can be made using various types of technology.

2.7.1.1 CAPACITIVE DEVICES

Capacitive devices consist of two conducting plates which are separated by an insulated layer of material called a dielectric. A capacitive based in-shoe pressure transducer uses a compressive dielectric material. Increasing pressures will tend to decrease the separation between the plates, thereby increasing the capacitance.

Such a device was used by Levin[56]. The dimensions of Levin's sensor were 3mm thick with a diameter of 14mm. The sensor was incorporated in a portable in-shoe gait analysis device which consisted of eight transducers positioned at selected anatomical points inside an insole.

2.7.1.2 PIEZOELECTRIC METHODS

The piezoelectric effect, found in natural materials such as quartz and manufactured materials such as PZT (lead ziconate titanate), results in the generation of charge when the material is deformed. This charge, once amplified, can be converted into a voltage which is proportional to an applied stress. The response of piezoelectric materials can be complex as it does not respond to a shear stress the same way it does to a vertical stress and is also sensitive to bending and temperature. Eight piezoelectric transducers were used by Gross et al[53] and six piezoelectric transducers were used by Ekstrom et al[54] in their studies of vertical in-shoe stresses. An illustration of the design of the discrete sensor is presented in *figure2.12*. The size of the sensor in the study by Gross et al[53] was (4.83*4.83*1.30 mm) and had a mass of 0.5g and in the study by Ekstrom et al[54] the size of the sensor was (4*4*1.2 mm).

2.7.1.3 HALL EFFECT AND MAGNETO-RESISTIVE DEVICES

When a current-carrying conductor is placed into a magnetic field, a voltage is developed perpendicular to both the direction of current flow and to the magnetic field. This principle is called the Hall-effect. Magneto-resistive devices operate on a similar principle except that resistance is changed rather than voltage output. Magneto-resistive devices were first implemented into gait analysis by Tappin et al[57] to measure the shear stresses on the sole of the foot. The design which is illustrated in *figure2.13* has been used in numerous other studies[46,49,58]. The device operates on the principle that the resistance of a semiconductor varies with the strength of the magnetic field in which it is placed.

By using a center-tapped magneto resistor bridge configuration, with a magnet placed centrally above it, any lateral movement of the magnet will unbalance the bridge and give an electric signal proportional to the movement of the magnet. It consists of two discs separated by a silicone rubber and a guiding middle disc. The silicone rubber supplies the restoring force and the guiding disc has the magnet attached to it while also only allowing movement in two orthogonal shear directions. The dimensions of the transducer are 2.7mm with a diameter of 15.96mm.

A similar sensor, based on the principle developed by Tappin et al[57], is used by Lord et al[16] to investigate the shear stresses acting on the plantar surface of the foot under the first metatarsal head. The motivation for locating the sensor under the first metatarsal is that although it is typically only the third highest area of stress in the forefoot region[35,50,58], the maximum shear stresses and maximum vertical stresses under the first metatarsal head have been suggested to occur at the same time[16,18,19]. There is also a high incidence of ulceration in this region[18,19,59]. The significance of the similar timing of the maximum vertical and maximum shear stresses is that pressure measuring devices can be used to locate the shear sensor[16].

Lord et al[16] found that locating the points of maximum pressure using the palpation method resulted in the points of maximum pressure being 20mm posterior to the points of maximum pressure found using a pressure measuring device (Tekscan matrix insole). They also found that peak pressures measured under the areas determined using the palpation method were substantially lower than those determined using the Tekscan matrix insole. These findings are illustrated in *figure2.15.* and *figure2.16.*

The deviation can be explained by the fact that gait is a dynamic phenomena and the palpation method measures the points of maximum pressure when the foot is static. When the foot is progressively loaded, the skin will tend to remain in the position at which it first came into contact with the shoe sole, whereas the underlying bony structure will distort[53]. Flattening of the longitudinal arch of the foot results in an anterior motion of the metatarsal heads as the midfoot lowers and the foot pronates[16]. This is consistent with a radiographic study done by Shereff et al[60] who showed that out of 20 normal subjects, 19 of them showed significant lengthening of the first metatarsal.

Once the location of the sensor has been determined, it is placed inside a customized insole as illustrated in *figure2.14.* The region surrounding the transducer must be of higher density than the rest of the insole so that the sensor remains flush with its surroundings during loading and provides stability for the sensor. To avoid interference with the flexibility of the foot during toe off, the higher density band is not extended too far anterior, similarly extending the band too far posterior would interfere with the flexibility of the foot at heel lift.

Findings :

Gross et al[53] studied a rearfoot striking runner running at 3.58 m/sec on a treadmill. Eight piezoelectric transducers are placed under the plantar surface to measure the magnitudes of the peak vertical stresses. The results of the study are presented in *Table2.3.*

Anatomical location	Mean peak stress	Standard deviation
	(kPa)	(kPa)
Big toe	420	90
Second metatarsal	340	50
Third metatarsal	305	35
First metatarsal	280	40

Table 2.3 Peak stresses in the forefoot region measured by Gross et al[53]

Lord et al[16] presented information on the two orthogonal axes of shear acting at the first metatarsal head using a shear transducer. The transducer was based on the magneto-resistive principle, mounted in a stock orthopedic shoe commonly prescribed for diabetic foot problems. In the study, a series of pilot trials were performed on normal subjects who walked at their own comfortable pace with the in-shoe device positioned inside an orthopedic shoe. The sampling rate of the data measured by the shear transducer for this particular study is 50Hz per channel. The results from one of the subjects of the study are illustrated in *figure2.17*.

Advantages / Benefits :

- Allows the two shear components of the applied force acting at a particular plantar area to be evaluated[16,57].
- They permit the most important interface, that between shoe and foot, to be monitored, thus providing a better means to understand the effects of shoe design modifications on the mechanics of the foot[52].
- They allow for increased versatility of measurement for the calculation of more robust statistical estimates[52].

- They allow a multiple step analysis to be performed thus allowing variability within a given condition to be examined[52].

- The problem of trying to target a force or pressure plate is eliminated[16].

- Measurements can be taken during a wide variety of activities, both indoors and outdoors, rather than being limited to a controlled lab environment[16,56].

Disadvantages / Limitations :

In-shoe stress measurement is technically more demanding than stress measurement on a flat walking surface. There are various factors which have the potential to increase measurement error and device failure.

- The transducer cables can experience bending as they travel from the sensor, through the insole and out of the shoe[52]. The repeated bending in the area around the transducer, unless reduced, can result in artifact information[16].

- The inside of the shoe can be described as a "hostile environment" since it can be warm, damp and contoured[52].

- The transducer may act as a foreign body in the shoe and alter the mechanical conditions at the foot-shoe interface. Not recessing the discrete sensor enough in an insole will result in it becoming a natural pressure point. Recessing it completely will result in it not being able to establish contact with the foot. Minimal contact between the sensor and the foot is regarded as ideal[57].

- Discrete sensors positioned at specific points are limited to gait patterns of a particular individual. Normalization of sensor locations so that any person can use the instrumented insole is not possible[52].

2.7.2 MATRIX DEVICES

Methodology :

Matrix systems consist of numerous pressure sensing elements arranged in rows and columns. Unlike discrete systems, this pattern permits a larger area, usually the entire surface of the foot, to be monitored at one time without the need for *a priori* decisions about the regions of particular interest[52].

At present there are two commercially available matrix systems, the EMED PEDAR insole shown in *figure 2.18,* (Novel GMBH, Beichstrasse 8, 8000 Munich 40, Germany) which consists of an array of 99 capacitive sensors per insole and the F - SCAN insole (Tekscan, Inc., Boston, MA, USA), which consists of an array of 960 force sensing resistors per insole. The F - SCAN consists of two printed circuits separated by a conductive ink layer. Applying pressure changes the composition of the ink layer, altering the output of the circuit elements which are variable resistors. An actual F - SCAN insole as developed by Tekscan is presented in the *Appendix E.*

Calibration is essential to the performance of matrix devices[49]. A matrix device should be treated as an assembly of discrete devices because individual elements do have markedly different calibration characteristics. As a result, Novel developed their own air bladder calibration device that applies a known uniform pressure to each sensor at the same time. In this manner each sensor can be calibrated individually. The air bladder calibration device, developed by Novel and used by McPoil et al[37] in their comparison of the EMED and F-SCAN insole systems, is shown in *figure2.19*. The normal F-SCAN calibration procedure involves the subject standing on the insole prior to movement.

Both systems use software to sampling data at a rate of 50 Hz.

Findings :

A study by McPoil et al[37] in 1995 compared the validity and reliability of the two insole systems manufactured by Novel and Tekscan. The study investigates three different loading conditions on the two insoles. The creep test involves applying a static uniform pressure of 150kPa over the entire area of the insoles for a fixed time period of 11 minutes using the air bladder calibration device. The second test also uses the air bladder device to apply a series of pressures from 0-500kPa to the insoles. The third test involves a series of actual dynamic tests. The performance of each insole during the dynamic tests is judged by the repeatability of each test to predict the two normal force peaks which are present in the normal gait pattern - either between the three steps of each trial, between each session on a particular day or between each day.

The results of the creep test are illustrated in *figure2.20*. The total creep of the EMED insoles is found to be 3.4% or less and linear whereas the total creep for the F-SCAN insoles is found to be 11.6% and non-linear.

The results of the calibration technique are shown in *figure2.21*. The average error at 50kPa for the EMED is 16% and 0.8% at 500kPa, whereas the error for the F-SCAN is 4% at 50kPa and 24% at 500kPa. The reproducibility and reliability of the two insoles is presented in *Table2.4*. The * indicates extremely poor reliability.

	Between trial	Between session	Between day
PEAK 1			
EMED	0.99	0.99	0.84
F - SCAN	0.82	0.97	0.76
PEAK 2			
EMED	0.99	0.99	0.97
F - SCAN	*	0.66	*

Table 2.4 The reproducibility and reliability of the EMED and FSCAN insoles[37]

The most important conclusion from this study is that although the normal force values and pressure values measured with the EMED insole demonstrated a high level of reliability and validity, those of the F-SCAN insole are less than satisfactory, raising serious questions regarding the ability of the F-SCAN insole system to accurately measure plantar pressures.

Advantages / Benefits :

- The matrix devices have the same advantages as the discrete devices except that matrix insoles, to date, are only able to measure the normal forces on the plantar surface of the foot and not the shear stresses[52].
- Matrix devices permit larger areas of the foot to be examined[52].
- Areas of the foot can be monitored without any need for *a priori* decisions about the regions of particular interest[52].

Disadvantages / Limitations :

- The position of the sensors inside the insole relative to the floor prevents the measurement of a true vertical force, especially during the initial and late portions of the walking cycle. At best the sensors can only measure the normal force because of their orientation to the ground[23].

- Only the normal force is calculated when using matrix devices. No information of the shear stresses is provided[57].

- A reliable means of calibrating each sensor is important to the performance of the matrix device as each sensor can have markedly different calibration characteristics[49].

FIGURES FOR CHAPTER 2

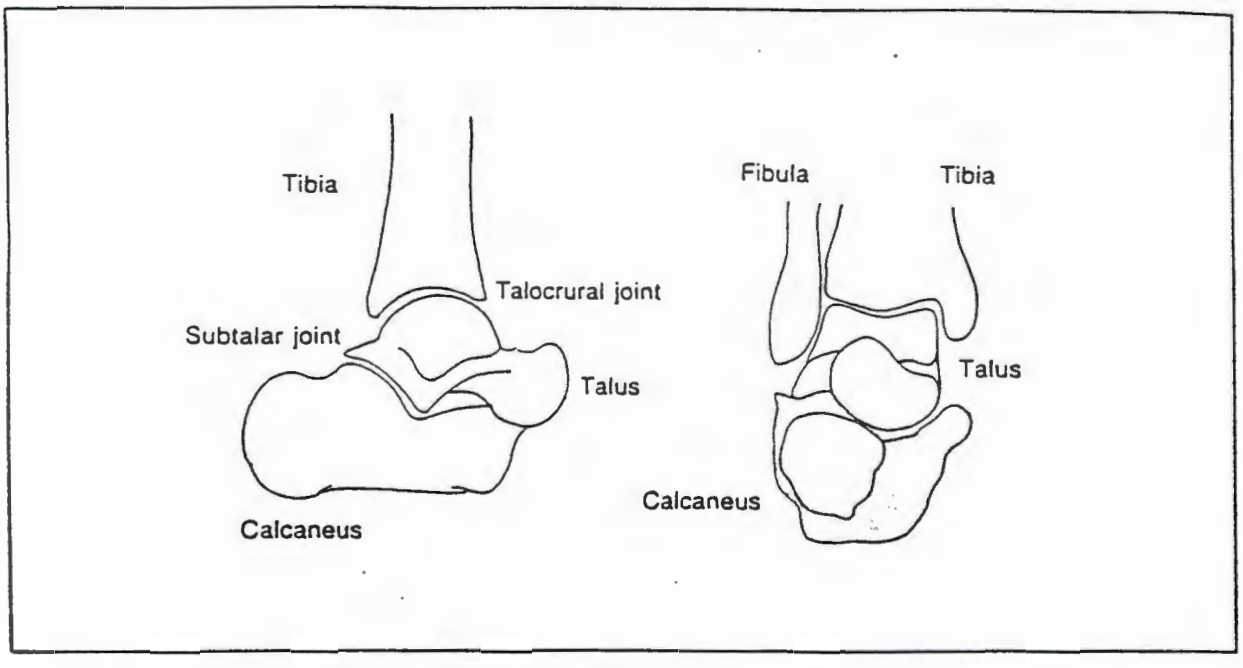

Figure 2.1 The bones of the rearfoot and ankle showing the location of the talocrural and subtalar joints
(See text, page10)

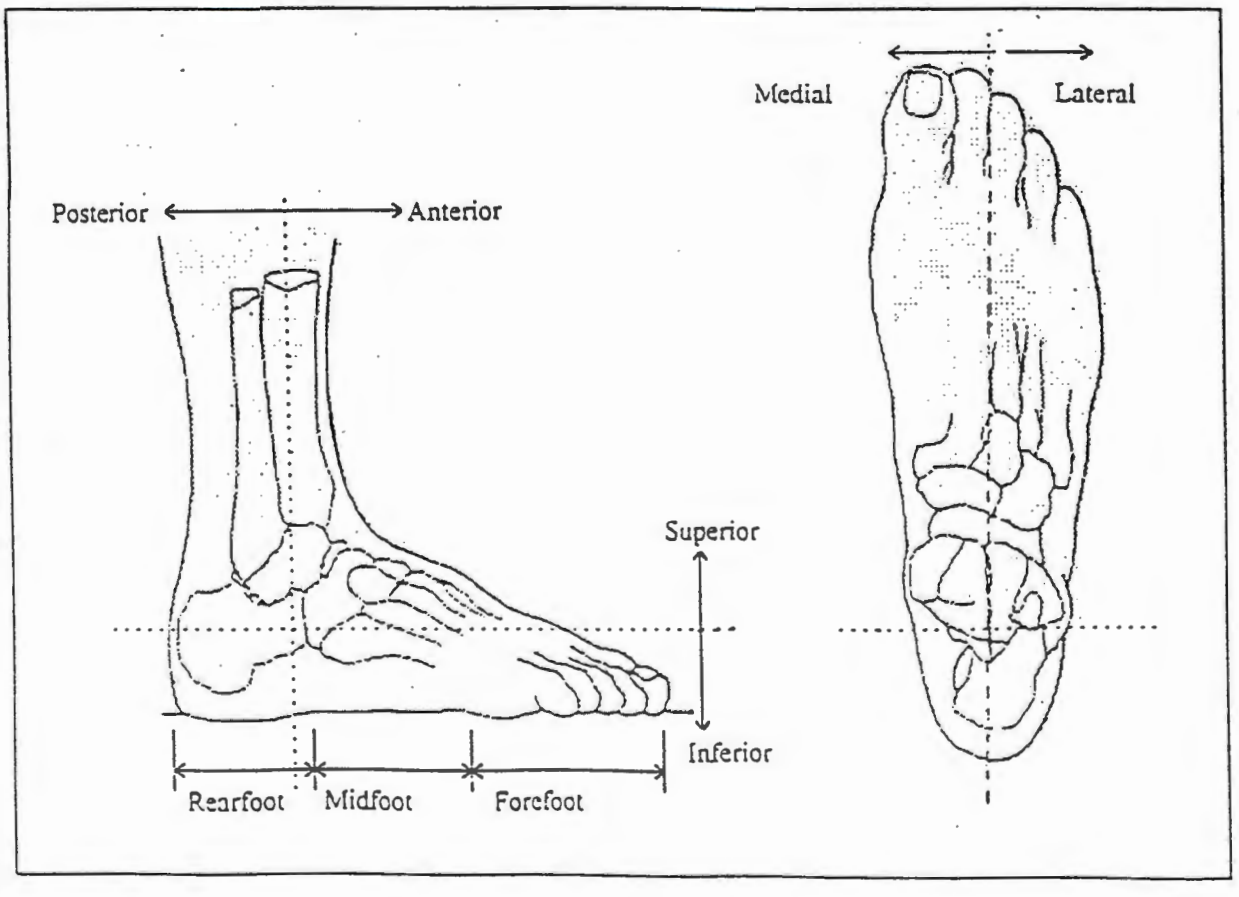

Figure 2.2 a Structure of the foot and terms used to define the foot
(See text, page11)

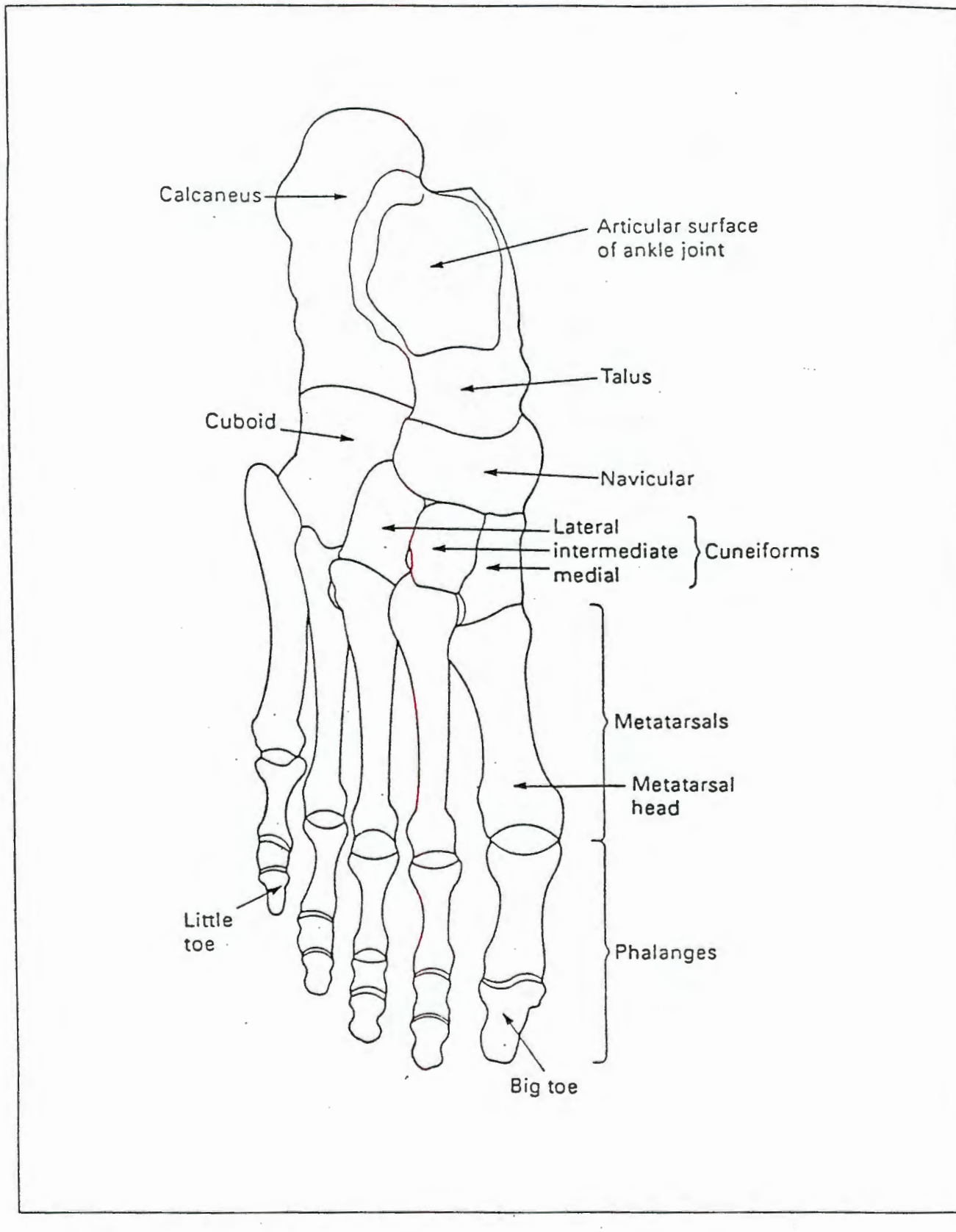

Figure 2.2 b The bones of the right foot from above
(See text, page11)

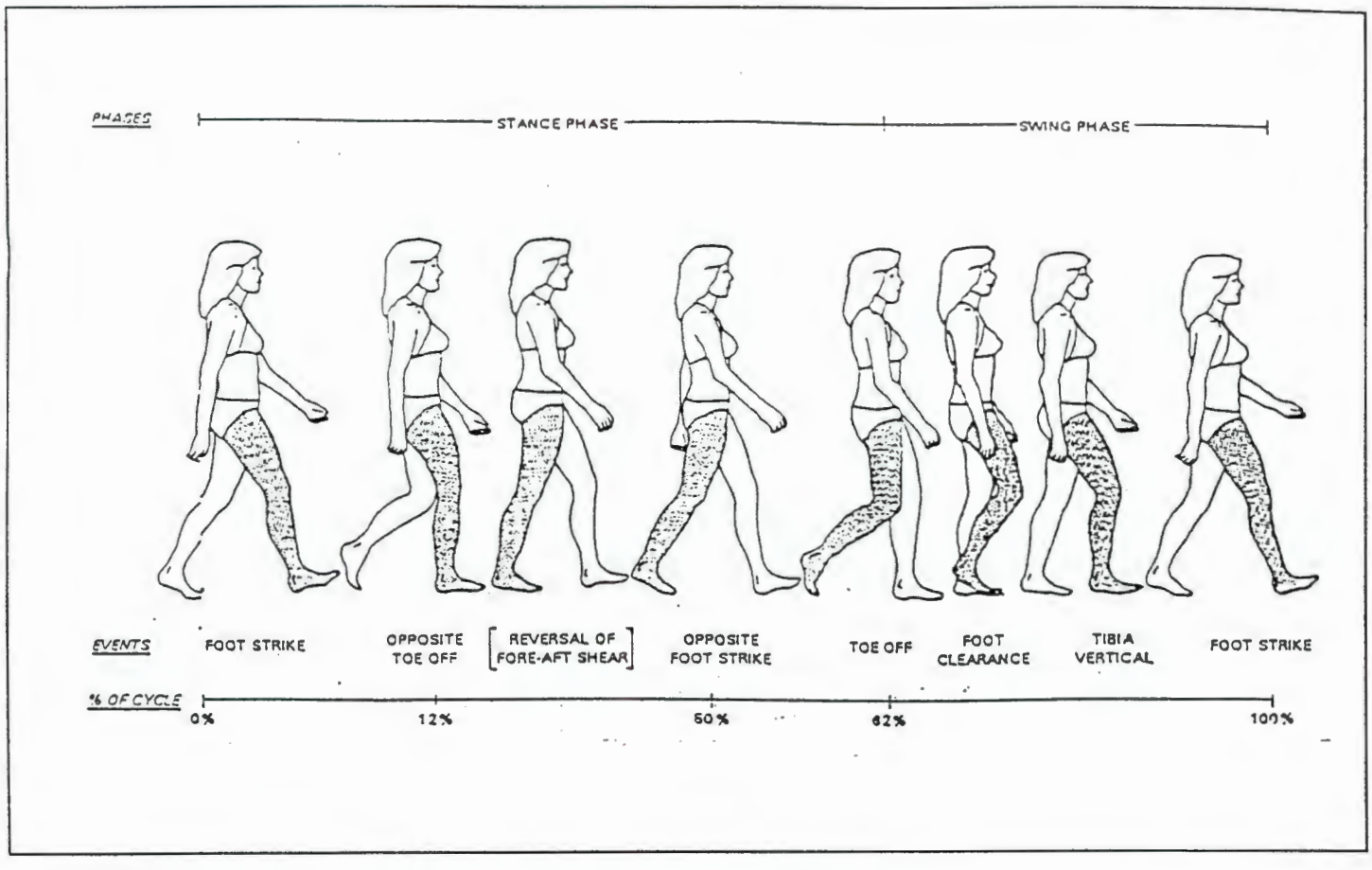

Figure 2.3 Typical normal walk cycle illustrating the events of gait
(See text, page13)

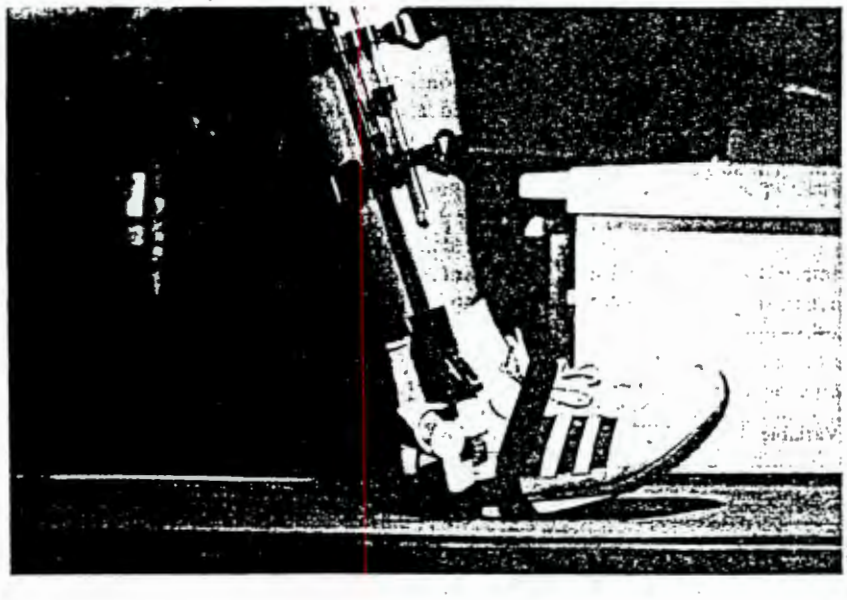

Figure 2.4 Electrogoniometer module positioned at the right ankle
(See text, page17)

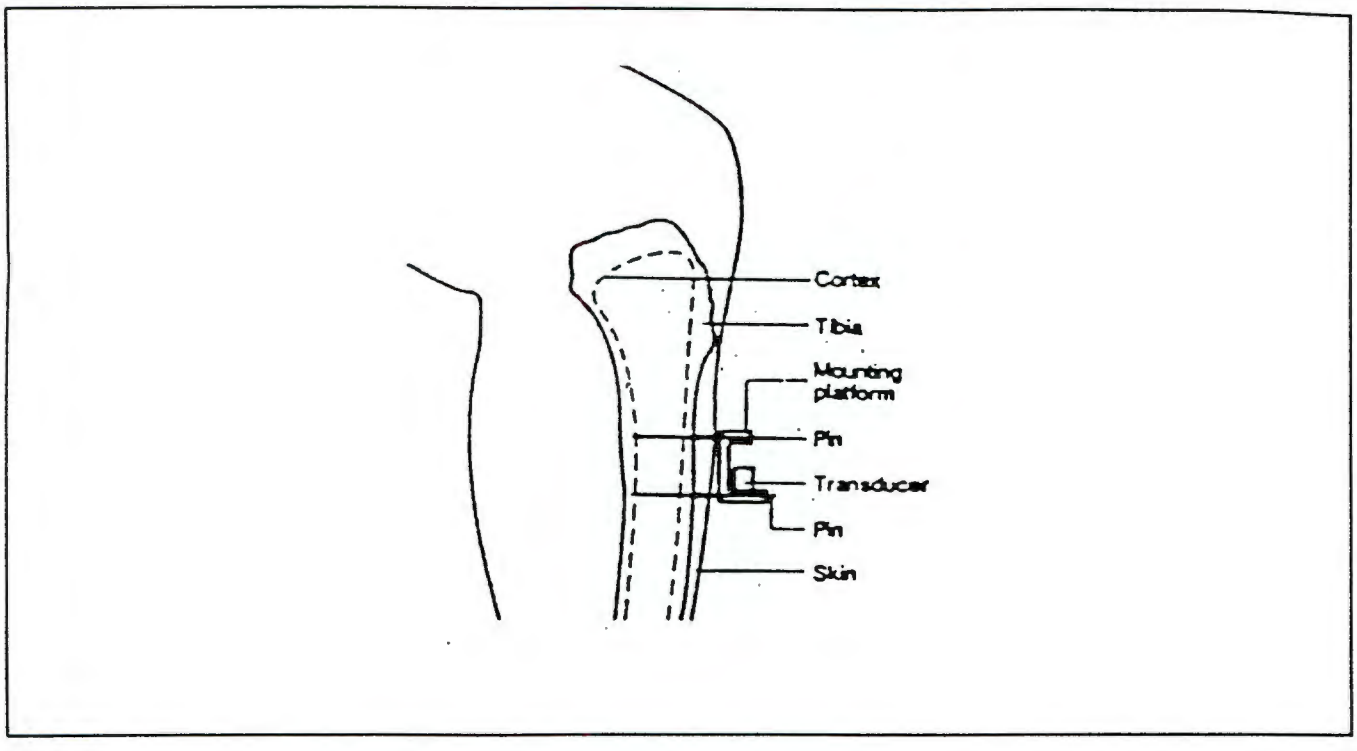

Figure 2.5 Cantilever mounting of miniature accelerometer in tibia
(See text, page18)

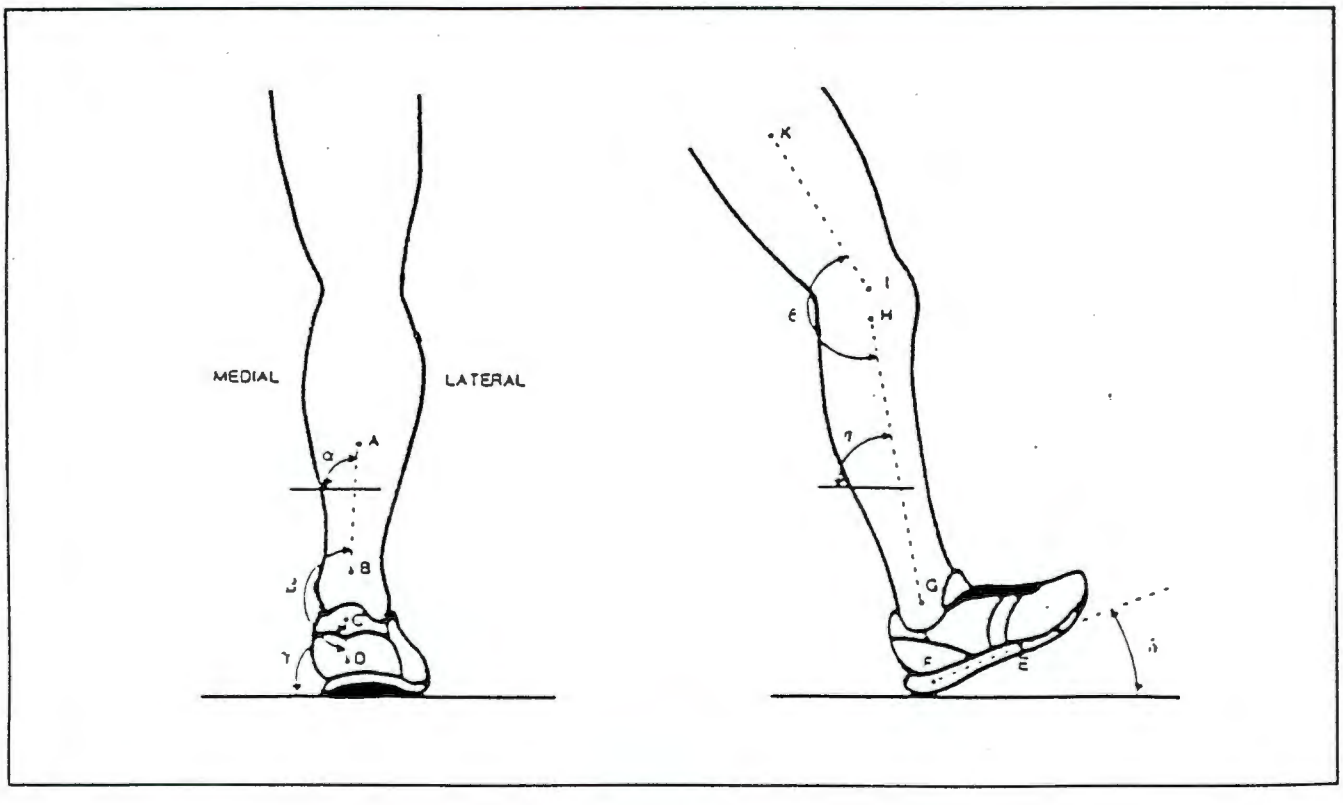

Figure 2.6 Illustration of the markers and angles used in the film analysis for the posterior and lateral view
(See text, page22)

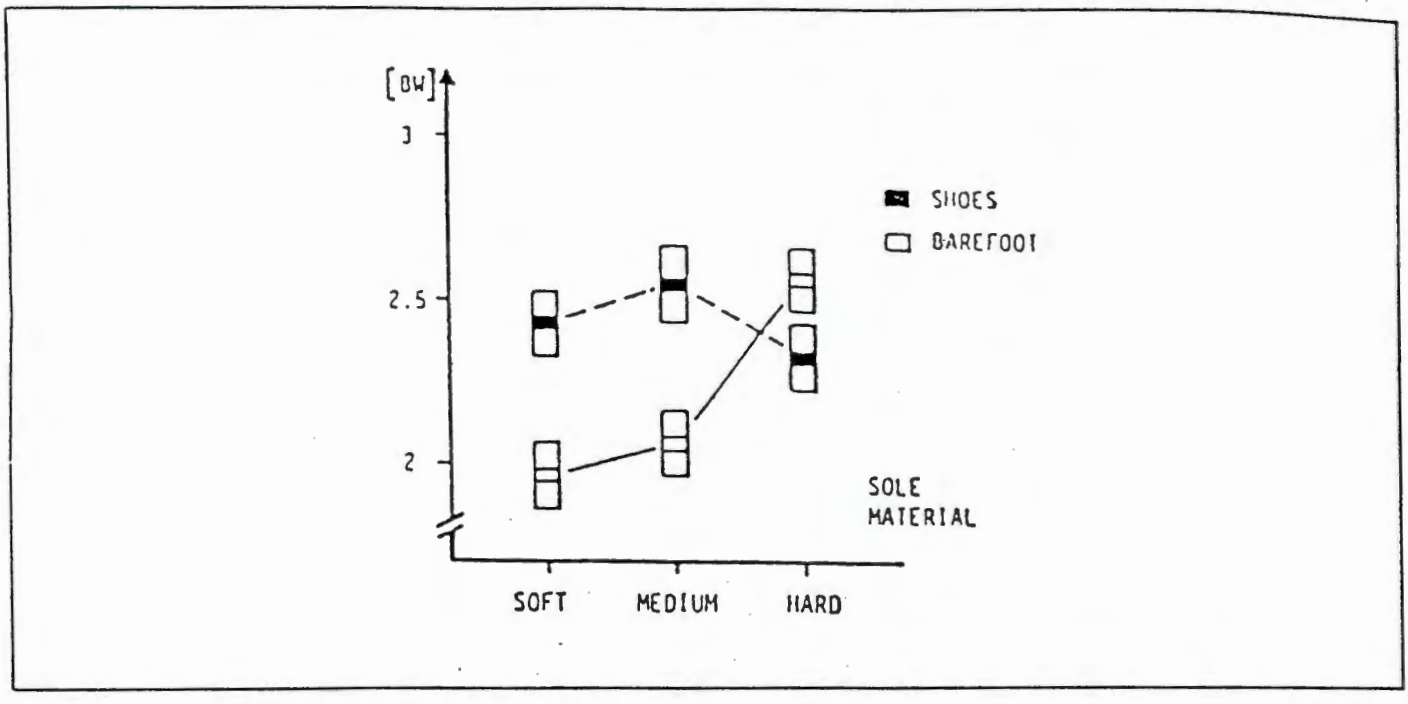

Figure 2.7 Illustration of the effect of hard insoles on the measured ground reaction forces
(See text, page23)

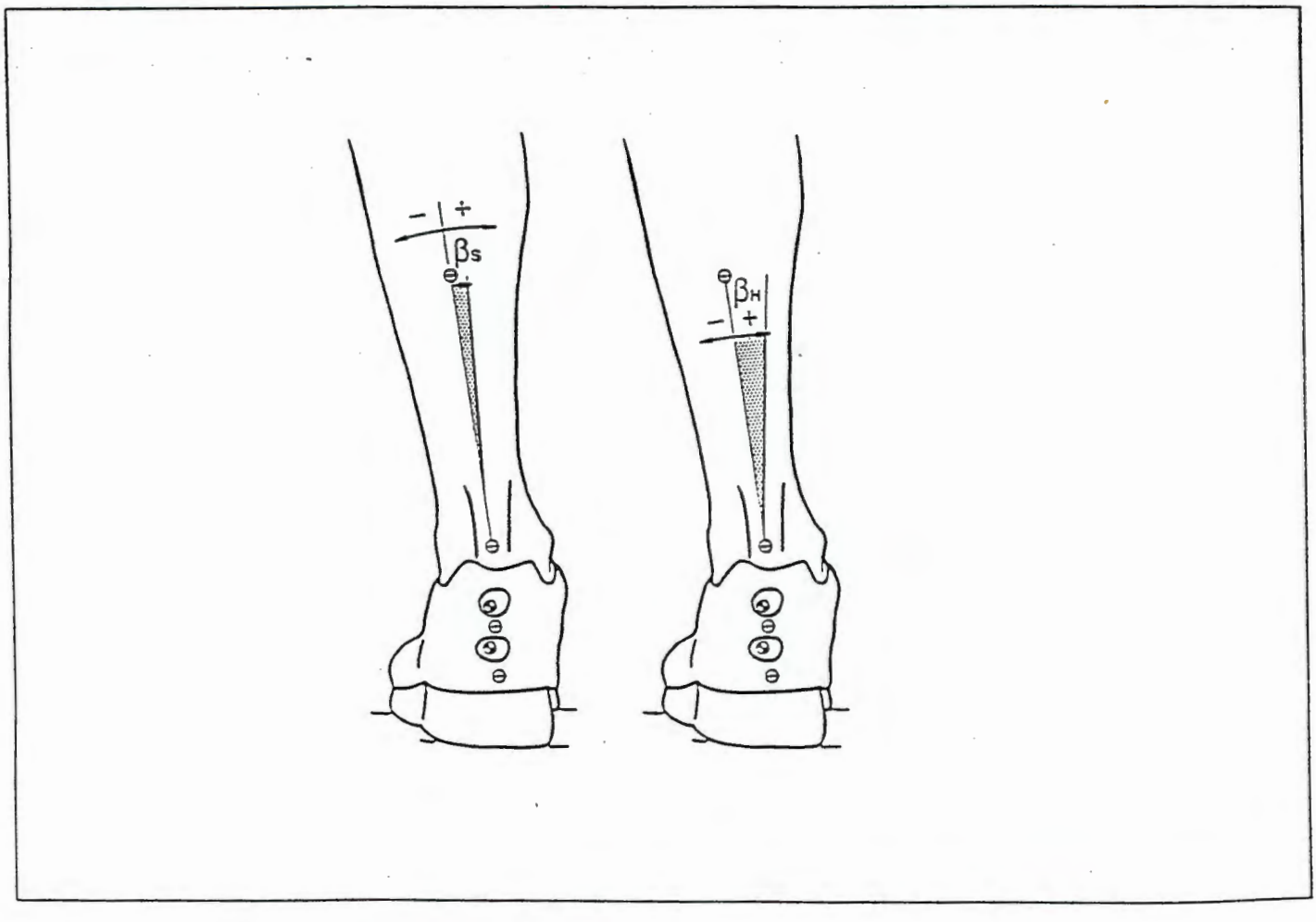

Figure 2.8 Illustration of the postions of markers on the heel of a shoe and the heel of a foot
(See text, page24)

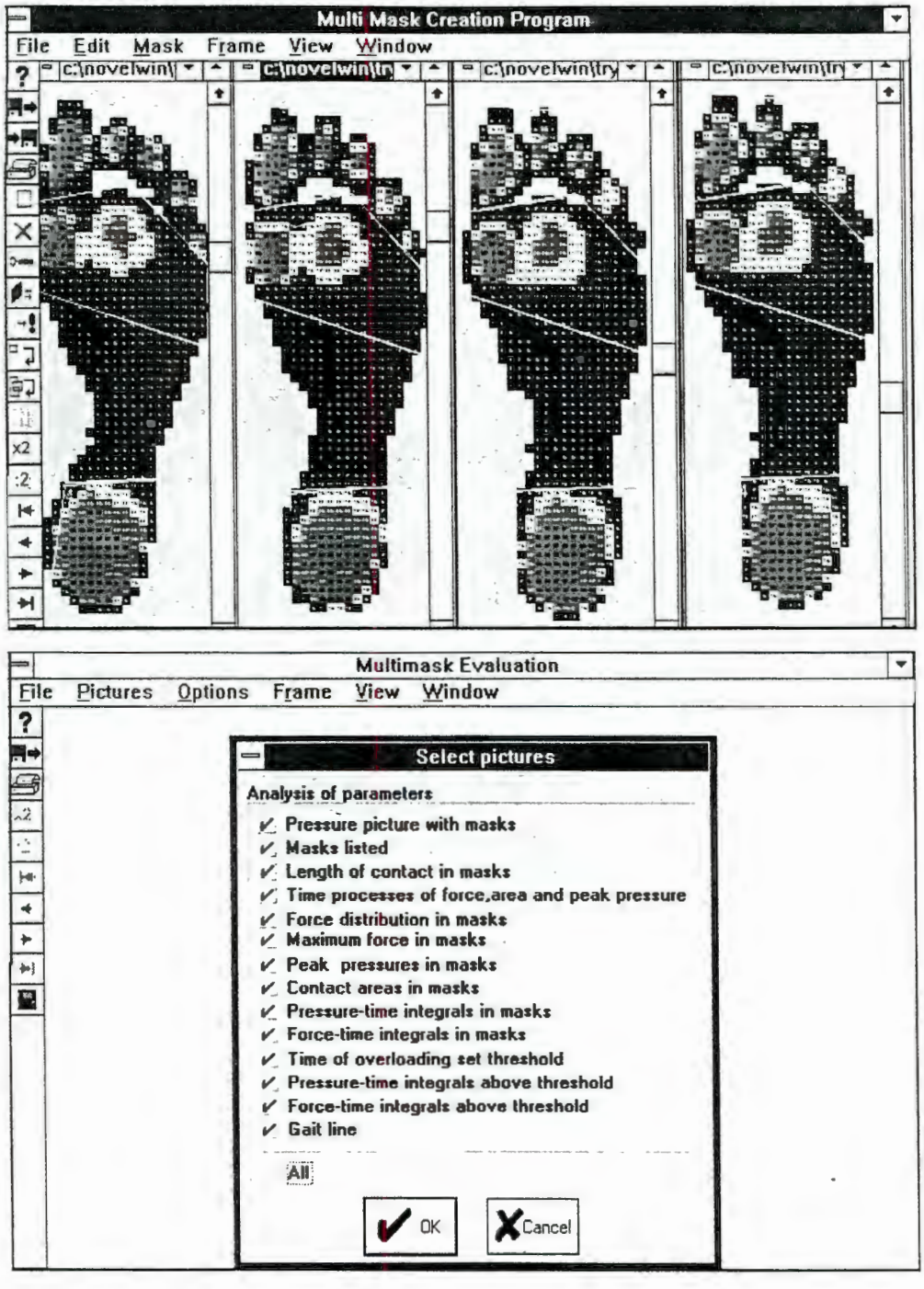

Figure 2.9 Illustration of the various windows that are available using the EMED - SF software
(See text, page27)

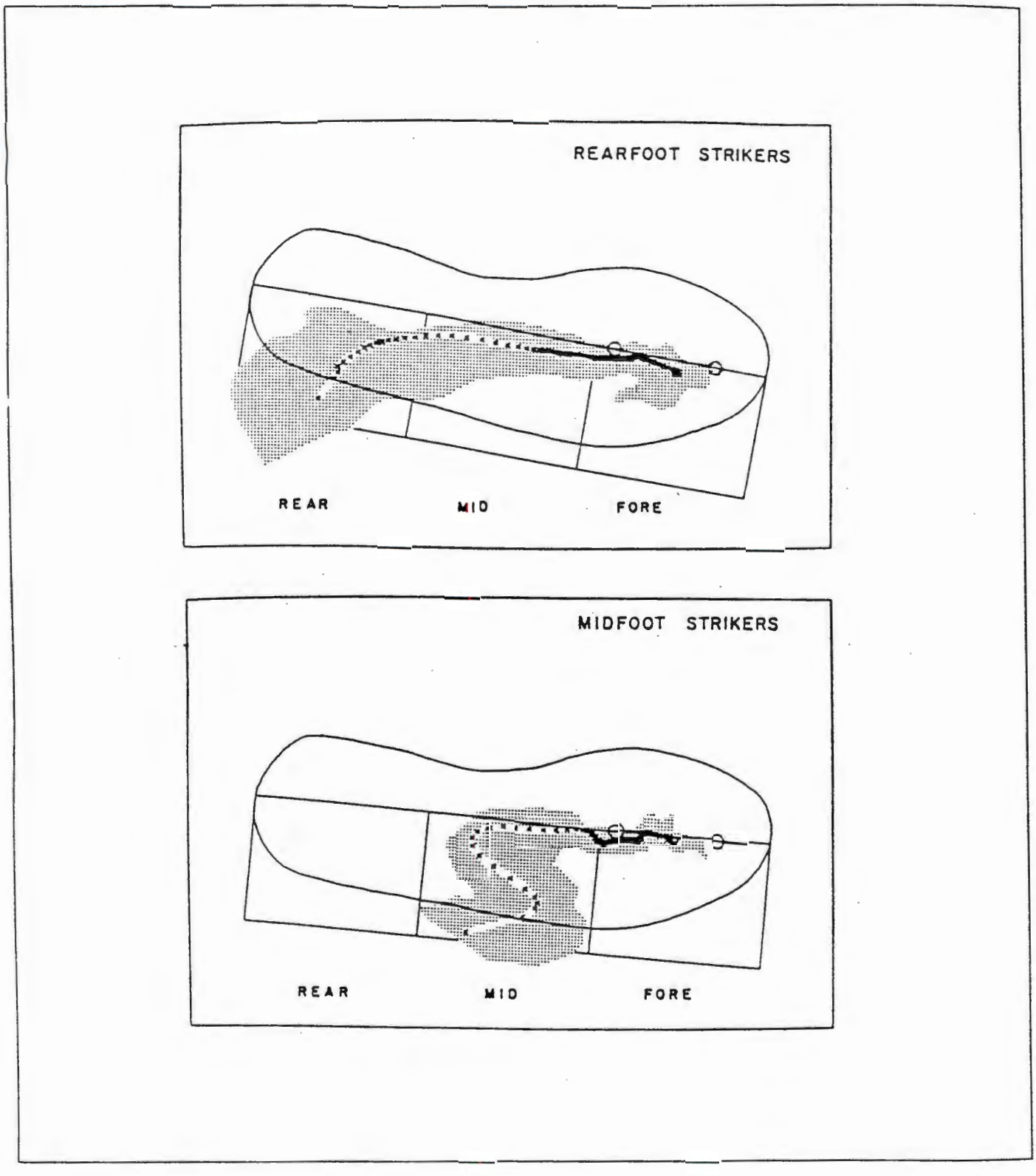

Figure 2.10 Mean centre of pressure (COP) locations under the shoe during gait
(See text, page28)

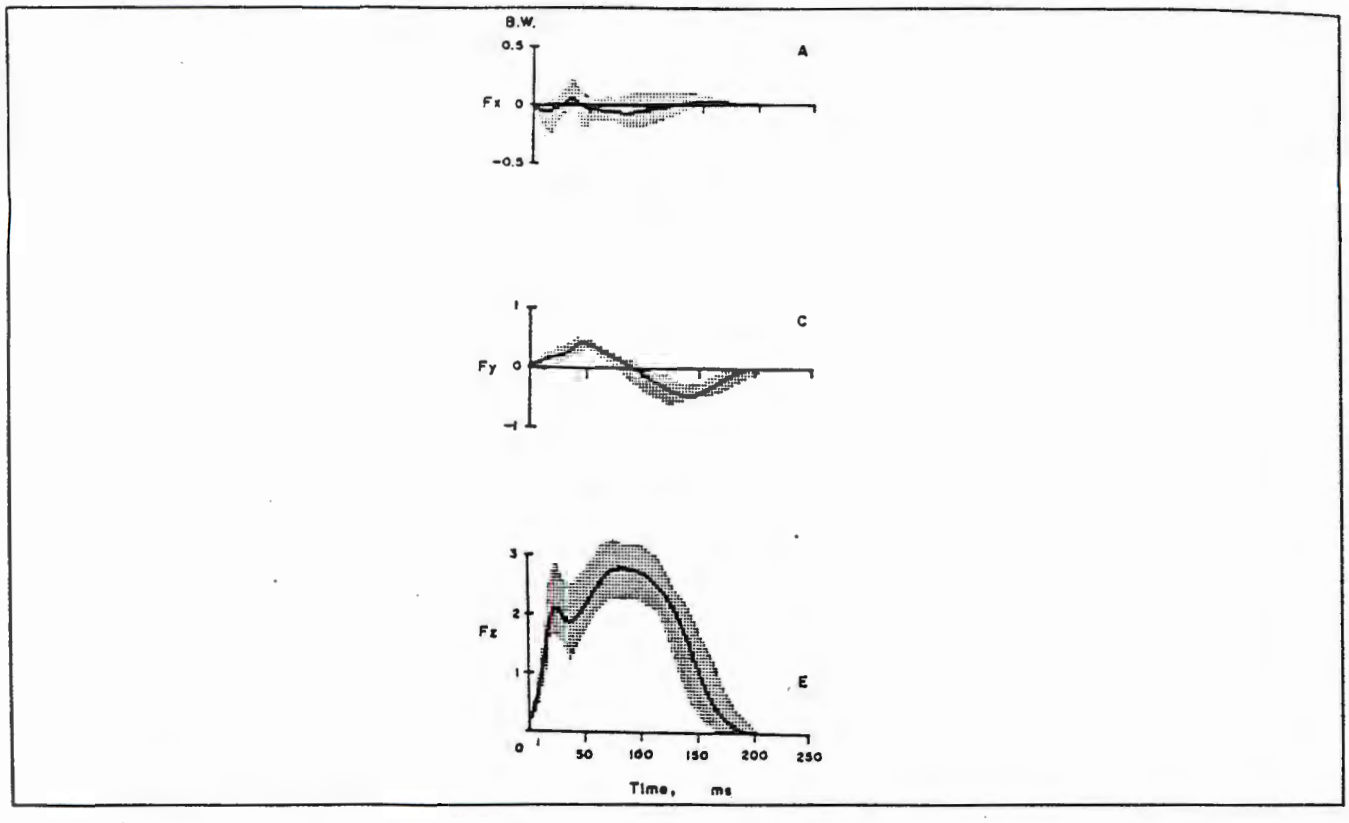

Figure 2.11 Mean force - time intervals (in units of body weight - BW) and range (shaded area) for the contact phase during gait
(See text, page32)

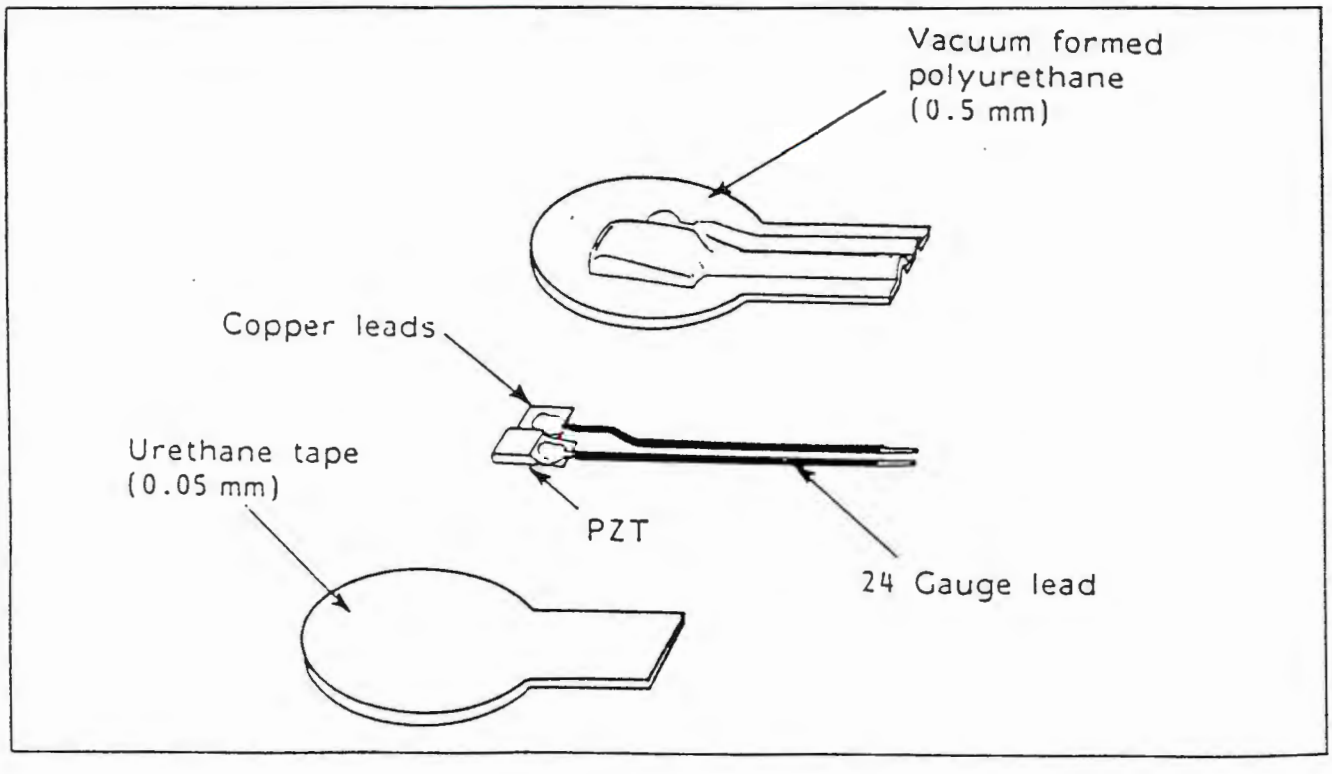

Figure 2.12 Exploded view of a discrete piezoelectric stress transducer
(See text, page34)

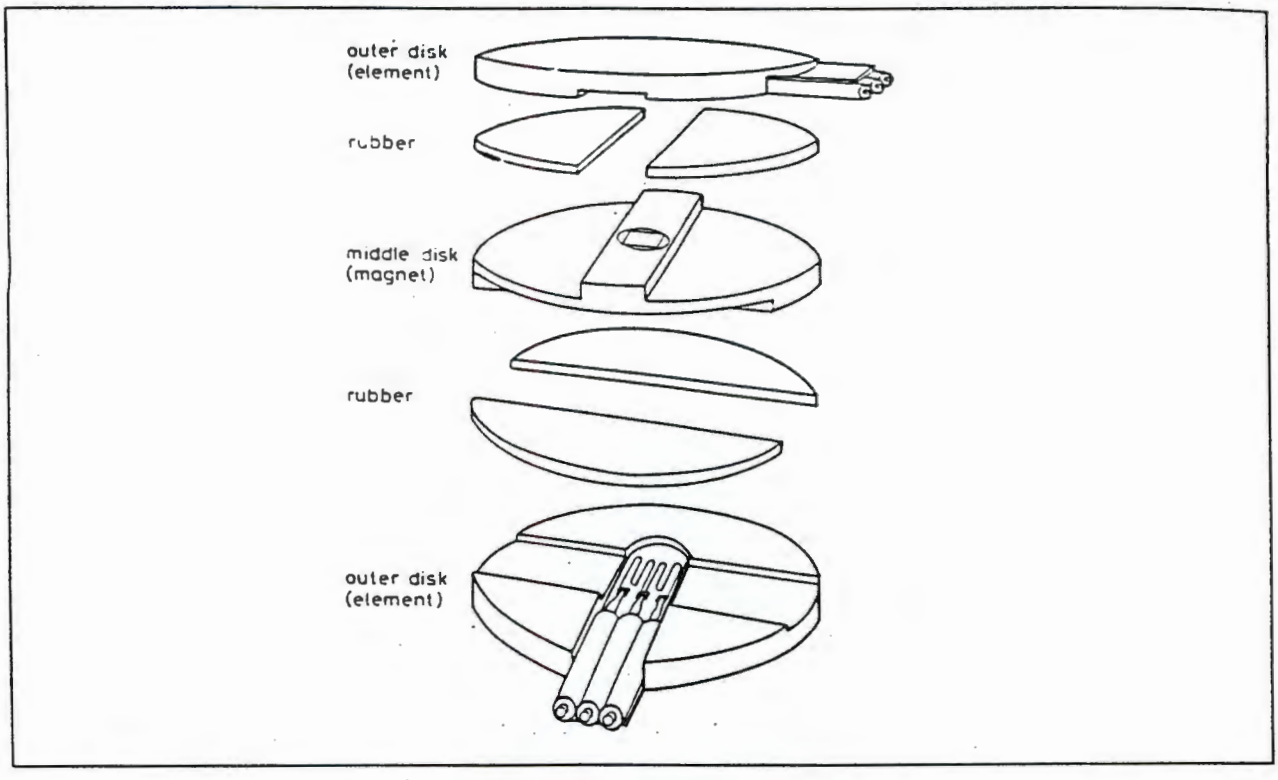

Figure 2.13 Exploded assembly of a biaxial shear transducer
(See text, page35)

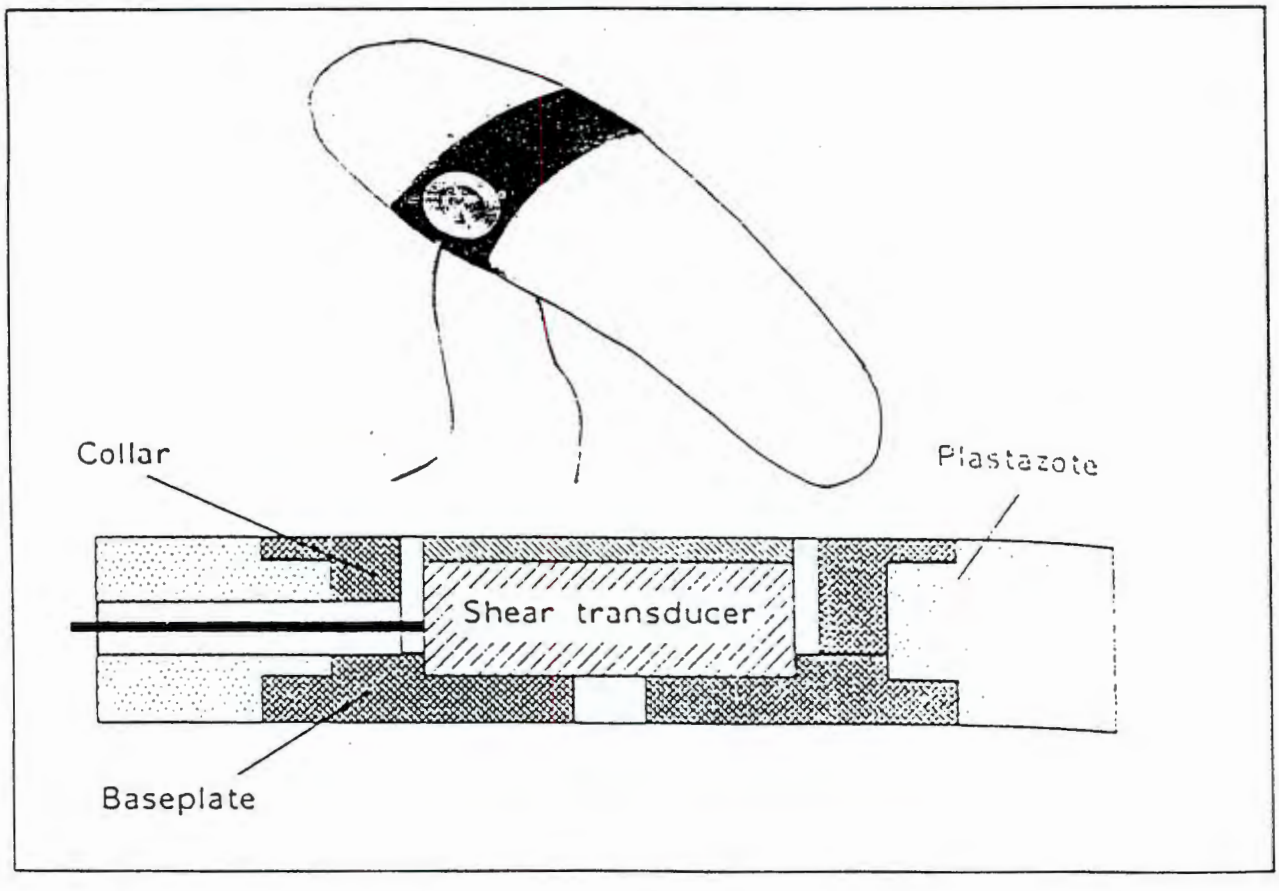

Figure 2.14 Illustration of a customized insole with an exploded view of the shear transducer mounting
(See text, page36)

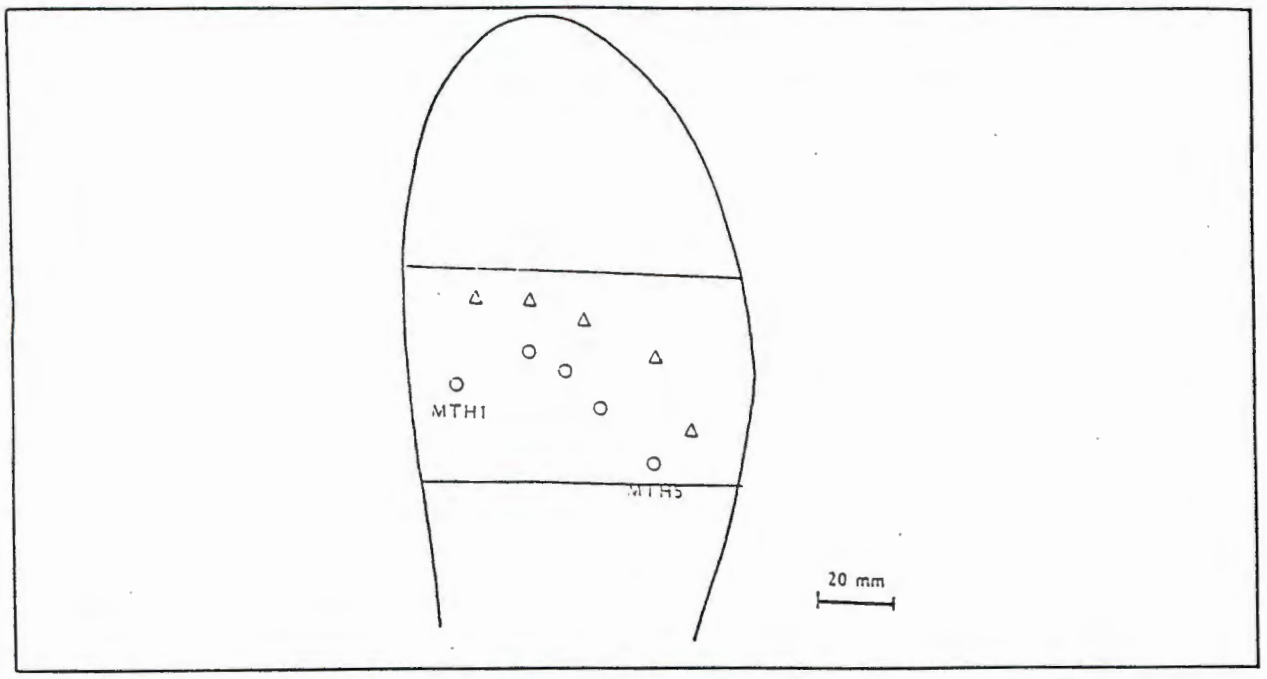

Figure 2.15 *(See text, page36)* Comparison of the location of the metatarsal heads by palpation ,O, and location of the peak pressures, Δ, recorded using the Tekscan gait device

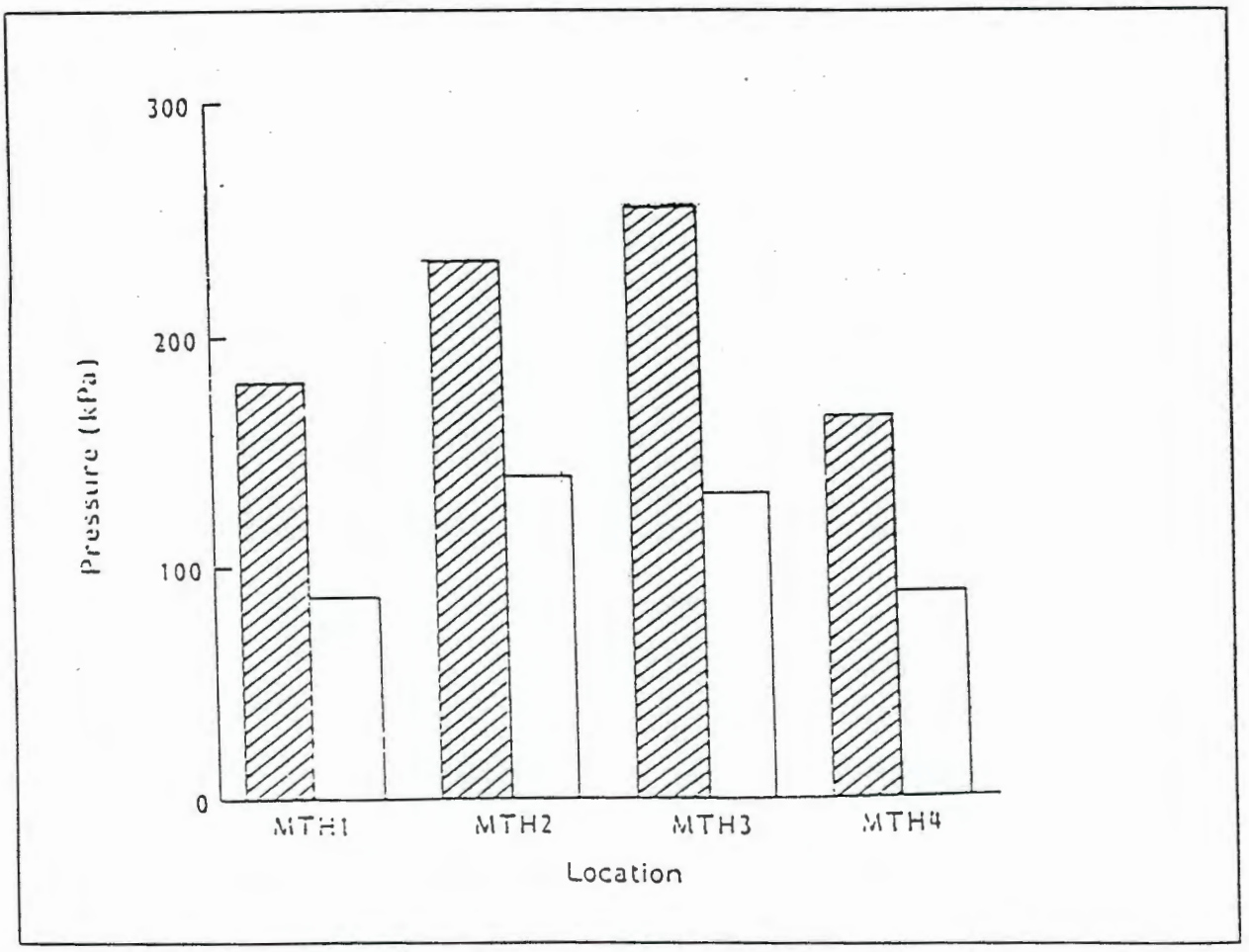

Figure 2.16 *(See text, page36)* Comparison of peak pressure, shaded, to pressure under the palpated markers (derived from Tekscan recordings and averaged over a 15 mm by 15 mm square area)-(MTH=Metatarsal Head)

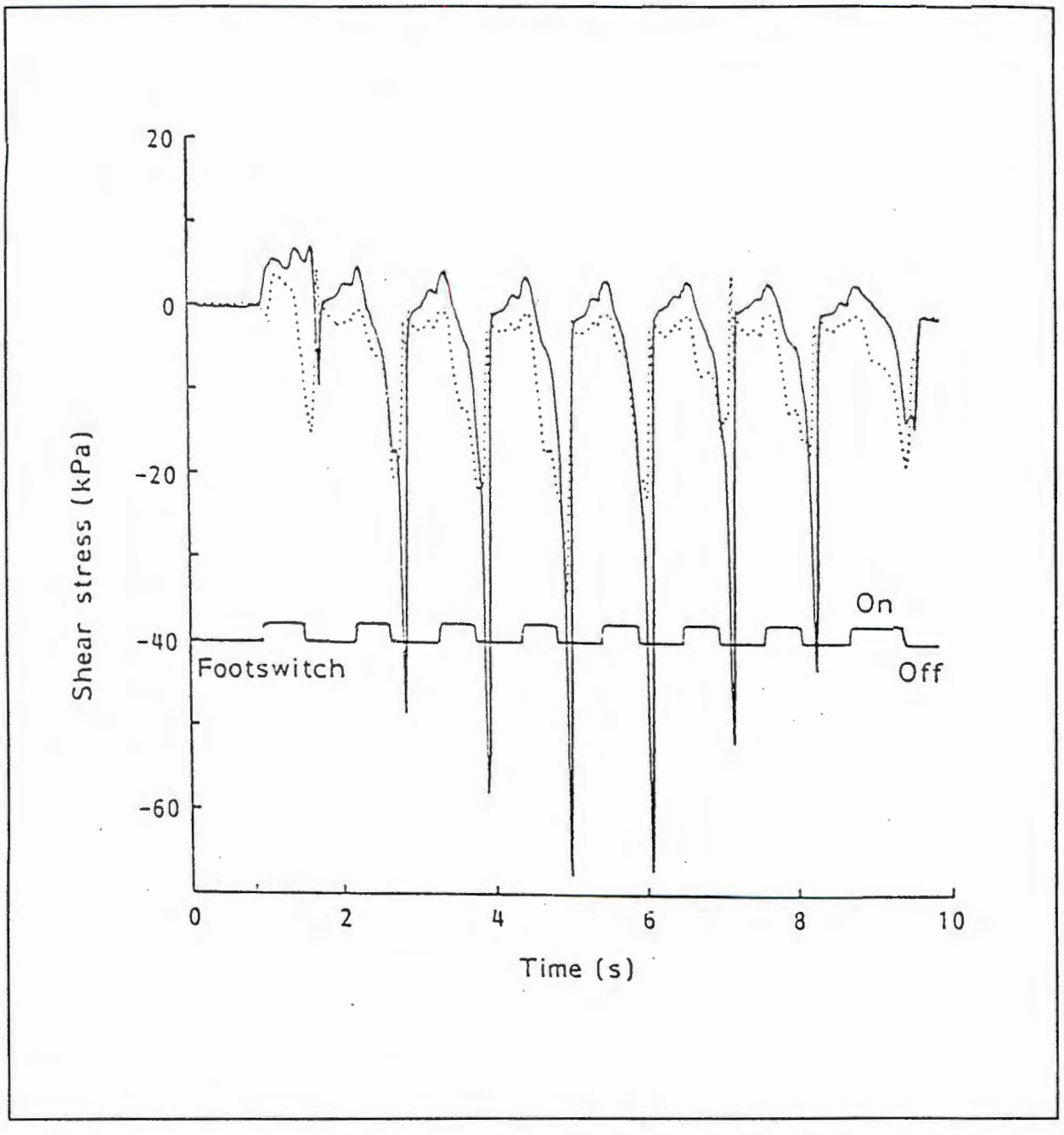

Figure 2.17 *(See text, page37)* The anterior-posterior (solid line) and medial-lateral (dotted line) shear stresses recorded in the trials performed by Lord et al[16]

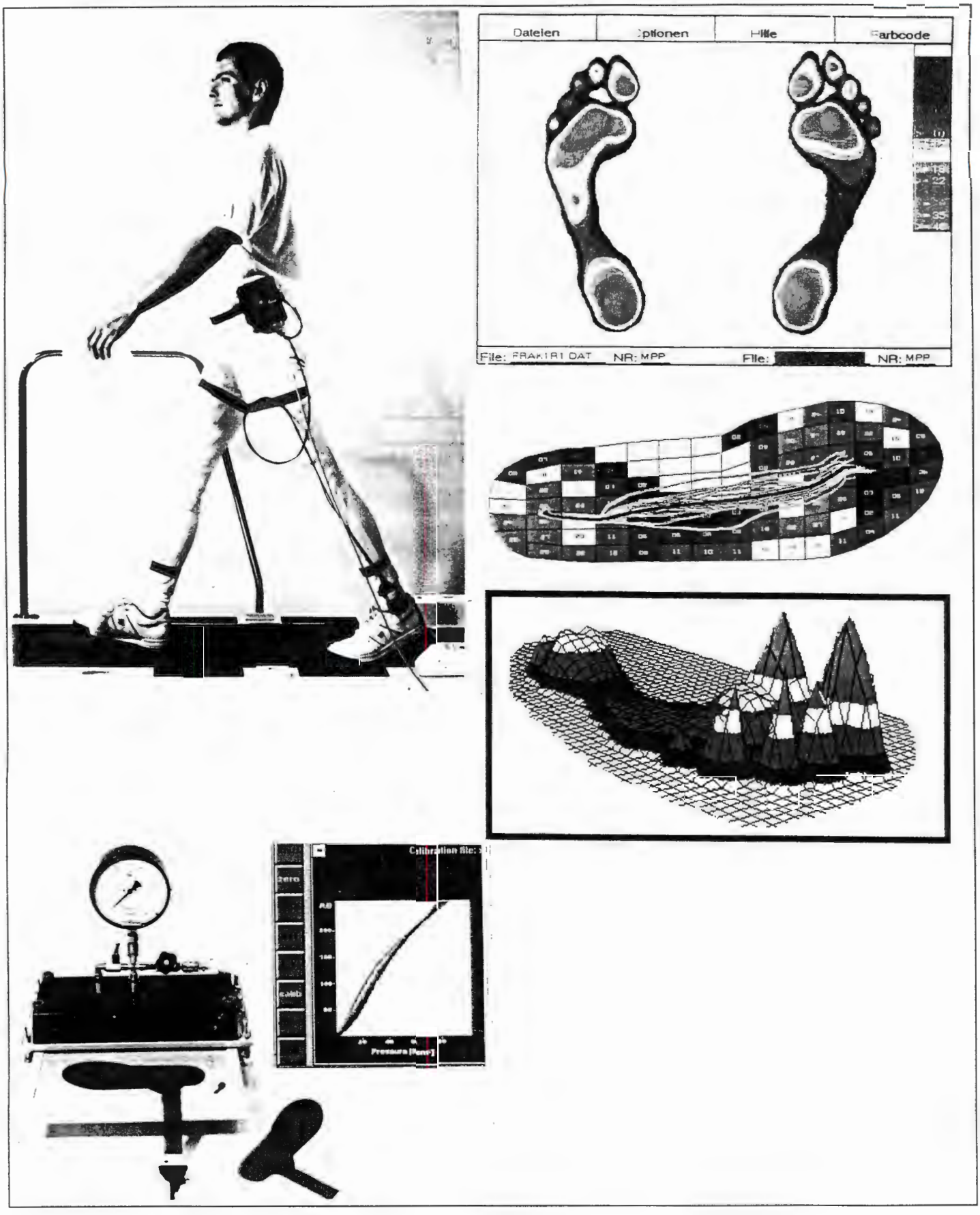

Figure 2.18 The Pedar in - shoe gait analysis device manufactured by Novel GMBH
(See text, page39)

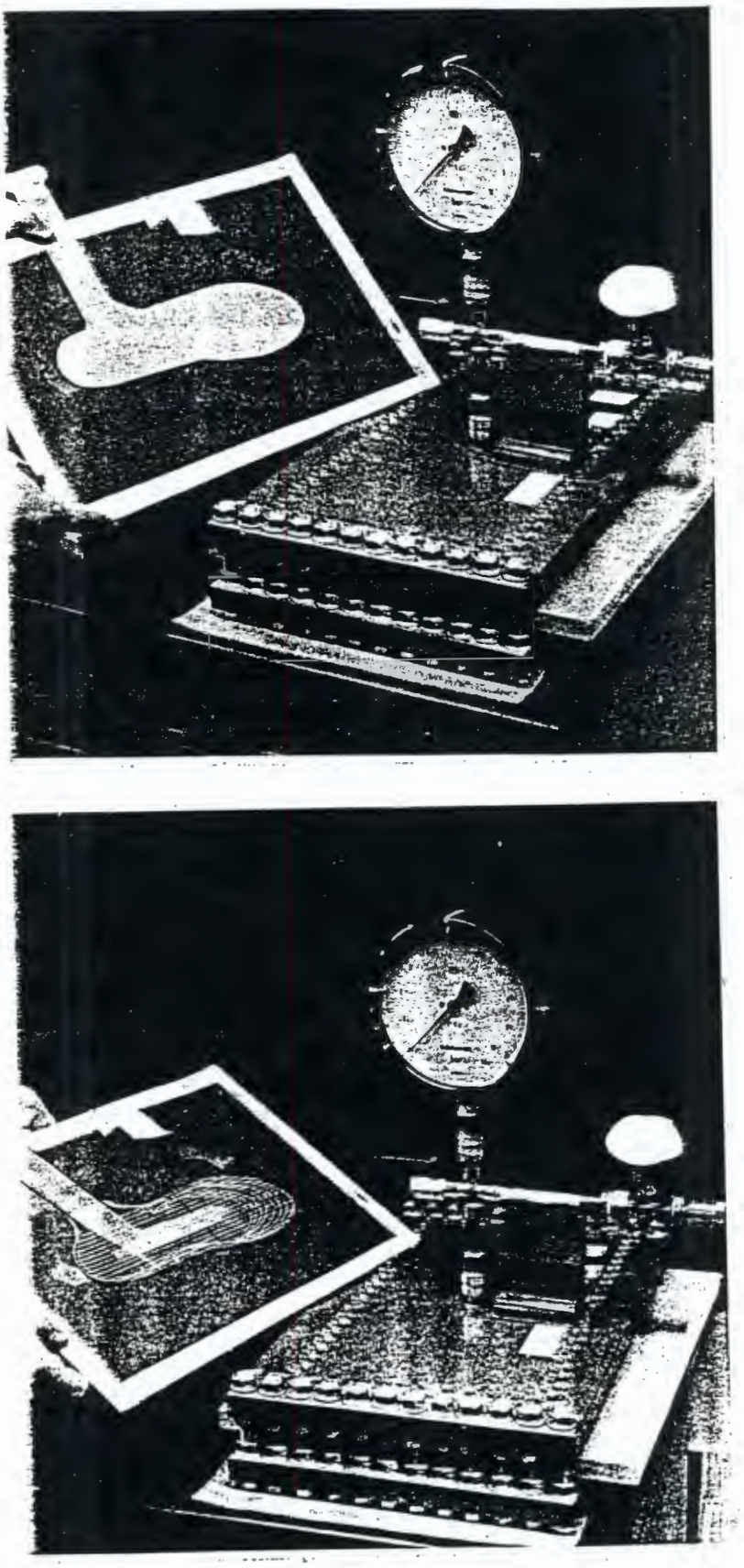

Figure 2.19 The EMED insole (above) and the F-SCAN insole (below) being postioned under the air bladder calibration device
(See text, page39)

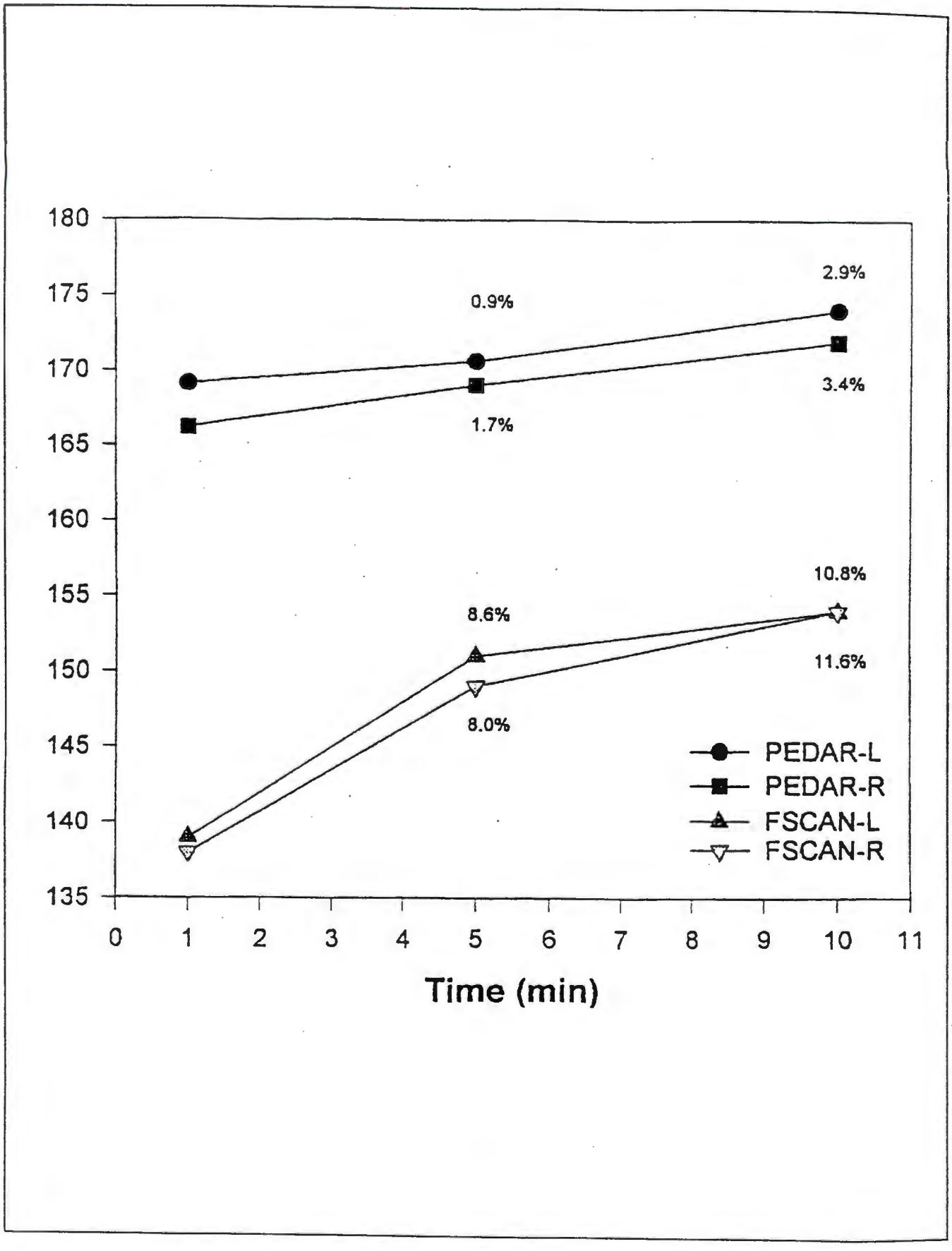

Figure 2.20 The effect of time and constant load on the actual pressures measured by the EMED Pedar and F-Scan systems
(See text, page40)

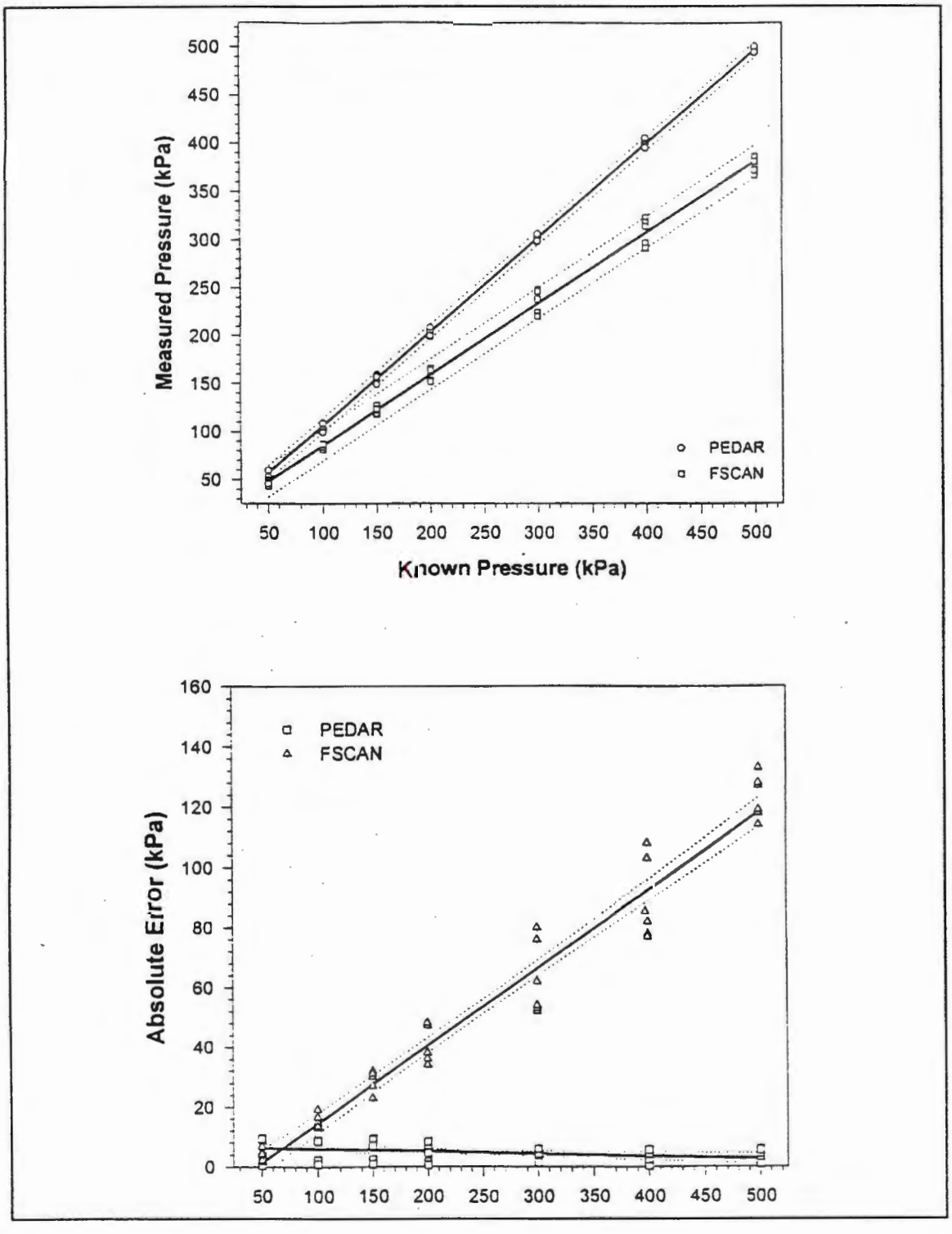

Figure 2.21 *(See text, page40)* The relationship between the known applied pressures versus the actual pressures measured by the EMED Pedar and F-Scan systems (above) and the amount of error associated with the actual pressures measured by the two systems (below).

CHAPTER 3

THE DEVELOPMENT OF AN IN - SHOE SHEAR STRESS MEASURING DEVICE

There are many different techniques which can be used to quantify the various parameters which affect gait. Only one however allows the shear stresses on the plantar surface of the foot to be examined at a specific anatomical point during uninterrupted gait. The technique involves placing a discrete transducer under the particular point of interest. The advantage of being able to quantify the stresses occurring under the foot inside the shoe, which is actual environment in which the foot is placed, is that it assists in the initial diagnosis, prognosis and monitoring of the recovery period of pathological gait conditions.

Discrete in-shoe transducer technology is being applied to the treatment and care of patients suffering from diabetes mellitus. Diabetes is a disease which is related to an inadequate amount of insulin being produced by the pancreas. Insulin is needed in the blood for the uptake of glucose, the removal of amino acids and the steady state repair and replacement of damaged tissues. An excessive amount of glucose in the blood can lead to numerous complications, one of which is the spontaneous attachment of glucose to proteins other than haemoglobin. This process can damage the basement membranes of certain cells of the lens of the eye and the peripheral neurons of tissue in the feet[61]. The reduced uptake of amino acids and damaged neurons means that the tissues of the lower extremities are vulnerable to trauma, can be become quickly infected, take longer to repair and injuries occur without any pain. The result is that patients are unaware of the trauma that they are inflicting upon themselves.

The loss of sensation means that diabetics do not adjust their gait patterns when they are causing harm to their feet. This results in the formation of large ulcers or long incisions on the plantar surfaces of their feet. The statistics relating to the treatment and care of diabetics suffering from gait related problems are presented in *section2.1.4.*

Findings relating to the treatment of diabetic related gait disorders tend to suggest that the shear stresses which the feet experience during gait could play a significant role in the damage process leading to ulceration in the regions of the first, fourth and fifth metatarsal[16]. It was also found that the vertical forces in these areas were also a maximum[18]. The compounding effect of shear and vertical force in these regions reduces the amount of blood to these areas, which has the effect of reducing the tissues resilience and increasing the likelihood of tissue damage, ulceration or infection. Although considerable research has gone into quantifying the vertical stresses at specific points on the plantar surface[14,15,18,19,26,32-35,38,39,50,51,53,54,56], very little work has been dedicated to quantifying the shear stresses[16,42,57]. The primary reason has been due to a lack of suitable instrumentation for its measurement.

This chapter presents the methodology which is adopted for the design of a new in-shoe gait analysis device that is intended to measure the shear stresses at the first metatarsal head (MTH 1) on the plantar surface of the foot during walking.

3.1 A DISCRETE TRANSDUCER

3.1.1 LOCATION OF THE SINGLE DISCRETE TRANSDUCER

The first metatarsal head was chosen as the point of interest for the following reasons:

- It is an area commonly associated with ulceration in diabetics[14,15,18,19,59].
- The maximum shear stresses and maximum vertical stresses are suggested to occur simultaneously at this point[16,18,19]. This phenomena allows a pressure measuring device, rather than a palpation technique to be used to locate the sensor. Palpation techniques have been shown to locate the point of maximum static pressure 20 mm posterior to the actual maximum pressure experienced during gait[16].
- The first metatarsal head typically experiences the third highest pressures in the forefoot region[35,50,53].

3.1.2 METHOD USED TO LOCATE SENSOR

It has been shown that the pressure distribution and weight bearing of the foot when a subject is stationary, is different to when the subject is walking[16,62]. When a subject transfers weight onto the foot during walking, the shape of the foot changes, altering the location of the maximum pressures[60,62] *(Figure 3.1).* It is also important to note that although there is commonly a 20 mm anterior shift of the maximum pressures in the forefoot region during walking, this can vary marginally from subject to subject.

Two separate methods were used to locate the area of maximum pressure under the first metatarsal of a person during walking. The person used to test the new in-shoe gait analysis device was referred to as the subject.

3.1.2.1 THE PODOTRACK PRESSURE MEASURING DEVICE

The Podotrack gait analysis device which was developed by Medical Gait Technology in The Netherlands consists of a specially designed mat which is placed on the ground for a subject to stand on, walk across or run over. The mat consists of a sheet of carbon paper which, when stood upon, leaves a black copy of the plantar surface on a scaled x -y grid positioned under the carbon paper. Darker areas left by the carbon paper are an indication of areas of higher pressure. Adhesive strips underneath the mat maintain its stability and an adhesive clear cover sheet which folds over the carbon imprint prevents any smudging when the imprints are being analysed. A reference card is provided to match the shades of grey left on the grid to known pressures established in the laboratory *(figure 3.2).*

Although there is evidence suggesting that walking velocity has little effect on the location of maximum pressure[49], conflicting evidence suggests that walking velocity does have a marked effect on the pressures on the plantar surface[32,53]. For this reason a controlled velocity of 1.3 m/sec (4.68 Km/h), which is regarded as a normal walking speed[19], was selected. It is also a velocity which allows a direct comparison between the results produced by the proposed sensor and the results presented in the literature to be made.

The controlled distance over which the tests were performed was 15m. The mean time between the controlled markers on the 15m runway at this velocity was 11.5±0.5 seconds. Once the subject had become used to the stride length and was comfortable with striking the area which marks the position of the mat, the mat was put into position and a series of five tests were conducted. Tests which did not occur within the given time limits were rejected.

To check that there was an anterior shift of the maximum pressures during walking as compared to standing, five static tests and five dynamic tests were performed.

The definitions below are illustrated in *figure 3.3* which is an actual template of a size 44 insole with the average bone structure of the foot for this size insole superimposed upon it. The size of the insole was the size which was suggested by a podiatrist for the subject[71].

The definitions used in *figure 3.3* are :

VDMP: Vertical Dimension for Maximum Pressure

TOP : Toe Off Point

MWF : Maximum Width of Foot

HDMP : Horizontal Dimension for Maximum Pressure - measured from MWF

AMBP : Anterior Metatarsal Break Point

PMBP : Posterior Metatarsal Break Point

HCP : Heel Contact Point

The MWF was the maximum width of the contact surface of the foot in the forefoot region. The maximum width of the insole was larger than the contact surface of the foot. To ensure that the sensor was in the correct position relative to the foot during walking, a correction was made when locating the sensor inside the insole.

Using the results from the Podotrack the maximum width of the foot was calculated to be 91mm. The maximum width of the insole, allowing for medial and lateral movement was 96mm. In order to place the sensor in the insole at the correct point of maximum pressure on the foot, it was assumed that the foot lies in the centre of the insole during walking. This equates to a 2 ½ mm clearance on either side. The importance of the MWF position is that the HDMP point for the sensor was measured from it. This effectively meant that the HDMP was 17 ½ mm from the medial border of the insole at the MWF position.

The AMBP and PMBP were the two limits which separated the last contact point of the metatarsal region from the first. These points are indicated in one of the walking imprints shown in *figure 3.4*. These limits were required in the design of the insole because a higher density band of material is necessary in this area to provide stability and support for the sensor, yet at the same time the higher density material must not interfere with the movement of the lower density material used in the rest of the insole. The lower density material allowed unhindered movement of the foot during the stance phase, particularly at heel off and toe off.

The results from the five different tests using the Podotrack for the static and walking imprints are presented in *Table 3.1*. The maximum errors and confidence intervals are also presented using statistical techniques described by Miller et al[63].

	TOP	PMBP	AMBP	MWF	HDMP	VDMP
Static (mean)	265.60	185.80	214.60	91.60		
Max error of mean with a 95 % confidence interval	0.68	1.04	0.68	1.42		
Max error of mean with a 98 % confidence interval	0.92	1.40	0.92	1.91		
Walking (mean)	292.80	202.80	232.60	90.80	14.60	219.40
Max error of mean with a 95 % confidence interval	1.40	1.40	0.92	1.40	0.92	1.50
Max error of mean with a 98 % confidence interval	1.04	1.04	0.68	1.04	0.68	1.11
Difference in means	27.50	17.00	17.00		0.50	
			Toe difference		9.00 - 10.00	
			Heel difference		16.50 - 17.50	

Table 3.1 Static and walking tests using Podotrack to locate the maximum pressures at MTH 1 (units are in mm)

According to Lord et al[16] the points of maximum pressure during walking are 20mm anterior to the points of maximum pressure when standing. When two imprints obtained from the static and dynamic tests were placed together with their heel contact points at the same level this certainly would seem to be the case. However, it is felt by the author that the 16.50mm to 17.50mm anterior shift was actually a roll effect which occurred when the heel initially came into contact with the ground. The roll effect was described as the section of the imprint created by the foot when it was in a non-horizontal contact position relative to the ground at heel strike and toe off. The same roll effect occurred at the big toe during toe off. The roll effect therefore only occurs during gait and not while standing. This would explain why a size 44 insole with a overall length of 292.8mm was better suited for the subject's foot, even though the actual static plantar contact surface of the subjects foot was 265.6 mm. The extra 27.5 mm was required for the rolling effects which occurred when the foot was in motion. The rolling effect was seen to occur in the walking imprint at the heel, big toe and the other four toes at heel strike and toe off respectively as shown in *figure3.4*. This effect was however not seen during the static imprint shown in *figure3.5*. Although there can be other reasons why there was the anterior shift of maximum pressures but the important fact about the tests performed using the Podotrack, was that the point of maximum pressure of the first metatarsal head was located at the point at which the maximum pressures occur during walking at 1.3m/sec.

3.1.2.2 THE ADIDAS PRESSURE MEASURING DEVICE

The ADIDAS *footscan* is a pressure mat consisting of 3500 pressure sensitive transducers. It is linked to a computer via an analogue to digital card which allows a recording speed of 300 images per second. The computer is also equipped with an extensive amount of software for gait analysis. The data is presented in a 2 dimensional and a turning 3 dimensional view. The image which is presented by the data is colour coded to represent the pressure values which occur on the plantar surface during the stance phase. The software performs an automatic self calibration before any test. The ADIDAS *footscan* is shown in *figure3.6*.

The *footscan* is customised to meet the specific needs of ADIDAS. The images which are generated by the *footscan* are compared to a data base of typical gait patterns from which the shoe most suitable to the particular client is recommended. The data base developed by Adidas is shown in *figure 3.7* as a selection of 12 different pressure traces. The data base offers a range of shoes for those with hypermobile feet (far left trace) to those with rigid feet (3rd trace from the right). The last two traces on the right are special cases indicative of forefoot strikers. Additional features include a frame by frame animation in 3-D, a playback option and the time elapsed of the pressure distribution under the plantar surface.

The total time of foot contact for the subject as determined by the footscan, walking at 1.3m/sec, was 647±52msec. This is equivalent to a gait cycle time of 1083±52msec.The maximum pressure at MTH 1 occurred at an average of 67% of the stance phase which clearly correlates with Tappin et al's[19] findings.

Another feature which is shown in *figure3.7* and *figure3.8* is the COP (Centre Of Pressure) line. The COP line for the subject indicates a pronatory movement at toe off. A final feature of the *footscan* is that it is able to recommend the correct size of shoe. The shoe size is determined during dynamic gait and not while standing. This is shown in *figure 3.8* by the dimension lines which include the roll effects which occur at the heel and at the big toe during walking.

Although the footscan offers a considerable number of software options, some of which have not been mentioned, the main purpose of using it in this thesis was to determine the point of maximum pressure at the first metatarsal head during walking.

The same testing environment and conditions were used as with the Podotrack, the only differences being that the subject struck the pressure mat of the footscan rather than Podotrack mat and that only walking conditions were analysed. The same parameters shown in *figure 3.3* were also used to locate the sensor.

The *shoesize* window shown in *figure 3.8* was used to scale the size of the foot and locate the green coloured area in the first metatarsal region. The conversion factor on the *shoesize* printout is 1mm is equal to 29.27 mm. Although the value in *figure 3.8* is correct a software problem located the width-indicating line and its length inaccurately. This problem was pointed out by the clinicians at ADIDAS during the tests. They did give assurance that the numeric value was correct and that the line should be located as shown in *figure3.3*. The results from the footscan tests are shown in *Table 3.2.*

	TOP	PMBP	AMBP	MWF	HDMP	VDMP
Walking (mean)	295.20	202.00	230.00	89.80	14.40	217.80
Maximum error of mean for 95% confidence interval	0.93	1.24	1.24	0.76	0.68	1.04
Maximum error of mean for 98% confidence interval	1.25	1.68	1.68	1.03	0.92	1.40

Table 3.2 Walking results using Footscan to locate the maximum pressure at MTH 1 (units=mm)

3.1.2.3 ANALYSIS OF RESULTS FROM THE PODOTRACK AND FOOTSCAN

Although there were marginal differences in the dimensional values between the two methods, combining the values from both methods enabled the point of maximum pressure at MTH 1 to be located at a gait velocity of 1.3 m/sec with a maximum error of 1mm at a chosen confidence level of 95% as shown in *Table 3.3*. The values presented in *Table 3.3* are the x-y values which were used to locate the sensor inside the insole. The actual test values are presented in the *Appendix A*.

	TOP	PMBP	AMBP	MWF	HDMP	VDMP
Walking (mean)	294.00	202.40	231.3	90.28	14.50	218.6
Maximum error of mean for a 95% confidence interval	0.93	0.62	1.00	0.56	0.34	0.75
Maximum error of mean for a 98% confidence interval	1.30	0.86	1.40	0.79	0.47	1.05

Table 3.3 Mean values and maximum error of combined dimensional values from Podotrack and Footscan maximum pressure location devices

Errors were most likely to occur during the measuring of the dimensional parameters from the imprints on the Podotrack and the plots from the *footscan*. A maximum error of 1mm with a 95% confidence level, was however, considered acceptable.

The results from the two test methods indicated that pressure was evenly distributed in an area of 12*12mm in the region of maximum pressure at the first metatarsal head . The area which indicates the location and size of the sensor using the Podotrack technique is shown in *figure3.4*. The green area in the first metatarsal region in *figure3.8* is the area where the sensor is located using the *footscan* technique. A detailed explanation of the shape and size of the sensor is presented in *section3.2*.

3.2 CONCEPTUAL DESIGN PARAMETERS

The proposed shear stress measuring device consists of a sensor mounted inside a specially designed insole which fits inside a size 44 diabetic shoe. It is mounted such a way that the transducer measures maximum shear stresses which occur under the first metatarsal head while the subject is walking at a controlled velocity of 1.3 m/sec.

This section is concerned with the theory used to design the sensor. The material properties of the sensor, as well as the calibration procedure which is used to assess the performance of the sensor, are presented in *section 3.3* and *section 3.6* respectively.

This section also provides information gathered from the literature which assisted in understanding the limitations of using discrete sensors and the environmental conditions inside the shoe which need to be considered. Previous discrete sensor designs which assisted in designing and dimensioning the discrete sensor are also examined.

Information which assisted in establishing the design parameters of the new discrete sensor positioned inside the shoe is presented first, followed by the design protocol which was used to design the new sensor.

3.2.1 ESTABLISHING THE DESIGN PARAMETERS FOR THE NEW DISCRETE IN-SHOE SENSOR

- Discrete sensors which do not have solid attachments can migrate from their original placement site thus producing results which are not indicative of the area which is being investigated. The cables travelling from these types of sensor and along the foot and inner lining of the shoe are also unsupported which makes them susceptible to damage or unwanted bending. Bending or movement of the sensor can affect the signal travelling from the sensor to the data recording equipment. Recessing the sensor inside a customised insole is a means of alleviating these problems as it provides a rigid support and protection for the sensor.

- Further support and stability is provided in an insole design by having a higher density strip of material over the entire width of the insole in the area of the transducer. As previously discussed the strip of material in the metatarsal region must not interfere with the movement of the foot, because it can create an unnatural gait pattern and itself impose bending on the sensor. The region requiring the higher density material is called the metatarsal break region and is shown in *figure3.3* as the band of material between the PMBP and AMBP limits.

- Recessing the sensor inside an insole creates new problems however, in that feet of different dimensions cannot be measured without altering the location of the sensor. This can be overcome by providing an array of custom insole sizes and designs for different people. Research by Miller et al[64] showed that variations in the angle of the metatarsal heads and the longitudinal axis of the foot remain relatively consistent under load bearing conditions. This allows for most feet of a given size to be studied with a single design of insole.

- The degree to which the transducer is recessed can also affect the results obtained. An overly exposed sensor results in it becoming a natural pressure point and a sensor that is recessed completely will not establish contact with the measurand. A compromise must be reached.

- The environmental conditions inside the shoe are important when designing sensors which are pyroelectric, affected by moisture or dependent on accurate alignment.

- An important consideration is the comparison between the measured stresses at specific anatomical sites which are recorded in the literature. Although stresses are related to the forces transmitted by the feet on a known area of a transducer, different results will be obtained at the same anatomical sites from transducers of different sizes.

- The sizes of the sensors used in previous studies to measure the shear stresses at the MTH1 are significant as they are indication of the accepted area over which the forces acting on the foot can be assumed to be uniform. Designing a sensor that is similar in size allows a direct comparison of results of the new sensor to be made. A list of the sizes of various discrete sensors that have been used by various researchers to measure plantar stresses at the first metatarsal head is presented below in *Table 3.4*.

Researcher	***Type of Stress/es***	***Contact Area Dimensions (mm)***	***Thickness (mm)***
Tappin et al[19]	Shear	Diameter = 16	t = 2.3
Pollard et al[18]	Shear	Diameter = 15.96	t = 2.3
Gross et al[39]	Vertical	Square 4.83 * 4.83	t = 1.3
Lord et al[16]	Shear	Diameter = 16	t = 4
Levin[56]	Vertical	Diameter = 14	t = 3

Table 3.4 Sizes of discrete sensors reported in the literature

3.2.2 EXPECTED MAGNITUDES OF MAXIMUM SHEAR STRESSES

The magnitude of the shear stresses which are commonly measured in the literature define the performance range of the new sensor. Lord et al[16] reported maximum shear stresses in the region of the MTH 1 of between 3.54kPa and 21.2kPa in the medial-lateral directions respectively and values of between 14kPa and 58kPa in the anterior-posterior directions respectively. The design range of the sensor developed by Lord et al[16] was 0 to 250kPa. The tests conducted by Lord et al[16] involved a normal subject walking in a standard diabetic shoe with an instrumented insole placed inside it. A typical output produced by the sensor is shown in *figure2.17*. A similar range of values to those presented by Lord et al[16] were measured by Pollard et al[55] in their study of forces under the foot. Pollard et al[55] reported values of 8.17kPa and 41.83kPa in the anterior-posterior directions respectively and 17.34kPa and 14.23kPa in the medial-lateral directions respectively.

In a study by Tappin et al[57] the maximum shear stress value in the posterior direction for subjects wearing leather shoes was 127kPa. For subjects wearing leather shoes plus a soft lining the maximum posterior shear stress value was 39kPa and for subjects wearing special soft fitting shoes was 69kPa.

The sampling rate for the studies by Lord et al[16], Pollard et al[55] and Tappin et al[57] was 50 Hz.

As the maximum shear stress values presented in the literature vary depending on the type of shoe the subject wears, the subject's weight, the size of the transducer and the anatomical shape and gait pattern of the subject's foot, the values presented in the literature act as a means of providing a guideline for determining the performance range of the new sensor.

3.2.3 DIMENSIONING OF THE INSOLE

The first stage of the design process involved dimensioning the insole into which the sensor was placed. The shape of the insole was taken from a template of a size 44 insole as was prescribed by a podiatrist for the size of the subject's foot. *Figure 3.3,* excluding the dimension lines, is an example of a template prescribed for a size 44 insole. The size of the insole, with the exception of the MWF dimension, corresponded to the dynamic dimensions which are presented in *Table 3.3.*

The MWF of the template was 96mm whereas the average MWF presented in *Table3.3* was 90.28mm. In order to account for this difference, the foot was assumed to be evenly positioned at the centre of insole. Based on this assumption there is a 2.86mm clearance at either side of the shoe at the MWF position. This meant that the sensor was located at 17.36mm (HDMP) from the MWF position and not 14.5mm as presented in *Table3.3.* The rest of the dimensions presented in *Table3.3* were mapped directly onto the template. The maximum length of the template insole, for example, corresponded to the TOP dimension measured using the Podotrack and Adidas *Footscan* as presented in *figure 3.3.* The HDMP and VDMP dimensions indicate the centre position of the sensor in the insole.

The insole was constructed from a 6 mm thick polyvinylacetate (PVA) material. Two different densities were used. A higher density PVA of Shore hardness 50 was used in the metatarsal break region to provide rigidity and support for the sensor. A lower density PVA of Shore hardness 25 was used in the rest of the insole to allow easier unrestricted movement of the foot inside the shoe. The lower density material prevented bending from being transmitted from the arch of the foot to the metatarsal region. The thickness of the higher density PVA was quality controlled so as to have thickness of 6.1±0.05 mm. This ensured that the sensor did not protrude from its housing in the insole by a more than 0.15mm and less than 0.05mm.

Cutting and shaping of the insole was done using a computer driven cutting machine. The tolerance allowances in shaping the insole were limited to a maximum of ± 0.05mm. The two different density PVA materials were joined at the metatarsal break region using a contact adhesive.

3.2.4 THE DESIGN OF THE SENSOR

The concept which was used in the design of the sensor is based on the assumption that stresses imposed upon a material can be predicted by measuring the deformational strains which they induce. The reliability and accuracy of the strain measurements depend on the properties of the material, its behaviour in its environment, the theory used to convert the strains to stresses and the equipment used to convert the material's deformations to measurable strains.

The theory which was used in the design of the sensor is based on the assumptions of linear Hookean mechanics for isotropic homogeneous materials. The theory states that below a certain stress, a material will behave in a predictable, repeatable and linear manner. The defining parameter which determines a material's ability to behave in such a manner is its stiffness. The defining parameter which quantifies a material's stiffness in the linear region is Young's modulus.

Young's modulus is the essential parameter which allows a conversion to be made from strain to stress. Any parameters which might change the value of Young's modulus therefore needed to be accounted for. Assuming that the parameters which can alter the value of Young's modulus can be accounted for, and that the material is subjected to loads well within its elastic range, then it is possible to use the governing equations and assumptions of linear elastic mechanics to predict the behaviour of a material and relate its deformational strains to the stresses applied to it.

The sensor was designed so as to measure the maximum shear stresses in two orthogonal directions. The two directions were the anterior-posterior and the medial-lateral directions. The design of the sensor consisted of a square block of material with a circular base of the same material incorporated in its bottom surface. The circular base provided stability and a mounting for the block of material in the customised insole. The top surface of the block was in contact with the foot, the bottom surface of the block was continuous with the top surface of the base and the bottom surface of the base was flush with the bottom surface of the customised insole. There was complete continuity between the base and block.

Two rectangular strain gauge rosettes, consisting of three gauges (0°,45°,90°) in each rosette, were placed on two of the lateral surfaces. These measured the shear angles induced on the lateral surfaces of the block by the uniform shear stresses acting on the top contact surface of the block. The assumption that the shear stresses were uniformly distributed over the top surface of the sensor was based on the findings in *section3.1.2* and the contact areas of other sensors used by other researches as presented in *Table3.4*. The magnitude and direction of the shear stresses that were applied to the top surface were calculated from the shear angles which were induced on the two lateral surfaces. The lateral surfaces of the block were orientated in the shoe such that the shear angles which were induced on its lateral surfaces were representative of shear stresses applied to its top surface in the anterior-posterior and medial-lateral directions. The base and block, together with the two rosettes, were termed the sensor.

The design of the sensor is illustrated in *figure3.9*. Gauge1 indicated in *figure3.9* was used to measure the shear strain produced by the uniformly distributed shear stress1. The same applies for gauge2 and the uniformly distributed shear stress2.

The desired performance range of the new sensor was to measure shear stresses between 7kPa and 350kPa over an area of 12*12 mm with a sampling rate of 50Hz. A shear stress of 7kPa corresponded to a shear strain of 10 microstrain which was the minimum recommended strain the amplifier could measure with a specified accuracy. The shear stress of 350kPa was approximately double the maximum shear stress expected inside the shoe.

The size of the sensor presented in *figure3.9* was determined by the following parameters :

1. The size of the rectangular rosettes which were commercially available.

2. The thickness of the material which forms the sensor. Machining the sensor to size changes the contact surface properties of the sensor and induces additional micro cracks or discontinuities which might alter the behaviour of the sensor. Machining was therefore kept to a minimum. Friction was considered to have a minimal effect on the magnitude of the stresses induced on the top surface as the skin in the contact area of the MTH 1 was assumed not to move during the walking cycle. This assumption was based on the foot being rigidly fastened in the shoe.

3. The area over which the pressure can be assumed to be uniformly distributed.

4. The size of previous discrete sensors which have been used by other researchers as presented in *Table 3.4.*

3.2.5 COMPUTATIONAL THEORY USED IN THE DESIGN OF THE NEW SENSOR

This section presents the computational method which was used to calculate maximum shear stresses which occur on the top surface of the sensor during walking.

To use the assumptions and conditions of linear elasticity, the parameters which define linear elasticity needed to be adhered to or accounted for. The most important of these parameters was the material the sensor was constructed from.

The material characteristics of the sensor are presented in *section 3.3.* The material had to behave in a linear isotropic homogeneous manner yet, its stiffness had be sufficiently low for the electronic equipment to detect and compute the strains which occurred in the material. Below a certain threshold the signal to noise ratio becomes too large. The result is that it is impossible to distinguish between noise and strain measurements. The performance characteristics and limitations of the recording equipment are discussed in *section 3.2.4.*.

Another factor which influenced the computational equations of linear elasticity was the geometrical shape of the sensor. Its governing equations could not account for this. The sensor had edges and elements which were unsupported, which meant that the linear elastic laws of continuity and compatibility were infringed upon. To account for the geometrical shape of the sensor a Shape Factor was determined using a Finite Element Method (FEM) which modelled the loads which the sensor was subjected to. The Shape Factor allowed the equations of linear elasticity to be used even though the laws of continuity were infringed upon. The FEM model is presented in *section3.4*.

3.2.5.1 THEORY AND ASSUMPTIONS OF LINEAR ELASICITY

The fundamental assumptions of linear elasticity are presented below, together with the assumptions which were made to allow the equations of two dimensional linear elasticity to be applied in the design of the sensor:

- The law of compatibility of linear elasticity states that each element which describes a structure must be continuous and compatible with every other element. Each element has to be properly strained so that when all the deformed elements are fitted together the entire structure is free of any discontinuities. The check to determine whether the elements are all properly strained, and hence compatible with each other, represents the compatibility relations. As the sensor does not have a planar shape being defined instead by boundaries and edges, certain elements of the structure are likely to experience discontinuity with other elements. This was accounted for by establishing a Shape Factor correction, specific to the design of the sensor and the location of the rosettes. The Shape Factor was determined using a FEM model.

- Equilibrium was maintained before and after deformation.

- Plane strain was assumed in the principle **x-x (1-1)** and **y-y (2-2)** directions of the sensor. The **z-z (3-3)** direction was taken as the vertical direction. The orientation convention which was used is shown in *figure3.9*. This assumption was based on the fact that on the deformations in these principle directions were so small that they could be neglected. The assumption of plane strain on the two lateral surfaces allowed the shear angles on the lateral surfaces to be calculated using the two dimensional equations of plane strain. The equations of linear elasticity which relate the shear angle to the shear stress and shear modulus are presented below.

$\gamma = \tau / G$ in **1 - 3** and **2 - 3** directions **(Equation 1)**

γ is defined as the shear angle induced in a given direction

τ is defined as the shear stress in a given direction

G is defined as the shearing modulus of elasticity

Where $G = E / 2*(1 + \upsilon)$ **(Equation 2)**

with **E** defined as the modulus of elasticity

and υ defined as Poisson's ratio

- In the formation of the transformation of plane strain equations which allows strains associated with one set of axes to be related to strains in any direction, the shear angle γ (gamma) is shown to consist of two $\gamma/2$'s measured from the horizontal and vertical axes. This analogy is based on the shear angle being induced by some component of a stress tensor. The shear strain is said to be pure or irrotational. The shearing strains are defined below.

$\gamma / 2 = \tau$ in **1 - 3** and **2 - 3** directions **(Equation 3)**

Provided the strains are small and that there is no reduction in area during loading the fundamental equation for the transformation of plane , is given for any angle θ by :

$$\varepsilon\theta = (\varepsilon x + \varepsilon y) / 2 + ((\varepsilon x + \varepsilon y) / 2) * \text{Cos } 2\theta + \gamma xy / 2 * \text{Sin } 2\theta$$

(Equation 4)

When the rectangular rosettes are separated by the angles $\theta 1 = 0°$, $\theta 2 = 45°$, **and** $\theta 3 = 90°$ and $0°$ defines the horizontal axis, the derivation for this equation is given by:

$$\varepsilon 1 = (\varepsilon x + \varepsilon y) / 2 + (\varepsilon x - \varepsilon y) / 2) = \varepsilon x \qquad \textbf{(Equation 5)}$$

$$\varepsilon 2 = (\varepsilon x + \varepsilon y) / 2 + \gamma xy / 2 \qquad \textbf{(Equation 6)}$$

$$\varepsilon 3 = (\varepsilon x + \varepsilon y) / 2 - (\varepsilon x - \varepsilon y) / 2) = \varepsilon y \qquad \textbf{(Equation 7)}$$

Solving for εx, γxy and εy,

$$\varepsilon x = \varepsilon 1 \qquad \textbf{(Equation 8)}$$

$$\varepsilon y = \varepsilon 3 \qquad \textbf{(Equation 9)}$$

$$\gamma xy = 2 * \varepsilon 2 - (\varepsilon 1 + \varepsilon 3) \qquad \textbf{(Equation10)}$$

These three strain readings enable the maximum shear strain to be calculated using the following formula. The formula is derived from the equations of transformation of stress.

$$\gamma max = ((\varepsilon x - \varepsilon y) ^ 2) + (\gamma xy)^2) ^ 0.5 \qquad \textbf{(Equation11)}$$

The maximum shear stress acts at an angle of (90 + φ), where φ is the angle between the direction of the maximum principle strain and the x axis.

$$\varphi = \tfrac{1}{2} \tan^{-1} (\gamma xy / \varepsilon x - \varepsilon y) \qquad \textbf{(Equation12)}$$

From **Equation 1** and **Equation 2** :

$$\tau max = (E / 2*(1 + \upsilon)) * \gamma max \qquad \textbf{(Equation13)}$$

To accurately model the loading conditions of the sensor as simple shear rather than a tensor induced shear, the shear angle γ_{xy} was assumed to be equal to the shear strain ε_{xy} and not $2*\varepsilon_{xy}$ as is the case when acted upon by a shear tensor. This assumption was based on the location of the gauges on the sensor. The deformation pattern of the elements at the locations of the gauges was indicative of simple shear as shown in *section 3.4* in FEM model rather than pure shear. The resulting equation which was used to represent the maximum shear stresses which occur on the top surface of the sensor is presented overleaf.

$$\tau \text{ max} = (E / 2*(1 + \upsilon)) * \gamma \text{ max} * S$$

(Equation14)

γ **max** = ε **xy**

S = **Shape Factor** developed using the FEM technique in *(section3.4)*

3.2.5.2 MEASURING METHODS AND EQUIPMENT USED TO COLLECT STRAIN DATA

A six channel strain gauge amplifier (KWS/6A-5) was used to amplify the strains measured on the sensor. The amplifier allowed each gauge to be amplified simultaneously or separately. Each measuring channel contained a static calibration unit which was used to reproduce a known transducer signal. The static calibration was acceptable in dynamic conditions up to a limiting frequency of 1500 Hz, which was well above the maximum expected frequency of 6Hz. Calibration was performed using switches on the gauge amplifier which supply a known resistance to gauge bridges. The known resistance was then calibrated to known strains. Using the gauge amplifier the minimum recommended strain which can be accurately measured was 10 microstrain. The gauge amplifier can measure strains as low as 1 microstrain but at such low levels it is difficult to distinguish between noise and the actual signal. As a result, the performance of the amplifier is not specified for strains below 10 microstrain.

The cross talk between the channels of the amplifier were neglected as this error is so small as not to have been addressed in the specifications brochure made available with the amplifier. The transverse sensitivity of the gauges which is supplied by the gauge manufacturer in cases where it is deemed necessary, was also not supplied for the particular gauges which were used and as such, these effects were also neglected.

Alternating current (a.c.) was used to amplify the voltage changes produced by the gauges. These amplified voltages allowed a measurement range of between -10V and +10V. The advantages of using a.c. rather than direct current (d.c.) are the simpler amplifications which are possible with a.c. Amplification was essential, given the small change in resistance produced by the gauges which was measured. Alternating current is also better suited to the measurement of low frequencies. Although d.c. does have the advantage that there is no interference from cable inductances or capacitances, these interferences can be reduced when using an a.c. supply voltage. The cables are screened and the a.c. gauge amplifier balances the resistances and inductances in its bridge circuit by using an equivalent offset proportional to the interferences. The use of an alternating current in a gauge amplifier has the additional problem of a common a.c. power supply. This gives rise to an interaction between the different bridges, such that the balancing of one bridge can lead to the imbalance of the others. This creates difficulties in adjusting the zero balance of the bridges.

The amplifier used the null method to balance the Wheatstone bridge by redressing variable elements incorporated in the bridge circuit. The Wheatstone bridge circuit transformed the resistance changes occurring in the strain gauges into measurable voltages. The K factor or gauge factor is the proportionality constant between the relative change in length and resistance of the gauge. The default setting for the gauge amplifier was K=2 but the gauge factor for the gauges which were used 2.1. All the readings were measured using a gauge factor of 2 and corrected using a gauge factor of 2.1 after the strain readings were taken.

A half bridge, which contains six additional temperature compensation dummy gauges, was used in conjunction with the sensor to allow for any temperature variations which may occur when the sensor was inside the shoe.

KYOWA *KFG-1-120-D17-XX-L5M-2S* triaxial, 3 element 45° rectangular stacked rosette gauges were used. Each had an individual resistance of 120 Ω ± 0.08, a gauge factor of 2.1, a gauge length of 1 mm, a grid width of 1mm and a matrix width of diameter 5mm. The gauges had screened leadwires 5m in length. When the leadwires were added to the cables (which are all screened) from the terminal box (containing the dummy gauges) to the amplifier and from the amplifier to the computer, the total cable length was approximately 9m. This length of cable amounted to a resistance of approximately 2Ω. This resistance was accounted for in the bridge circuit of the gauge amplifier.

The gauges were bonded to the surface of the sensor using cyano-acrylate strain gauge cement as supplied by KYOWA.

Once the six gauges were balanced and zeroed, the tests were performed and sampled by a computer controlled analogue to digital converter. A PC30FG analogue to digital converter was used to sample the data at 50 Hz. The software provided by the a-d card allowed each channel to be sampled simultaneously and written to a numeric data file which could be examined using any spreadsheet package. Options within the software allowed the displayed voltage range to be between +10Vand -10 V which corresponded to the voltage range of the strain gauge amplifier. Any voltage measured by the strain amplifier was therefore exactly represented by the software available on the PC30FG card.

3.3 MATERIAL MORPHOLOGY

The theory used to predict the shear stresses acting on the top surface of the sensor required that the material chosen was isotropic, homogeneous and responded in a repeatable, strain rate independent and linear manner within its elastic range.

The material selected was required to have a sufficiently low modulus to allow strains produced by a shear stress as low as 7kPa to be measured. Materials with high moduli, such as metals and ceramics, could not be used as the materials do not strain more than 10microstrain when a shear stress of 7kPa is applied. Elastomers produce substantial strains when loaded at 7kPa but do not behave in a linear, strain rate independent or hysteresis- free manner. They, however, behave in an viscoelastic manner.

Many types of polymers have suitable moduli. It was however necessary for the material used to have the same properties in any orientation of its molecular structure. Crystalline polymers have distinctly orientated fibres and a different stiffness matrix in each of their orientations. This makes them non-homogeneous. Amorphous polymers, which are orientation independent, were therefore the only type of polymers which can be used.

The type of amorphous polymer which was selected was required to behave in the same manner in tension or compression. The effect of stain rate on its Young's modulus as well as the effect of temperature and moisture on its material properties also had to be accounted for.

The most suitable amorphous polymer found to serve as the new sensor was Ultra High Impact Polymethylmethacrylate (UHI-PMMA).

3.3.1 ULTRA HIGH IMPACT POLYMETHYLMETHACRYLATE

UHI-PMMA is manufactured in South Africa by Ampaglas from an impact modified high molecular weight acrylic polymer. It is a brittle polymer which has a glass temperature of 105° making it solid at room temperature. It is a lightweight material which can be machined easily because it has excellent forming characteristics.

Ampaglas provide an extensive amount of information concerning the material properties of their product. The technical information relating to the performance of the material is presented in a four page specification brochure which is provided with delivery of the material. Ampaglas also provide literature and additional information on the material, specifically relating to the effect of strain rate and temperature on its Young's modulus, the material's behaviour in tension and compression and its Poisson's ratio.

3.3.1.1 MATERIAL SPECIFICATIONS PROVIDED BY AMPAGLAS

The data presented in *Table3.5* was determined using the equipment and the technical expertise at Ampaglas. The tests were conducted using ASTM standards at a room temperature of 23°C±2°C.

Tensile strength at yield	**Tensile modulus**	**Compressive modulus**	**Thermal conductivity**	**Water absorption**	**Poisson's ratio**
(MPa)	**(MPa)**	**(MPa)**	**(W/m°C)**	**24hrs@23°C (%)**	
40	1520	1510	0.19	0.3	0.35

Table 3.5 Material properties of UHI - PMMA as supplied by Ampaglas

Table 3.5 illustrates that the difference between the tensile and compressive modulus of UHI-PMMA is just 10 MPa. The similarity between the behaviour of the material in tension and compression is further illustrated in the tensile-compressive graph shown *figure3.10.* The graph was obtained from tests conducted by Ampaglas using ASTM A 370 standards. The value of 0.35 for Poisson's ratio concurs with other literature on Poisson's ratio for a UHI-PMMA[65].

Given that the modulus of the material selected was over 1GPa, the material was brittle with a yield stress of approximately 40MPa and the stresses which were expected on the sensor were less than 350kPa, the following assumption was made. The engineering strain was assumed to be the same as the true strain of the material which meant that the area reductions which occurred in the material during loading were so small that they do not to have to be accounted for.

UHI-PMMA only absorbs 0.3% moisture after being totally submerged in water for 24 hours. This property coupled with the fact that a foot in an enclosed shoe only provides about 0.6ml/min of sweat after 15 minutes of walking at 1.56 m/sec in a 20°C and 35 % humidity environment[66] and the fact that the foot was is in contact with the sensor for a period no longer than a minute removed the need to compensate for moisture absorption. Given that the tests conducted on the new sensor were done using an open strapped diabetic shoe which provides increased evaporation, the contribution of moisture to the behavioural properties of the sensor was now regarded as even less insignificant.

An important environmental condition which *could* alter the performance of the sensor was temperature. Data supplied by Ampaglas stated that a change of 1°C between 15°C and 30°C results in an average change in the Young's modulus of the material of 25.1MPa. This amounts to a change in the value of the shear stress of 1.3% for every degree which the sensor varies from its initial temperature. The modulus measured by Ampaglas and the tensile tests conducted in this thesis were performed at a room temperature of 23°C±2°C.

Although the core temperature of the body remains remarkably steady at 37°C, it is difficult to calculate the temperature of the body's skin. It varies according to the circulation and the environment that the particular anatomical area of interest is exposed to. The extremities of the body such as the hands and feet can be five to eight degrees cooler than other areas of the body such as under the arms or the chest depending on the environmental conditions. This is the body's natural means of ensuring that the vital areas of the body receive the required amount of circulation in preference to other areas.

For a subject walking barefoot at 1.56 m/sec in a 20°C and 35% humidity environment the surface of the skin in the chest area is approximately 32.5°C while the temperature of the skin of the feet is approximately 26.8°C[66].

As the circulation amongst subjects for different studies varies, even in an area of the foot, the temperature of the foot in the region of the MTH1 was controlled before and after the experiments. In this way the difference between the temperature of the skin and the sensor was kept to a minimum. Controlling the temperature of the sensor and the foot was regarded as the simplest and most efficient means of catering for any temperature changes which might occur before or during the experimental tests *(See Chapter4)*. The temperature of the foot and sensor were measured using an infra-red mini-laser temperature sensor. The temperature sensor determines the intensity of infra-red radiation emitted by an object. The only information which the temperature sensor required was the emissivity of the object which it was measuring. The emissivity of skin is 0.97 and that of UHI-PMMA 0.90.

Monitoring the temperature of the sensor before and after the tests also allowed a quality control technique to be applied. All the tests where the temperature of the sensor was found to be ±0.5°C greater or less than its initial temperature were excluded. Consequently a maximum error of approximately ±0.65% could exist for any temperature changes which affected the material properties of the sensor.

In addition to the environmental conditions during testing, the chemical properties of the material were also investigated. As the strain gauges required a cleaning agent and a special adhesive it was essential that the chemicals used do not react with the UHI-PMMA. UHI-PMMA reacts with strong acids, esters, ketones, aliphatic alcohols and detergents. This meant that the common method of preparing a material's surface with trichloroethylene before applying an adhesive was not possible. Acetone which is an inexpensive cleaning agent which does not react with cyano-acrylate (adhesive used to bond the gauges to the sensor) or UHI-PMMA was used.

Cyano-acrylate has extremely good adhesive properties. It allows a bonded area of 12.7*25.4 mm to have shear strength of approximately 6000N which amounts to a shear stress of 18.6 MPa[67]. For cyano-acrylate to be effective, the surface it is applied to has to be smooth because the adhesive has poor flow properties. This is one of the reasons why the sensor was not machined on its contact surfaces.

As the properties of the material were essential to the performance of the sensor, a series of tests were performed on the material. The specification data supplied by Ampaglas was confirmed and it was verified that the material supplied by Ampaglas's supplier in Cape Town, Cape Plastics, was indeed the material specified in the brochure. The first series of tests involved confirming that the Young's modulus was the same as that specified by Ampaglas. The second series of tests involved assessing the effects of strain rate on the material's Young's modulus.

3.3.1.2 CONFIRMATION OF TENSILE MODULUS

Given that there is only a 10MPa difference between the compressive and tensile moduli of UHI-PMMA up to a proof stress of approximately 30 MPa taken at 0.2 % strain, it was assumed that they were identical in the expected load range. Tensile tests were therefore used to confirm the material's properties rather than compressive tests. The reason for selecting tensile rather than compressive tests was the complications associated with compression testing. If the specimen and platen in a compressive test are not of the same size and of the same material, friction tends to retain the ends of the specimen. This prevents the specimen from expanding freely in the lateral directions, resulting in errors in the measurement of the specimen's strain.

A series of five rectangular specimens were tested using ASTM A 370 tensile testing standards at a room temperature of 23°C±1°C. The average temperature of the specimens during the testing was 23.0°C. The tests were carried out at the Department of Materials Engineering at the University of Cape Town. The testing apparatus consisted of a computer driven tensile testing machine and an extensiometer. The testing environment and equipment are illustrated in *figure3.11*. All the data obtained during the experiments were digitally recorded at a sampling rate of 50Hz. The dimensions of the specimens are presented in *Table3.6*.

Gauge Length	Specimen Width	Specimen Thickness	Overall Length	Strain Rate	Cross Head Speed
(mm)	(mm)	(mm)	(mm)	(/sec)	(mm/min)
25 ± 0.08	6.25 ± 0.05	6.18 ± 0.05	100	0.001	1.5

Table 3.6 Tensile testing parameters used to confirm Young's modulus

The proportional limit is the stress necessary to produce the onset of curvature in the tensile stress-strain relationship. To detect this limit a line with a slope of 1520MPa and an intercept on the strain axis of 0.2% was added to the tensile test data. This line corresponded to the slope of the Young's modulus as specified by Ampaglas. The point, at which this line intersected the test data corresponded to the particular stress value which was used to produce a new regression line indicative of the Young's modulus of the specimens. The results from the first specimen's test together are shown in *figure3.12* together with the specimen's Young's modulus. The average modulus determined from the five tests was 1554MPa which was only a difference of 2.2% to the Young's modulus of 1520MPa specified by Ampaglas.

Given the inherent possibilities for error in the testing procedure, such as alignment of the specimens in the grips or possible grip slippage, an error of 2.2 % was not regarded as substantial enough to indicate that the material supplied was not the material specified by Ampaglas. The specifications produced by Ampaglas were therefore used with confidence.

3.3.1.3 THE EFFECT OF STRAIN RATE ON YOUNG'S MODULUS

Determining Young's modulus by drawing a line parallel to the initial linear section of the stress-strain curve from 0.2% strain was regarded as inappropriate given the loading which was expected on the sensor. *Figure3.12* shows that the data used to calculate Young's modulus was not entirely linear up to the point where the linear regression was fitted. Given that the design loads expected on the material were no more than 1000 kPa, using a modulus calculated up to 30 MPa was regarded as inappropriate. A lower limit in the elastic range of Young's modulus was therefore selected.

The tests indicated that the values of Young's modulus, although 1% higher with the higher strain rate, do not vary significantly enough to doubt the claims made by Kitagawa et al[68]. The value of Young's modulus was therefore regarded as independent of strain rate. The average value of Young's modulus was 1874MPa with a standard deviation of 6.81MPa and a maximum error of 6.1MPa at a 98% confidence level. A maximum error of 6.1MPa produces a maximum of a 0.32 % error in the strain predictions.

3.4 FEM TO ESTABLISH THE SHAPE FACTOR (" S ")

The finite element method (FEM) is a computational technique for obtaining approximate solutions for engineering analysis problems[69]. The advantage of using the FEM was the relative simplicity with which it could be used to generate approximate solutions to the complex mathematical equations which describe the physical phenomena which the sensor experiences.

The primary objective of using ABAQUS was to determine the Shape Factor which accounts for the geometrical discontinuities of the sensor inside the shoe. The Shape Factor was used with the equations presented in *section 3.2* to develop a means of predicting the maximum shear stresses which occur on the top surface of the sensor.

The particular FEM technique used was ABAQUS/Standard[70]. The essence of the method consists of evaluating approximate solutions to partial differential equations. The equations are computed using a numerical iterative process at particular points called (nodes), in a geometrical representation of a model, (mesh). Boundary and loading conditions are assigned and applied to the prospective nodes within the mesh.

Once the nodes are defined, the appropriate elements which would best describe the behavioural patterns and material properties of the model are selected. These discrete elements form the global matrix which is solved using standard linear algebra techniques. The accuracy of the model therefore lies within the assumptions made and the simplifications of the theory applied.

Inputting the data related to the model so that it is compatible with ABAQUS is done in the form of an input deck. The deck contains all the necessary information about the model in such a way that ABAQUS can translate the information into a mathematical analysis of the physical phenomena. Once the analysis is complete, the results are viewed either graphically using ABAQUS/Post, or numerically using an ABAQUS/data file.

3.4.1 PURPOSE OF USING ABAQUS

The purpose of using ABAQUS was to determine the Shape Factors for the sensor in the calibration technique and inside the insole. The input decks modelled the shape of the sensor, its material properties, boundary conditions and loading conditions. The first input deck modelled the entire sensor whereas the second input deck modelled only the block of the sensor without its base. This allowed the effect of the base to be analysed. The first input deck was also used to model the different loading conditions the sensor experienced in the calibration technique and inside the customised insole. (*See section3.4.2* and *section 3.4.3*).

Once the computational analysis of the two decks was complete, the shear stresses at discrete points called the sensor nodes, on two of the lateral surfaces of the block were analysed. The sensor nodes represented the possible locations of the strain rosettes when they were attached to the lateral surface of the block. *Figure 3.16* illustrates the positions of the sensor node sets.

Three sensor node sets were presented as it is reasonable to assume that although every attempt was made to position the gauges at sensor node set 2, it was possible that the gauges were not accurately positioned which meant that the strains measured at node set 2 could be influenced by the strains which occur at the sensor node sets1 and 3.

The results from the FEM analysis presented in *section 3.4.3.5* give the average values of the strains determined at sensor node set 2 together with a variance interval associated with the strains measured at sensor node sets 1 and 3. The shear strains measured at the sensor nodes in the direction of the applied shear stresses were then inserted into Equation 14 without the Shape Factor and compared with the shear stresses which were calculated by ABAQUS in the same direction. This was done to confirm whether the assumptions made and the theory used in *section 3.2.5* were valid.

The shear stresses which were predicted at the sensor nodes were expected to be greater than the shear stresses acting on the top surface of the sensor because of the geometrical discontinuities in the design of the sensor. The Shape Factor was used to correct these shear stresses measured at the sensor nodes so that they were equal to the shear stresses which occur on the top surface of the sensor.

3.4.2 DEFINING THE INPUT DECK

The input decks were constructed by defining analysis procedures which are listed below :

- Node generation
- Element generation
- Boundary conditions
- Material properties
- Load definitions

3.4.2.1 NODE GENERATION

The base of the sensor was made rectangular to simplify the geometry of the model. The distance between the nodes was refined to 1mm. The effect of the base on the shear angles measured at the sensor nodes was analysed to ensure that simplifying the geometry of the base was feasible. This is shown in *section 3.4.3*. The model geometry varied from the actual sensor geometry as shown in *Table 3.8*. These simplifications were made to reduce the complexity of the mesh. A model of the sensor is presented in *figure 3.16.*

	Base **thickness**	Base **Geometry**	Block **Geometry**
Actual	1.08	Sphere r = 11	12 * 12 * 5.12
ABAQUS Model	1	Rectangle of 12 * 12	12 * 12 * 5

Table 3.8 Simplifications made on the mesh of the model of the sensor (units are in mm)

The simplifications presented in *Table 3.8* were considered acceptable given that the area of interest in the model was located a significantly large distance away from these geometrically different sections of the model. As such, the changes would not have an effect on the stresses measured at the sensor nodes. The effect of making these geometrical simplifications is assessed in *section 3.4.3.5*.

Two input decks with different node generations were constructed. The one was representative of the sensor (Input Deck 1), and the other was representative of the block without the base (Input Deck 2). The two input decks are presented in Appendix C(i). In Input Deck 1 the base was continuous with the block and the only boundary conditions imposed on the system were those which act to pin the bottom surface of the base. In Input Deck 2 there was no base and the bottom surface of the block was pinned. A schematic, showing the definitions and the different node generations used in the two Input Decks, is shown in *figure3.16* and *figure3.17.*

3.4.2.2 ELEMENT DEFINITION

The particular type of elements chosen for the base and block were 8-node linear three dimensional continuum brick elements (designation C3D8). These elements are stress/displacement elements and are suited to meshes that do not necessarily have to be very finely defined. The elements do not take into account any thermal effects. They have three active degrees of freedom in the form of displacement in the x(1), y(2), z(3) directions. These elements are generally preferred for most cases because they are usually the more cost effective of the elements which are provided in ABAQUS[70]. The only limitation of using C3D8 elements was their inability to rotate. This attribute was not however, detrimental to the behaviour of the model but did not allow the FOLLOWER load option (ABAQUS load definition) to be used. The FOLLOWER option allows loads applied to a surface to always remain orthogonal to the loaded surface. The FOLLOWER option can only be used with beam or shell elements which allow rotational and displacement degrees of freedom. Shell elements allow the load applied to the top surface to always be normal to the shell surface.

A thin layer of 0.1mm shell elements was therefore added to the top surface of the block so that the FOLLOWER option could be used when inputting the load parameters. Its stiffness had no significant effect (1*10E7 times smaller) on the global stiffness matrix of the sensor. The shell element chosen was a (S4R) shell element, which is a 4-node doubly curved, reduced integration, thin shell. These shell elements have six degrees of freedom, both in the form of rotational and displacement freedom in the principle 1,2,3 directions. The C3D8 and the S4R elements are shown in *figure3.18* and *figure3.19* with their corresponding node ordering and face numbering.

3.4.2.3 BOUNDARY CONDITIONS

The bottom surface of the base was pinned. This meant that the nodes which form the bottom surface of the base were free to rotate but not free to displace in any of the principle directions. The rest of the nodes in the model had no boundary conditions.

3.4.2.4 MATERIAL DEFINITIONS

As the analysis was for a homogeneous, isotropic, linear, elastic material, only the Young's modulus and Poisson's ratio of the material were needed. The material's properties are presented in *Table 3.9*.

Element type	**Young's modulus**	**Poisson's ratio**
	(Pa)	
C3D8	$1874 * 10^6$	0.35
S4R	100	0.35

Table 3.9 Type of elements used in the model

3.4.2.5 LOADING CONDITIONS

As the analysis was for an isotropic homogeneous linear elastic material, the material's properties were assumed to remain constant when loaded. This meant that analysing the material response at any point in time with any particular load in the elastic range would produce a response that would, without any geometrical discontinuities, directly relate the input stresses on the top surface of the sensor to the shear stresses measured at the sensor nodes. This elevated the need to do a continuous analysis of varying loads through time. As a result, a single set of values (see *section3.4.3*) representing the three components of the input stresses on the top surface in the vertical, medial-lateral and anterior-posterior direction were imposed on the top surface of the sensor. The independence of the Shape Factor to the magnitude of the input loads is presented in *section3.4.3*.

As the material was an isotropic linear elastic material a STATIC analysis with the AMPLITUDE option was used to model the loading of the sensor. The AMPLITUDE option allowed a uniform load to be applied the top surface of the sensor for a fixed time interval of 1sec. As the material was elastic, the length of time for which the material is loaded was arbitrary. Given the time interval over which the actual loading was expected to occur, between 0.4sec and 1sec, creep was not considered to be relevant in the analysis.

Having two input decks served for three purposes. The first was to assess the effect of the base on the strains measured at the sensor nodes. The second was to verify the computational theory constructed in *section 3.2.5*. The third was to simulate the different types of loading conditions which were expected when the foot was in the shoe and when the sensor was tested in the calibration technique. The calibration technique distributed the shear load evenly over the top surface of the sensor without allowing any movement in the vertical direction. To simulate this accurately using ABAQUS, a condition was built into the STEP definition which prevented the top surface from moving in the vertical direction. This is shown Input Deck 1. When the sensor was placed inside the insole however, the top surface was no longer restricted in the vertical direction and therefore the condition which prevented the top surface from moving in the vertical direction in the STEP definition was omitted. This is shown in Input Deck 2. Illustrations and comparisons between the two conditions used within the STEP definition are shown in *section 3.4.3*.

The loads on the top surface of the sensor were defined using the CLOAD option. This option allowed concentrated forces to be applied to all of the nodes on the top surface of the sensor. Based on the assumption that the load was distributed evenly over the entire top surface of the sensor, the loads were applied to the top surface of each node in the model such that total load on the top surface was the sum of all the individual nodal loads. Each node then experienced the correct proportion of the overall load applied to the top surface of the sensor. Loads were simultaneously applied in the three principle directions by using three separate CLOAD definitions (Z-Load, X-Load and Y-Load). In this way a realistic model was developed which described an actual loading condition at some point in time in the contact process. It also allowed one or two of the load components to be isolated in order to check that the theory of superposition was maintained.

3.4.3 ANALYSIS OF THE RESULTS PREDICTED USING ABAQUS

These results aimed to show that the ABAQUS model could predict the correct Shape Factor to calculate τ**13**, which was the shear stress in the anterior-posterior direction and τ**23**, which was the shear stress in the medial-lateral direction on the top surface of the sensor from the strain measurements calculated at the sensor nodes on the lateral faces 3 and 4 respectively.

The results which are presented were extracted from the ABAQUS data file which was produced by ABAQUS during its analysis of the model. The numerical data could also be presented in the form of graphical plots, which illustrate the stresses developed in the sensor during actual loading. *Figure3.20* is representative of the response of the sensor to an applied load during the calibration technique and *figure3.21* is representative of the response of the sensor to an applied load when it was mounted inside the insole.

The following parameters, which are defined as **Parameter Numbers No° 1, 2, 3 and 4** were examined using ABAQUS :

No1. The effects of the base on the strains measured at the sensor nodes.

No2. The theory of superposition of stresses.

No3. The Shape Factor was independent of the magnitude of the applied stresses within the design range.

No4. A Shape Factor for the sensor during the calibration procedure and for the sensor when it was mounted in the insole.

3.4.3.1 THE EFFECT OF THE BASE ON THE STRAINS MEASURED AT THE SENSOR NODES

Input Deck 2 differed from Input Deck 1 in that it did not have a base. Its geometrical mesh is shown in *figure 3.17*. If the base was found to have no effect on the readings taken at the sensor nodes, then it could be assumed that the geometry of the base had no effect on the readings either.

3.4.3.2 THE THEORY OF SUPERPOSTION OF STRESSES

To ensure that the laws of superposition of stresses were obeyed, the three components of the induced stresses were applied to the top surface of the sensor simultaneously or as individual components. This allowed the theory of superposition of stresses to be confirmed.

3.4.3.3 THE EFFECT OF THE MAGNITUDE OF THE APPLIED STRESSES

In the ABAQUS model the maximum component of stress, which is the vertical direction, was 1000 kPa. The loads which were applied to the model were the loads which are expected to occur on the sensor during gait. As the Shape Factor was independent of the magnitude of the load applied to it, the loads which were applied to the model were randomly designated within the design range.

3.4.3.4 SHAPE FACTOR PREDICTED FOR CALIBRATION PROCEDURE AND SENSOR MOUNTED INSIDE THE INSOLE

As the sensor cannot be calibrated inside the shoe, a separate calibration technique was developed to ensure that the assumptions made and the theory used to relate the strains on the lateral surfaces to the shear stresses occurring on the top surface of the sensor were valid. The only difference between the calibration technique and the conditions describing the behaviour of the sensor inside the shoe was the type of loading which the sensor experiences. The loading experienced by the sensor in the vertical direction during the calibration technique was ideally zero whereas the sensor inside the shoe experienced a vertical component of the stresses applied to it by the foot.

If the calibration procedure produced the correct results using the theory developed in *section 3.2,* then all that needed to be examined to confirm the effectiveness of the in-shoe sensor was the effect of a load applied to it in the vertical direction.

If a load applied in the vertical direction was shown to have no effect on the strains measured at the sensor nodes, then the same theory used in the calibration procedure could be used for the sensor inside the shoe. Assuming the same theory could be used, then there was a single difference between the two procedures. The single difference being the different element restrictions in the vertical direction. The Shape Factors were intended to account for this difference.

Input Deck1 and Input Deck 2 were also modified to allow the different loading conditions expected on the sensor in the calibration procedure and inside the shoe to be examined. Input Deck 1 restricted the top surface of the sensor from moving in the vertical direction during loading whereas Input Deck 2 allowed the top surface to move freely in the vertical direction during loading. The response of the sensor in the calibration technique to a single shear stress of a magnitude of 33kPa applied in the 1-3 direction is shown in *figure3.22*. The loading of the sensor in the calibration procedure is referred to in *section3.4.3.5*. as the *restricted case*. The response of the sensor to an expected in-shoe single shear stress of a magnitude of 33 kPa applied in the 1-3 direction is shown in *figure3.23*. The loading of the sensor inside the shoe is referred to in *section 3.4.3.5* as the *free case*. Both *figure3.22* and *figure3.23* are magnified by a factor of 5000. These figures are not to scale because images become distorted when revolved in ABAQUS. The images were revolved to present a three-dimensional view of the sensor.

The response of the sensor shown in *figure3.23* is the type of response which was expected. The side closest to the direction from which the stress was applied being "lifted up" and the side furthest from the direction from which the stress was applied being "pushed down". The "lifting up" phenomena occurred because of the pulling effect the supported elements further down from the direction of the applied stress had on the unsupported edge elements closest to the side the stress was being applied from. The "pushing down" phenomena was because the edge of elements furthest down from the direction of the applied stress was not supported by any elements on its boundary and as a result the elements were free to collapse downwards.

To examine the effect of a vertical stress on the response of the sensor inside the shoe, the three components of stress were applied separately as well as simultaneously to the top surface of the sensor. This method provided a means of examining the effect of the vertical component on the deformation of the sensor and the strains which were produced at the sensor nodes.

3.4.3.5 RESULTS PREDICTED FROM THE FEM ANALYSIS

The results produced using ABAQUS were used to examine the parameters presented in *section 3.4.3*. Each parameter number is presented in *Table3.10* and *Table3.11* to indicate which of the parameters presented in *section3.4.3* is being assessed. *Table3.10* represents the measurements taken at node set 2 on face 3 for the *restricted case* and *Table3.11* represents the measurements taken at node set 2 on face 3 for the *free case*. *Appendix C(ii)* illustrates an example of the results on face 3 of the sensor for the *restricted case* for the *free case*. The results were extracted from the ABAQUS/data file.

NODE SET 2					
RESTRICTED CASE	**DIRECTION AND MAGNITUDE OF STRESS**	**AVERAGE τ_{13}**	**AVERAGE ε_{13}**	**SHAPE FACTOR**	**PARA-METER *No°***
	(kPa)	**(kPa)**		**"S"**	
BASE AND BLOCK	1 - 3 = 33	1 - 3 = 37.2	1 - 3=5.35E-5	0.89	**1,2**
BASE AND BLOCK	1-3=33, 2-3=15	1 - 3 = 37.3	1 - 3=5.35E-5	0.89	**2,3**
BLOCK	1 - 3 = 33	1 - 3 = 37.3	1 - 3=5.36E-5	0.89	**1**
BLOCK	1-3=66, 2-3 = 22	1 - 3 = 74.5	1 - 3=1.07E-4	0.89	**3**

Table 3.10 Results of measurements at node set 2 on face 3 for the restricted case

NODE SET 2					
FREE CASE	**DIRECTION AND MAGNITUDE OF STRESS**	**AVERAGE τ_{13}**	**AVERAGE ε_{13}**	**SHAPE FACTOR**	**PARA-METER *No°***
	(kPa)	**(kPa)**		**"S"**	
BLOCK	1 - 3 = 33	1 - 3 = 43.3	1 - 3=6.23E-5	0.76	**1**
BASE AND BLOCK	1 - 3 = 33	1 - 3 = 43.3	1 - 3=6.24E-5	0.76	**1,2,3**
BASE AND BLOCK	1 - 3 = 33 2 - 3 = 15 3 - 3 = 1000	1 - 3 = 43.3	1 - 3=6.24E-5	0.76	**2,3**

Table 3.11 Results of measurements at node set 2 on face 3 for the free case

The results presented in *Table 3.10* and *Table 3.11* indicate that the first three **Parameter No°'s,** defined in *section 3.4.3*, were not affected by the changes of magnitudes of the stresses applied to the sensor. They also show that the theory of superposition was valid and that the base and vertical component of the applied stress had no effect on the strains measured at the sensor nodes. These results confirmed that the material behaved in a linear isotropic homogenous elastic manner. Based on these findings, only one separate loading case for the restricted and free case was examined for face 4. The results are summarised below in *Table 3.12.*

NODE SET2				
CASE EXAMINED	**MAGNITUDE AND DIRECTION OF STRESS**	**AVERAGE** τ_{23}	**AVERAGE** ε_{23}	**SHAPE FACTOR**
	(kPa)	**(kPa)**		**"S"**
RESTRICTED BASE AND BLOCK	1 - 3 = 33 2 - 3 = 15 3 - 3 = 1000	2 - 3 = 16.8	2 - 3 = 2.42E-5	0.89
FREE BASE AND BLOCK	1 - 3 = 33 2 - 3 = 15 3 - 3 = 1000	2 - 3 = 19.7	2 - 3 = 2.83E-5	0.76

Table 3.12 Results of measurements taken at node set 2 on face4 for the free and restricted cases

The results presented in *Table3.12* indicate that the same **Parameter No°'s** which were examined and presented in *Table3.10* and *3.11* for face3 were directly applicable to face4.

The possibility that the gauge rosettes were not positioned exactly on node set 2 was also examined. This would result in the gauges at node set 2 being influenced by the two neighbouring node sets. The variance in the strain measurements between the node sets was therefore determined. The Shape Factors which were determined for node set 1 and 3 are presented in *Table 3.13.* The range of the average Shape Factors for both the restricted and free case at all the node sets is presented in *Table 3.14.*

NODE SET	CASE	DIRECTION AND MAGNITUDE OF STRESS	AVERAGE ε_{13}	AVERAGE τ_{13}	SHAPE FACTOR
		(kPa)		(kPa)	
1	Restricted	1 - 1 = 33	5.41E-5	37.41	0.88
3	Restricted	1 - 1 = 33	5.41E-5	37.41	0.88
1	Free	1 - 1 = 33	6.21E-5	43.53	0.76
3	Free	1 - 1 = 33	6.21E-5	45.53	0.76

Table 3.13 Shape factors determined at sensor nodes 1 and 3 on face 3

	RESRICTED CASE SHAPE FACTOR	FREE CASE SHAPE FACTOR
Node Set1	0.89	0.76
Node Set2	0.88	0.76
Node Set3	0.89	0.76

Table 3.14 Variance of Shape Factors with node sets

The average Shape Factor which was determined for the calibration technique was **0.887** with a standard deviation of **0.0049.** For the sensor inside the shoe it was **0.760**. The following section (*section 3.5*) is concerned with the calibration technique which was used to validate the assumptions and theory used in the design of the sensor.

3.5 CALIBRATION PROCEDURE

Although the calibration procedure did not exactly represent the type of loading of the sensor inside the shoe, it did provide a method to confirm that the sensor with the appropriate Shape Factor could predict the magnitude of shear stresses applied to its top surface. The response and performance of the sensor to the calibration procedure was assessed and used as a means of gaining an insight into the type of response which the sensor experienced when it was inside the shoe.

The Shape Factors took into account the different loading conditions which allowed the calibration measurements and the in-shoe measurements to be compared. The Shape Factor was a single number which decreased every strain measurement by a fixed amount when it was applied to Equation14. The amount was a uniform percentage less than the amount the strains were reduced when the sensor was inside the shoe. The results from the calibration procedure were therefore regarded as a good indication of the in-shoe sensor's response. The Shape Factor determined for the in-shoe sensor reduces the strains by 24%. For the calibration procedure the Shape Factor reduces the strains by 11%.

The sensor was placed between two parallel surfaces of a specially designed jig. The jig which was made from mild steel with a compliance far exceeding the compliance of the sensor by more than 210 times was designed to fasten between the two crossheads of a computer controlled ZWICK tensile/compressive testing machine. When the crossheads were separated from one another, the top surface of the sensor between the two separate parallel surfaces of the jig experienced simple shear. The strains experienced by the jig were not considered to affect the response of the sensor.

The force-time history which was applied to the jig was recorded by the ZWICK's computer at a sampling rate of 50 Hz. This was the same as the sampling rate at which the PC30FG card recorded the shear angle changes of the sensor. The force-time history recorded by the ZWICK was converted into a shear stress-time history. The ZWICK therefore provided a known shear stress to the sensor during testing. For the calibration technique a single rosette was attached to the lateral surface of the sensor. The lateral surface was parallel to the applied load on the top surface of the sensor. The location of the rosette on the lateral surface is illustrated in *figure 3.24*. The shear angles measured by the rosette were converted to the shear stresses acting on the lateral surface. These shear stresses were then corrected by the Shape Factor, to produce the shear stresses acting on the top surface of the sensor . The results from the sensor were compared to the known shear stresses applied by the ZWICK. In comparing these results, the accuracy of the sensor was evaluated. The controlled environment and apparatus used during the calibration procedure are shown in *figure3.25*. A schematic illustration of the apparatus shown in *figure 3.25* is shown in *figure3.26*.

As the material was assumed to be strain rate independent at the loads expected, a slow cross head speed of 0.06 mm/min was chosen. This cross head speed provided an adequate amount of data with a high resolution.

3.5.1 THE DESIGN OF THE CALIBRATION JIG AND ATTACHMENT OF THE SENSOR TO THE JIG

The calibration jig which housed the sensor was made in two pieces. The top jig was attached to the top crosshead of the ZWICK and remained stationary during loading. It was the jig onto which the base of the sensor was attached. The bottom jig provided the load. The top surface of the sensor was attached to it. The distance between the parallel surfaces of the top and bottom jigs was the thickness of the sensor i.e. 6.2±0.01mm.

The sensor was attached onto the two jigs using cyano-acrylate adhesive. Cyano-acrylate has a shear strength of 6000N which is well above the maximum applied shear load of 50N. The top jig was pinned to the top crosshead with a locking pin and fastening nut. The bottom jig was pinned to the bottom crosshead with approximately a 0.2mm clearance in the pin hole diameter. The clearance allowed the entire jig to align itself axially when loaded. This reduced the possibility of any misalignment which might be present in the system. A collar with two locking grub screws was designed to fit around the jig in the region of the sensor so that, once the sensor was fitted, the entire jig with the sensor could be removed from the ZWICK and transported without disturbing the environment of the sensor. The calibration jig with the sensor mounted in the ZWICK is shown in *figure3.27*. The design drawings of the calibration jig are presented in *Appendix D*.

When loading the jig the objective was to apply a load through the entire jig which matched the load which was being applied to the sensor by the ZWICK. The axial load applied by the ZWICK was the load which was translated to the shear stress applied on the sensor. Changing the orientation of this load results in the data recorded by the ZWICK not being a representation of the shear stresses applied to the sensor but rather of some component of a force applied to the sensor. The sensor could not detect a misaligned force component applied by the ZWICK. Therefore a misalignment of the jig could result in an error in the correlation between the data recorded by the ZWICK and the data recorded by the sensor. Additional methods which were adopted to keep misalignment to a minimum are presented below.

- The bottom and top jigs were scribed with centre line markers during the machining process. The centre lines allowed the sensor to be placed between the two parallel surfaces of the jigs such that the top surface of the sensor experienced a force parallel to the centre line of the entire jig.

- The ZWICK was used to mount the sensor in the calibration jig. The process involved gluing the sensor to the top jig. The jig was then attached to the top crosshead of the ZWICK. A special level surface was then created on the bottom crosshead. The apparatus used to create the level surface is shown in *figure 3.28*. The bottom jig was stood upright on the level plate. The bottom crosshead was raised until it was at the correct height to bring it into contact with the top surface of the sensor. Once at that height the bottom jig was moved laterally until it touched the top surface of the sensor. This process involved using two guiding parallel blocks positioned on the parallel plate. The process was confirmed five times. The guiding blocks were then secured, adhesive applied to the top surface of the sensor and the bottom jig moved to make contact with the sensor. With the sensor now glued to the bottom jig, the locking collar was slid over the two jigs and fastened into place. The bottom jig was then lowered and the level plate removed. The lower crosshead was moved back up to fit neatly into the bottom jig. With the bottom crosshead in position the bottom locking pin was placed into the bottom jig. Once the entire jig was stable and in its testing position, the collar was lowered and the tests conducted. The advantage of using the ZWICK to set up the calibration jig, was that small increments of movement could be applied with a known force.

3.5.2 TESTING PROTOCOL

The calibration procedure tested the sensor up to a maximum shear stress of 350 kPa at a crosshead speed of 0.06 mm/min. Ten tests were performed and the results analysed to check the correlation between the shear stresses measured by the sensor to the known shear stresses applied by the ZWICK. The data presented by the ZWICK is termed the ZWICK data and the data presented by the sensor the Experimental data. The correlation between the two sets of data was used to validate the design and theory used to develop the sensor.

The temperature of the sensor was maintained at 23°C±0.5°C throughout the testing. The maximum error possible in the stress calculation from the measured strains as a result of a temperature variation ±0.5°C was therefore ±0.65% of the Full Scale Output. Recording of the gauge data was started first. The data recorded by the ZWICK began as soon as the tests commenced. The load cell used was a 1000N load cell with an accuracy of ±1N.

A pre-load of 4 N, which corresponds to a shear stress of 27.8 kPa, was applied to the sensor before the tests commenced. It was important to confirm that the jig was aligned and completely stable before any results were gathered. The pre-load takes up any slack in the calibration jig and crossheads and ensures that a simple shear axial force is applied to the sensor. The sensor could not be calibrated from 7 kPa, as it was believed that an applied force of 1N is too low and too close to the limitations of the equipment. It would not be high enough to take out the slack in the calibration jig and crossheads and as such would resemble noise rather than a response from the sensor. Although the sensor was, as a result, only calibrated from 27.8 kPa, it is felt that this is not a limitation of the performance of the sensor but rather a limitation of the calibration technique.

The equipment used to amplify the strains produced by the gauges can, according to the specifications provided the manufacturer, ROHLOFF Inc., measure strains above 10 microstrain with an error margin of ±0.75 % of the Full Scale Output. Although the gauge amplifier has the ability to measure strains as low as 1 microstrain, strains below 10 microstrain are not guaranteed with the same level of accuracy and as such are not specified by the manufacturer. The possible errors which were induced as a result of attempting to measure strains below 10 microstrain are assessed in *section 3.5.3.1.* The error margins of the gauge amplifier as specified by the manufacturer for strains above 10 microstrain are presented overleaf:

- Calibration = ± 0.5 %
- Linearity Deviation = ± 0.05% Full Scale Deflection
- Influence of Adjusted Measuring Sensitivity by 10 % Mains Voltage Fluctuation

  = ± 0.1%
- Influence on Zero Point by 10% Mains Voltage Fluctuation Deflection

  = ± 0.1% Full Scale

Once the ten tests were complete, a best fit equation was fitted to both series of data to allow a correlation to be made between the strains measured by the sensor and the forces applied by the ZWICK at discrete points in time during the calibration. An average error with a 99 % confidence interval was determined for all ten tests.

3.5.3 THE RESULTS FROM THE CALIBRATION PROCEDURE

The results from the calibration procedure are presented in the *AppendixD. Figure3.29* is an illustration of one of the response curves of the sensor to the forces applied by the ZWICK. Three additional response curves are presented in *AppendixD(ii). AppendixD(iii)* is an illustration of the analysis which was used to convert the voltages produced by the gauge amplifier to shear stresses acting on the top surface of the sensor.

The best curves which were fitted to the data produced by the ZWICK and the gauges are presented in *Appendix D(v)*. The forms of the equations were second order polynomials. *Section 3.5.4.* discusses the form of these equations and how they were used as an indication of the performance of the sensor during the calibration technique. The equations describing the behaviour of the ZWICK and the gauges were used to generate two new digitally filtered series of data. These new sets of data were used to predict the error of the strain readings measured by the sensor and the forces applied by the ZWICK.

The statistical equation used to predict the confidence intervals of the mean error is presented below:

$$X - z\,\alpha/2 * \sigma / \sqrt{n} < \mu < X + z\,\alpha/2 * \sigma / \sqrt{n} \quad \textbf{(Equation 15)}$$

X =Mean

z α/2=Degree of Confidence

n=Size of Sample

σ=Variance

μ=Confidence Interval

A summary of the statistical analysis which was performed on the two sets of data for all ten tests is presented in *Table 3.15.* A graphical illustration of the random error between ZWICK data and the gauge data of the ten tests is presented in *AppendixD(vi).*

Shear Stress			**Force**		
Mean Error	**Confidence Interval 99%**	**Maximum Error of Estimate**	**Mean Error**	**Confidence Interval 99%**	**Maximum Error of Estimate**
(kPa)	**(kPa)**	**(kPa)**	**(N)**	**(N)**	**(N)**
6.03	3.70<μ<8.36	2.33	0.87	0.53<μ<1.21	0.34

Table 3.15 Mean error between the shear stresses measured by the ZWICK and gauges

3.5.3.1 POSSIBLE SOURCES OF ERROR DURING THE CALIBRATION

The results presented in *Appendix D(iii)* indicate that the strains on the horizontal gauge3 at stresses below approximately 50 kPa were below 10 microstrain. Although the gauge amplifier has the capacity to measure strains below 10 microstrain, these measurements are not guaranteed by the manufacturer with the same degree of accuracy (±0.75% Full Scale Deflection). However, it is believed the errors which were incurred during the calibration technique as a result of strains being below 10 microstrain were no greater than the errors which were induced into the results by the amplifier for strains above 10 microstrain. This assumption is based on the magnitudes of the strains which were measured by the amplifier at gauge3. Gauge 3 was the only gauge where strains below 10 microstrain were experienced.

The results indicated that the strains, starting from the initial strain of 8 microstrain, increased with a similar margin of consistency and repeatability as the strains which were measured above 10 microstrain to a value of 12 microstrain. This is shown in *Appendix D(iv)* where the average slope of the data from 8 to 10 microstrain is consistent with the data from 10 to 12 microstrain. The graphs presented in *AppendixD(iv)* also indicate the continuity at the transition between the strains measured below and above 10 microstrain. This continuity is what was expected, given that the load applied to sensor was linear. Strains below 10 microstrain in the calibration procedure were therefore regarded as having the same specified degree of accuracy as those above 10 microstrain.

Additional errors which could account for the errors presented in *Table 3.15* are presented below.

- Any misalignment of the sensor in the calibration jig. This would result in a non-axial load being applied to the sensor. Only a purely axial load could be used to equate the force measured by the ZWICK to simple shear applied to the top surface of the sensor.

- The inadequate removal of all the slack in the calibration jig and crossheads. A pre-load of 4N was hoped to be adequate to avoid this error yet is possible that all the slack was not entirely removed. Slippage of the calibration jig or sensor is not regarded as a possible source of error owing to the design of the jig and crossheads.

- Any errors or non linearity's present in the ZWICK. The performance of the load cell is rated to ± 0.1% of its Full Scale Deflection of 1000N.

- Errors associated with the performance of the gauge amplifier. The accumulated errors associated with the gauge amplifier amount to ± 0.75% Full Scale Deflection for the adjusted measuring range of 1000 microstrain.

- Errors associated with any material property changes which might have occurred as a result of a change in the temperature of the sensor. The mean temperature of the sensor during the testing was maintained between 23°C±0.5°C. The mean temperature of the sensor during the tests was 23.3°C. This resulted in a maximum error of ±0.39% when the stresses were calculated from the strains measured by the gauges. The error was induced because a modulus corresponding to a temperature of 23.0°C was used during all the tests.

3.5.4 THE OVERALL PERFORMANCE OF THE SENSOR

Based on the results of the calibration procedure the following performance characteristics of the sensor are presented:

- The mean error of the sensor from the ZWICK data is 0.87 N. The mean error will, with a 99% probability be between 0.53 N and 1.21 N. The maximum error of the estimate of the mean with a 99% confidence interval is 0.34N. This corresponds to mean error of ±1.7% of the Full Scale Deflection of the measured range. Although the average curve of the data measured by the gauges was not linear but a second order polynomial, the response of the sensor was still regarded as linear. This is because the input load supplied by the ZWICK was also a second order polynomial. Any non linearity of the force applied by the ZWICK, which were as a result of the errors mentioned in *section3.5.3.1*, was not regarded as a limiting factor in assessing the performance of the sensor as the same inherent error was also applied to the sensor.

The results indicate that the sensor could be used to measure the shear stresses on the top surface of the sensor with a low degree of error (±1.7% of Full Scale Output). The performance of the sensor during the calibration technique validated and gave confidence to the theory and assumptions used in the design of the sensor.

3.6 MOUNTING THE SENSOR IN THE CUSTOMISED INSOLE

The centre of the gauge was located using the data presented in *figure 3.3*. The high density PVA band was 6.1mm± 0.05 mm thick with the bottom of the sensor flush with the insole and the top surface protruding from the insole by a maximum of 0.16mm and a minimum of 0.04mm. A 1±0.05 mm spacing was provided around the sensor so that the PVA material never came into contact with the lateral surfaces of the sensor during loading. Care was taken in ensuring the sensor was aligned parallel to the anterior-posterior and medial-lateral axes. Computer driven machinery performed all the shaping of the insole to house the sensor. A tolerance of ± 0.02 mm was provided for the area in which the sensor and its cables were located. The cables for each rosette were led out of the lateral side of the insole and bonded to the insole using cyano-acrylate. The gutters made for the cables were 6.5mm and 1.08mm deep. This was the same depth as the area cut away to house the base of the sensor. The base of the sensor was also bonded to the high density PVA using cyano-acrylate. The sensor and it's cables mounted inside the insole is shown in *figure3.30.*

The newly instrumented insole was then fixed to the bottom insole of a diabetic shoe. The instrumented insole inside a diabetic shoe is shown in *figure 3.31.*

3.7 INSHOE TESTING PROCEDURE

The tests were conducted using a treadmill laboratory at the Sports Science Institute of South Africa. The laboratory was climate controlled and the horizontal treadmill had recently been calibrated. The testing environment is shown in *figure 3.32*. The tests were conducted at a gait velocity of 1.3 m/sec ± 0.083 m/sec. This velocity was chosen because it allowed the results from the tests conducted in this thesis to be compared with the literature and it provided a controlled environment for the analysis of the results. It also allowed the effects of any increase or decrease in velocity to be neglected. The velocity chosen was the highest comfortable walking velocity. The subject had a body mass of 82 Kg and a height of 1.86m. Although the average mass of the subjects used in the literature was 70Kg, the subject was still selected, as the convenience of having the subject available at any time during the thesis outweighed the limitations which were introduced as a result of the differences in body mass. The shear stresses measured in this thesis were therefore expected to be greater than those stresses presented in the literature as a result of the higher mass of the subject. The profiles of the stresses were however not expected to be indistinguishably different.

Before the tests were conducted the subject attached the instrumented shoe onto his right foot and a diabetic shoe with an equivalent height onto his left foot. He then became accustomed to walking on the treadmill at the test velocity. No socks or items were worn on the feet during the testing. (*figure 3.33*)

The results from each of the tests performed on the sensor and its equipment are discussed and analysed in *Chapter 4* under the headings presented below.

Temperature Regulation. There were three variables whose temperature's were controlled during the testing. These were the temperature of the room, the foot and the sensor. The temperature of the laboratory was set and maintained at a temperature of 23°C±1°C for the tests using the climate control. The temperature of the foot in the region of first metatarsal was measured before and after each test using a infra-red mini-laser. The mini-laser is shown in *figure 3.34*. The temperature of the foot was controlled using a heater or a ice pack until it was 23°C±1°C.

The temperature of the sensor was also controlled to within the same limits. Maintaining the temperature of the environment, the foot to within 23°C±1°C and the sensor to within 23°C±0.5°C reduced the possibility of any changes in the material properties of the sensor which could result as a result of temperature variances. This kept the error induced when calculating the stresses from the strains measured by the gauges to a value no greater than ±0.65%. If the temperature of the sensor was not within the required limits before and after each test, the test data was rejected.

Gauge Amplifier Balancing. The six gauges on the gauge amplifier were balanced prior to the commencement of the tests. The gauges were balanced using the highest sensitivity of the amplifier (full scale deflection of 100 microstrain). At this setting a 0.1 change in voltage represented 10 microstrain. Once the gauges were balanced the range of amplifier was set such that the full scale deflection was a 1000 microstrain for the tests.

The protocol which was adopted for the testing of the instrumented diabetic shoe involved a series of *pilot tests* and a series of *analysis tests*.

Pilot Tests. Five pilot tests were conducted. The pilot tests were performed to assess a number of parameters. The drift of the sensor at zero load, the scuffling which occurred as the foot was placed into the instrumented shoe, the validity and purpose of using a standing position prior to walking as a datum from which the stresses measured when the subject was walking could be referenced and the magnitudes and profiles of the stresses which occur during walking. The pilot tests were also used to establish and justify the testing protocol which was used during the analysis tests.

The procedure for the pilot tests was as follows:

- The analogue to digital card used to sample the data was activated when there was zero load on the instrumented shoe.
- After approximately 12 seconds, the right foot was placed into the shoe and the velcro around the shoe tightened.

- Once the foot was correctly located and fastened into the instrumented shoe, the subject stood stationary with both feet horizontal to the treadmill for approximately 1 second.

- The treadmill was then started and after approximately 6 gait cycles, the sampling being performed by the analogue to digital recorder was deactivated. The results were stored on disk.

Analysis Tests. A series of five tests were conducted. The testing protocol used during the analysis tests was identical to the pilot tests, with the only difference being that the recorder began sampling when the subject was standing on the treadmill with the instrumented shoe attached and ready to begin walking. The reason and purpose for doing this is discussed in detail in *section4.2.*

FIGURES FOR CHAPTER 3

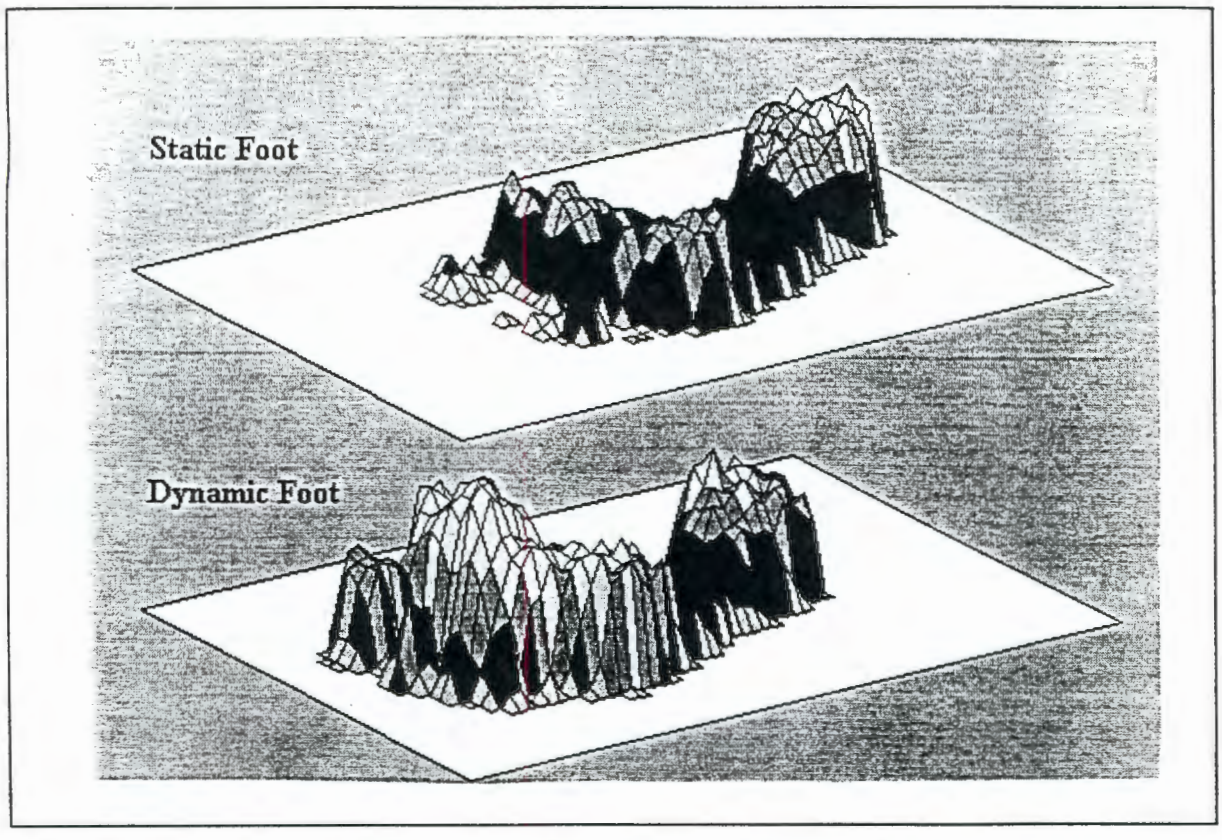

Figure 3.1 The difference between a static foot and dynamic foot imprint
(See text, page60)

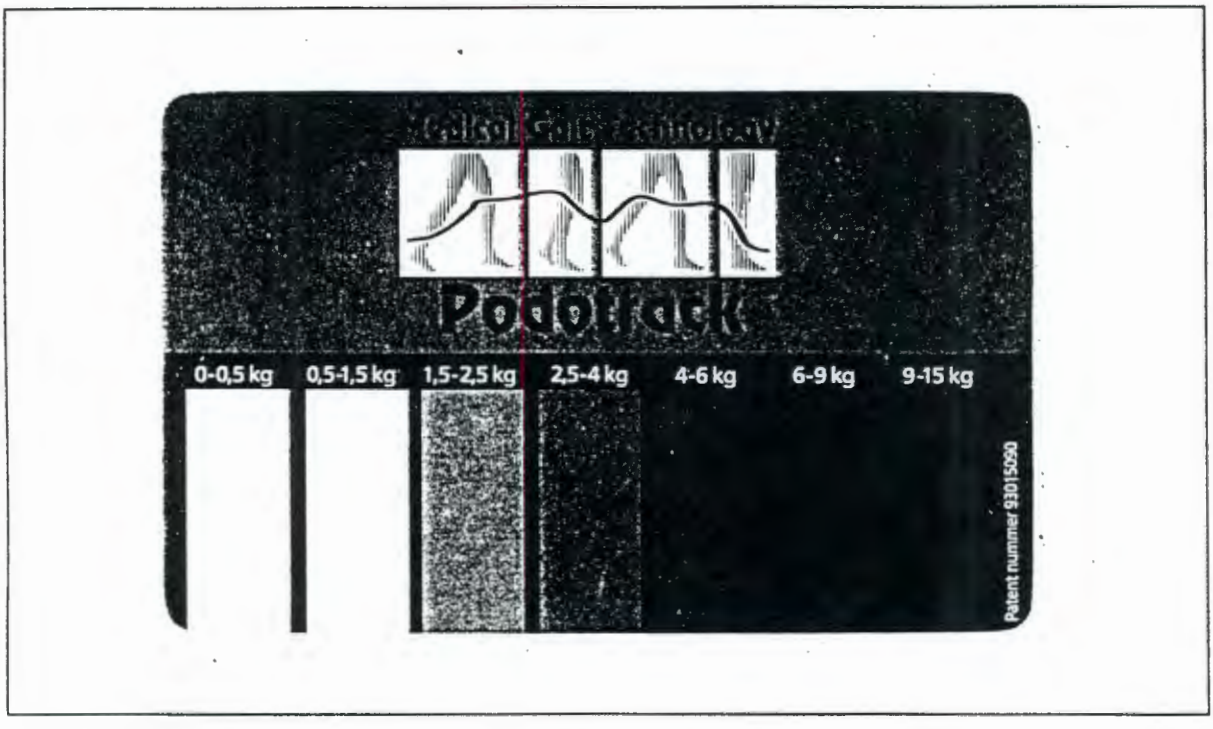

Figure 3.2 The Podotrack grey scale reference card
(See text, page60)

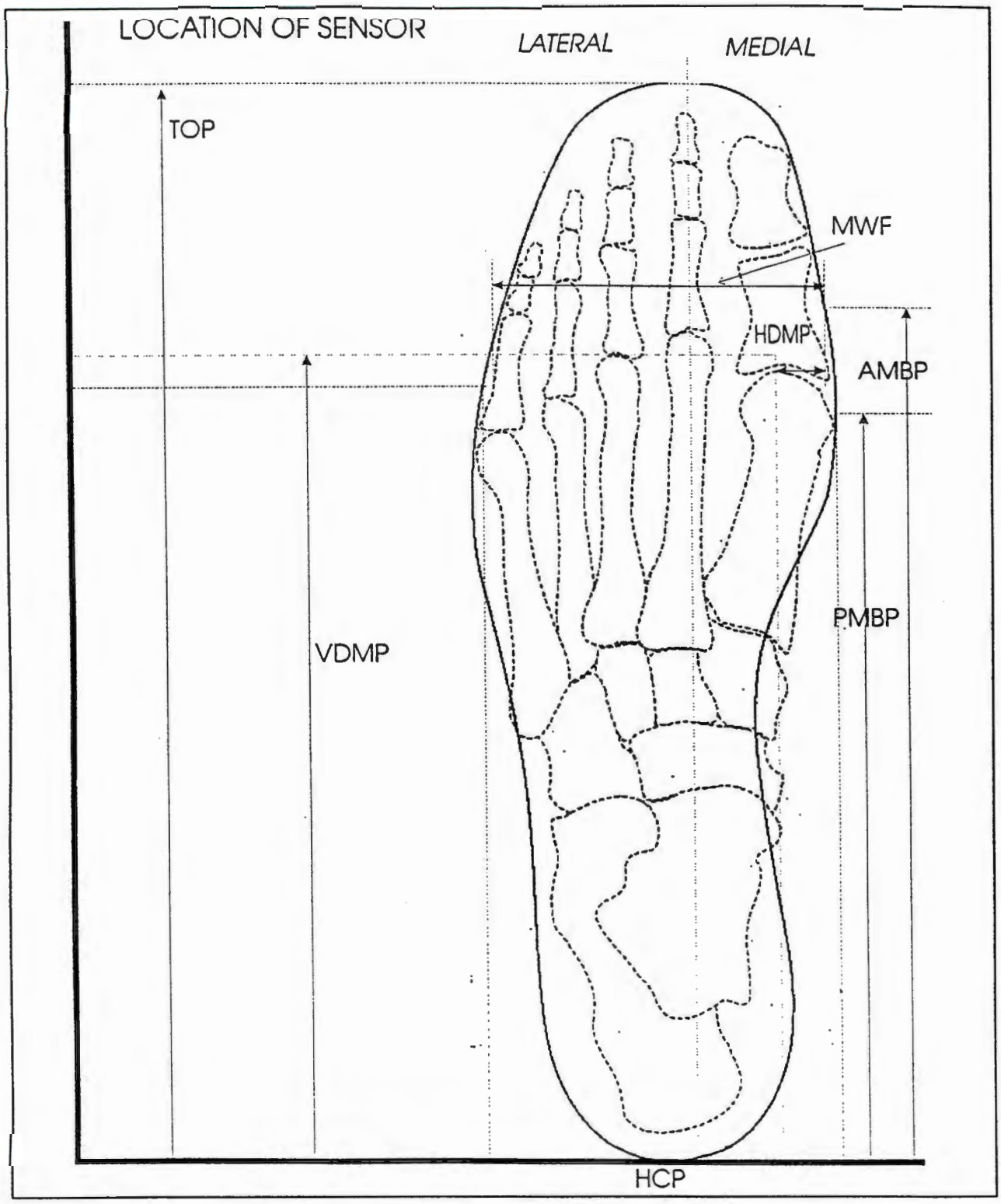

Figure 3.3 Template of a size 44 in sole and dimension lines used to locate the new sensor

(See text, page61)

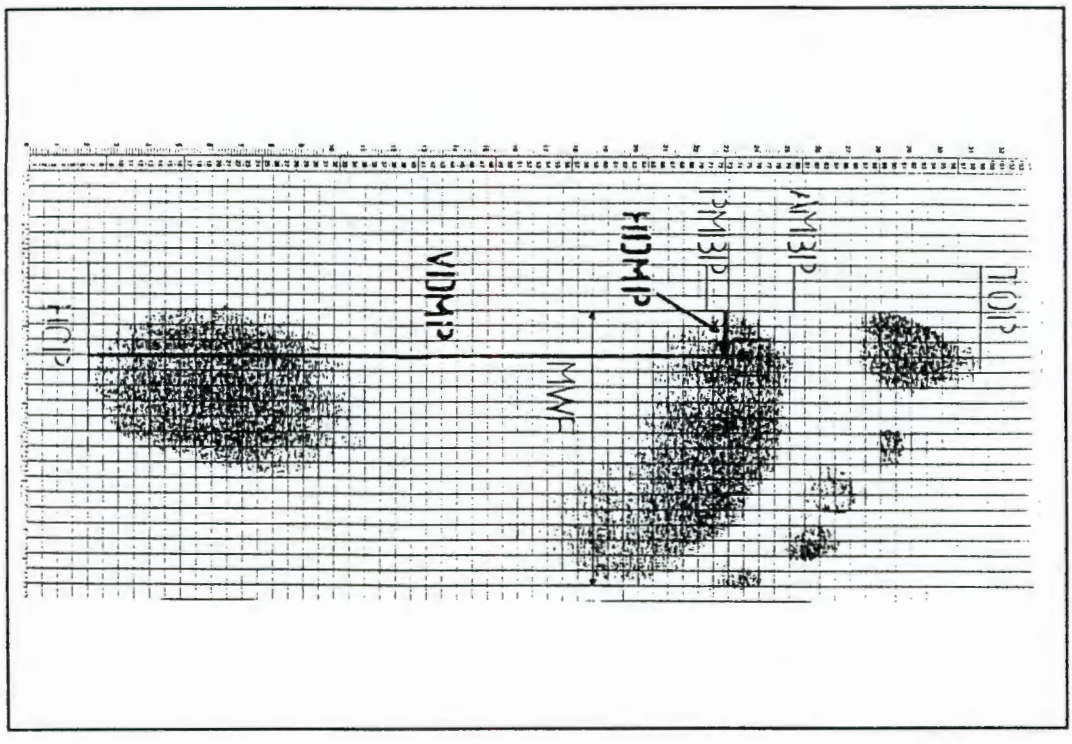

Figure 3.4 Carbon print of dynamic foot produced using the Podotrack mats with dimension lines included

(See text, page62)

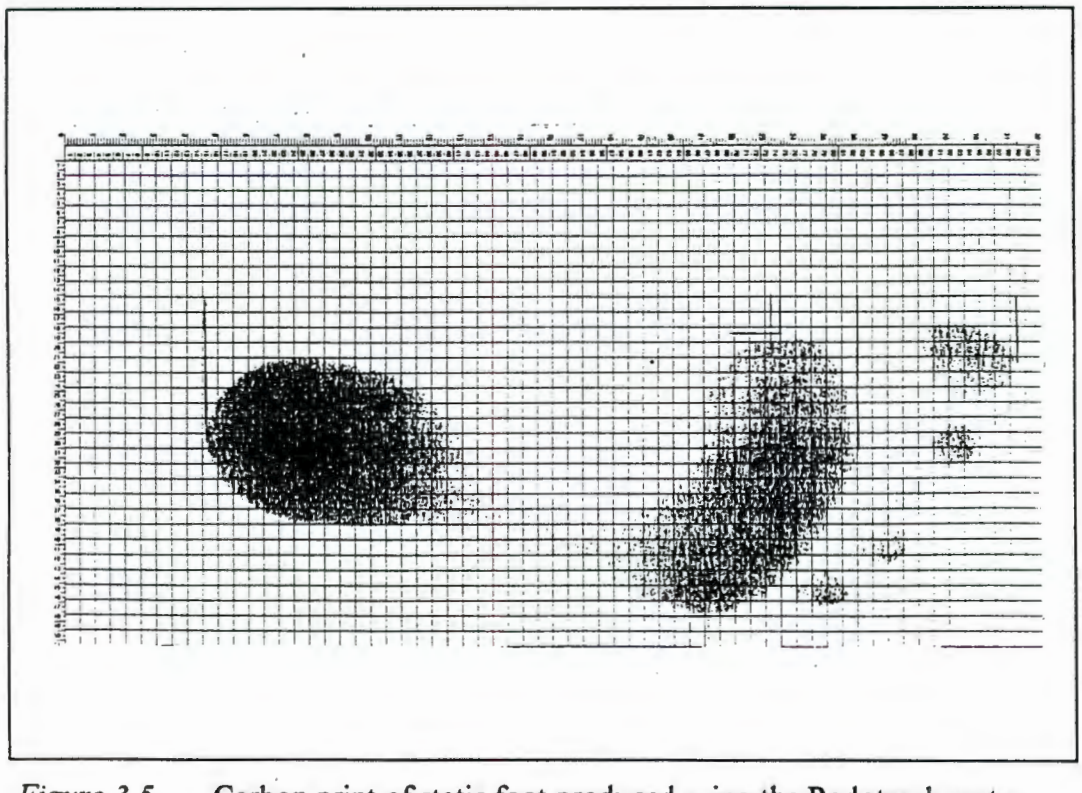

Figure 3.5 Carbon print of static foot produced using the Podotrack mats

(See text, page64)

Figure 3.6 The Adidas *footscan* equipment

(See text, page64)

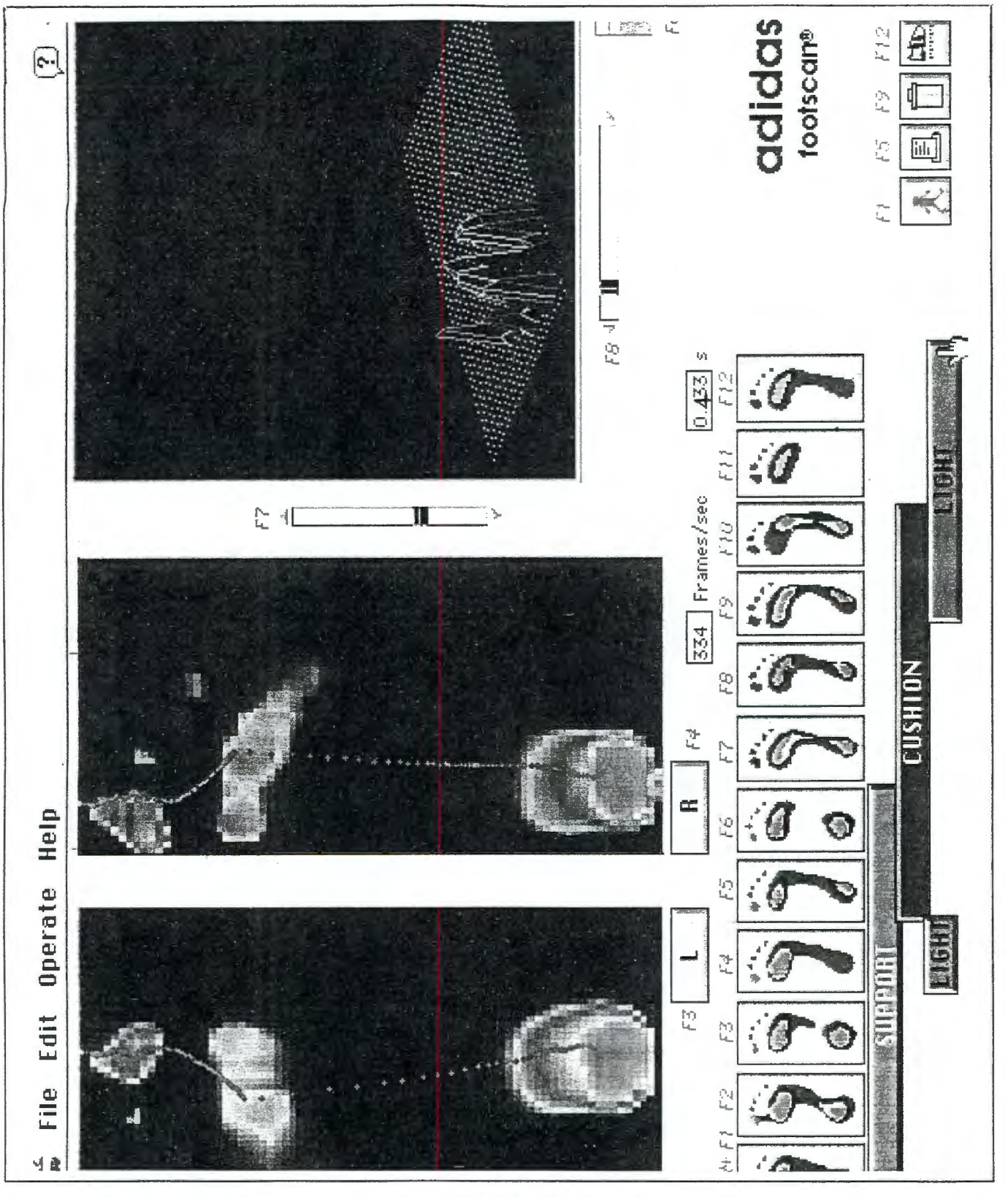

Figure 3.7 Printout produced by the Adidas *footscan* during walking at 1.3 m/sec showing the 3 D pressure image and the reference pressure distributions developed by Adidas

(See text, page65)

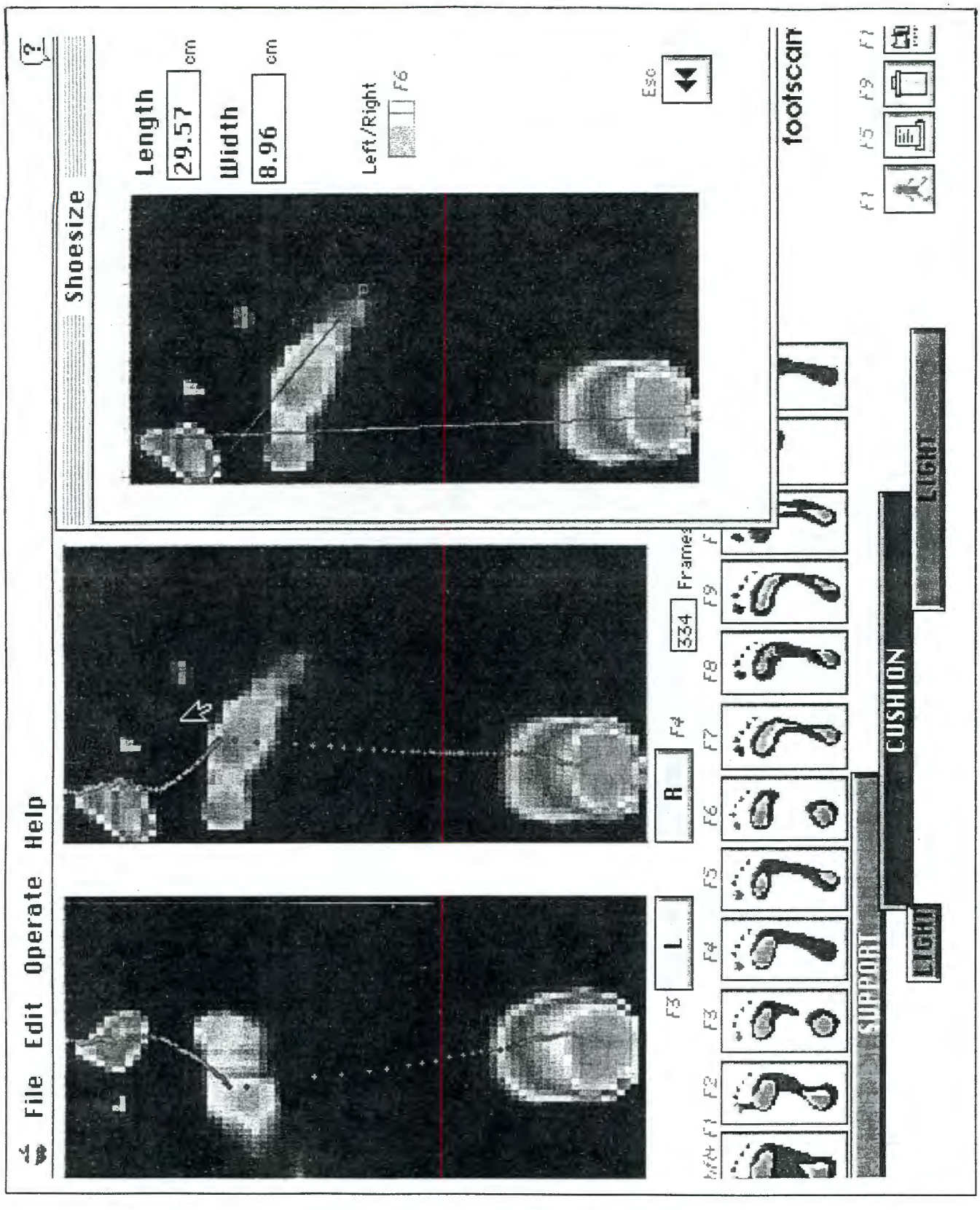

Figure 3.8 Printout produced by the Adidas *footscan* during walking at 1.3 m/sec illustrating the Shoesize window

(See text, page65)

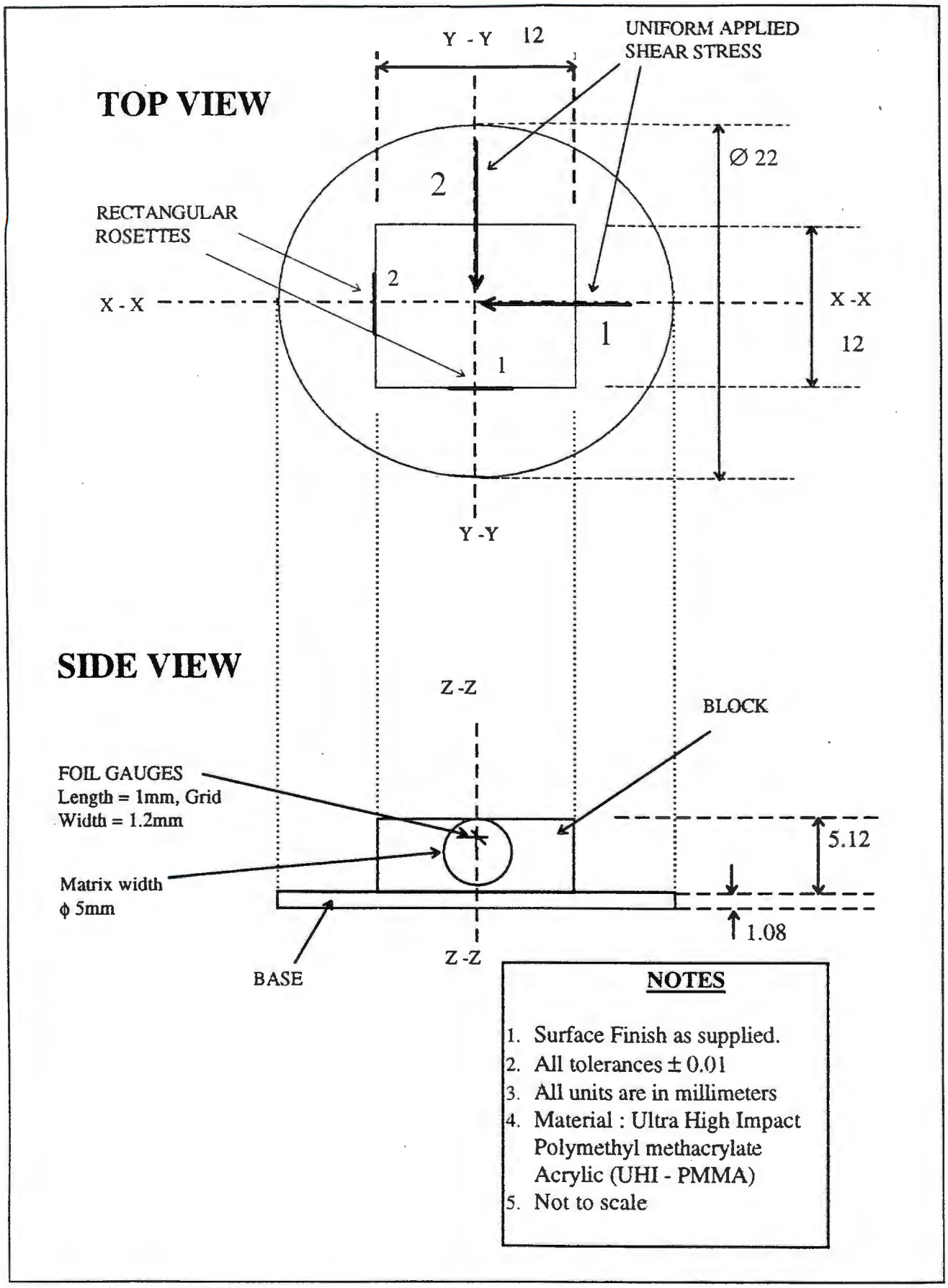

Figure 3.9 The design of the new sensor

(See text, page74)

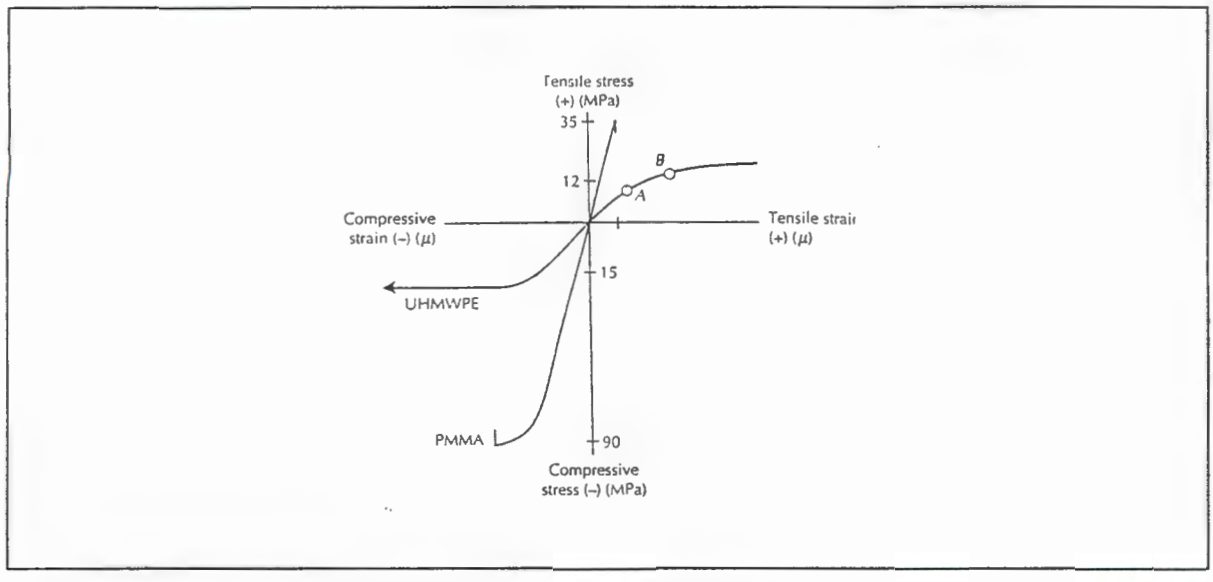

Figure 3.10 Tensile - Compressive behaviour of PMMA

(See text, page84)

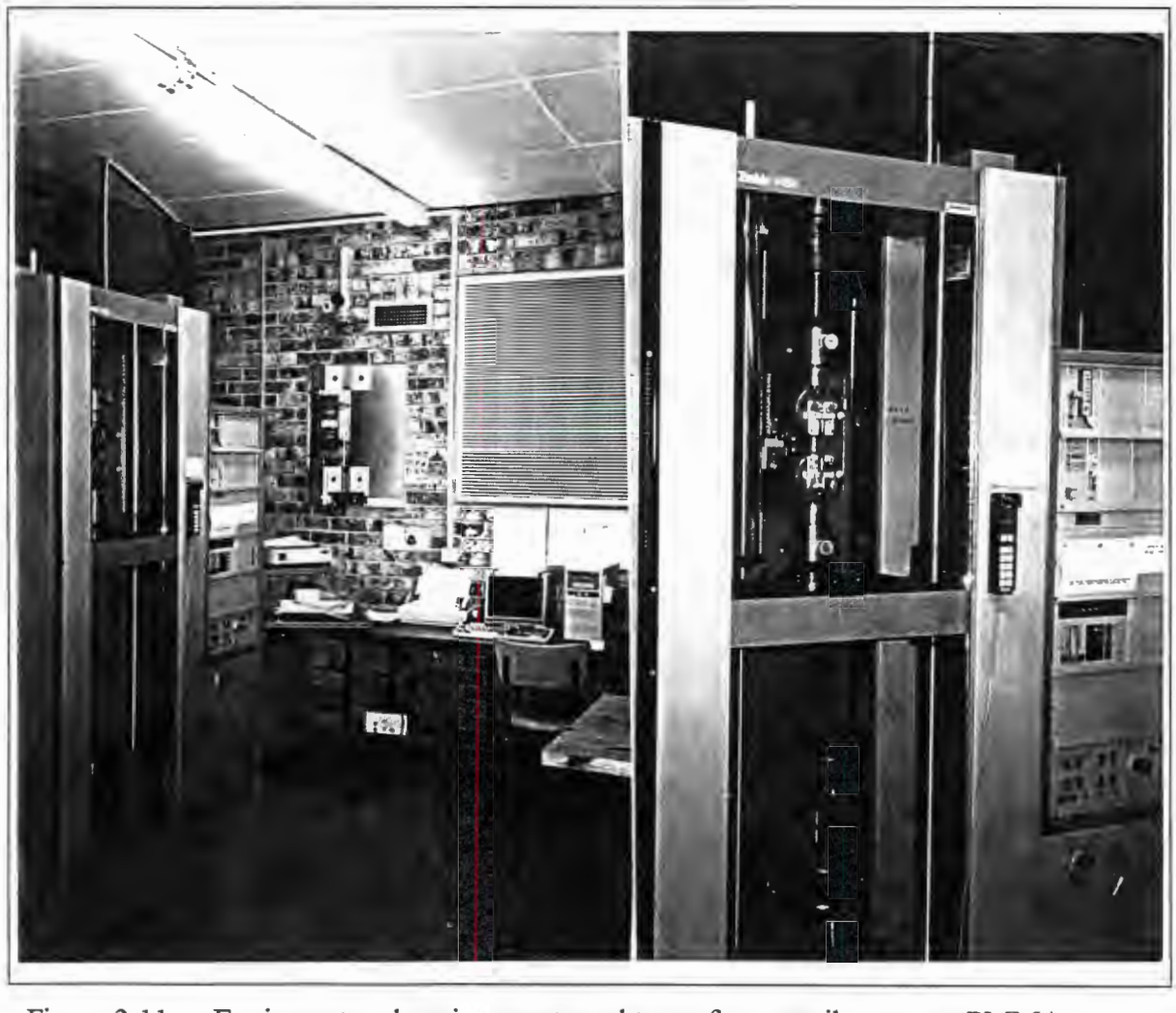

Figure 3.11 Equipment and environment used to perform tensile tests on PMMA

(See text, page87)

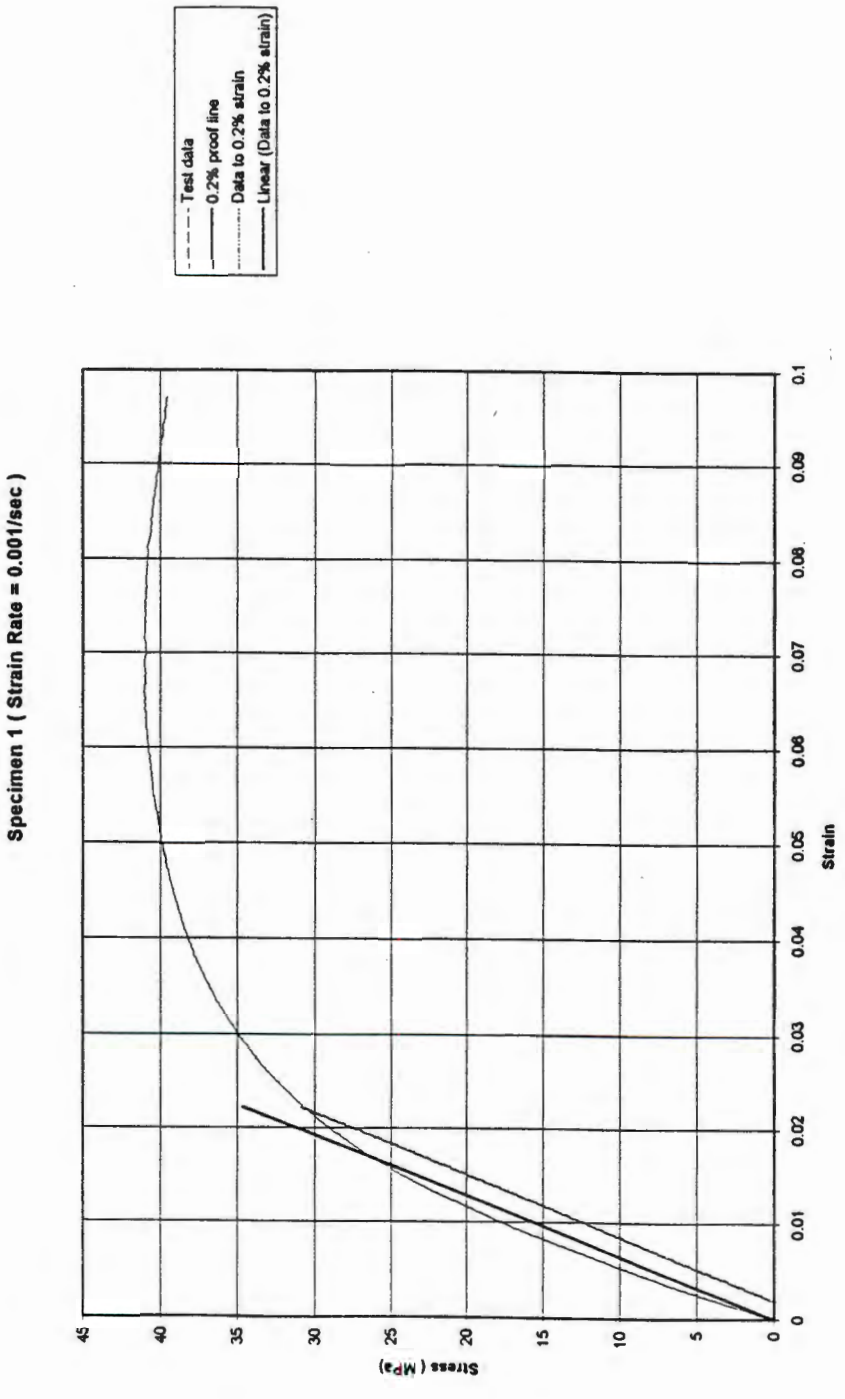

Figure 3.12 Predicted Young's modulus using ASTM standards

(See text, page88)

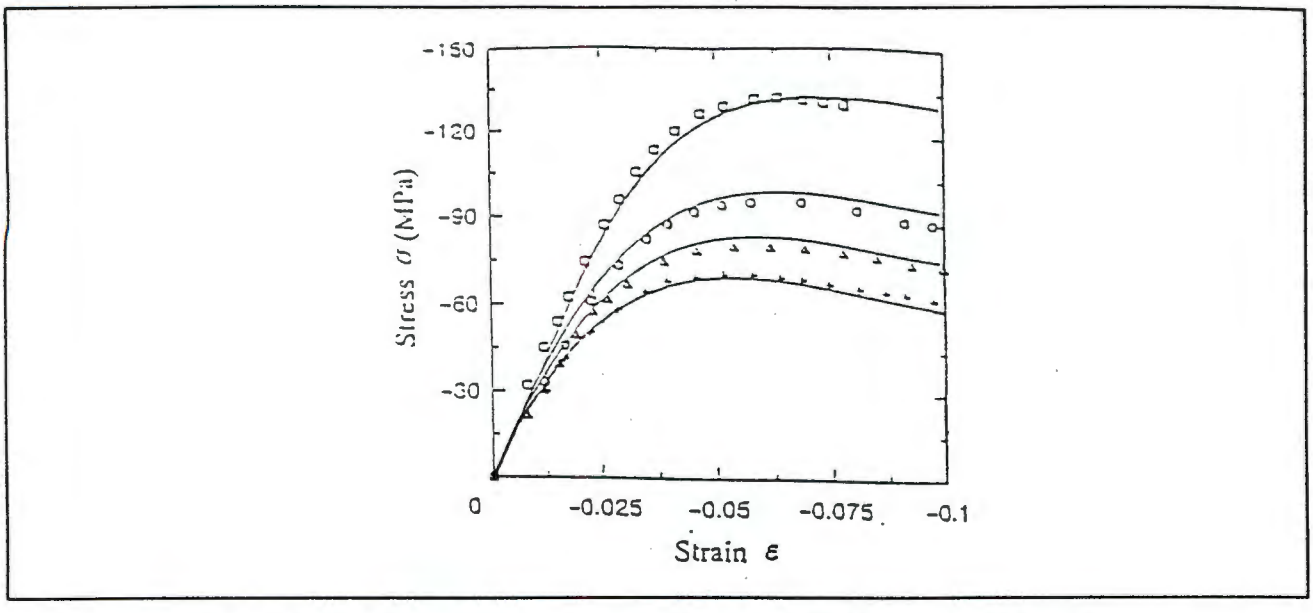

Figure 3.13 The effect of strain rate on the Young's modulus of PMMA as determined by Kitagawa et al[63]

(See text, page89)

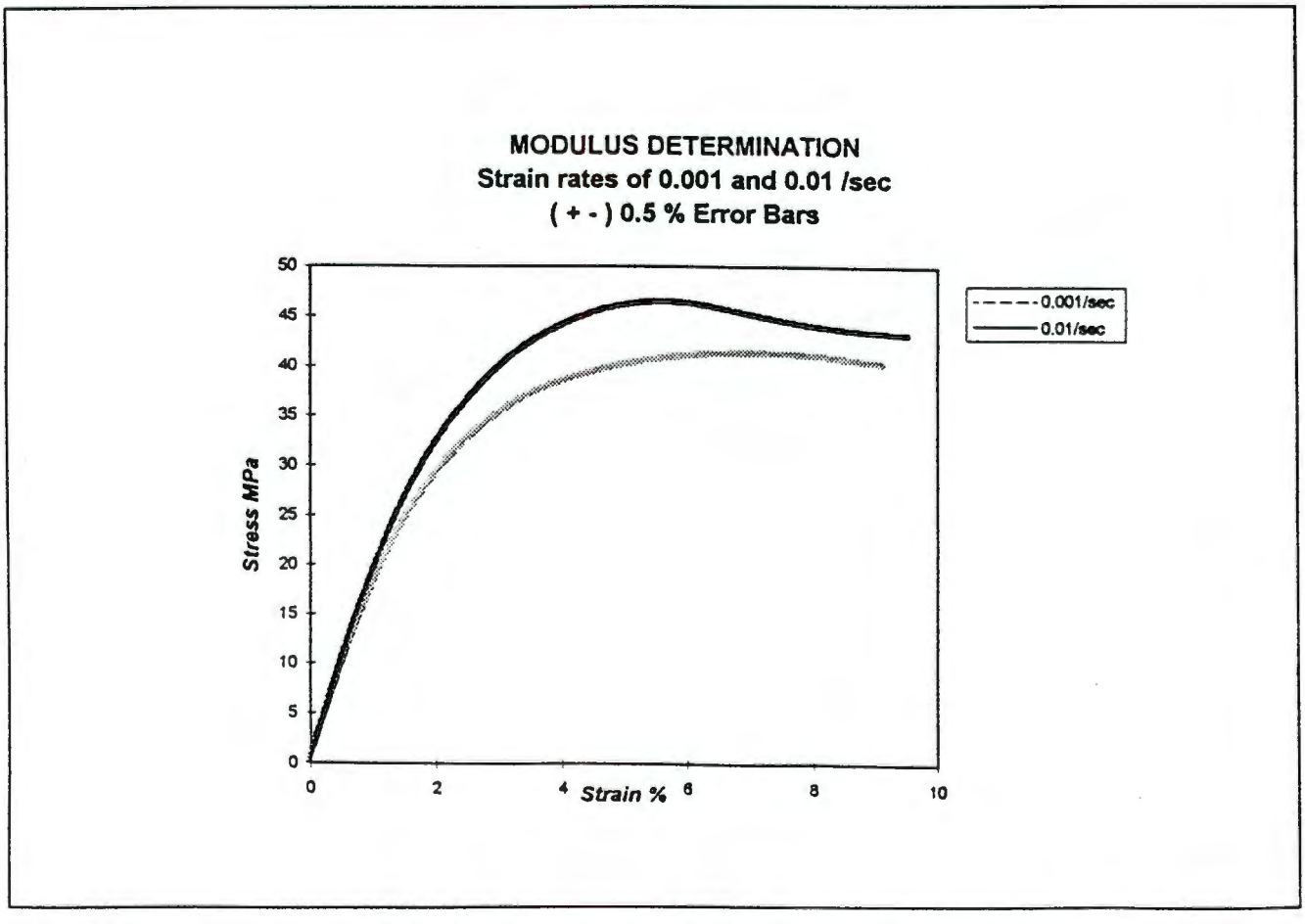

Figure 3.14 The effect of strain rate on the Young's modulus of PMMA as determined in tensile tests

(See text, page89)

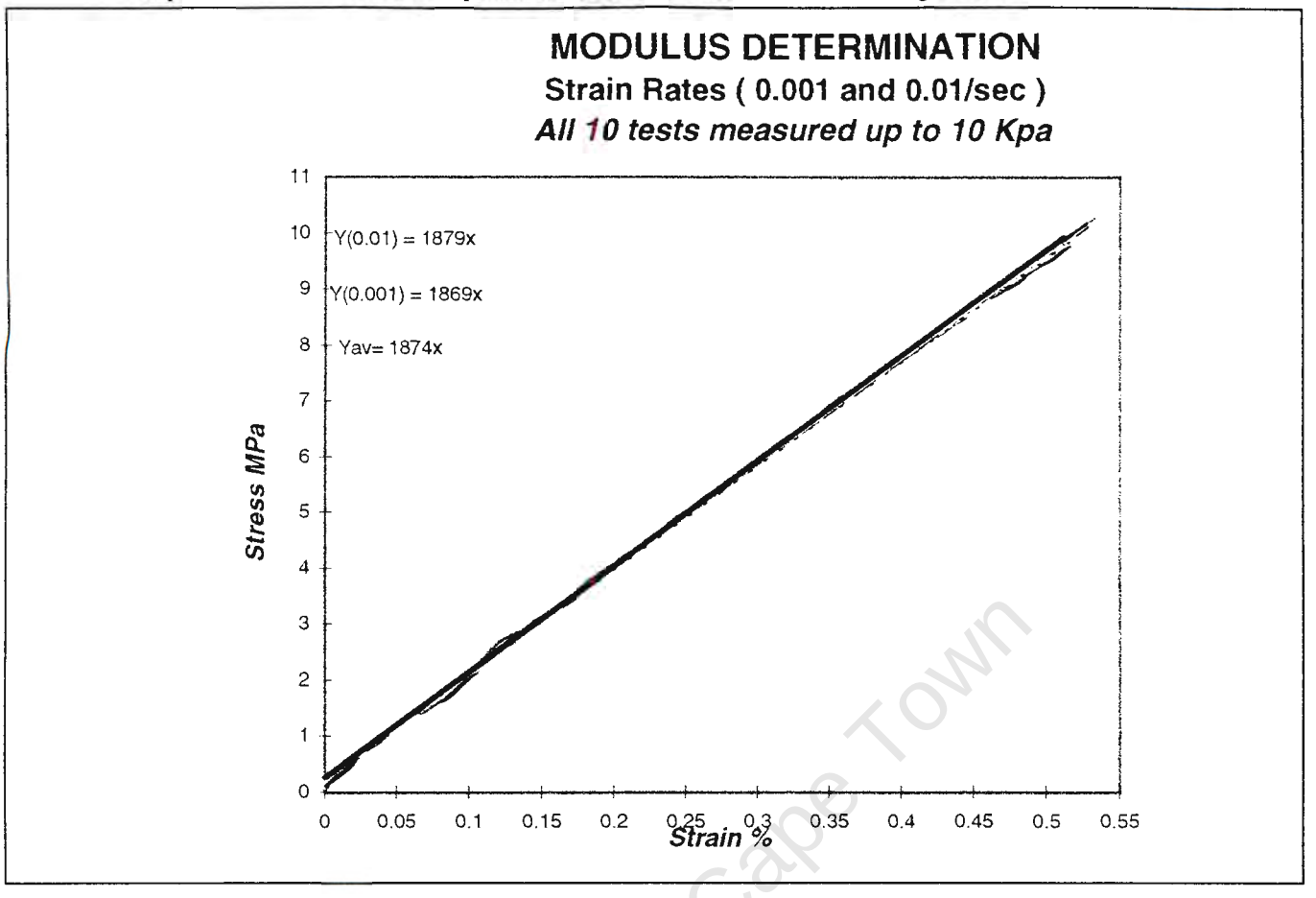

Figure 3.15 Young's modulus as measured in the tensile tests up to a stress of 10 Mpa

(See text, page89)

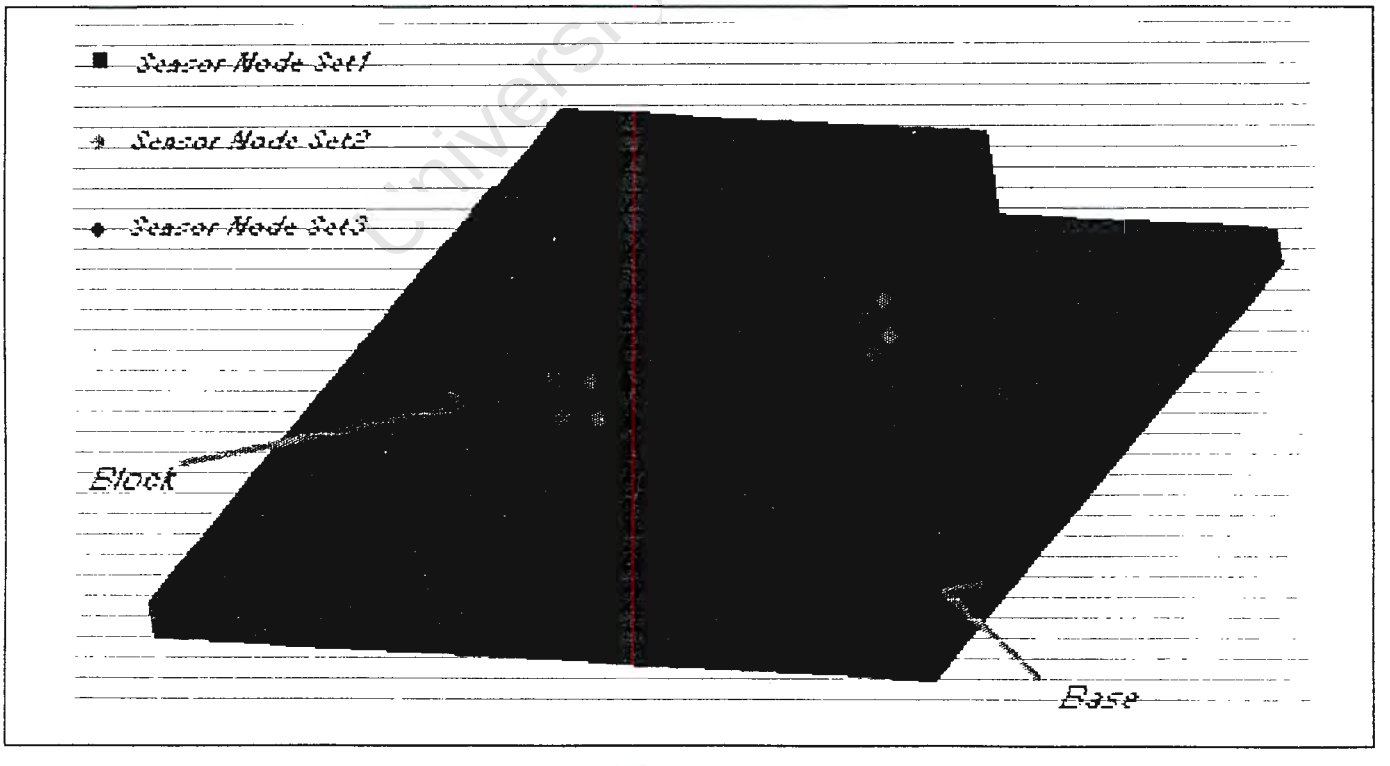

Figure 3.16 ABAQUS model of the sensor

(See text, page91)

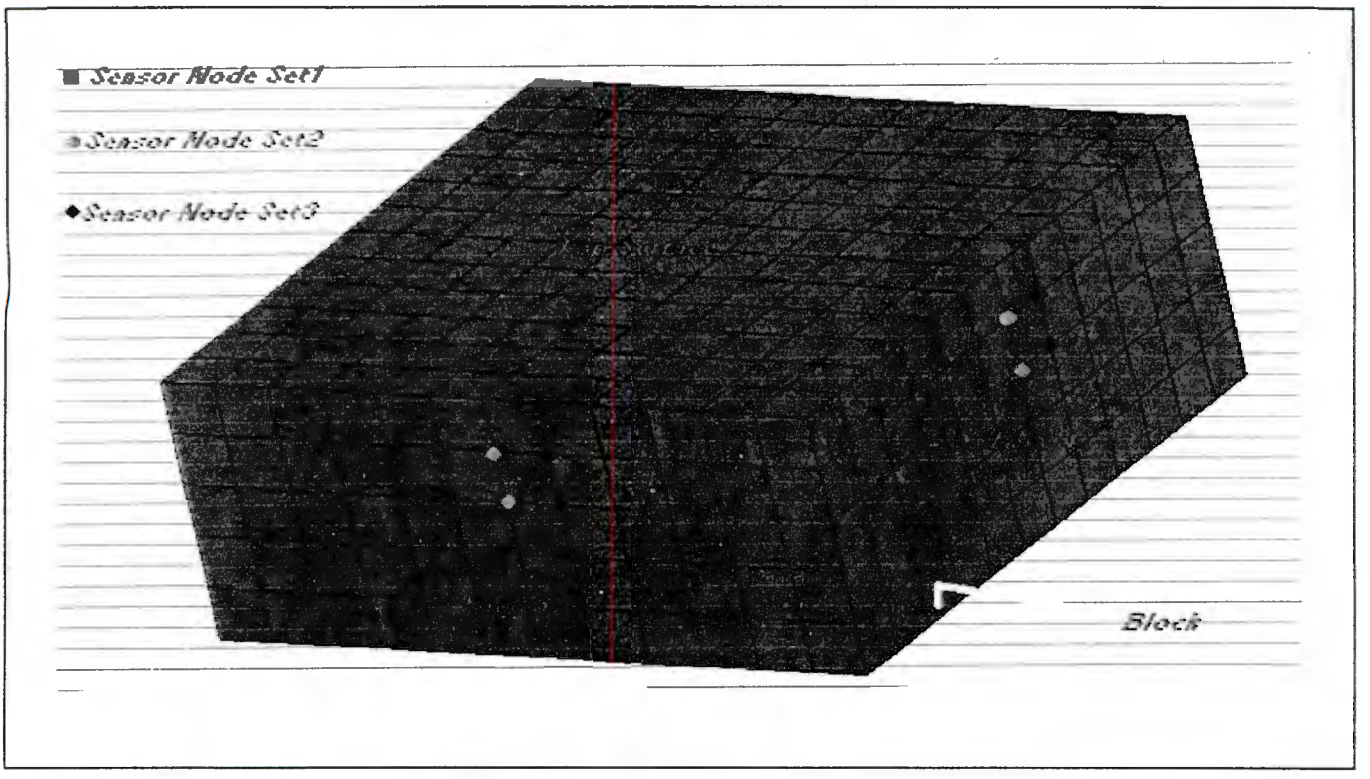

Figure 3.17 ABAQUS model of the block
(See text, page93)

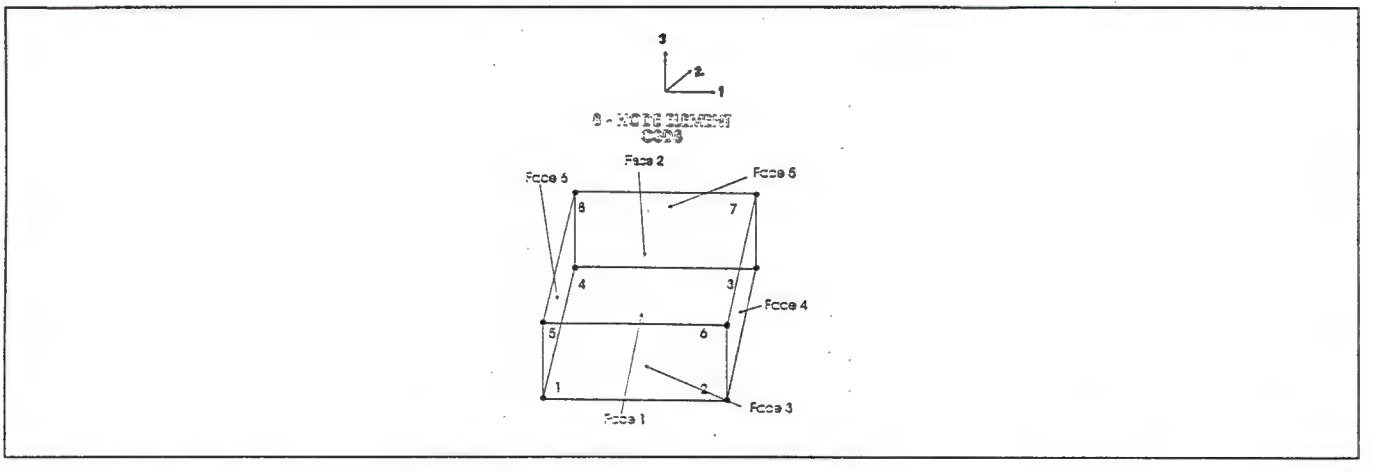

Figure 3.18 Continuum 8 - Noded C3D8 element
(See text, page94)

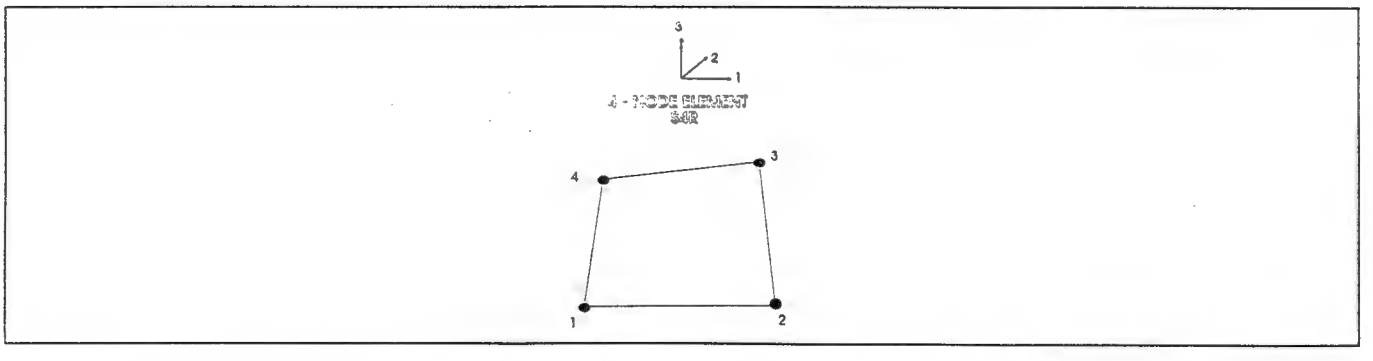

Figure 3.19 4 - Noded S4R shell element
(See text, page94)

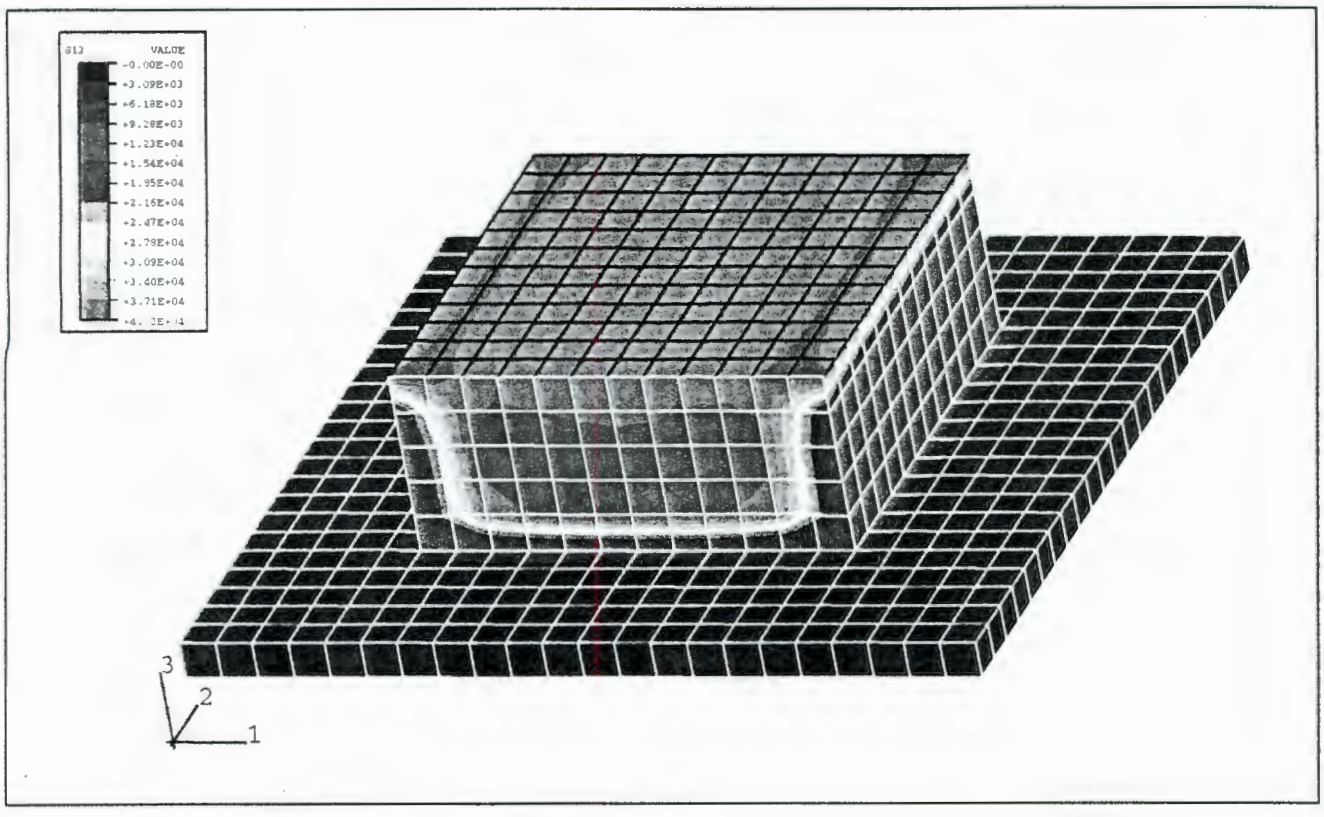

Figure 3.20 Typical predicted stress distribution experienced by the sensor during the calibration procedure

(See text, page97)

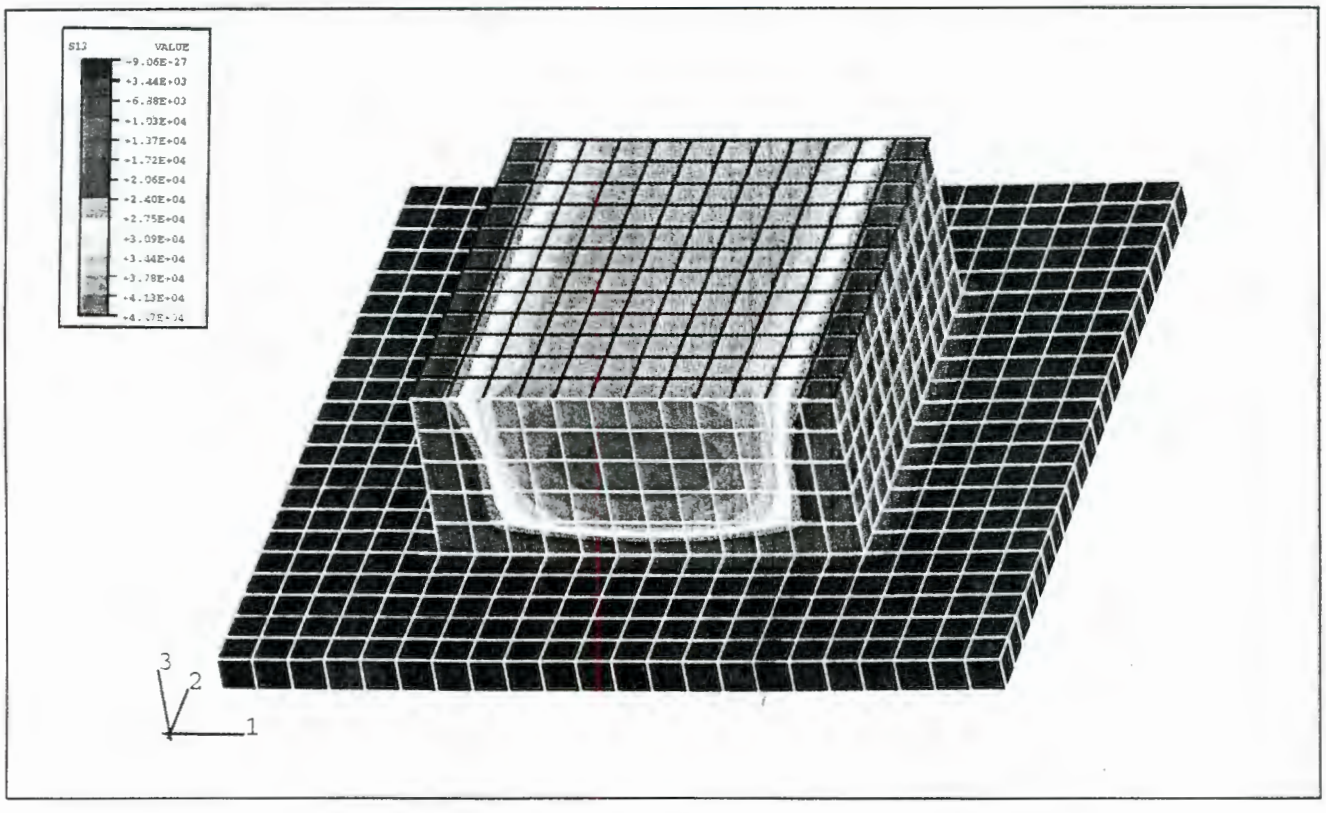

Figure 3.21 Typical predicted stress distribution experienced by the sensor when the sensor is located inside the insole

(See text, page97)

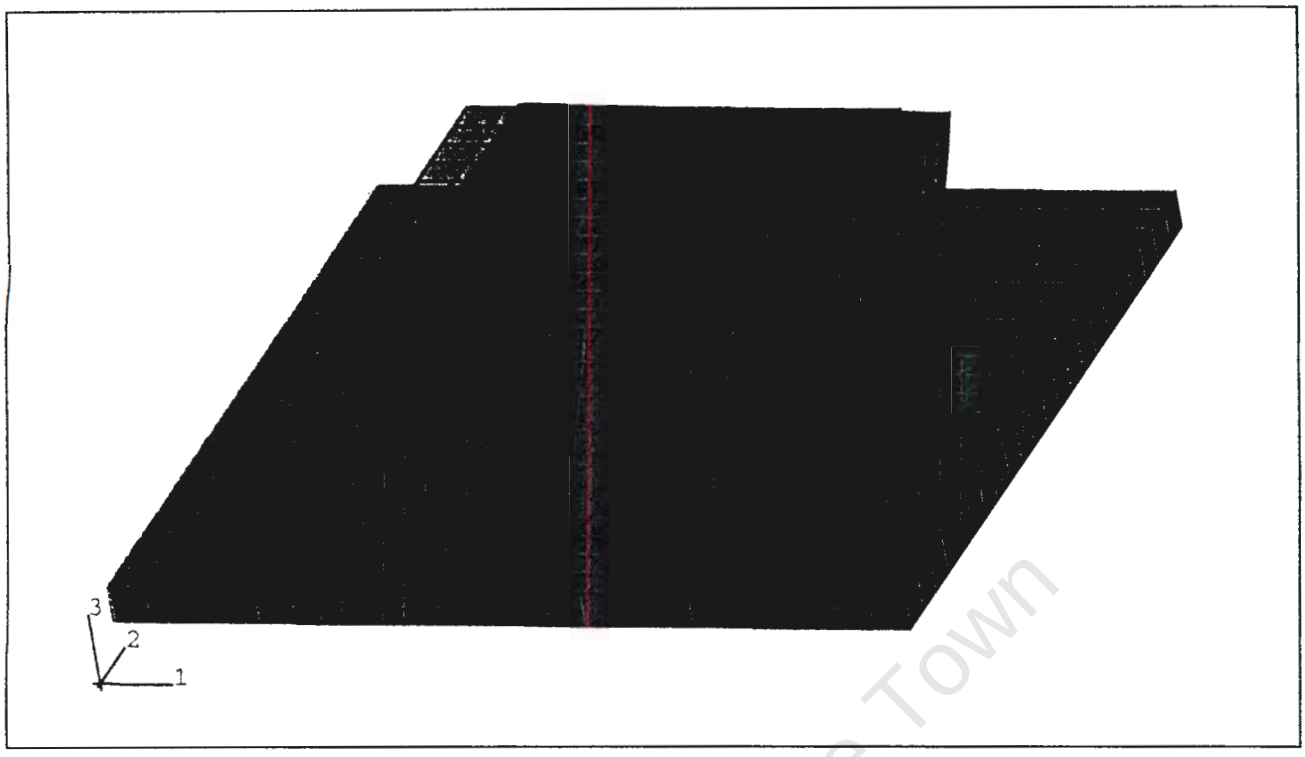

Figure 3.22 Typical predicted deformation characteristics of the sensor when a single component of shear stress is applied to the sensor during the calibration procedure

(See text, page100)

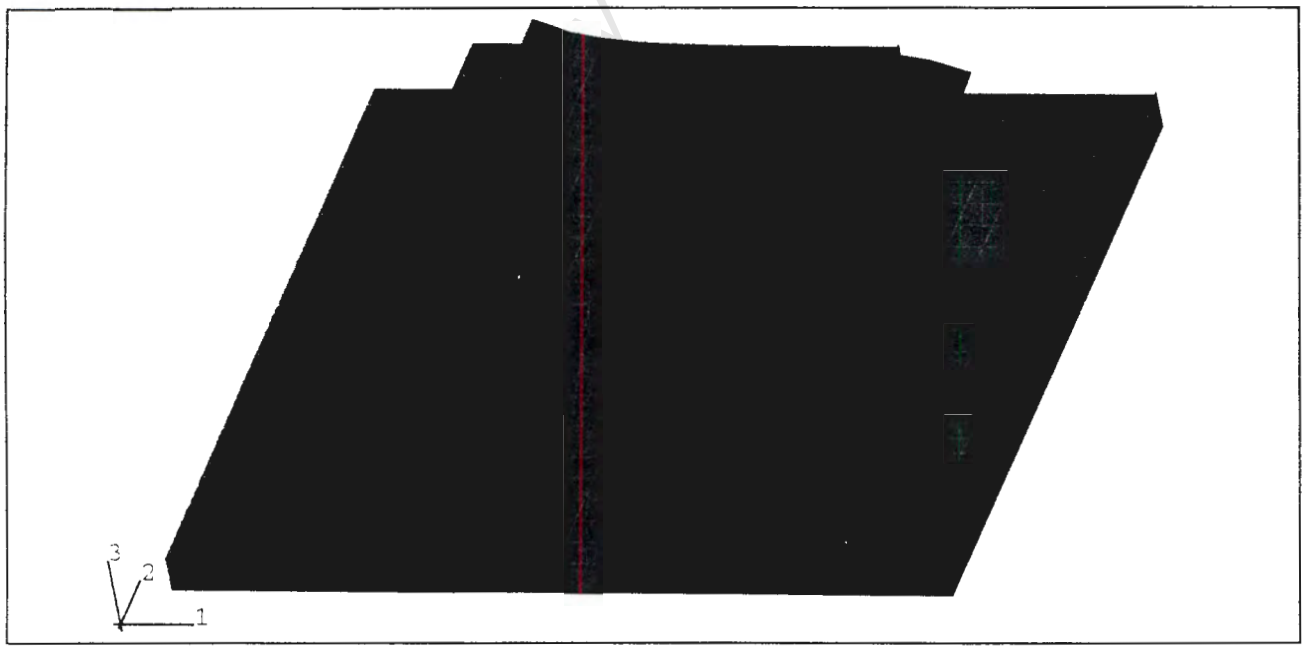

Figure 3.23 Typical predicted deformation characteristics expected of the sensor when a single component of shear stress is applied to the sensor when the sensor is inside the shoe

(See text, page100)

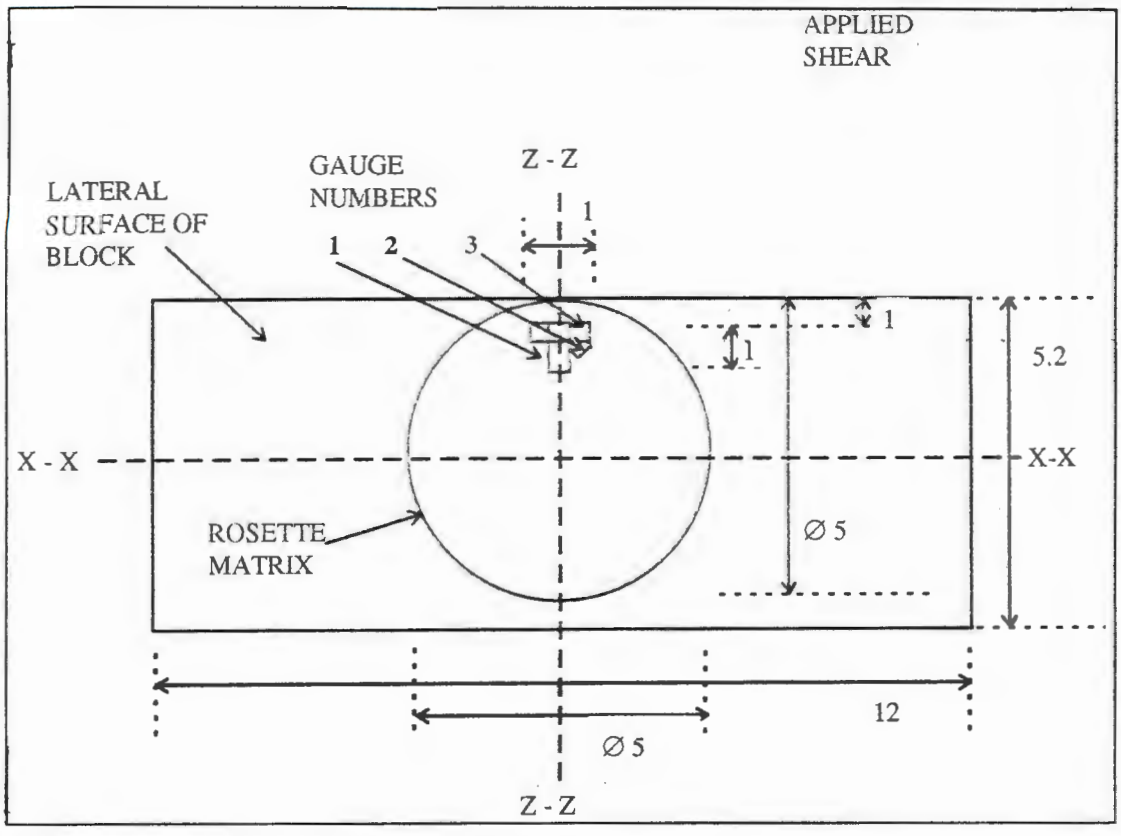

Figure 3.24 Illustration of the position of the strain gauge rosettes on one of the lateral surfaces of the sensor

(See text, page106)

Figure 3.25 The testing equipment and environment used in the calibration procedure

(See text, page106)

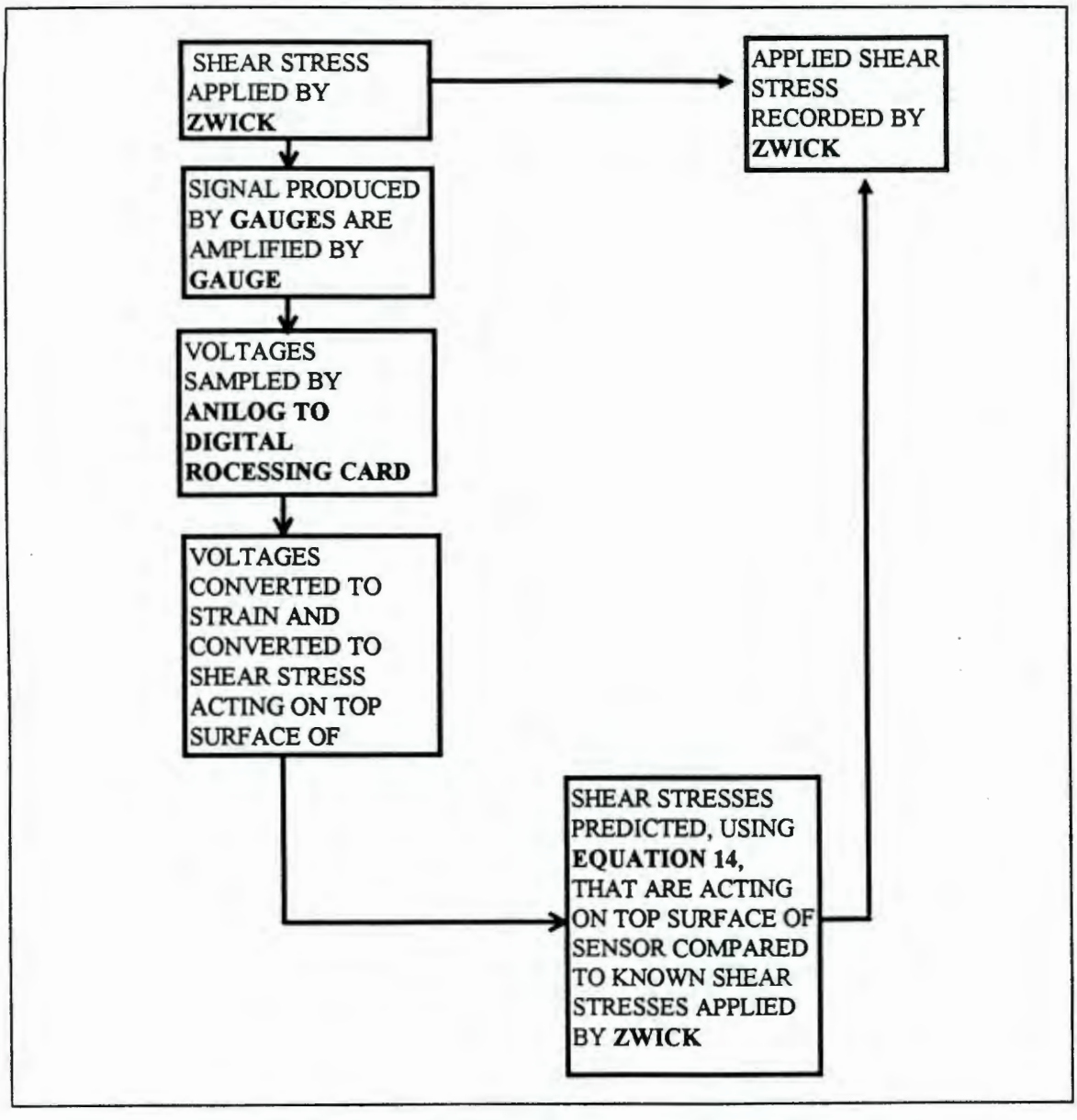

Figure 3.26 Schematic illustration of protocol used in calibration procedure

(See text, page106)

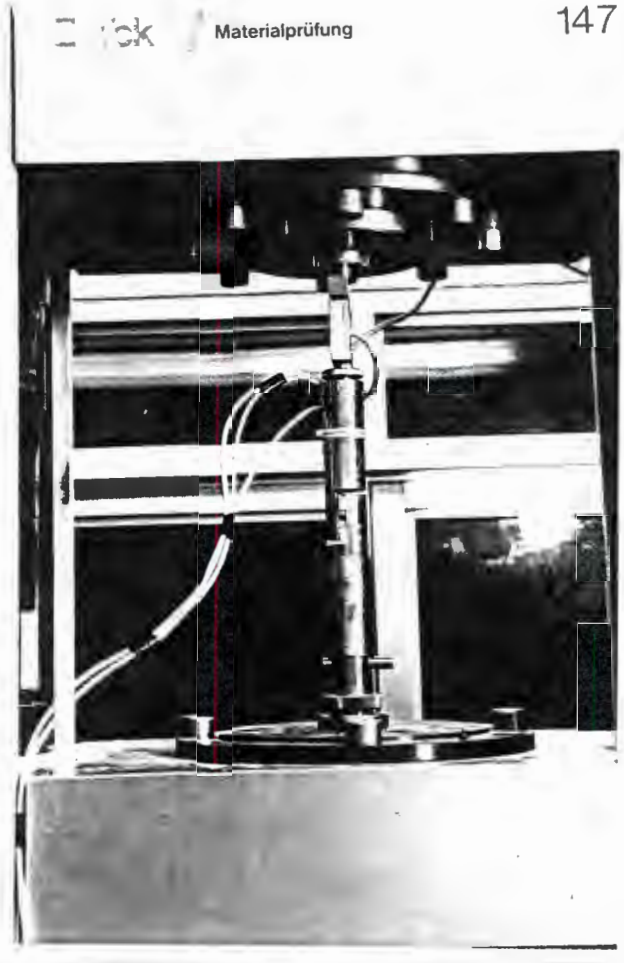

Figure 3.27 Illustration of the calibration jig

(See text, page107)

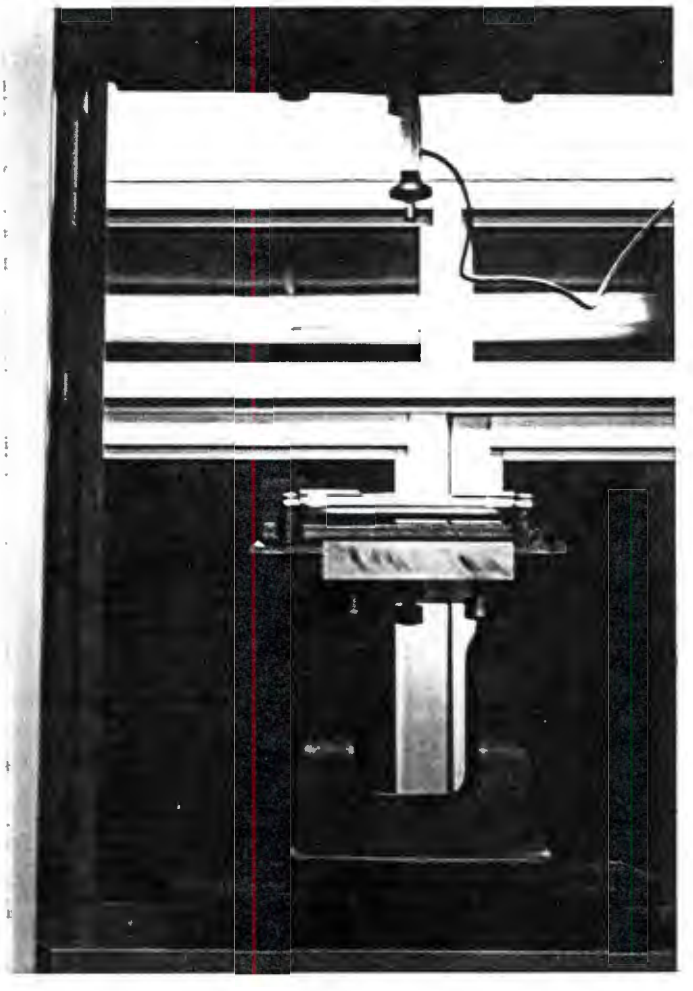

Figure 3.28 Illustration of method used to level the bottom jig of the calibration jig

(See text, page108)

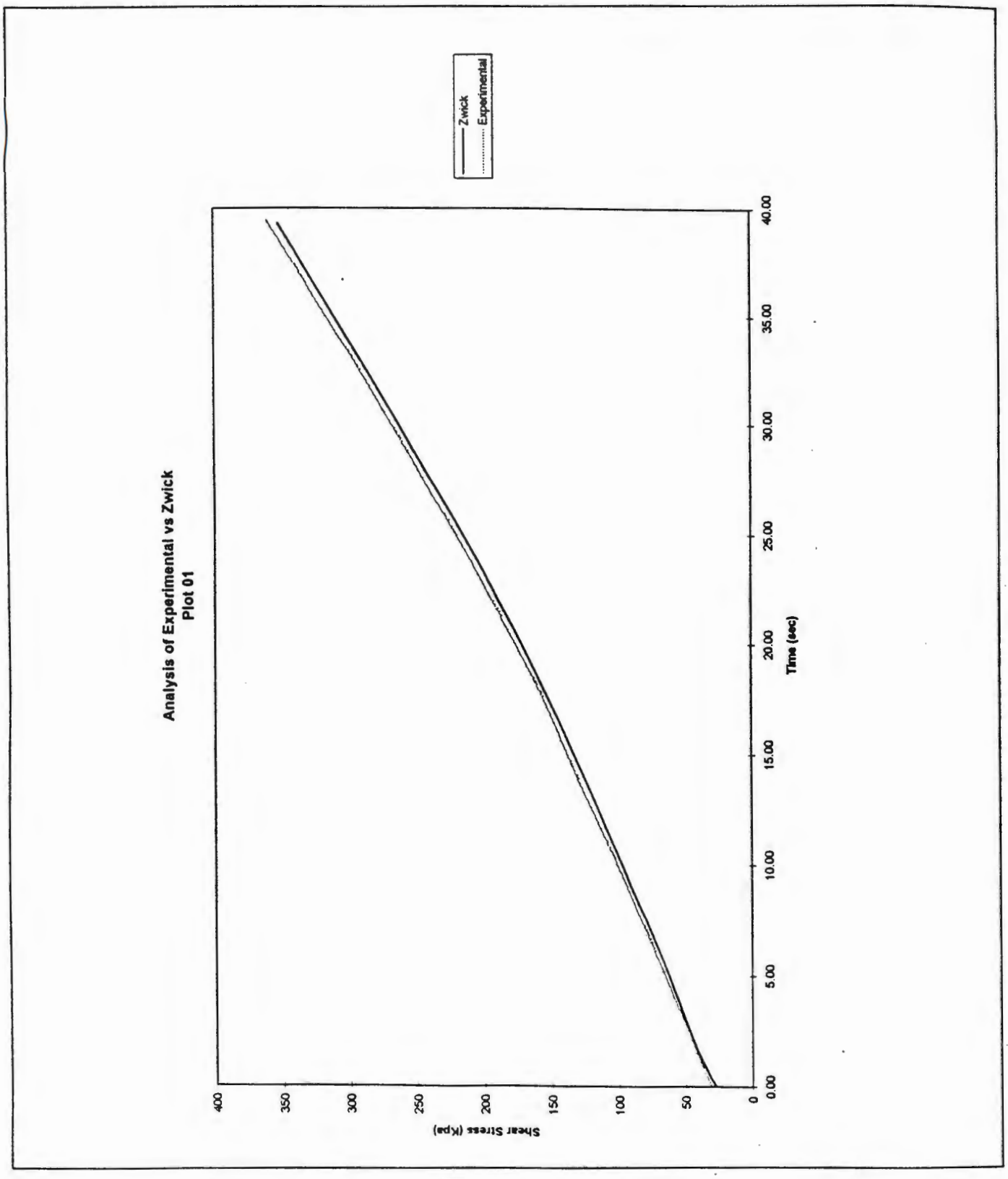

Figure 3.29 Sample illustration of the results obtained during the calibration procedure

(See text, page 110)

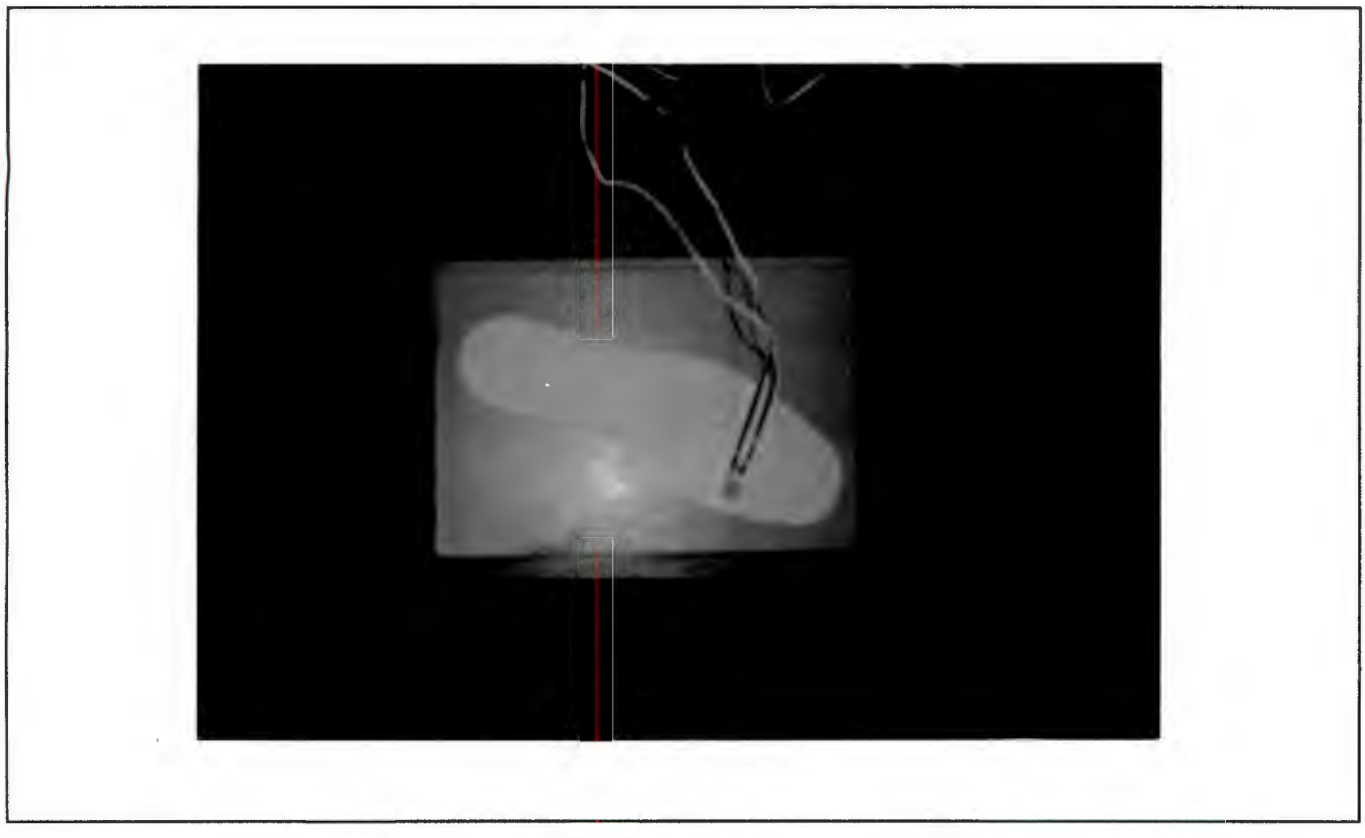

Figure 3.30 Illustration of the new in - shoe instrumented insole
(See text, page115)

Figure 3.31 Illustration of the new instrumented insole fitted to the standard diabetic shoe
(See text, page115)

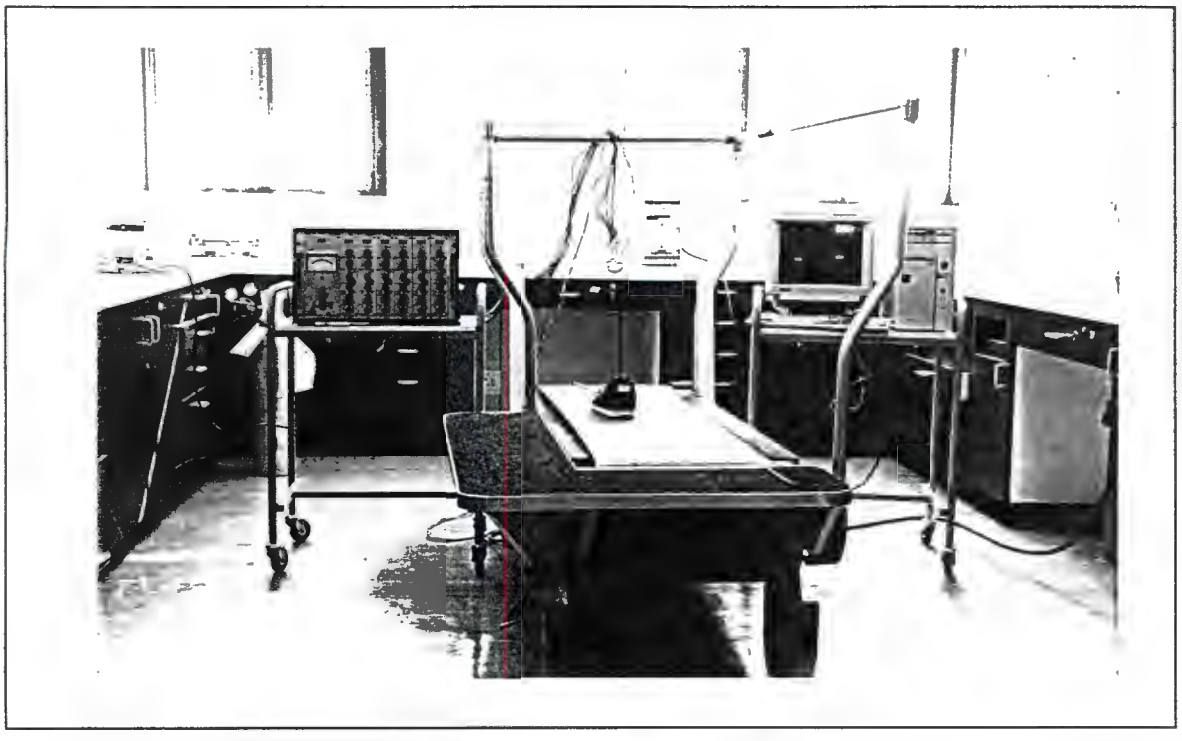

Figure 3.32 Illustration of the testing environment
(See text, page116)

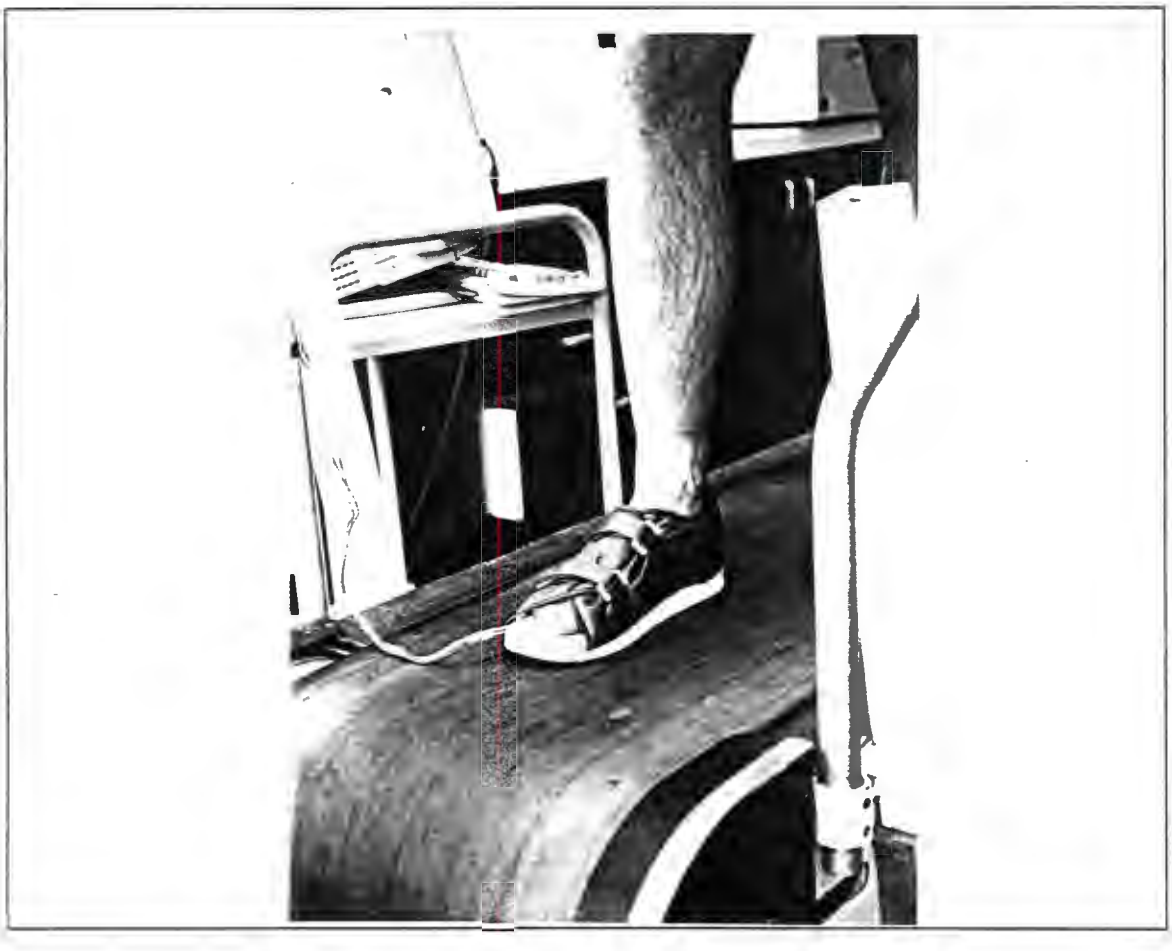

Figure 3.33 Illustration of the instrumented diabetic shoe fastened to the foot of the subject
(See text, page116)

Figure 3.34 The infra-red mini-laser temperature sensor

(See text, page116)

CHAPTER 4

IN - SHOE TEST RESULTS

4.1 TEMPERATURE REGULATION

A mini-laser (*figure3.34*) was used to measure the temperature of the sensor and the foot before and after each test. To ensure that the mini-laser performed at its maximum accuracy (±0.1°C), a ruler was fastened to it so that the sensor always measured at a distance of 30 mm from its object. When the ruler was in contact with the foot or sensor it ensured that the same area was measured with the same intensity during all tests.

The temperature of the foot was controlled so that it would not increase the temperature of the sensor when the two came into contact. To lower the temperature of his foot the subject stood on the tiled floor of the laboratory. Keeping his foot off the ground allowed his own circulation to raise the foot's temperature. In this way the temperature of the foot in the region of the first metatarsal was easily controlled at 23°C±0.5°C for the duration of each test.

It was discovered prior to testing that the two strain rosettes contained enough current to increase the temperature of the sensor to an equilibrium temperature of approximately 27°C. Although the tests could have been conducted with the sensor at this temperature by correcting its modulus, it was decided to control the temperature of sensor at 23.0°C±0.5°C by placing the instrumented insole inside a fridge prior to testing. The reason for selecting this method was that the modulus which was being used, had been determined at 23.0°C±1°C.

The shoe was removed from the fridge at a temperature of approximately 21°C. A test was conducted when the sensor was at 23°C±0.2°C. It was found that the temperature of the sensor had increased by an average of 0.3°C after each test. This is attributed to the contact of sensor with the skin and the heat generated by the sensors. The average temperature of the sensor during all the tests was 23.2°C. Any test whose final temperature was greater than 23.5°C was rejected. Using this quality control procedure allowed the errors induced by temperature to be kept below an average of ±0.26% of the Full Scale Output when calculating the stresses from the strains measured by the gauges.

4.2 PILOT TESTS

The pilot tests were used to examine the following four phases.

1. Zero Load Phase.
2. Scuffling Phase.
3. Standing Phase.
4. Walking Phase.

An illustration of one of the pilot tests, illustrating the four parameters presented above, is shown in *figure 4.1*.

4.2.1 THE ZERO PHASE

The sensor was allowed to experience zero load for an average of 12 seconds before the foot was placed inside the instrumented shoe. This time period is explained in *section 4.2.5*. *Figure4.2a* and *b* illustrate the drift which was experienced during one of the pilot tests.

A linear regression provided the means of predicting the average value of stress after 12 seconds. The difference between the initial value and final value of stress indicated the error which was imposed on the sensor as a result of drift. The average drift over 12 seconds for the five tests was ±0.92Kpa (±0.263% of Full Scale Output) for the Medial-Lateral gauge and ±0.99Kpa (±0.283% of Full Scale Output) for the Anterior-Posterior gauge. Although it is impossible for the amplifier to measure strains at this level, the results which were obtained were used to indicate the ability of the amplifier to maintain a fixed setting.

4.2.2 SCUFFLING ANALYSIS

The scuffling phase (2) illustrated in *figures 4.1a* and *4.1b* showed that when the foot was placed inside the shoe, the sensor was initially subjected to stresses in the posterior and lateral directions. The initial stresses in the lateral direction are attributed to the position of the foot inside the shoe and the tightening of the velcro around the foot which pulled the foot laterally. The initial stresses in the posterior direction are attributed to the foot being placed in the shoe from the front and the presence of the small camber in the front part of the shoe. The camber is visible in *figure3.31* and *figure3.33*. The variation of these stresses is attributed to the movement of the foot inside the shoe and shoe having being partially lifted off the ground to allow the shoe to be attached to the foot.

4.2.3 STANDING ANALYSIS

The subject stood on the treadmill in the standing position for an average time of one second before it was switched on. One second of standing provided 50 data points. The reason for having the subject stand stationary prior to walking was to provide an alternative means of obtaining footswitch data.

Footswitch data enables the contact time of the foot with the ground, i.e. the stance phase, or the time of one gait cycle to be evaluated. Footswitch data is usually obtained using video techniques or highly sensitive pressure transducers placed on the heel and big toe of the foot. The footswitch data must be synchronised with the data being gathered by the transducers inside the shoe.

Synchronising the footswitch data with the transducer data enabled a trigger, controlled by the footswitch data, to activate the shear transducer when the foot first came into contact with the ground. This enabled the data presented in the literature to be referenced to zero and the effects of any scuffling which occurred inside the shoe prior to walking to be ignored. An illustration of footswitch data is presented in *figure2.17*. The time between each "on" signal in Lord et al's study[16] is indicative of a gait cycle.

To reduce the complexity and costs of the experimental apparatus, a simpler method of obtaining a datum was used. The datum was produced using the average stress which occurred during the standing position. Any deviation of stress above or below this datum was indicative of a stress in either the Medial/Anterior or Lateral/Posterior directions respectively. The datum also allowed the total time of the gait cycle to be determined. The use of the datum is shown during the walking phase discussed in *section 4.2.4*. The datum therefore allowed the data measured during the walking phase of the tests conducted in this thesis to be compared to data presented in the literature. An illustration of the standing phase, the datum line and the walking phase is presented in *figure4.3*.

4.2.4 WALKING ANALYSIS

The final stage of the pilot tests was the walking phase. In order to present the data in a format comparable to the literature, the average value of the stress which determined the datum line was normalised to zero (*figure4.4a and b*). Although a full analysis was not performed on all the results of the pilot tests, being done rather on the analysis tests, the following parameters were investigated to assess the validity of the magnitude and profiles of the stresses measured by the sensor.

- The results showed repeatability, which indicated the consistency and reliability of the sensor*(figure4.4a and b)*. The magnitude of the stresses experienced by the foot in the anterior and posterior directions were in close agreement with the results produced by Lord et al[16] and Pollard et al[55]. The results produced by Lord et al[16] are summarised in *Table 4.1*.

The values presented in *Table 4.1* are the mean maximum shear stresses. The negative medial shear stress which is presented was indicative of a medial shear which has occurred with a value was than the lateral pre-stress which existed on the sensor during the test. This resulted in it being presented as a negative value. As a number of normal subjects were used during Lord et al's[16] studies, a range of the mean maximum shear stresses measured in this study are presented. The range of values indicates the variation which is possible between subjects, who present different shear profiles as a result of their individual gait patterns even though they have a similar mass. This further illustrates the necessity for normative data bases and the development of new devices.

Range of Anterior Shear Stresses	**Range of Posterior Shear Stresses**	**Range of Medial Shear Stresses**	**Range of Lateral Shear Stresses**
(kPa)	**(kPa)**	**(kPa)**	**(kPa)**
4.23±0.8 and 14.13±0.8	33.14±1.26 and 58.4±8.08	-1.53±0.62 and 3.54±2.12	14.5±4.95 and 21.2±1.48

Table 4.1 Shear data presented by Lord et al[16]

A series of experiments were also performed by Pollard et al[55]. A single subject was used in their tests. The results presented in *Table 4.2* are the mean maximum shear stresses which were measured during Pollard et al's[55] tests.

Anterior Shear Stresses	**Posterior Shear Stresses**	**Medial Shear Stresses**	**Lateral Shear Stresses**
(kPa)	**(kPa)**	**(kPa)**	**(kPa)**
8.17±1.3	41.83±12.97	17.34±0.73	14.23±1.65

Table 4.2 Shear data presented by Pollard et al[55]

The mean maximum posterior and anterior shear stress measured during the pilot tests conducted in this thesis were 69.3kPa ±8.93kpa and 9.9kpa±2.61kpa respectively. The anterior stresses were in close agreement to the literature but the posterior stresses although significantly higher, were considered close enough to the literature to validate the performance of the sensor. Justification for this is given in *section4.2.5*.

The maximum stresses measured in the medial and lateral directions during the pilot tests were 18.8kpa±1.57kpa and 67.9±7.82kpa respectively. The range of medial stresses were in close agreement with the literature but the lateral stresses were significantly (approximately 3.7 times) greater than those presented in the literature. The lateral shear stresses measured using the new device are nevertheless regarded as being accurate for reasons given in *section 4.2.5*.

- The average time of the gait cycle for one of the tests (test 2) was examined. It was determined by measuring the time taken for a repeated series of stress data to re-intercept the datum line. This is illustrated as the time "T 1" in *figure4.5a* and *b*. The average gait cycle time for test 2 was 1146±46.8msec which corresponds to a stance time of 710±46.8msec. This is because the stance phase occurs for 62% and the swing phase 38% of the gait cycle[1]. This correlates well with the stance times measured by the footscan (647±52msec) used in this thesis and the average gait cycle times measured by Lord et al[16](1112.32±21.79msec) and Pollard et al[55](1101.55±11.27msec). The differences between the times could be attributed to the controlled stride lengths which were experienced during treadmill tests.

  Although it is only possible to determine the beginning and end of the gait cycle using footswitch equipment, a technique was developed in this thesis to give an approximation of the correct position of the gait cycle. The position is shown as "T2" in *figure4.5a* and *b*. "T1" was relocated to "T2" ("T2" has exactly the same magnitude as "T1") because maximum shear stresses typically occur at approximately 68% of the stance phase[19,32] (i.e. 42% of the gait cycle). With the gait cycle in the correct position, the shear profiles produced by the new sensor correlate well with the profiles produced by Lord et al[16]. Examining the "on" position of the footswitch data presented by Lord et al[16] showed that the beginning and end of the gait cycle occur in the dip just before the maximum anterior shear stress *(figure2.17)*. This coincides well with the beginning and end of the gait cycle measured by the proposed sensor*(figure4.5b)*.

4.2.5 DISCUSSION OF THE PILOT TESTS

4.2.5.1 SELECTION OF A 12 SECOND PERIOD FOR DRIFT EVALUATION

The average time from the beginning of the standing phase to the end of the walking phase was a time less than 12 seconds. The average maximum time of each analysis test was expected to be 10 seconds. As a result of the findings of the pilot tests and the format of the data presented in the literature, it was decided that the analysis tests would only start from the beginning of the standing phase. The analysis tests would therefore exclude the zero load and scuffling phases. The drift experienced by the sensor during the zero load phase was therefore calculated to be used as an indication of the drift of the sensor during the analysis tests. This allowed any errors associated with drift to be accounted for during the analysis tests.

4.2.5.2 SCUFFLING PHASE STRESSES

The scuffling phase produced interesting results, as the sensor consistently experienced the same type of stresses in the posterior and lateral directions. The reasons for this pre-load, including the fastening of the foot inside the shoe and small camber present in the shoe, have been discussed, but another important consideration is the fact that any measurement made with a sensor is ultimately relative to the sensor's orientation to the foot, not to the ground. There is a camber at the front part of the shoe which points upward. This type of camber will tend to orientates the foot inside the shoe causing the sensor to experience a posterior stress. This provides another possible explanation for initial posterior stress in the sensor.

Although the zero and scuffling phase results are omitted during the analysis tests, the data obtained from these phases during the pilot tests provides essential information relating to the understanding of the pre-stress which was present on the sensor when the foot was inside the shoe. The data provided by the zero phase also allowed the drift of the sensor to be measured.

4.2.5.3 WALKING PHASE STRESSES

The shear profiles, relative timing of the maximum stresses and repeatability produced during the walking phase compared well with the literature. However, as the stresses in the medial-lateral direction were 3-5 times greater than the medial-lateral shear stresses presented in the study by Lord et al[16] a series of performance-checks were performed on the sensor to ensure that the media-lateral gauge was not mis-functioning.

The sensor was loaded separately with approximately the same pressure in both orthogonal directions. The stresses were applied evenly using the middle finger of the hand. This test provided a means of insuring that the medial-lateral rosette did not measure a stress three times greater than the anterior-posterior rosette. The two rosettes were found to measure approximately the same shear angle. The effect of additional bending of the shoe in the region around the sensor and the cables leading through the shoe were also investigated to examine any artefact data.

All the checks tended to indicate that the stresses measured by the medial-lateral gauge were indeed accurate. There was also no local square pressure mark left in the region where the sensor had been in contact with the foot. A swelling or redness might have suggested that the soft tissues of the foot were extruded significantly into the clearance between the sensor and the high density PVA. The lack of any redness indicated that the sensor had not been a natural pressure point.

Given the favourable performance of the sensor in the anterior-posterior direction, it is conceivable that these high stresses in the medial-lateral direction are as a result of the particular gait pattern and anatomical structure of the subject. The first factor is the weight of the subject. The subject was approximately 10 kg heavier than the average mass of the subjects used in the literature. Although every attempt was made to allow a direct comparison of the performance of the sensor with the literature, the subject was selected because of the availability and convenience which is provided in selected one's self as the test subject.

There are additional factors which tend to indicate that the performance of the sensor is not limiting but rather that the higher lateral shear stresses were as a result of the physiological and anatomical condition of the subject. These factors include the present condition of the subject's skin in the forefoot area and the condition of his shoes. The subject's shoes showed a natural tendency to deteriorate first in the region of the first metatarsal. The subject also has an abductory twist during the push off phase of the gait cycle. This twisting of the forefoot when the heel is in the air can result in higher than normal lateral shear stresses being experienced by the sensor.

4.3 THE ANALYSIS TESTS

A series of five tests were conducted using the testing protocol developed during the pilot tests. One of the test results which was obtained is graphically illustrated in *figure4.6.* The remainder of the results are presented in *Appendix F(i).* The first step on a treadmill was regarded more as an adjusting step rather than a true established gait pattern. During the analysis of the results, presented in *Appendix F(ii),* the first recorded step was therefore rejected. The analysis examined the following aspects of each test:

- The time of each gait cycle and the number of gait cycles.
- The maximum shear stresses which occurred.
- The mean value of the maximum shear stresses.
- The datum stress which was measured during the standing phase.

A summary of the results performed in the analysis is presented in *Table4.3* and *Table4.4.*

Average Gait Cycle Time	Mean Maximum Medial Shear	Mean Maximum Lateral Shear	Mean Maximum Posterior Shear	Mean Maximum Anterior Shear	Anterior-Posterior Datum Stress	Medial-Lateral Datum Stress
(sec)	(kPa)	(kPa)	(kPa)	(kPa)	(kPa)	(kPa)
1145.27±39.47	20.02±0.58	65.6±9.00	63.4±9.42	11.72±2.98	109.64±11.31	97.86±16.07

Table 4.3Mean gait times, maximum shears and datum stresses experienced during the analysis testing

Average Number of Gait Cycles measured during tests	Average Duration of Tests	Maximum Medial Shear	Maximum Lateral Shear	Maximum Posterior Shear	Maximum Anterior Shear
	(sec)	(kPa)	(kPa)	(kPa)	(kPa)
6.6±1.34	10.12±1.3	24.01±2.48	91.32±13.01	76.58±15.64	13.12±4.67

Table 4.4Number of gait cycles, average duration of tests and maximum shear stresses experienced during the analysis testing

4.3.1 DISCUSSION OF RESULTS

The gait cycle time of 1145.27±39.47msec correlates well with the gait cycle time of 1083±52msec recorded using the footscan pressure plate (*section 3.1.2.2*) and the literature. This indicates the sensor's ability to repeatably measure the changes in the shear stresses as they occurred during the gait cycle.

The average duration of each test was 10.12±1.3 seconds and the average number of gait cycles was 6.6±1.3. The consistency with which the shear stresses were measured by the sensor indicated that the number of cycles was adequate. The duration of all five of the analysis tests was kept below 12 seconds, so as to allow the drift determined during the pilot tests to be equivalent to the drift experienced by the sensor during these tests.

The magnitude of the mean maximum shear stresses, presented in *Table 4.3,* in the anterior-posterior directions compared well with the results presented by Lord et al[16], Tappin et al[57] and Pollard et al[55]. The medial-lateral stresses, as was the case with the pilot tests, were found to be higher than those presented in the literature.

An explanation of the profiles of the shear data is presented below. The described gait cycle uses the adjusted gait cycle time "T2". An illustration of the gait cycle time "T2" is presented in *figure4.5a* and *b.*.

Anterior - Posterior Shear Profiles *(figure4.5b)*:

Heel-strike → Peak anterior shear stress → Peak posterior shear stress → Toe off occurs at zero load → Gradual increase in anterior shear stress during swing phase → Heel-strike.

Medial - Lateral Shear Profiles *(figure4.5a)*:

Heel-strike → Peak medial shear stress → Peak lateral shear stress → Toe off at zero load → Increase in medial shear followed by a reduction in medial shear. (The initial increase and then reduction in medial shear was also experienced by Lord et al[16]. It could be attributed to a movement of the bones in the foot after toe off or a movement of the foot relative to the leg at the beginning of the swing phase) → Gradual increase in medial shear → Heel-strike.

The gradual increases in the medial and anterior shear stresses during the swing phase prior to heel-strike were expected. The increased medial shear stress is attributed to the supine position of the foot during the swing phase. The gradual increase in anterior shear stress is a result of the direction in which the subject walks (the foot during the swing phase is always swinging in the forward direction).

4.3.1.1 ASSESSMENT OF POSSIBLE SOURCES OF ERROR INHERENT IN THE AMPLIFIER

As was previously mentioned, the performance of the gauge amplifier was not guaranteed for strains below 10 microstrain. An assessment of the strains which were experienced by each individual gauge during the pilot and analysis tests was therefore made. It was found that during the walking phase, two of the three gauges from both rosettes always measured more than 20 microstrain and that periodically, the third gauge measured strains below 10 microstrain. These strains were however never less than 8 microstrain. The same error (±0.75% of Full Scale Output) associated with strains measured above 10 microstrain was therefore used for the strains measured above 8 microstrain.

4.4 THE DESIGN RANGE OF THE PROPOSED SENSOR

The sensor was originally designed to perform in a range from 7kpa to 350kpa. This range was intended to allow specific measurement of the range of maximum shear stresses presented in the literature. Given that the amplifier was shown to maintain its performance to strains as low as 8 microstrain the design range was extended to a range of 5.5kpa to 350kpa. However, as there were pre-stresses on the sensor when the foot was placed inside the shoe, the strains which it experienced were predominately greater than 8 microstrain(20 microstrain and greater). The pre-strains on the sensor therefore allowed the performance of the sensor to be increased to a range between 0kPa and 350kPa. The shear data is in a format which represents this stress range when it was normalised to zero from the pre-stress datum determined during the standing phase.

4.5 OVERALL PERFORMANCE OF THE SENSOR

The aim of this thesis was to develop a technique to measure the maximum shear stresses at the first metatarsal. The literature was used to provide a means of validating the technique which was developed. To be able to compare the data with the literature, the environment and conditions under which the sensor was tested were strictly controlled. Controlling the temperature and running speed and various other parameters such as the duration of the tests eliminated the number of variables which might have affected the data measured by the sensor. The correlation between the data presented in the literature and that obtained using the sensor developed in this thesis was used as an indication of the validity, performance and accuracy of the proposed sensor.

The close correlation between the results of the proposed sensor and the literature showed that the proposed sensor was able to measure the maximum shear stresses which occurred at the first metatarsal.

The specifications and performance characteristics of the sensor during the in-shoe experiments conducted in this thesis are summarised below:

- The design of the sensor consists of 12*12*5.2 block of PMMA. A circular base of diameter 22 mm and thickness 1.08mm of the same material is incorporated into its bottom surface. Two rectangular strain gauge rosettes were positioned on two of its lateral surfaces.

- The performance range of the sensor is 0 to 350kPa.

- The maximum error as a result of any temperature variations is equivalent to ±0.26% or ±0.91kpa of the Full Scale Output.

- The drift of the sensor is ±0.92kpa (±0.263% of Full Scale Output) for the Medial-Lateral gauge and ±0.99kpa (±0.283% of Full Scale Output) for the Anterior-Posterior gauge.

- The error associated with the performance of the amplifier is equivalent to ±2.63kpa which is ±0.75% of Full Scale Output.

- The error associated in determining Young's modulus during the compression tests is 0.32%. This is equivalent to 1.12kPa of the Full Scale Output.

- Cross talk effects were neglected.

The maximum error associated with the sensor during the in-shoe tests was found to be ±5.65kPa. Given the extremely small strains which were measured, the environment in which the sensor operated, the assumptions and theory used in the design of the sensor and the limitations of the equipment which was available, this error was not regarded as being substantial enough to make the proposed sensor non-viable. The ability of the sensor to measure shear stresses which were repeatable, of similar magnitude and timing to the shear stresses reported in the literature indicates that the assumptions, theory and concepts used to design and locate the proposed sensor are valid.

With an appropriate means of controlling temperature and a modern amplifier with enhanced amplification and drift characteristics, it is believed that the proposed sensor will be able to measure the two shear stresses with even greater accuracy. As these are considered to be the two main limitations of the proposed sensor, making modifications to eliminate errors associated with these variables will also allow the sensor to be more versatile in the clinical environment.

FIGURES FOR CHAPTER 4

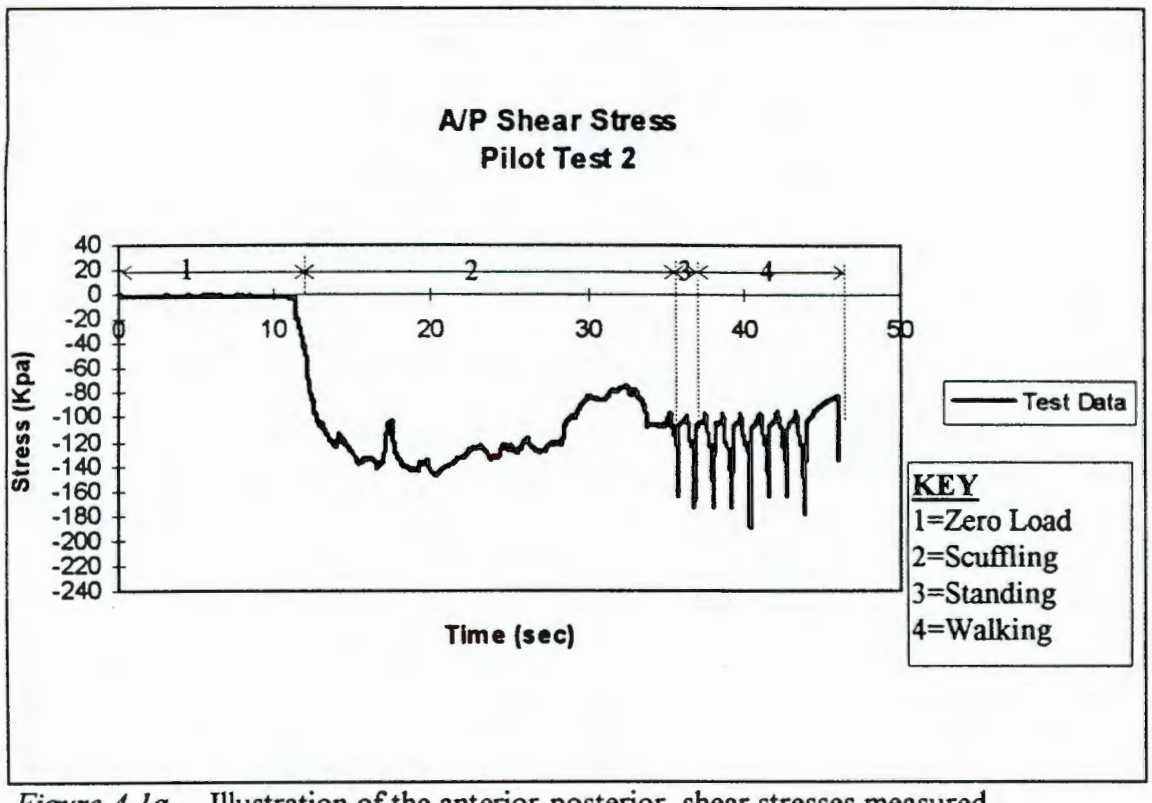

Figure 4.1a Illustration of the anterior-posterior shear stresses measured during the pilot tests

(See text, page142)

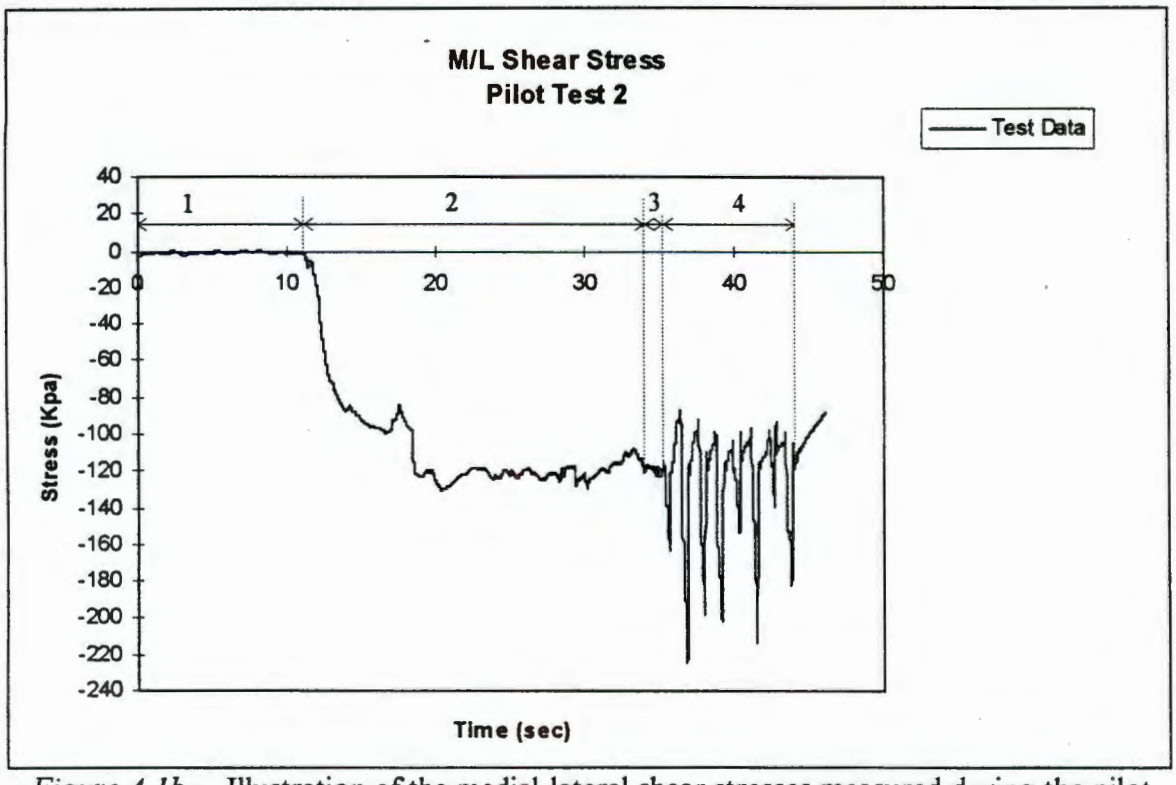

Figure 4.1b Illustration of the medial-lateral shear stresses measured during the pilot tests

(See text, page142)

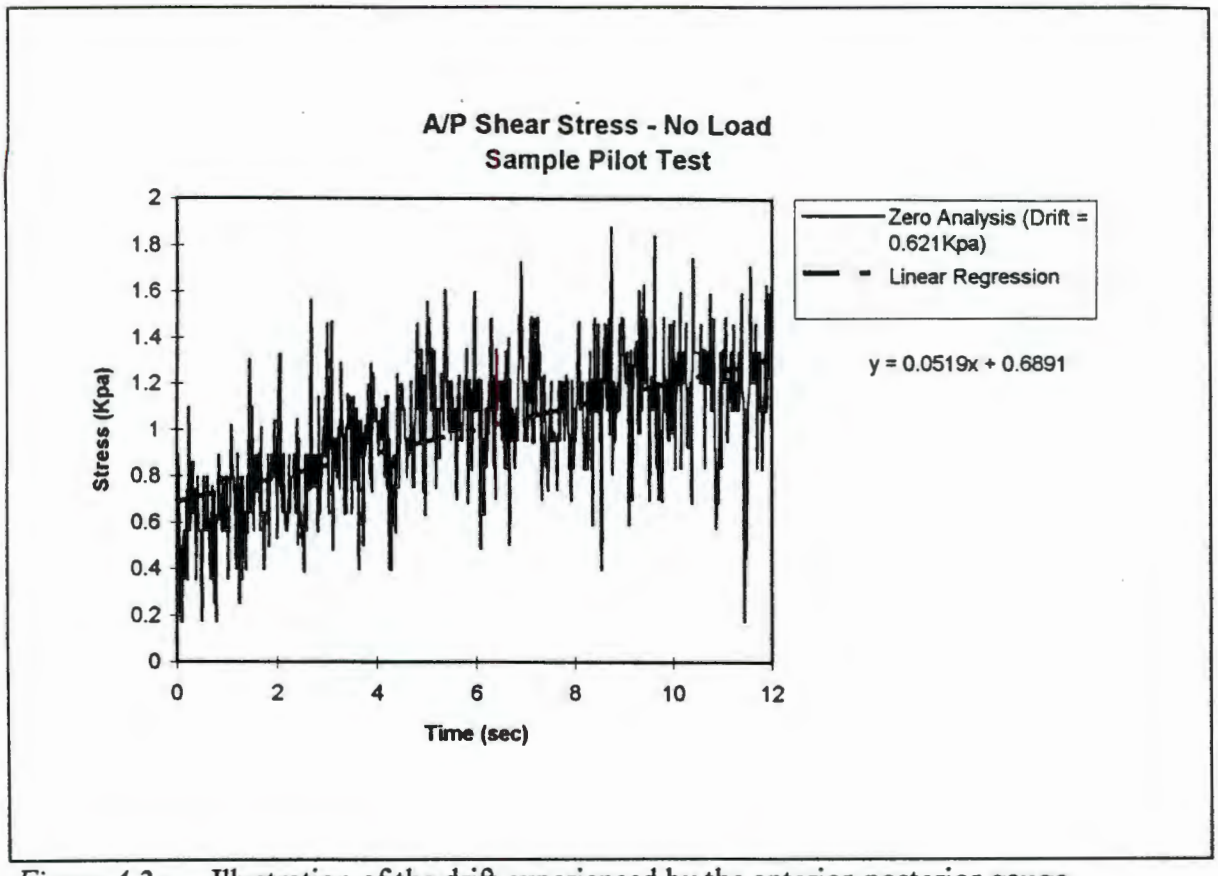

Figure 4.2a Illustration of the drift experienced by the anterior-posterior gauge during the pilot tests
(See text, page142)

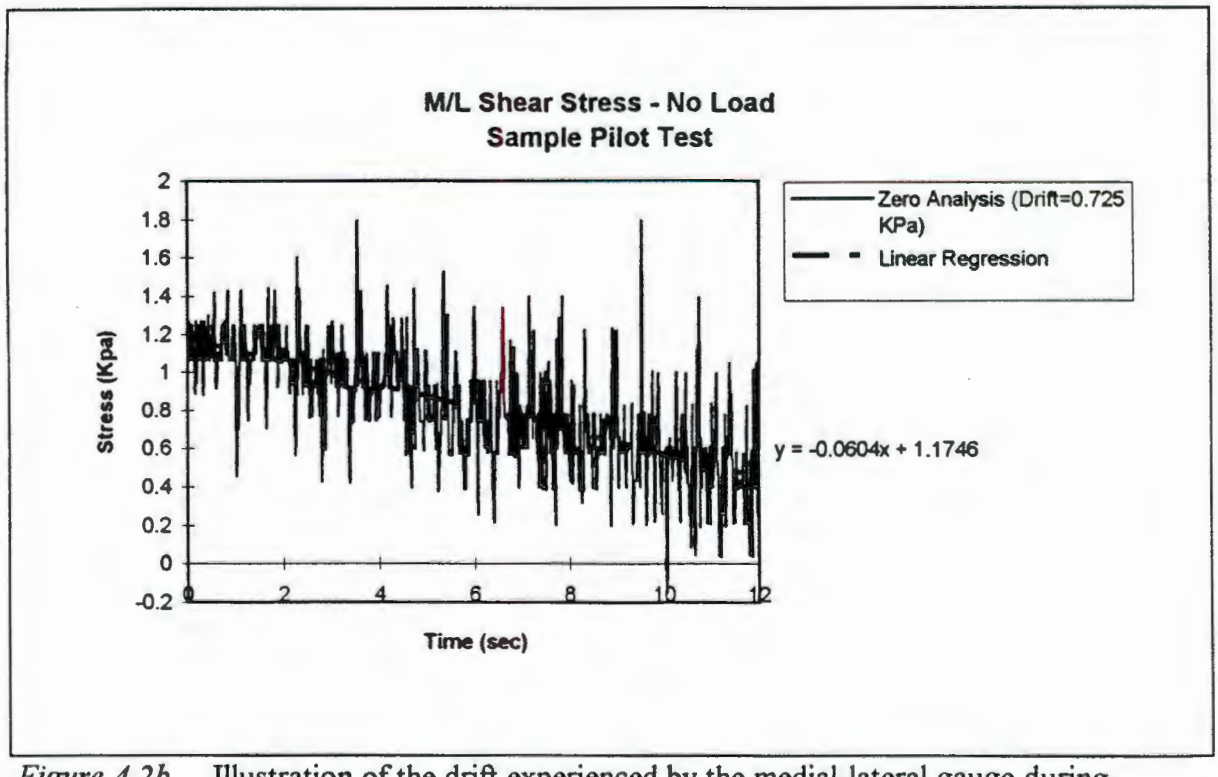

Figure 4.2b Illustration of the drift experienced by the medial-lateral gauge during the pilot tests
(See text, page142)

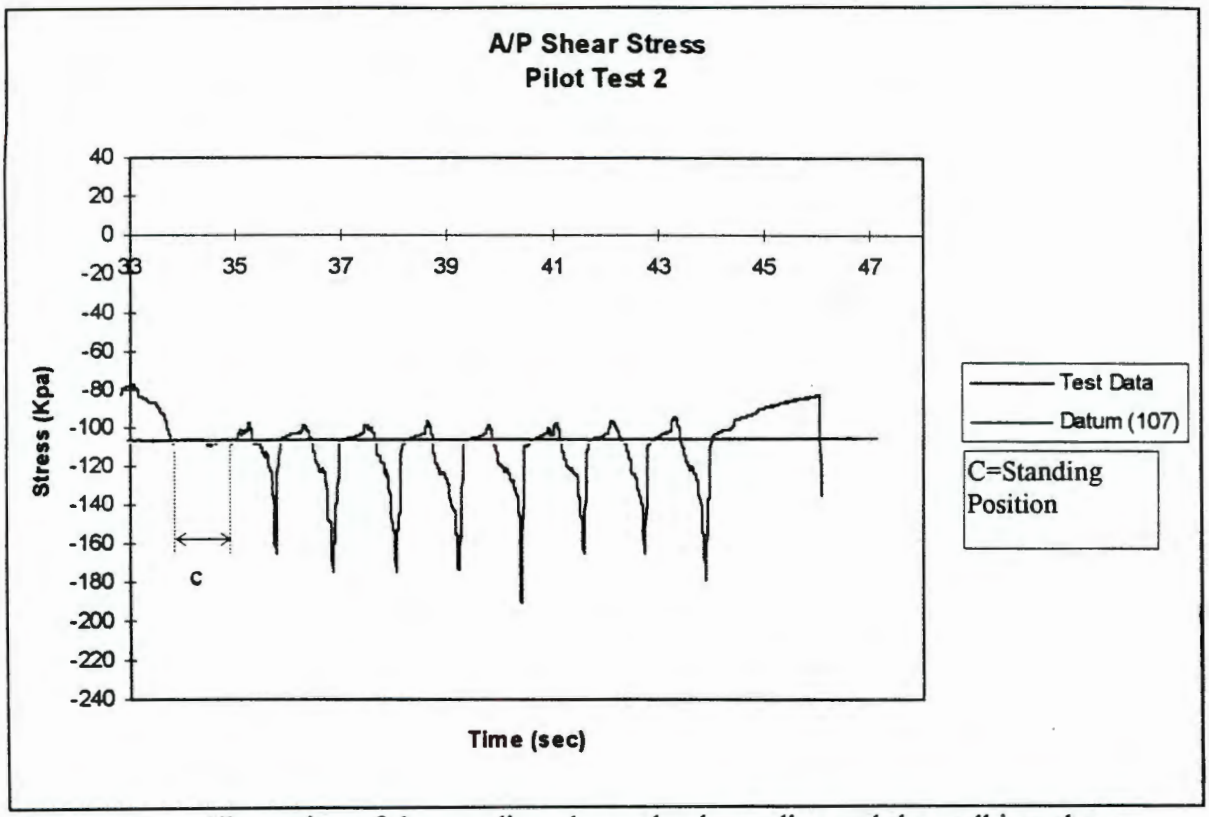

Figure 4.3a Illustration of the standing phase, the datum line and the walking phase measured by the anterior-posterior gauge
(See text, page144)

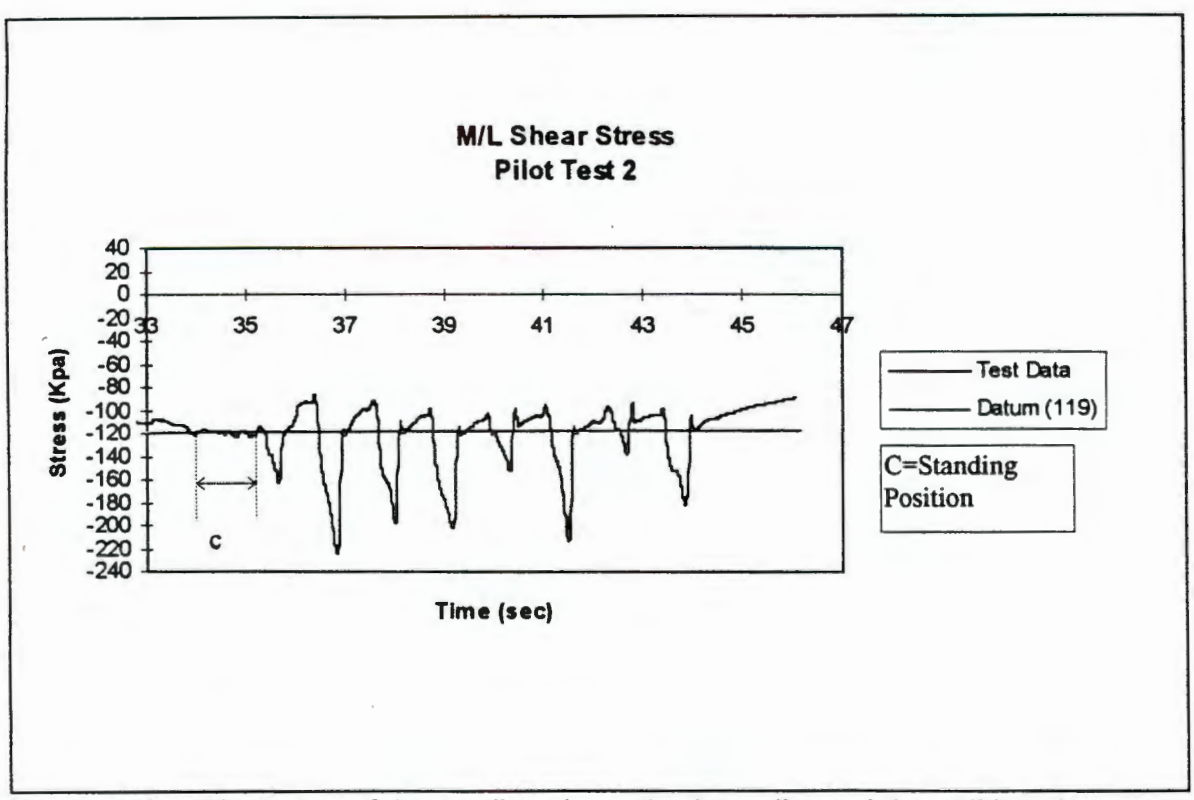

Figure 4.3b Illustration of the standing phase, the datum line and the walking phase measured by the medial-lateral gauge
(See text, page144)

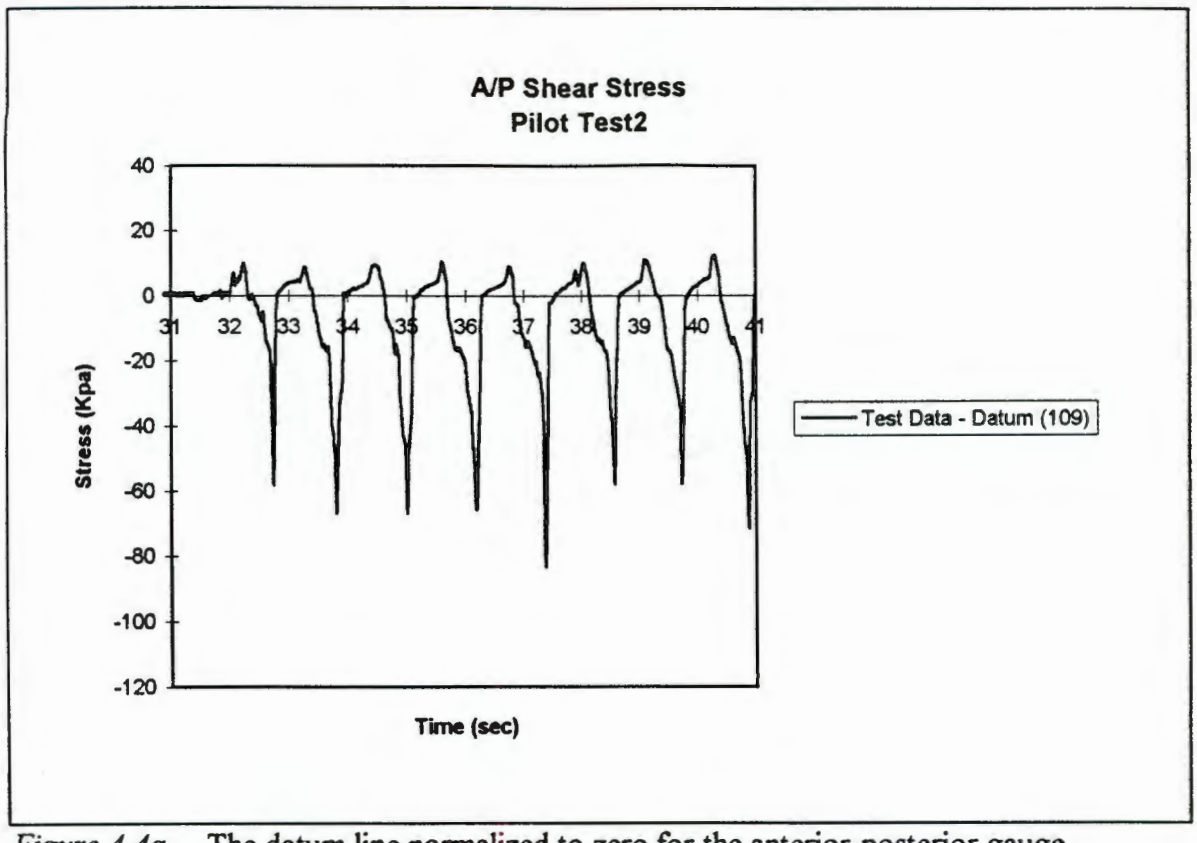

Figure 4.4a The datum line normalized to zero for the anterior-posterior gauge
(See text, page144)

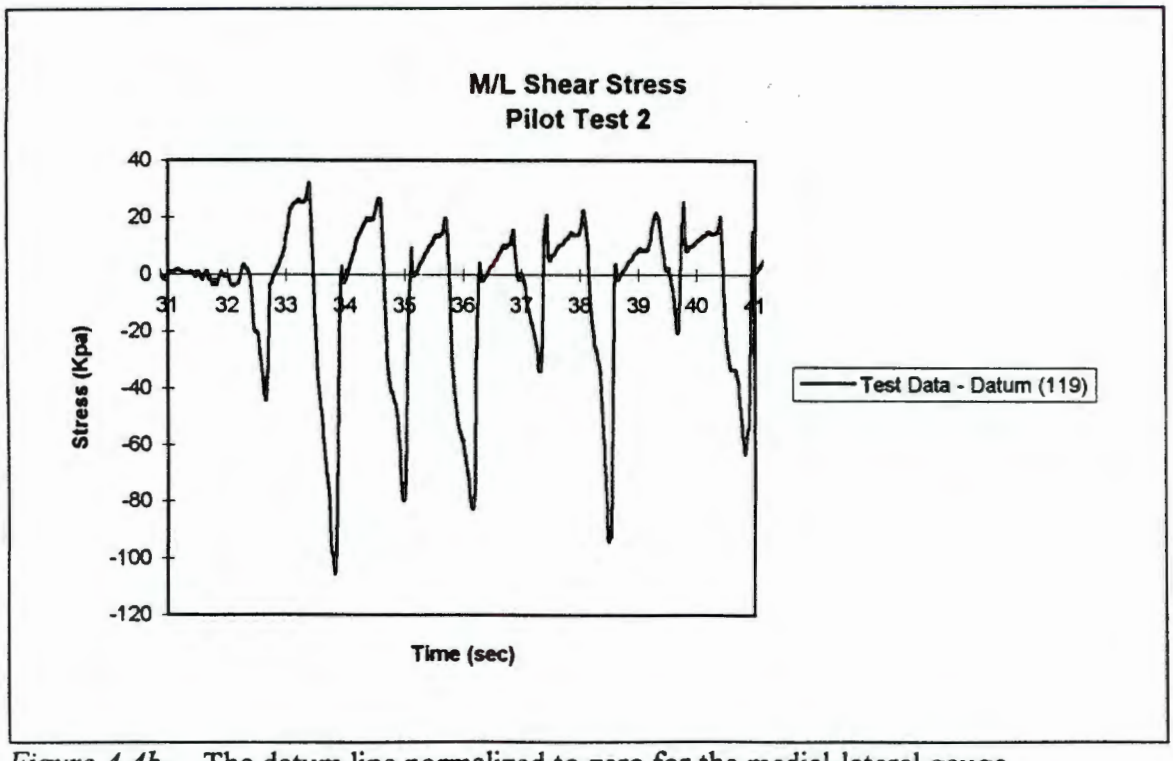

Figure 4.4b The datum line normalized to zero for the medial-lateral gauge
(See text, page144)

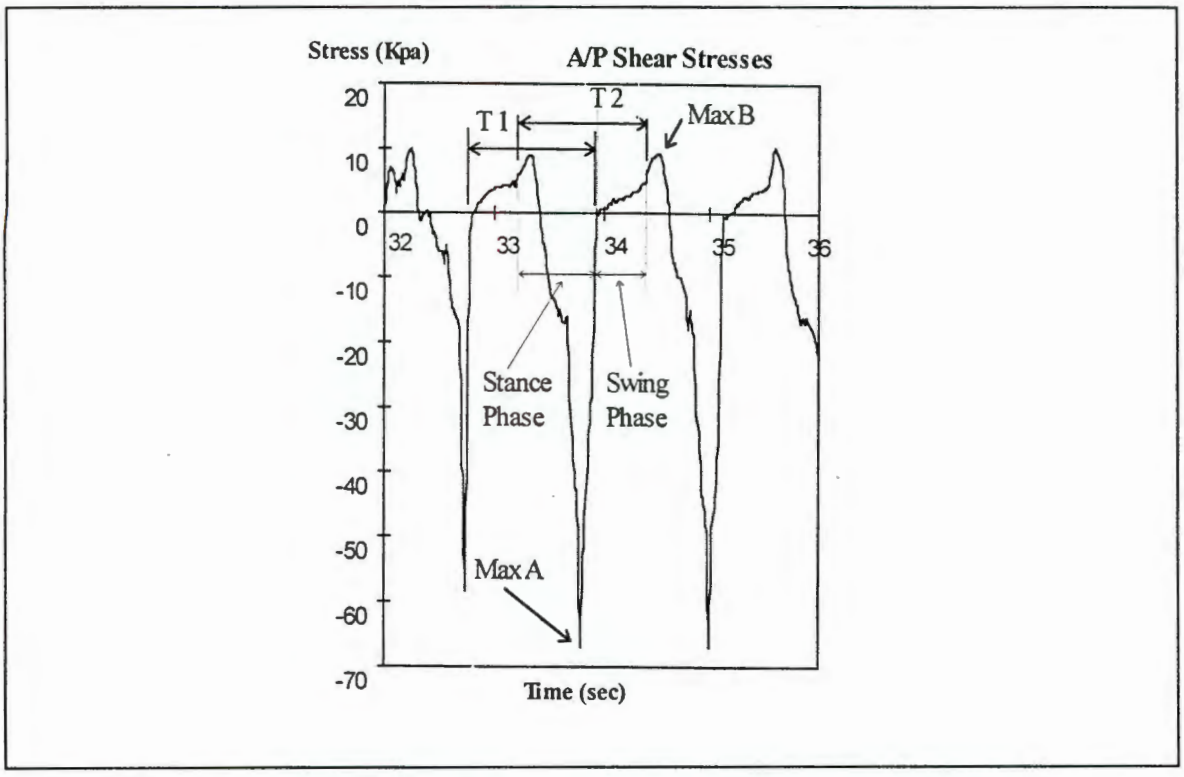

Figure 4.5b Relative and suggested position of the gait cycle for the anterior-posterior gauge
(see text, page 146)

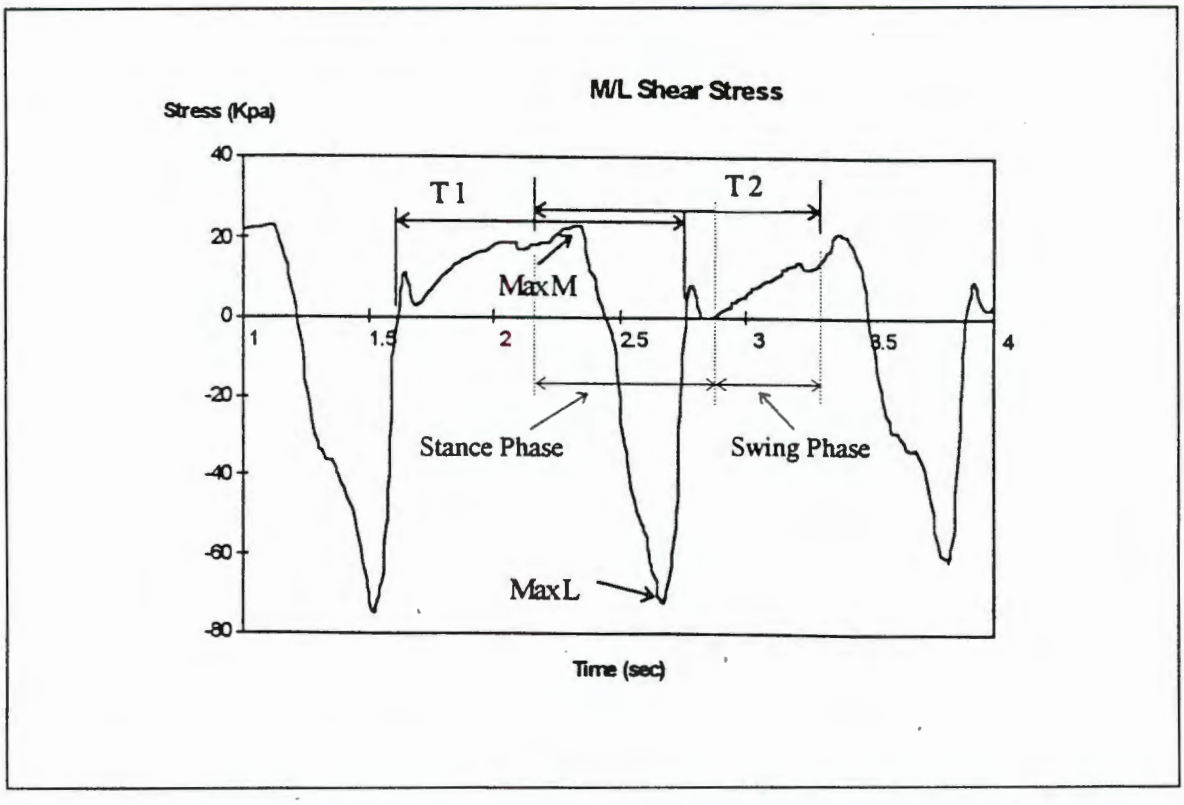

Figure 4.5a Relative and suggested position of the gait cycle for the medial-lateral gauge
(see text, page146)

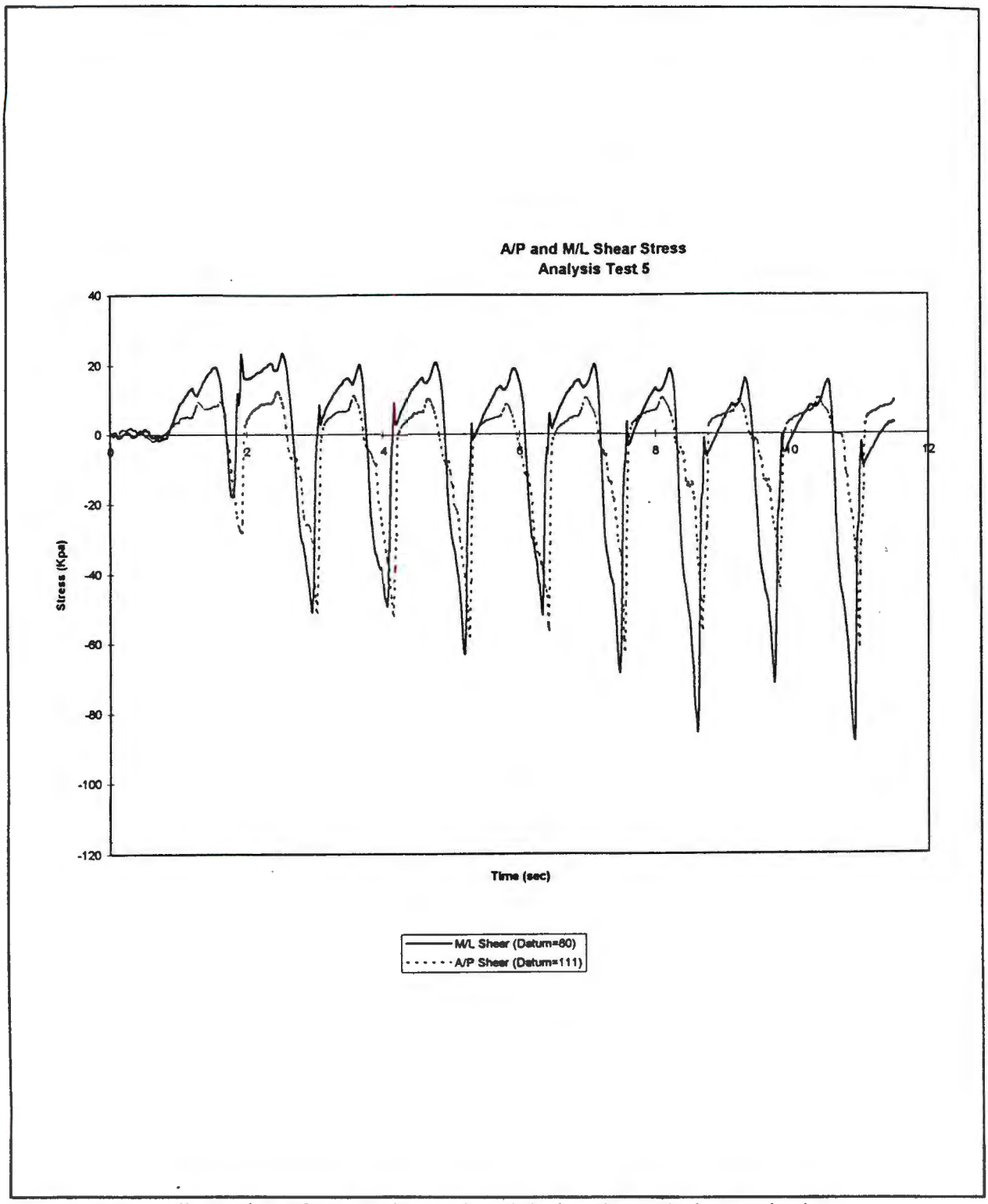

Figure 4.6 Illustration of the results produced during the analysis tests in the medial-lateral and anterior-posterior directions
(See text, page149)

CHAPTER 5

DISCUSSION

This investigation can be divided into the following primary and secondary objectives:

Primary objectives:

1. The ability of the sensor to measure the maximum shear stresses which were repeatable, of similar magnitude and timing to the shear stresses reported in the literature with a maximum associated error of ±5.65kPa indicates that the assumptions and theory used to design and construct the proposed sensor are feasable. The mean maximum shear stresses measured by the sensor compared to the literature are summarised below in *Table 5.1a* and *5.1b* and *figure 5.1a* and *5.1b*.

Researcher	Range of Anterior Shear Stresses	Range of Posterior Shear Stresses	Range of Medial Shear Stresses	Range of Lateral Shear Stresses
	(kPa)	(kPa)	(kPa)	(kPa)
Pollard et al[55]	8.17±1.3	41.83±12.97	17.34±0.73	14.23±1.65
Lord et al[16]	4.23±0.8 and 14.13±0.8	33.14±1.26 and 58.4±8.08	-1.53±0.62 and 3.54±2.12	14.5±4.95 and 21.2±1.48

Table 5.1a Shear data presented in the literature

Anterior Shear Stresses	Posterior Shear Stresses	Medial Shear Stresses	Lateral Shear Stresses
(kPa)	(kPa)	(kPa)	(kPa)
9.9±2.61	69.3±8.93	18.8±1.57	67.9±7.82

Table 5.2b Shear data measured by the sensor during the pilot tests

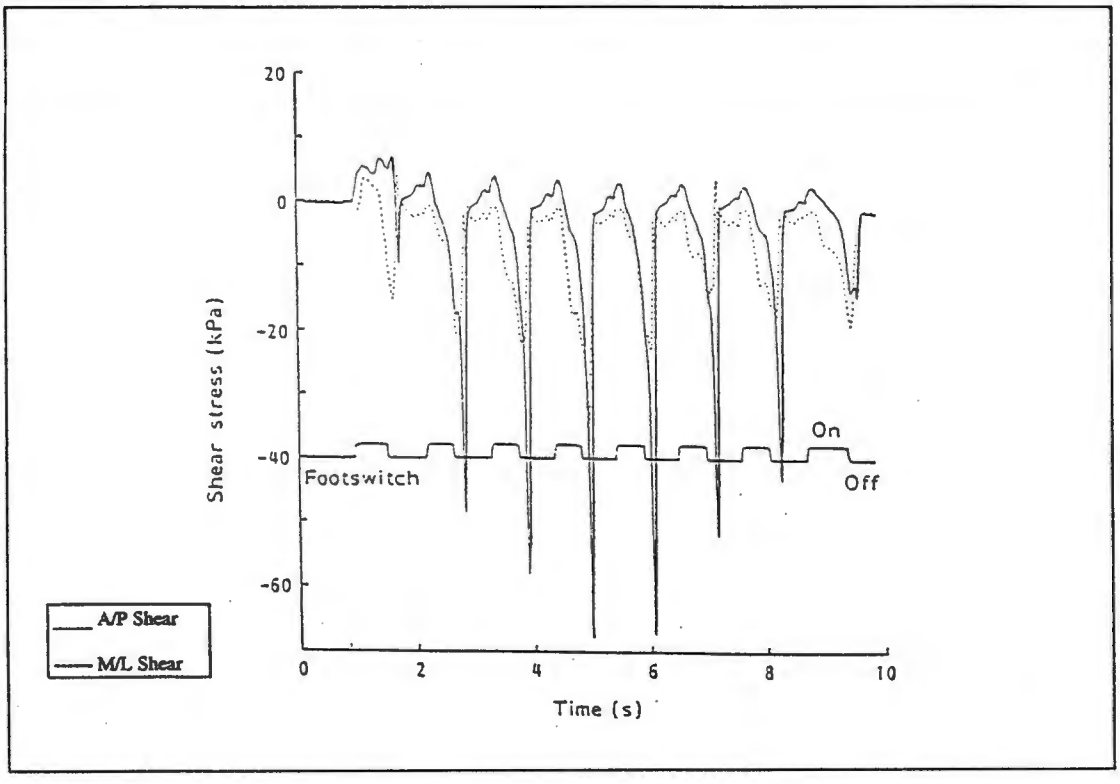

Figure 5.1a Sample shear data presented by Lord et al[16]

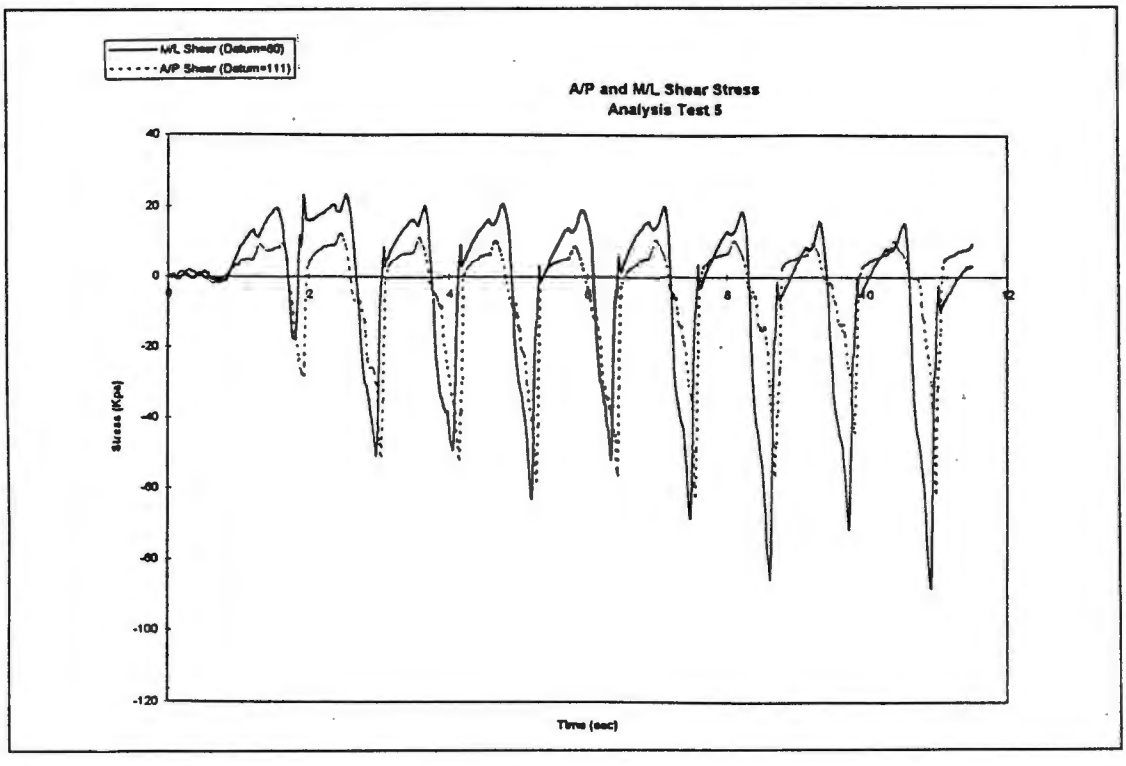

Figure 5.1b Sample shear data measured by the transducer during the analysis tests

7. Aspects in the design which would have improved the performance, accuracy and versatility of the proposed sensor were regarded as:

- Footswitch data - this would have provided an accurate means of determining the timing of the gait cycle.

- Amplification and drift characteristics of the amplifier- Enhanced amplification properties would allow lower strains to be measured in cases where the pre-stresses are less than 8 microstrain. It is possible that the existing amplifier can measure strains below 8 microstrain with the same accuracy as it does for strains above this value but this was not examined. Less drift would also reduce the overall error associated with the sensor.

- An alternative means of allowing for the effects of temperature on the material properties of the sensor. The method which was used is very specific to the pre-determined conditions assigned to the experimental procedure used in this thesis.

- A software program which would present the shear stresses in a visual format immediately after a test had been conducted. The existing procedure involves converting the data from the format in which is presented by the amplifier and the analogue to digital card to the form which allows it to be compared with the literature.

CHAPTER 6

CONCLUDING REMARKS

Based on the performance of the proposed in-shoe gait analysis device and the discussion presented in the previous chapter, the following concluding remarks are made:

1. A wider range of strain rates should be applied to the material so as to confirm the findings presented by Kitagawa et al[68] and those found during this thesis.

2. The calibration technique must be modified or improved upon so as to confirm that the performance of sensor is the same to 7kPa as it is above 27.8kPa.

3. A dynamic analysis should be performed on the sensor using ABAQUS to confirm that the simplification of using a static analysis is valid.

4. An alternative means of accounting for the temperature changes which occur in the sensor must be found. This could be achieved by placing a temperature transducer on the sensor so that the correct modulus corresponding to the measured temperature can be used. This will allow the sensor to be more versatile in the clinical environment.

5. The performance of the amplifier below 8 microstrain must be checked or an alternative amplifier sought.

6. Footswitch equipment must be incorporated into the testing protocol. This will indicate the accurate time at which the measured shear stresses occur during the gait cycle.

7. A software program should be written to allow the data measured by the gauges to be presented after each test in a form which is directly recognisable as the shear stresses occurring at the first metatarsal during the gait cycle.

8. As technology progresses, it is hoped that these improvements will be made on the proposed sensor, and that eventually it will be used in the clinical environment assisting clinicians in their diagnosis and treatment of the side-effects associated with patients suffering from diabetes mellitus.

REFERENCES

1. ESQUENAZI A. and M.A.KEENAN. Gait Analysis. Rehabilitation Medicine: Principles and Practice. 2nd Edition, 1993.

2. MUTSCHLER G. and G. FAESSLER. Evaluation of Gait Disorder Following Complex Foot Trauma. Scientific Exhibit, AAOS, Anaheim, Feb 7 - 11, 1991.

3. DE HEUS-VAN-PUTTEN M.A. and N.C. SCHAPER. The Clinical Examination of the Diabetic Foot in Daily Practice. Diabetic medicine : 13, S55 - S57, 1996.

4. NOAKES T. The Lore of Running.

5. NIGG, B.M. and B. SEGESSER. Biomechanical and Orthopedic Concepts in Sport Shoe Construction. Medicine and Science in Sports and Exercise. 24:595 - 601, 1992.

6. HARKLESS L.B. and K.J. DENNIS. You see what you look for and recognize what you know. Clinics Podiatr Med Surg 4 : 331, 1987.

7. WHEAT L.J. and S.D. ALLEN. Diabetic Foot Infections, Bacteriological Analysis. Arch Int Med 146 :1935, 1986.

8. DYCK P.J. and P.K. THOMAS. Diabetic Neuropathy, WB Saunders, Philadelphia, 1987.

9. KOSAK G.P. and C.S. HOAR. Management of Diabetic Foot Problems, WB Saunders, Philadelphia, 1984.

10. LEVIN M.E. and M.W. O'NEAL. The Diabetic Foot, 3rd Ed, CV Mosby, St Loius, 1983.

11. BOTHANNON N. Oral Hypoglycemic Agents. Digest for Family Practice, 35, 26, 1987.

12. GIBBONS G.W and A. BOTHE. Diabetic Foot Management, Harvard Medical School, Cambridge, MA, 1988.

13. BILD E.D. and J.V. SELBY. Lower Extremity Amputations in People with Diabetes, Epidemiology, and Prevention. Diabetes Care 12: 1, 1989.

14. BOULTON A.J.M. and T.DUCKWORTH. Dynamic Foot Pressure and other Studies as Diagnostic and Management Aids in Diabetic Neuropathy. Diabetes Care: 6, 26 - 33, 1983.

15. DUCKWORTH T. and A.J.M. BOULTON. Plantar Pressure Measurements and the Prevention of Ulceration in the Diabetic Foot. J Bone Joint Surg: 67,79-85, 1985.

16. LORD M. , R. WILLIAMS and R. HOSEIN. Method for In - Shoe Shear Stress Measurement. J of Biomedical Engineering: 14,181-186, 1992.

17. WILLIAMS R.B. , PORTER D. and V.C. ROBERTS. Triaxial Force Transducer for Investigating Stresses at the Stump / Socket Interface. Medical and Biological Engineering and Computing: 30, 89 - 96, 1992.

18. POLLARD J.P., L.P. LeQUESNE and J.W TAPPIN. Forces Under the Foot. J of Biomedical Engineering: 5,37-40, 1983.

19. TAPPIN J.W. and K.P. ROBERTSON. Study of Relative Timing of Shear Forces on the Sole of the Forefoot During Walking. J of Biomedical Engineering: 13,39-42, 1991.

20. BENNETT I. and D. KEVNER. Shear versus Pressure as a Causative Factor in Skin Blood Flow Occlusion. Arch Phys Med Rehabil: 60,309-314, 1979.

21. HALL CRAGGS E.C.B. Anatomy as a Basis for Clinical Medicine.2nd Edition.

22. ROSE J. and J.G. GAMBLE. Human Walking 2 nd Edition.

23. WINTER. Biomechanics of Human Movement 2 nd Edition.

24. WEBER W and E. WEBER. Mechanik du Meschlichen. Gottingen: Gehwerkzeugen, 1836.

25.BRIDGER R.S. Department of Biomedical Engineering Activity Report. Biostereometrics Group: 23-29,1991.

26.LaFORTUNE M. and E.HENNING. Cushioning Properties of Footwear during Walking: Accelerometer and Force Platform Measurements. Clinical Biom: 7, 181 -184, 1992.

27.SMART G. and G. ROBERTSON. Triplanar Electrogoniometer Analysis of Running Gait. B.C. Sports Medicine Clinic, Vancouver, Canada, 1982.

28.BRAUNE W. and FISHER O. Der Gang des Menschen. I - IV. Teil, B.G. Teschner, Leipzig.

29.AMAR J. The Human Motor. E.P. Dutton, New York, 1920.

30.ELFTMAN H. A Cinematic Study of the Distribution of Pressure in the Human Foot. Anat Record: 59, 481 - 491, 1934.

31.MILLER D.I. Biomechanics of Running - what should the future hold ? Can. Journal of Applied Sports Science: 3, 229 - 236, 1978.

32.CAVANAGH P. and M. LaFORTUNE. Ground Reaction Forces in Distance Running. J. of Biomechanics: 13, 397 - 406, 1980.

33.CAVANAGH P. and A. MICHIYOSHI. A Technique for the Display of Pressure Distributions Beneath the Foot. Journal of Biomechanics: 13, 69 - 75, 1980.

34.GERBER H. A System for Measuring Dynamic Pressure Distribution under the Human Foot. Journal of Biomechanics: 15, 225 - 227, 1982.

35.BENNETT P. and L.R. DUPLOCK. Pressure Distribution Beneath the Human Foot. Journal of the American Podiatry Medical Association: 83, 674 - 678, 1993.

36.LaFORTUNE M. and M.J. LAKE. Pendulum Modality to Simulate Foot - Ground Impact during Locomotion Activities. Int. Soc. of Biomechanics:XIV Congress, 744 - 745, 1993.

37.McPOIL T. , CORNWALL P.T. and W. YAMADA. A Comparison of Two In - Shoe Plantar Pressure Measurement Systems. The Lower Extremity:2, 95 - 103, 1995.

38.PHILLIPSON A. and S. DHAR. Forefoot Arthroplasty and changes in Plantar Foot Pressures. Foot and Ankle:15, 595 - 598, 1994.

39.GROSS T.S. and BUNCH R.P. Measurement of Discrete Vertical In - Shoe Stress with Piezoelectric Transducers. Journal of Biomedical Engineering: 10, 261 - 265, 1987.

40.SCHWARTZ R.P. and HEATH A.L. Kinetics of Human Gait: The Making and Interpretation of Electrobasographic Records of Gait. Journal of Bone and Joint Surgery: 16, 343 - 350, 1934.

41.SCHWARTZ R.P. and HEATH A.L. The Definition of Human Locomotion on the basis of Measurement. Journal of Bone and Joint Surgery: 29, 203 - 214, 1947.

42.SPOLEK G.A. and F.G. LIPPERT. An Instrumented Shoe - A Portable Force Measuring Device. Journal of Biomechanics: 9, 779 - 783, 1976.

43.VALIANT G. , McMAHON A. and FREDERICK E. A New Test to Evaluate the Cushioning Properties of Athletic Shoes. J of Biomechanics: 937 - 941, 1983.

44.HENNING E. and M. LaFORTUNE. Tibial Bone Acceleration and Ground Reaction Parameters during Running. Abstract # 266, June 1989.

45.NIGG B. , HERZOG W. and L.J. READ. Effect of Viscoelastic Shoe Insoles on the Vertical Impact Forces in Heel - Toe Running. The American Journal of Sports Medicine: 16, 70 - 75, 1988.

46.LEUTHI S. , DENOTH J. and X. KAELIN. The Influence of the Shoe on Foot Movement and Shock Attenuation in Running. Biomechanics: Current Interdisciplinary Research: 931 - 935, 1985.

47.STACOFF A. , KALIN X and E. STUSSI. The Effects of Shoes on the Torsion and Rearfoot Motion in Running. Medicine and Science in Sports and Exercise: 23, 482 - 490, 1991.

48.STUSSI E. , STACOFF A. and C. REINSCHMIDT. The Movement of the Heel within a Running Shoe. Medicine and Science in Sports and Exercise: 24, 695 - 701, 1992.

49.HUGHES J. , PRATT L. and L. KLENERMAN. Reliability of Pressure Measurements: the EMED F System. Clinical Biomechanics: 61, 14 -18, 1991.

50.HENNING E. , A. STAATS and D. ROSENBAUM. Plantar Pressure Distribution Patterns of Young Children in Comparison to Adults. Foot and Ankle: 15, 35 - 40, 1994.

51.CLARKE T.E. The Pressure Distribution Under the Foot during Barefoot Walking. Doctoral Dissertation, The Pennsylvania State University, 1980.

52.CAVANAGH P.R. , HEWITT F.G. and J.E. PERRY. In - Shoe Plantar Pressure Measurement: A Review. The Foot: 2, 185 - 194, 1992.

53.GROSS T.S. and R.P. BUNCH. Measurement of Discrete Vertical In - Shoe Stress with Piezoelectric Transducers. Journal of Biomedical Engineering: 10, 261 - 265, 1988.

54.EKSTROM H. and J. KARLSSON. Direct Force Measurement in Biomechanical Investigations. Journal of Biomechanics, 201 - 205, 1982.

55.POLLARD J.P , LeQUESNE L.P. and J.W. TAPPIN. Forces Under the Foot. Journal of Biomedical Engineering: 5, 37 - 40, 1983.

56.LEVIN M. Portable In Shoe Gait Analysis Device. Department of Electrical Engineering, University of Cape Town, 1987.

57.TAPPIN J.W. , POLLARD J. and E.A. BECKETT. Method of Measuring "Shearing" Forces on the Sole of the Foot. Clin. Phys. Physiol. Meas. : 1, 83 - 85, 1980.

58.WILLIAMS R.B. , PORTER D. and V.C. ROBERTS. Triaxial Force Transducer for Investigating Stresses at the Stump / Socket Interface. Medical and Biological Engineering and Computing: 30, 89 - 96, 1992.

59.CTERCTEKO G.C and L.P LeQUESNE. Vertical Forces Acting on the Feet of Diabetic Patients with Neuropathic Ulceration. Br. Journal of Surgery: 68, 608 - 614, 1981.

60.SHEREFF M.J. , DiGIOVANNI L. and F.J. KUMMER. A Comparison of Non Weight - Bearing and Weight Bearing Radiographs of the Foot. Foot and Ankle: 10, 306 - 311, 1990.

61.BIOCHEMISTRY - A Functional Approach, McGilvery Goldstein, 3rd Edition, 1983.

62.MUSGRAVE FOOTPRINT SYSTEM - Information Pack, Preston Communications, United Kingdom, 24 - 25.

63.PROBABILITY AND STATISTICS FOR ENGINEERS - Prentice - Hall International Editions, 3rd Edition, 1985.

64.MILLER G.F and I.A. STOKES. A Study of the Duration of Load - Bearing Under Different Areas of the Foot. Engineering Medicine : 8, 128 - 132, 1979.

65.CARSONS E. Poisson's ratio. Modern plastics: 63, 609 - 610, 1986.

66.KRANING K.K. Temperature Regulation of the Skin, 1085 - 1095.

67.SHIELDS. Adhesive Bonding. 1 - 18.

68.KITAGAWA M. and D. ZHOU. Stress - Strain Curves for Solid Polymers. Polymer Engineering and Science: 35, 1725 - 1732, 1995.

69.PEARCE H. An Introduction into Finite Elements. 1995.

70.HIBBERT, KARLSSON AND SORENSEN. ABAQUS Standard Users Manual 1. 1995.

71.MULDER H. Uresil Prosthetic Supplies, Cape Town.

BIBLIOGRAPHY

1. DAINTY.D and NORMAN R. *Standardising Biomehanical Testing In Sport.* Human Kinetics Publishers. 1987

2. PERRY C.C and LISSNER H.R. *The Strain Gauge Primer,* 2 nd Edition

3. ASM INTERNATIONAL. *Tensile Testing.* 1993

4. ASHBY M. and JONES D. *Engineering Materials 1 - An Introduction To Their Properties And Applications.*1989

5. ASHBY M. and JONES D. *Engineering Materials 2 - An Introduction to Microstructures, Processing And Design.* 1989

6. POPOV E. *Introduction To Mechanics Of Solids.* Prentice - Hall. 1968

7. DALL and RILEY. *Experimental Stress Analysis.* McGraw - Hill Book Company. 1965

APPENDIX A

RESULTS FROM PODOTRACK AND FOOTSCAN

Podotrack and Footscan Results

Results of Sensor location tests	TOP	AMBP	PMBP	MWF	HDMP	VDMP	
Podotrack							
"Standing"	266	214	186	90			
	266	215	187	91			
	265	215	186	92			
	265	214	185	93			
	266	215	185	92			
Stdev	0.54772256	0.5477226	0.83666	1.140175			
Mean	265.6	214.6	185.8	91.6			
max error	0.91782298	0.917823	1.401998	1.910601			98%
	0.67997774	0.6799777	1.038683	1.415487			95%
Podotrack							
"Walking"	292	232	203	92	15	220	
	294	233	202	91	14	220	
	292	233	203	90	15	219	
	293	233	204	91	14	218	
	293	232	202	90	15	220	
Stdev	0.83666003	0.5477226	0.83666	0.83666	0.547723	0.894427	
Mean	292.8	232.6	202.8	90.8	14.6	219.4	
max error	1.40199775	0.917823	1.401998	1.401998	0.917823	1.498799	98%
	1.03868315	0.6799777	1.038683	1.038683	0.679978	1.110399	95%
Footscan	295.7	231	203	89.6	14	217	
"Walking"	294.3	229	201	90.3	15	218	
	294.6	230	203	89.3	14	218	
	295.2	231	202	90.5	14	217	
	296.1	229	201	89.1	15	219	
Stdev	0.74632433	1	1	0.614817	0.547723	0.83666	
Mean	295.18	230	202	89.76	14.4	217.8	
max error	1.25062151	1.6757078	1.675708	1.030254	0.917823	1.401998	98%
	0.92653465	1.2414638	1.241464	0.763273	0.679978	1.038683	95%

Combined Results of Podotrack and Footscan "Walking"	TOP	AMBP	PMBP	MWF	HDMP	VDMP
	292	232	203	92	15	220
	294	233	202	91	14	220
	292	233	203	90	15	219
	293	233	204	91	14	218
	293	232	202	90	15	220
	295.7	231	203	89.6	14	217
	294.3	229	201	90.3	15	218
	294.6	230	203	89.3	14	218
	295.2	231	202	90.5	14	217
	296.1	229	201	89.1	15	219
Mean	293.99	231.3	202.4	90.28	14.5	218.6
Stdev	1.46017503	1.5670212	0.966092	0.882924	0.527046	1.173788
Max error 98% Confidence	1.30258159	1.3978961	0.861824	0.787632	0.470163	1.047103
Max error 95% Confidence	0.93173941	0.9999181	0.616464	0.563395	0.336309	0.748995

APPENDIX B

RESULTS FROM TENSILE TESTS PERFORMED ON THE PMMA

Modulus Determination

Strain Rate 0.001	Modulus	Error		R^2	intercept		
	Kpa	%					
1	1869	0.01	-	0.9993	0.2776	**Average**	**1869.2**
2	1876	0.38	+	0.9998	0.2471	**Stdev**	**4.816638**
3	1867	0.12	-	0.9998	0.2499		
4	1863	0.33	-	0.9994	0.2654		
5	1871	0.11	+	0.9996	0.2548		
Strain Rate 0.01							
1	1885	0.31	+	0.9997	0.2505	**Average**	**1879.2**
2	1881	0.11	+	0.9996	0.2567	**Stdev**	**4.32435**
3	1876	0.17	-	0.9994	0.2645		
4	1880	0.04	+	0.9997	0.2632		
5	1874	0.27	-	0.9998	0.2635		
		Overall	**1874.2**				
		modulus					
		Stdev	**6.811755**				
		Max Error	**6.1 Kpa**				
		98%					
		Max Error					
		95%	**4.87 Kpa**				

APPENDIX C

RESULTS FROM FINITE ELEMENT ANALYSIS

I. ABAQUS INPUT DECK 1

II. ABAQUS INPUT DECK 2

III. RESULTS FROM DATA FILES ON FACE 3 (FREE CASE)

IV. RESULTS FROM DATA FILES ON FACE 3 (RESTRICTED CASE)

```
*HEADING
SIMULATED RESPONSE OF PMMA SENSOR WITH A BASE INSIDE A SHOE DURING GAIT
*RESTART,WRITE,FREQUENCY=1
**
**------------------------------------------------------------------
                          **NODE GENERATION
**------------------------------------------------------------------
**
*NODE
1,0.,0.,0.
23,0.022,0.,0.
1101,0.,0.022,0.
1123,0.022,0.022,0.
20001,0.,0.,0.001
20023,0.022,0.,0.001
21101,0.,0.022,0.001
21123,0.022,0.022,0.001
20256,0.005,0.005,0.001
20268,0.017,0.005,0.001
20856,0.005,0.017,0.001
20868,0.017,0.017,0.001
120256,0.005,0.005,0.006
120268,0.017,0.005,0.006
120856,0.005,0.017,0.006
120868,0.017,0.017,0.006
*NGEN,NSET=B1
1,23,1
*NGEN,NSET=B2
1101,1123,1
*NFILL,NSET=BASE
B1,B2,22,50
*NGEN,NSET=T2
20001,20023,1
*NGEN,NSET=T3
21101,21123,1
*NFILL,NSET=TOP
T2,T3,22,50
*NFILL,NSET=BOTTOM
BASE,TOP,1,20000
*NSET,NSET=TOM, GENERATE
20256,20268,1
20306,20318,1
20356,20368,1
20406,20418,1
20456,20468,1
20506,20518,1
20556,20568,1
20606,20618,1
20656,20668,1
20706,20718,1
20756,20768,1
20806,20818,1
20856,20868,1
*NGEN,NSET=T5
120256,120268,1
*NGEN,NSET=T6
120856,120868,1
*NFILL,NSET=JERRY
T5,T6,12,50
*NFILL,NSET=CUBE
TOM,JERRY,5,20000
*NSET,NSET=FACE3, GENERATE
20256,20268,1
40256,40268,1
60256,60268,1
80256,80268,1
100256,100268,1
120256,120268,1
**FACE3 ASSOSIATED WITH MEASURING OF ANTERIOR/POSTERIOR SHEAR
*NSET,NSET=FACE4, GENERATE
20268,20868,50
40268,40868,50
60268,60868,50
80268,80868,50
100268,100868,50
120268,120868,50
**FACE4 ASSOSIATED WITH MEASURING OF MEDIAL/LATERAL SHEAR
```

```
*NSET,NSET=FILL1, GENERATE
120307,120317,1
120357,120367,1
120407,120417,1
120457,120467,1
120507,120517,1
120557,120567,1
120607,120617,1
120657,120667,1
120707,120717,1
120757,120767,1
120807,120817,1
*NSET,NSET=FILL2
120256,120268,120856,120868
*NSET,NSET=FILL3, GENERATE
120257,120267,1
120318,120818,50
120306,120806,50
120857,120867,1
*NSET,NSET=UPPER
FILL1,FILL2,FILL3
**
**----------------------------------------------------------------
                        **ELEMENT GENERATION
**----------------------------------------------------------------
**
*ELEMENT,TYPE=C3D8
1,1,2,52,51,20001,20002,20052,20051
*ELGEN,ELSET=BOTTOM
1,22,1,1,22,50,50,1,20000,5000
*ELEMENT,TYPE=C3D8
1000000,20256,20257,20307,20306,40256,40257,40307,40306
*ELGEN,ELSET=BLOCK
1000000,12,1,1,12,50,50,5,20000,5000
*ELSET,ELSET=TOTAL
BOTTOM,BLOCK
*ELEMENT,TYPE=S4R
2000000,120256,120257,120307,120306
*ELGEN,ELSET=LAYER
2000000,12,1,1,12,50,50
*ELSET,ELSET=MEASURE3, GENERATE
1000004,1000007,1
1005004,1005007,1
1010004,1010007,1
1015004,1015007,1
1020004,1020007,1
*ELSET,ELSET=MEASURE4, GENERATE
1000211,1000361,50
1005211,1005361,50
1010211,1010361,50
1015211,1015361,50
1020211,1020361,50
*ELSET,ELSET=FACE3A, GENERATE
1000000,1000011,1
1005000,1005011,1
1010000,1010011,1
1015000,1015011,1
1020000,1020011,1
*ELSET,ELSET=FACE4A, GENERATE
1000011,1000561,50
1005011,1005561,50
1010011,1010561,50
1015011,1015561,50
1020011,1020561,50
**
**----------------------------------------------------------------
                        **BOUNDARY CONDITIONS
**----------------------------------------------------------------
**
*BOUNDARY
BOTTOM,PINNED
**
**----------------------------------------------------------------
                        **MATERIAL DEFINITION
**----------------------------------------------------------------
**
*SOLID SECTION,ELSET=TOTAL,MATERIAL=PMMA
*MATERIAL,NAME=PMMA
```

```
*ELASTIC
1874E6,0.35
*DENSITY
1150
** PAGE 8.14.1-1
*SHELL SECTION,ELSET=LAYER,MATERIAL=CHOICE
0.0001
*MATERIAL,NAME=CHOICE
*ELASTIC
100,0.35
**
**----------------------------------------------------------------
                          **LOAD DEFINITION
**----------------------------------------------------------------
**
*AMPLITUDE,NAME=ZLOAD
0.,1, 1,1
*AMPLITUDE,NAME=XLOAD
0.,1, 1,1
*AMPLITUDE,NAME=YLOAD
0.,1, 1,1
**
**----------------------------------------------------------------
                          **STEP DEFINITION
**----------------------------------------------------------------
**
*STEP,NLGEOM,INC=20
*STATIC
0.1,1.0,0.01,0.2
*BOUNDARY
UPPER,3
**
**----------------------------------------------------------------
                          **NODAL LOADS
**----------------------------------------------------------------
**
*CLOAD,FOLLOWER,AMPLITUDE=ZLOAD
FILL1,3,-1.0
FILL3,3,-0.5
FILL2,3,-0.25
*CLOAD,FOLLOWER,AMPLITUDE=XLOAD
FILL1,1,0.033
FILL2,1,0.00825
FILL3,1,0.0165
*CLOAD,FOLLOWER,AMPLITUDE=YLOAD
FILL1,2,0.015
FILL2,2,0.00375
FILL3,2,0.0075
*EL PRINT,ELSET=MEASURE3,POSITION=AVERAGED AT ALL NODES,FREQUENCY=1
S
E
*EL PRINT,ELSET=MEASURE4,POSITION=AVERAGED AT ALL NODES,FREQUENCY=1
S
E
*EL FILE,ELSET=MEASURE3,POSITION=AVERAGED AT ALL NODES,FREQUENCY=1
E
*EL FILE,ELSET=MEASURE4,POSITION=AVERAGED AT ALL NODES,FREQUENCY=1
*E
*EL FILE,ELSET=MEASURE3,POSITION=AVERAGED AT ALL NODES
S
E
*EL FILE,ELSET=MEASURE4,POSITION=AVERAGED AT ALL NODES
S
E
*END STEP
**----------------------------------------------------------------
                          **END OF ANALYSIS
```

```
*HEADING
SIMULATED RESPONSE OF PMMA SENSOR WITHOUT A BASE INSIDE THE SHOE DURING
GAIT
*RESTART,WRITE,FREQUENCY=1
**
**------------------------------------------------------------------
                          **NODE GENERATION
**------------------------------------------------------------------
**
*NODE
20256,0.,0.,0
20268,0.012,0.,0
20856,0.,0.012,0
20868,0.012,0.012,0
120256,0.,0.,0.005
120268,0.012,0.,0.005
120856,0.,0.012,0.005
120868,0.012,0.012,0.005
*NGEN,NSET=B1
20256,20268,1
*NGEN,NSET=B2
20856,20868,1
*NFILL,NSET=BASE
B1,B2,12,50
*NGEN,NSET=T2
120256,120268,1
*NGEN,NSET=T3
120856,120868,1
*NFILL,NSET=TOP
T2,T3,12,50
*NFILL,NSET=RUBY
BASE,TOP,5,20000
*NSET,NSET=FACE3, GENERATE
20256,20268,1
40256,40268,1
60256,60268,1
80256,80268,1
100256,100268,1
120256,120268,1
**FACE3 ASSOSIATED WITH MEASURING OF ANTERIOR/POSTERIOR SHEAR
*NSET,NSET=FACE4, GENERATE
20268,20868,50
40268,40868,50
60268,60868,50
80268,80868,50
100268,100868,50
120268,120868,50
**FACE4 ASSOSIATED WITH MEASURING OF MEDIAL/LATERAL SHEAR
*NSET,NSET=FILL1, GENERATE
120307,120317,1
120357,120367,1
120407,120417,1
120457,120467,1
120507,120517,1
120557,120567,1
120607,120617,1
120657,120667,1
120707,120717,1
120757,120767,1
120807,120817,1
*NSET,NSET=FILL2
120256,120268,120856,120868
*NSET,NSET=FILL3, GENERATE
120257,120267,1
120318,120818,50
120306,120806,50
120857,120867,1
*NSET,NSET=BOUND
FILL1,FILL2,FILL3
**
**------------------------------------------------------------------
                          **ELEMENT GENERATION
**------------------------------------------------------------------
**
*ELEMENT,TYPE=C3D8
1000000,20256,20257,20307,20306,40256,40257,40307,40306
*ELGEN,ELSET=BLOCK
```

```
1000000,12,1,1,12,50,50,5,20000,5000
*ELEMENT,TYPE=S4R
2000000,120256,120257,120307,120306
*ELGEN,ELSET=LAYER
2000000,12,1,1,12,50,50
*ELSET,ELSET=MEASURE3, GENERATE
1000004,1000007,1
1005004,1005007,1
1010004,1010007,1
1015004,1015007,1
1020004,1020007,1
*ELSET,ELSET=MEASURE4, GENERATE
1000211,1000361,50
1005211,1005361,50
1010211,1010361,50
1015211,1015361,50
1020211,1020361,50
*ELSET,ELSET=FACE3A, GENERATE
1000000,1000011,1
1005000,1005011,1
1010000,1010011,1
1015000,1015011,1
1020000,1020011,1
*ELSET,ELSET=FACE4A, GENERATE
1000011,1000561,50
1005011,1005561,50
1010011,1010561,50
1015011,1015561,50
1020011,1020561,50
**
**----------------------------------------------------------------
                        **BOUNDARY CONDITIONS
**----------------------------------------------------------------
**
*BOUNDARY
BASE,PINNED
**
**----------------------------------------------------------------
                        **MATERIAL DEFINITION
**----------------------------------------------------------------
**
*SOLID SECTION,ELSET=BLOCK,MATERIAL=PMMA
*MATERIAL,NAME=PMMA
*ELASTIC
1874E6,0.35
*DENSITY
1150
*SHELL SECTION,ELSET=LAYER,MATERIAL=CHOICE
0.0001
*MATERIAL,NAME=CHOICE
*ELASTIC
100,0.35
**
**----------------------------------------------------------------
                        **LOAD DEFINITION
**----------------------------------------------------------------
**
*AMPLITUDE,NAME=ZLOAD
0.,1, 1,1
*AMPLITUDE,NAME=XLOAD
0.,1, 1,1
*AMPLITUDE,NAME=YLOAD
0.,1, 1,1
**
**----------------------------------------------------------------
                        **STEP DEFINITION
**----------------------------------------------------------------
**
*STEP,NLGEOM,INC=20
*STATIC
0.05,1.0,0.001,0.1
**
**----------------------------------------------------------------
                        **NODAL LOADS
**----------------------------------------------------------------
**
*CLOAD,FOLLOWER,AMPLITUDE=ZLOAD
FILL1,3,-1.0
```

```
FILL3,3,-0.5
FILL2,3,-0.25
*CLOAD,FOLLOWER,AMPLITUDE=XLOAD
FILL1,1,0.033
FILL2,1,0.00825
FILL3,1,0.0165
*CLOAD,FOLLOWER,AMPLITUDE=YLOAD
FILL1,2,0.015
FILL2,2,0.00375
FILL3,2,0.0075
*EL PRINT,ELSET=MEASURE3,POSITION=AVERAGED AT ALL NODES,FREQUENCY=1
S
E
*EL PRINT,ELSET=MEASURE4,POSITION=AVERAGED AT ALL NODES,FREQUENCY=1
S
E
*END STEP
**-----------------------------------------------------------------
                          **END OF ANALYSIS
```

RESULTS FROM FREE CASE ON FACE 3

	Free case	Face 3			
	X = 33	Y = 15	Z = 1000		
Node Set	NODE	S13		NODE	E13
	20260	-3.16E+04		20260	-4.55E-05
	20261	4694		20261	6.76E-06
	20262	3.72E+04		20262	5.36E-05
	20263	6.82E+04		20263	9.82E-05
	20264	1.00E+05		20264	1.44E-04
	20310	-3.01E+04		20310	-4.33E-05
	20311	5722		20311	8.24E-06
	20312	3.81E+04		20312	5.49E-05
	20313	6.94E+04		20313	1.00E-04
	20314	1.02E+05		20314	1.47E-04
	40260	-2.56E+04		40260	-3.69E-05
	40261	8270		40261	1.19E-05
	40262	3.86E+04		40262	5.56E-05
	40263	6.74E+04		40263	9.70E-05
	40264	9.82E+04		40264	1.41E-04
	40310	-2.35E+04		40310	-3.39E-05
	40311	9661		40311	1.39E-05
	40312	3.95E+04		40312	5.69E-05
	40313	6.82E+04		40313	9.82E-05
	40314	9.93E+04		40314	1.43E-04
	60260	-1.09E+04		60260	-1.57E-05
	60261	1.74E+04		60261	2.51E-05
	60262	4.27E+04		60262	6.15E-05
	60263	6.70E+04		60263	9.65E-05
	60264	9.53E+04		60264	1.37E-04
	60310	-9477		60310	-1.37E-05
	60311	1.80E+04		60311	2.60E-05
	60312	4.22E+04		60312	6.08E-05
	60313	6.56E+04		60313	9.45E-05
	60314	9.34E+04		60314	1.35E-04
	80260	8314		80260	1.20E-05
1	80261	2.75E+04	*1*	80261	3.96E-05
2	80262	4.47E+04	*2*	80262	6.44E-05
3	80263	6.14E+04	*3*	80263	8.84E-05
	80264	8.27E+04		80264	1.19E-04
	80310	8439		80310	1.22E-05
	80311	2.70E+04		80311	3.90E-05
	80312	4.32E+04		80312	6.22E-05
	80313	5.87E+04		80313	8.46E-05
	80314	7.94E+04		80314	1.14E-04
	100260	2.09E+04		100260	3.00E-05
1	100261	3.28E+04	*1*	100261	4.73E-05
2	100262	4.17E+04	*2*	100262	6.01E-05
3	100263	5.05E+04	*3*	100263	7.27E-05
	100264	6.65E+04		100264	9.58E-05
	100310	2.03E+04		100310	2.92E-05
	100311	3.20E+04		100311	4.61E-05
	100312	4.01E+04		100312	5.77E-05
	100313	4.79E+04		100313	6.91E-05
	100314	6.36E+04		100314	9.16E-05
	120260	2.53E+04		120260	3.64E-05
	120261	3.38E+04		120261	4.87E-05

	120262	3.79E+04		120262	5.46E-05
	120263	4.18E+04		120263	6.03E-05
	120264	5.51E+04		120264	7.93E-05
	120310	2.47E+04		120310	3.55E-05
	120311	3.31E+04		120311	4.77E-05
	120312	3.65E+04		120312	5.26E-05
	120313	3.97E+04		120313	5.73E-05
	120314	5.29E+04		120314	7.62E-05
	MAXIMUM	1.02E+05		MAXIMUM	1.47E-04
	NODE	20314		NODE	20314
	MINIMUM	-3.16E+04		MINIMUM	-4.55E-05
	NODE	20260		NODE	20260

RESULTS FROM RESTRICTED CASE ON FACE 3

Restricted case	Face 3				
X=33 Kpa					
Node set	NODE	S13	Node Set	NODE	E13
	20260	3.70E+04		20260	5.33E-05
	20261	3.78E+04		20261	5.45E-05
	20262	3.80E+04		20262	5.48E-05
	20263	3.78E+04		20263	5.45E-05
	20264	3.70E+04		20264	5.33E-05
	20310	3.69E+04		20310	5.32E-05
	20311	3.76E+04		20311	5.41E-05
	20312	3.77E+04		20312	5.44E-05
	20313	3.76E+04		20313	5.41E-05
	20314	3.69E+04		20314	5.32E-05
	40260	3.81E+04		40260	5.49E-05
	40261	3.84E+04		40261	5.53E-05
	40262	3.85E+04		40262	5.54E-05
	40263	3.84E+04		40263	5.53E-05
	40264	3.81E+04		40264	5.49E-05
	40310	3.77E+04		40310	5.43E-05
	40311	3.79E+04		40311	5.46E-05
	40312	3.80E+04		40312	5.48E-05
	40313	3.79E+04		40313	5.46E-05
	40314	3.77E+04		40314	5.43E-05
	60260	3.98E+04		60260	5.74E-05
	60261	3.91E+04		60261	5.63E-05
	60262	3.88E+04		60262	5.60E-05
	60263	3.91E+04		60263	5.63E-05
	60264	3.98E+04		60264	5.74E-05
	60310	3.89E+04		60310	5.61E-05
	60311	3.84E+04		60311	5.53E-05
	60312	3.82E+04		60312	5.50E-05
	60313	3.84E+04		60313	5.53E-05
	60314	3.89E+04		60314	5.61E-05
	80260	3.98E+04		80260	5.73E-05
1	80261	3.86E+04	*1*	80261	5.57E-05
2	80262	3.83E+04	*2*	80262	5.52E-05
3	80263	3.86E+04	*3*	80263	5.57E-05
	80264	3.98E+04		80264	5.73E-05
	80310	3.87E+04		80310	5.57E-05
	80311	3.78E+04		80311	5.45E-05
	80312	3.76E+04		80312	5.42E-05
	80313	3.78E+04		80313	5.45E-05
	80314	3.87E+04		80314	5.57E-05
	100260	3.72E+04		100260	5.36E-05
1	100261	3.64E+04	*1*	100261	5.25E-05
2	100262	3.62E+04	*2*	100262	5.21E-05
3	100263	3.64E+04	*3*	100263	5.25E-05
	100264	3.72E+04		100264	5.36E-05
	100310	3.65E+04		100310	5.26E-05
	100311	3.59E+04		100311	5.17E-05
	100312	3.57E+04		100312	5.15E-05
	100313	3.59E+04		100313	5.17E-05

	100314	3.65E+04		100314	5.26E-05
	120260	3.49E+04		120260	5.02E-05
	120261	3.44E+04		120261	4.96E-05
	120262	3.43E+04		120262	4.94E-05
	120263	3.44E+04		120263	4.96E-05
	120264	3.49E+04		120264	5.02E-05
	120310	3.46E+04		120310	4.99E-05
	120311	3.43E+04		120311	4.94E-05
	120312	3.42E+04		120312	4.92E-05
	120313	3.43E+04		120313	4.94E-05
	120314	3.46E+04		120314	4.99E-05
	MAXIMUM	3.98E+04		MAXIMUM	5.74E-05
	NODE	60264		NODE	60264
	MINIMUM	3.42E+04		MINIMUM	4.92E-05
	NODE	120312		NODE	120312

APPENDIX D

RESULTS FROM CALIBRATION PROCEDURE

I. DRAWINGS OF THE CALIBRATION JIG

II. ILLUSTRATION OF RESULTS FROM CALIBRATION PROCEDURE

III. ILLUSTRATION OF NUMERICAL RESULTS FROM CALIBRATION PROCEDURE

IV. ANALYSIS OF DATA BETWEEN 8 AND 12 MICROSTRAIN

V. BEST FIT CURVE EQUATIONS

VI. RANDOM ERROR PLOTS

Drawings of the Calibration Jig

COLLAR

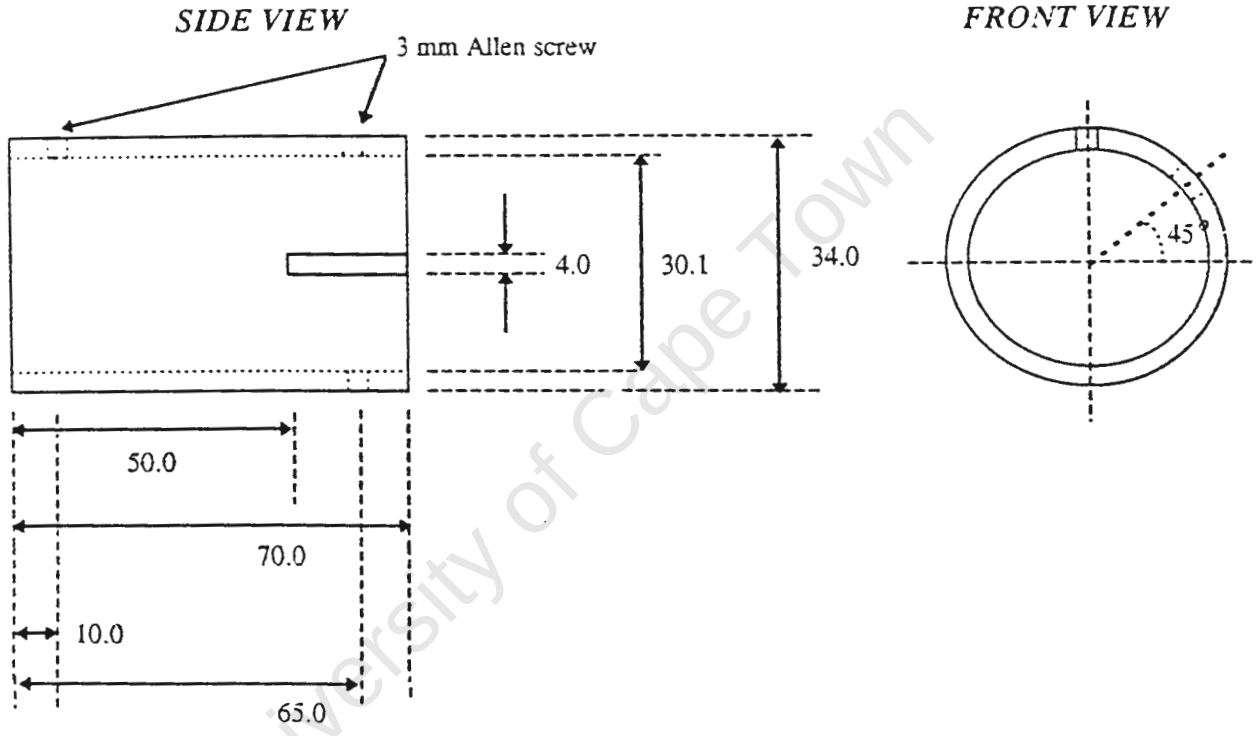

DRAWING 1

NOT TO SCALE
Dimensions - mm
Material - Mild Steel
All tolerances ± 0.1 mm

Drawings of the Calibration Jig

LOCKING PIN (1) and TOP JIG (2)

(1.)

SIDE VIEW

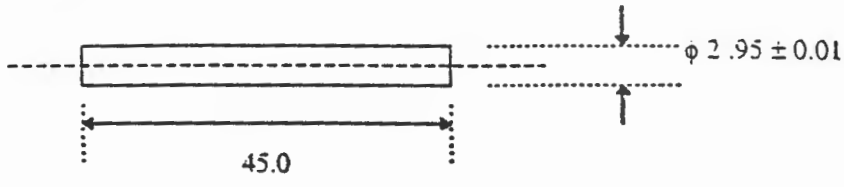

(2.)

SIDE VIEW

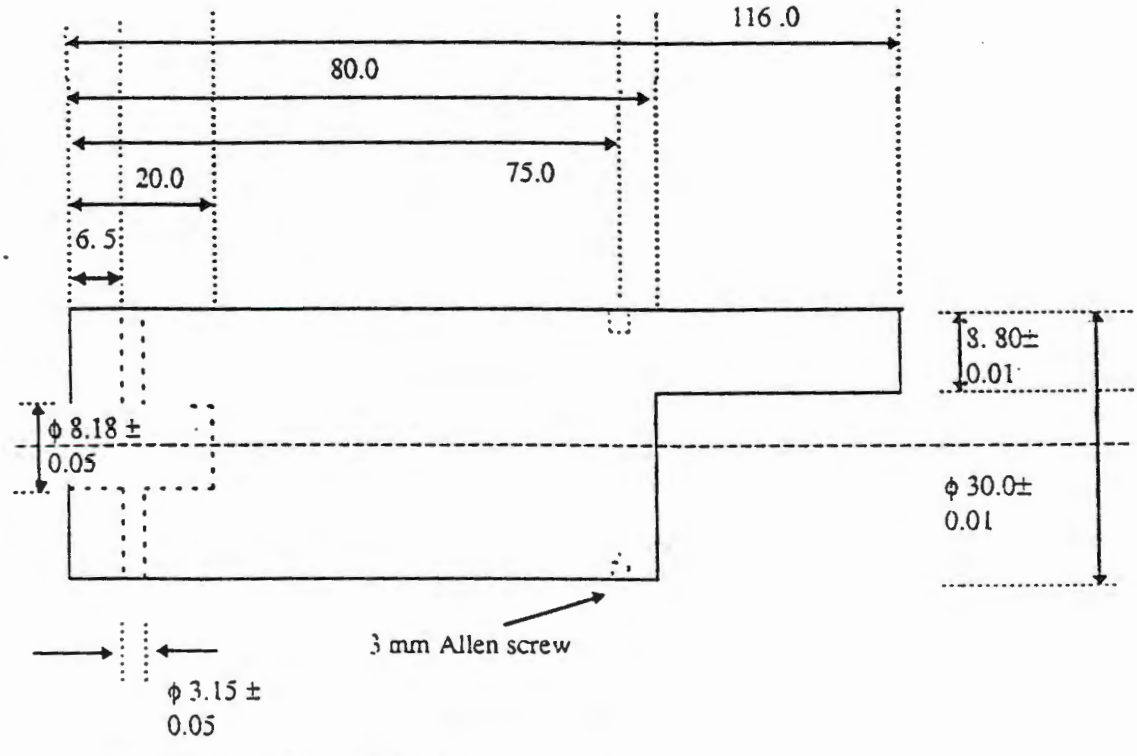

DRAWING 2

NOT TO SCALE
All Tolerances ± 0.1 mm
unless otherwise specified
Material : Mild Steel
Units : mm

Drawings of the Calibration Jig

LOCKING PIN (1) and BOTTOM JIG (2)

(1.)

SIDE VIEW

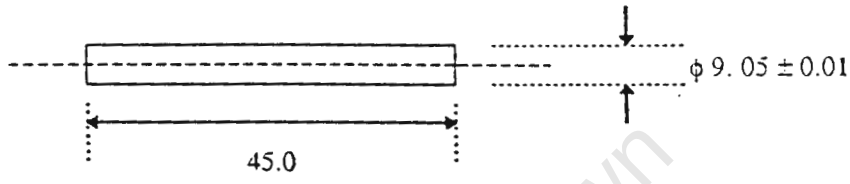

(2.)

SIDE VIEW

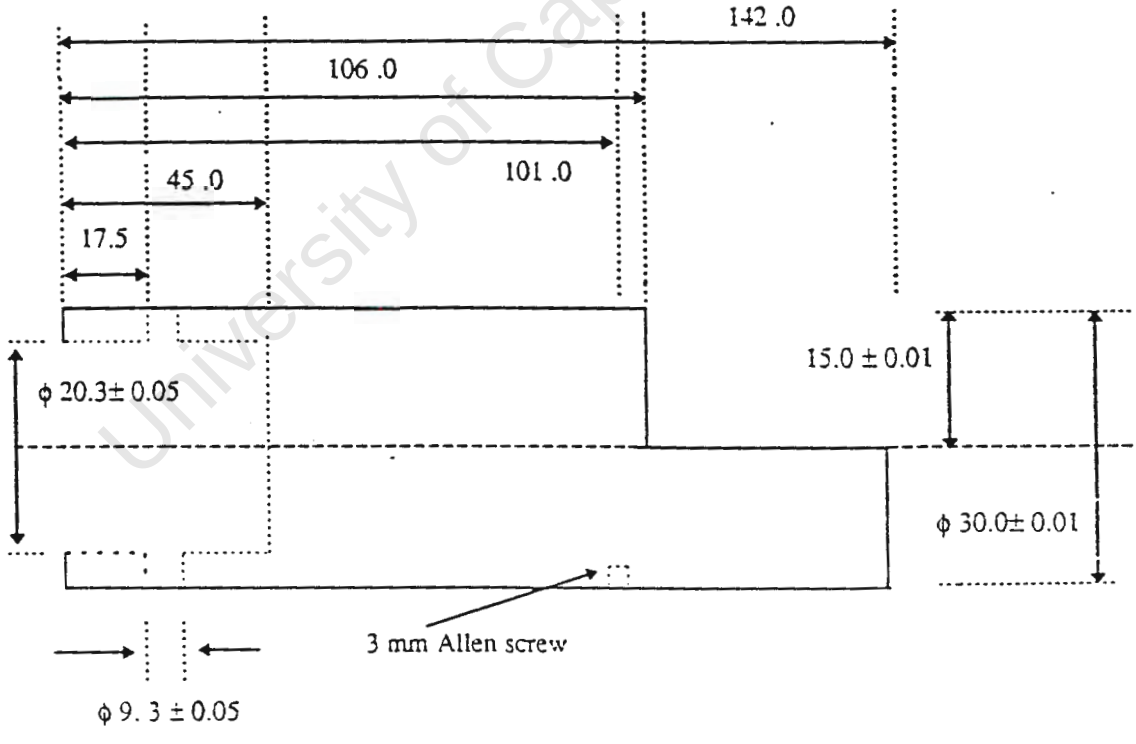

DRAWING 3
NOT TO SCALE
All Tolerances ± 0.1 mm unless otherwise specified
Material : Mild Steel
Units : mm

Illustration of Results from Calibration Procedure

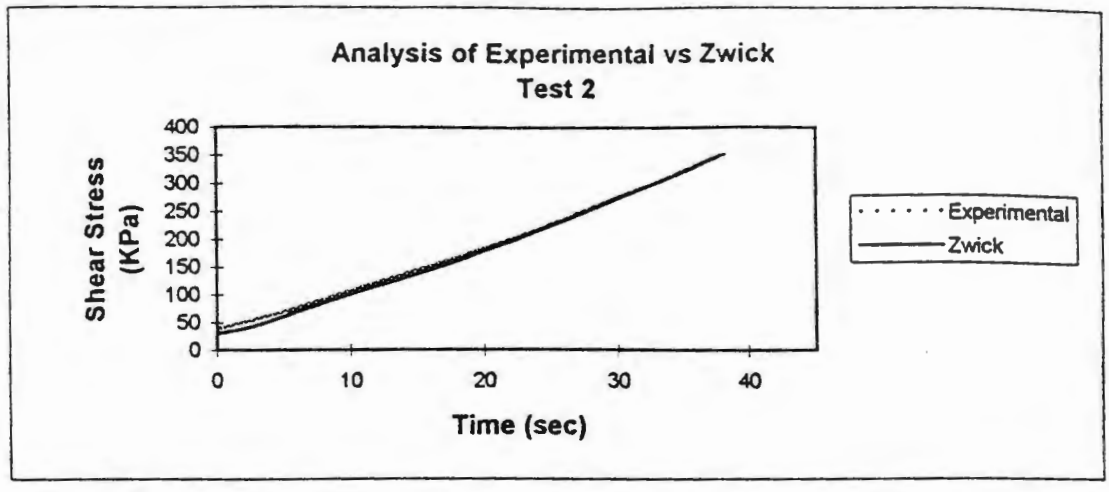

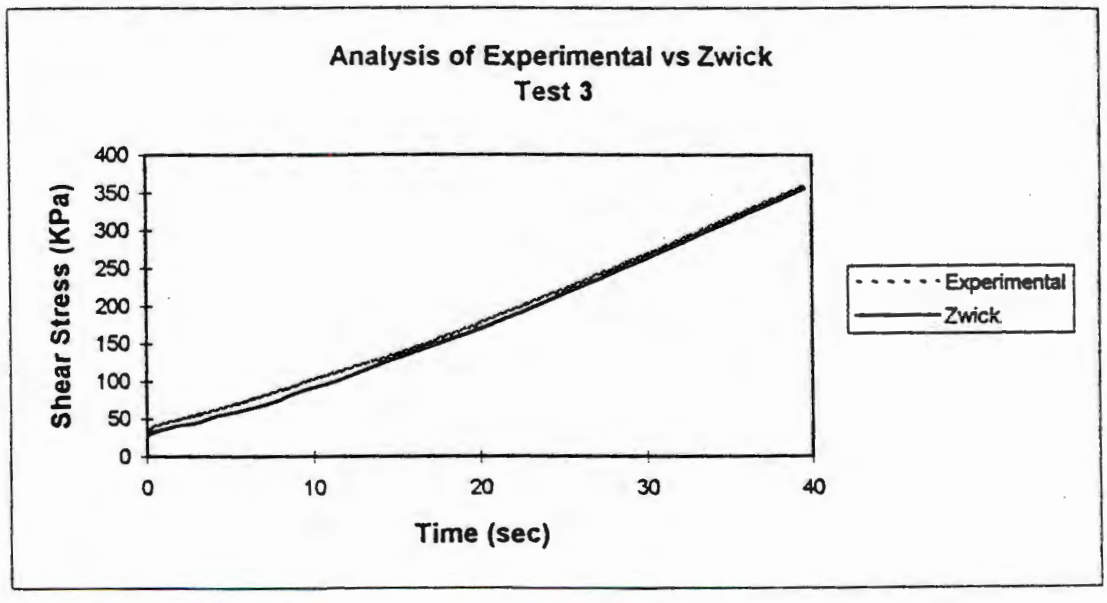

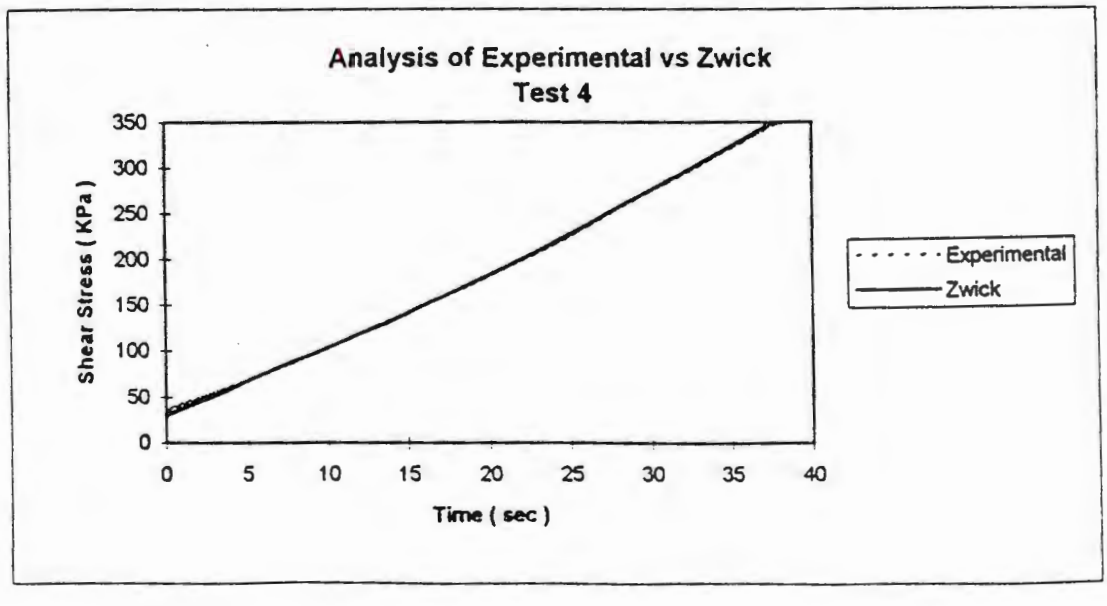

Illustration of Numerical Results from the Calibration Procedure

Wave View for Dos 1.24 Multiboar		Modulus	Poisson	Abaqus	Amp	Zwick		
5682 samples at 50 Hz in burst m		1.87E+09	0.35	0.887	347.28	347.359		
Input range: -10 to +10 volts								
3 channels sampled: 0 1 2								
First sample taken at 03/06/96 14:39:02								
Test No 5								
Data is in float (volts) format					Vertical	45	Horizontal	Shear
		Experimental	Voltage	Voltage	Voltage	Strain	Strain	Strain	Angle
number	time(s)	Stress (Kpa)	*1*	*2*	*3*	*1*	*2*	*3*	
0	0	27.95951588	0.242	0.579	0.168	1.2E-05	5.5E-05	8.00E-06	4.54E-05
3	0.02	29.02253748	0.261	0.603	0.173	1.2E-05	5.7E-05	8.2E-06	4.71E-05
6	0.04	28.9128431	0.3	0.613	0.183	1.4E-05	5.8E-05	8.7E-06	4.7E-05
9	0.06	29.83827865	0.291	0.628	0.188	1.4E-05	6E-05	9E-06	4.85E-05
12	0.08	31.39015269	0.286	0.652	0.183	1.4E-05	6.2E-05	8.7E-06	5.1E-05
15	0.1	31.29120454	0.33	0.662	0.188	1.6E-05	6.3E-05	9E-06	5.08E-05
18	0.12	31.84127436	0.344	0.676	0.193	1.6E-05	6.4E-05	9.2E-06	5.17E-05
21	0.14	33.34921851	0.325	0.696	0.188	1.5E-05	6.6E-05	9E-06	5.42E-05
24	0.16	35.43515814	0.335	0.73	0.173	1.6E-05	7E-05	8.2E-06	5.76E-05
27	0.18	34.81745542	0.379	0.735	0.193	1.8E-05	7E-05	9.2E-06	5.66E-05
30	0.2	35.71924147	0.383	0.75	0.188	1.8E-05	7.1E-05	9E-06	5.8E-05
33	0.22	35.97581686	0.354	0.745	0.178	1.7E-05	7.1E-05	8.5E-06	5.84E-05
36	0.24	35.5060547	0.383	0.745	0.183	1.8E-05	7.1E-05	8.7E-06	5.77E-05
39	0.26	35.85847691	0.418	0.759	0.183	2E-05	7.2E-05	8.7E-06	5.82E-05
42	0.28	35.87733458	0.393	0.755	0.188	1.9E-05	7.2E-05	9E-06	5.83E-05
45	0.3	36.65899872	0.374	0.764	0.188	1.8E-05	7.3E-05	9E-06	5.95E-05
48	0.32	35.84469279	0.413	0.759	0.188	2E-05	7.2E-05	9E-06	5.82E-05
51	0.34	37.15853009	0.418	0.784	0.193	2E-05	7.5E-05	9.2E-06	6.04E-05
54	0.36	37.12208371	0.393	0.779	0.198	1.9E-05	7.4E-05	9.4E-06	6.03E-05
57	0.38	37.73005237	0.393	0.784	0.178	1.9E-05	7.5E-05	8.5E-06	6.13E-05
60	0.4	37.07908304	0.418	0.784	0.198	2E-05	7.5E-05	9.4E-06	6.02E-05
63	0.42	37.23809614	0.418	0.784	0.188	2E-05	7.5E-05	9E-06	6.05E-05
66	0.44	38.31436147	0.393	0.794	0.178	1.9E-05	7.6E-05	8.5E-06	6.22E-05
69	0.46	38.11405756	0.418	0.799	0.188	2E-05	7.6E-05	9E-06	6.19E-05
72	0.48	37.76893293	0.432	0.799	0.198	2.1E-05	7.6E-05	9.4E-06	6.13E-05
75	0.5	38.78573614	0.413	0.808	0.183	2E-05	7.7E-05	8.7E-06	6.3E-05
78	0.52	38.10137143	0.403	0.794	0.183	1.9E-05	7.6E-05	8.7E-06	6.19E-05
81	0.54	37.62295932	0.427	0.794	0.193	2E-05	7.6E-05	9.2E-06	6.11E-05
84	0.56	38.97481659	0.403	0.813	0.198	1.9E-05	7.7E-05	9.4E-06	6.33E-05
87	0.58	39.06542504	0.418	0.818	0.198	2E-05	7.8E-05	9.4E-06	6.35E-05
90	0.6	38.58647038	0.432	0.813	0.198	2.1E-05	7.7E-05	9.4E-06	6.27E-05
93	0.62	39.23718262	0.427	0.823	0.198	2E-05	7.8E-05	9.4E-06	6.37E-05
96	0.64	39.02449421	0.437	0.823	0.203	2.1E-05	7.8E-05	9.7E-06	6.34E-05
99	0.66	38.95800983	0.432	0.818	0.193	2.1E-05	7.8E-05	9.2E-06	6.33E-05
102	0.68	39.46255632	0.432	0.828	0.198	2.1E-05	7.9E-05	9.4E-06	6.41E-05
105	0.7	39.62154805	0.432	0.828	0.188	2.1E-05	7.9E-05	9E-06	6.44E-05
108	0.72	39.80930338	0.422	0.833	0.203	2E-05	7.9E-05	9.7E-06	6.47E-05
111	0.74	39.34319124	0.447	0.828	0.193	2.1E-05	7.9E-05	9.2E-06	6.39E-05
114	0.76	39.0376509	0.442	0.823	0.198	2.1E-05	7.8E-05	9.4E-06	6.34E-05
117	0.78	40.11351903	0.427	0.838	0.198	2E-05	8E-05	9.4E-06	6.52E-05
120	0.8	40.35969125	0.442	0.847	0.203	2.1E-05	8.1E-05	9.7E-06	6.56E-05
123	0.82	40.43912218	0.442	0.847	0.198	2.1E-05	8.1E-05	9.4E-06	6.57E-05
126	0.84	40.87716246	0.437	0.852	0.193	2.1E-05	8.1E-05	9.2E-06	6.64E-05
129	0.86	40.28037039	0.432	0.842	0.198	2.1E-05	8E-05	9.4E-06	6.54E-05
132	0.88	40.65175607	0.442	0.852	0.203	2.1E-05	8.1E-05	9.7E-06	6.6E-05
135	0.9	41.15673421	0.432	0.857	0.198	2.1E-05	8.2E-05	9.4E-06	6.69E-05

Illustration of Numerical Results from the Calibration Procedure

138	0.92	40.58513151	0.447	0.852	0.203	2.1E-05	8.1E-05	9.7E-06	6.59E-05
141	0.94	40.82401317	0.447	0.852	0.188	2.1E-05	8.1E-05	9E-06	6.63E-05
144	0.96	41.39465302	0.442	0.862	0.193	2.1E-05	8.2E-05	9.2E-06	6.72E-05
147	0.98	41.23593248	0.432	0.857	0.193	2.1E-05	8.2E-05	9.2E-06	6.7E-05
150	1	41.47417405	0.452	0.867	0.198	2.2E-05	8.3E-05	9.4E-06	6.74E-05
153	1.02	41.24864426	0.447	0.862	0.198	2.1E-05	8.2E-05	9.4E-06	6.7E-05
156	1.04	41.97872797	0.452	0.877	0.203	2.2E-05	8.4E-05	9.7E-06	6.82E-05
159	1.06	41.62016599	0.447	0.867	0.193	2.1E-05	8.3E-05	9.2E-06	6.76E-05
162	1.08	42.25838452	0.437	0.877	0.198	2.1E-05	8.4E-05	9.4E-06	6.86E-05
165	1.1	42.65049056	0.447	0.886	0.198	2.1E-05	8.4E-05	9.4E-06	6.93E-05
168	1.12	42.21735827	0.452	0.877	0.188	2.2E-05	8.4E-05	9E-06	6.86E-05
171	1.14	42.45090707	0.462	0.886	0.198	2.2E-05	8.4E-05	9.4E-06	6.9E-05
174	1.16	41.60730951	0.452	0.872	0.208	2.2E-05	8.3E-05	9.9E-06	6.76E-05
177	1.18	42.65049056	0.447	0.886	0.198	2.1E-05	8.4E-05	9.4E-06	6.93E-05
180	1.2	42.42968935	0.452	0.882	0.193	2.2E-05	8.4E-05	9.2E-06	6.89E-05
183	1.22	42.75637827	0.457	0.886	0.183	2.2E-05	8.4E-05	8.7E-06	6.94E-05
186	1.24	43.60604915	0.447	0.901	0.193	2.1E-05	8.6E-05	9.2E-06	7.08E-05
189	1.26	43.26043074	0.457	0.896	0.188	2.2E-05	8.5E-05	9E-06	7.03E-05
192	1.28	43.46000454	0.462	0.906	0.208	2.2E-05	8.6E-05	9.9E-06	7.06E-05
195	1.3	43.69836373	0.462	0.906	0.193	2.2E-05	8.6E-05	9.2E-06	7.1E-05
198	1.32	43.38075573	0.452	0.901	0.203	2.2E-05	8.6E-05	9.7E-06	7.05E-05
201	1.34	43.71164235	0.471	0.911	0.203	2.2E-05	8.7E-05	9.7E-06	7.1E-05
204	1.36	42.70356032	0.471	0.891	0.193	2.2E-05	8.5E-05	9.2E-06	6.94E-05
207	1.38	43.5656558	0.466	0.906	0.198	2.2E-05	8.6E-05	9.4E-06	7.08E-05
210	1.4	44.44163385	0.466	0.921	0.198	2.2E-05	8.8E-05	9.4E-06	7.22E-05
213	1.42	44.14962565	0.476	0.921	0.208	2.3E-05	8.8E-05	9.9E-06	7.17E-05
216	1.44	44.21617595	0.471	0.921	0.208	2.2E-05	8.8E-05	9.9E-06	7.18E-05
219	1.46	44.81315051	0.466	0.926	0.193	2.2E-05	8.8E-05	9.2E-06	7.28E-05
222	1.48	45.12630992	0.466	0.93	0.188	2.2E-05	8.9E-05	9E-06	7.33E-05
225	1.5	45.04674913	0.466	0.93	0.193	2.2E-05	8.9E-05	9.2E-06	7.32E-05
228	1.52	44.91404992	0.476	0.93	0.193	2.3E-05	8.9E-05	9.2E-06	7.3E-05
231	1.54	44.83435208	0.476	0.93	0.198	2.3E-05	8.9E-05	9.4E-06	7.28E-05
234	1.56	44.90074885	0.481	0.935	0.208	2.3E-05	8.9E-05	9.9E-06	7.29E-05
237	1.58	45.26268303	0.471	0.94	0.212	2.2E-05	9E-05	1E-05	7.35E-05
240	1.6	45.40536654	0.471	0.94	0.203	2.2E-05	9E-05	9.7E-06	7.38E-05
243	1.62	45.64387586	0.481	0.945	0.198	2.3E-05	9E-05	9.4E-06	7.41E-05
246	1.64	45.36557595	0.486	0.94	0.193	2.3E-05	9E-05	9.2E-06	7.37E-05
249	1.66	45.8562718	0.471	0.945	0.193	2.2E-05	9E-05	9.2E-06	7.45E-05
252	1.68	45.84347846	0.476	0.95	0.208	2.3E-05	9E-05	9.9E-06	7.45E-05
255	1.7	46.01549155	0.481	0.95	0.193	2.3E-05	9E-05	9.2E-06	7.47E-05
258	1.72	45.71027188	0.486	0.95	0.208	2.3E-05	9E-05	9.9E-06	7.42E-05
261	1.74	46.09524478	0.491	0.955	0.198	2.3E-05	9.1E-05	9.4E-06	7.49E-05
264	1.76	45.72618036	0.496	0.955	0.217	2.4E-05	9.1E-05	1E-05	7.43E-05
267	1.78	46.44030814	0.481	0.96	0.203	2.3E-05	9.1E-05	9.7E-06	7.54E-05
270	1.8	46.66579451	0.486	0.965	0.203	2.3E-05	9.2E-05	9.7E-06	7.58E-05
273	1.82	46.51979494	0.491	0.965	0.208	2.3E-05	9.2E-05	9.9E-06	7.56E-05
276	1.84	46.89940138	0.486	0.969	0.203	2.3E-05	9.2E-05	9.7E-06	7.62E-05
279	1.86	46.66579451	0.486	0.965	0.203	2.3E-05	9.2E-05	9.7E-06	7.58E-05
282	1.88	46.83584267	0.496	0.974	0.217	2.4E-05	9.3E-05	1E-05	7.61E-05
285	1.9	47.04541034	0.491	0.974	0.208	2.3E-05	9.3E-05	9.9E-06	7.64E-05
288	1.92	47.62948137	0.491	0.984	0.208	2.3E-05	9.4E-05	9.9E-06	7.74E-05
291	1.94	47.50996741	0.496	0.979	0.193	2.4E-05	9.3E-05	9.2E-06	7.72E-05
294	1.96	47.27091934	0.496	0.979	0.208	2.4E-05	9.3E-05	9.9E-06	7.68E-05
297	1.98	47.56599479	0.491	0.984	0.212	2.3E-05	9.4E-05	1E-05	7.73E-05
300	2	47.66914009	0.51	0.989	0.208	2.4E-05	9.4E-05	9.9E-06	7.74E-05

Illustration of Numerical Results from the Calibration Procedure

303	2.02	47.59211923	0.505	0.989	0.217	2.4E-05	9.4E-05	1E-05	7.73E-05
306	2.04	48.31948775	0.501	0.994	0.193	2.4E-05	9.5E-05	9.2E-06	7.85E-05
309	2.06	48.16003305	0.501	0.994	0.203	2.4E-05	9.5E-05	9.7E-06	7.82E-05
312	2.08	48.59798195	0.496	0.999	0.198	2.4E-05	9.5E-05	9.4E-06	7.89E-05
315	2.1	48.3060124	0.496	0.994	0.198	2.4E-05	9.5E-05	9.4E-06	7.85E-05
318	2.12	48.95968802	0.496	1.009	0.212	2.4E-05	9.6E-05	1E-05	7.95E-05
321	2.14	48.74397211	0.501	1.004	0.203	2.4E-05	9.6E-05	9.7E-06	7.92E-05
324	2.16	48.60090429	0.501	1.004	0.212	2.4E-05	9.6E-05	1E-05	7.89E-05
327	2.18	48.83966774	0.505	1.009	0.212	2.4E-05	9.6E-05	1E-05	7.93E-05
330	2.2	49.035963	0.501	1.009	0.203	2.4E-05	9.6E-05	9.7E-06	7.96E-05
333	2.22	49.25678652	0.496	1.013	0.208	2.4E-05	9.6E-05	9.9E-06	8E-05
336	2.24	49.72091033	0.505	1.023	0.208	2.4E-05	9.7E-05	9.9E-06	8.08E-05
339	2.26	49.44200541	0.51	1.018	0.203	2.4E-05	9.7E-05	9.7E-06	8.03E-05
342	2.28	50.22509391	0.501	1.028	0.198	2.4E-05	9.8E-05	9.4E-06	8.16E-05
345	2.3	49.65438171	0.51	1.023	0.208	2.4E-05	9.7E-05	9.9E-06	8.07E-05
348	2.32	50.01295437	0.505	1.028	0.208	2.4E-05	9.8E-05	9.9E-06	8.12E-05
351	2.34	49.9494689	0.505	1.028	0.212	2.4E-05	9.8E-05	1E-05	8.11E-05
354	2.36	50.17191615	0.515	1.033	0.208	2.5E-05	9.8E-05	9.9E-06	8.15E-05
357	2.38	49.94638457	0.51	1.028	0.208	2.4E-05	9.8E-05	9.9E-06	8.11E-05
360	2.4	50.17191615	0.515	1.033	0.208	2.5E-05	9.8E-05	9.9E-06	8.15E-05
363	2.42	50.38759957	0.51	1.038	0.217	2.4E-05	9.9E-05	1E-05	8.18E-05
366	2.44	50.62314826	0.515	1.038	0.198	2.5E-05	9.9E-05	9.4E-06	8.22E-05
369	2.46	50.33382086	0.52	1.038	0.212	2.5E-05	9.9E-05	1E-05	8.18E-05
372	2.48	50.75898441	0.51	1.043	0.212	2.4E-05	9.9E-05	1E-05	8.24E-05
375	2.5	51.06105289	0.52	1.048	0.203	2.5E-05	1E-04	9.7E-06	8.29E-05
378	2.52	50.83835428	0.52	1.048	0.217	2.5E-05	1E-04	1E-05	8.26E-05
381	2.54	51.11787897	0.515	1.053	0.222	2.5E-05	0.0001	1.1E-05	8.3E-05
384	2.56	51.05106647	0.52	1.053	0.222	2.5E-05	0.0001	1.1E-05	8.29E-05
387	2.58	50.99735542	0.53	1.053	0.217	2.5E-05	0.0001	1E-05	8.28E-05
390	2.6	51.78980161	0.51	1.062	0.217	2.4E-05	0.0001	1E-05	8.41E-05
393	2.62	51.58946609	0.525	1.062	0.217	2.5E-05	0.0001	1E-05	8.38E-05
396	2.64	52.39610352	0.525	1.072	0.203	2.5E-05	0.0001	9.7E-06	8.51E-05
399	2.66	51.87855817	0.52	1.062	0.203	2.5E-05	0.0001	9.7E-06	8.43E-05
402	2.68	51.735437	0.52	1.062	0.212	2.5E-05	0.0001	1E-05	8.4E-05
405	2.7	52.39610352	0.525	1.072	0.203	2.5E-05	0.0001	9.7E-06	8.51E-05
408	2.72	52.46563845	0.525	1.077	0.217	2.5E-05	0.0001	1E-05	8.52E-05
411	2.74	52.31960199	0.53	1.077	0.222	2.5E-05	0.0001	1.1E-05	8.5E-05
414	2.76	52.69102993	0.53	1.082	0.217	2.5E-05	0.0001	1E-05	8.56E-05
417	2.78	52.47845513	0.54	1.082	0.222	2.6E-05	0.0001	1.1E-05	8.52E-05
420	2.8	53.19586572	0.52	1.087	0.212	2.5E-05	0.0001	1E-05	8.64E-05
423	2.82	52.91647649	0.535	1.087	0.217	2.5E-05	0.0001	1E-05	8.6E-05
426	2.84	53.4211928	0.525	1.092	0.212	2.5E-05	0.0001	1E-05	8.68E-05
429	2.86	53.42955396	0.53	1.096	0.222	2.5E-05	0.0001	1.1E-05	8.68E-05
432	2.88	53.28797779	0.535	1.092	0.212	2.5E-05	0.0001	1E-05	8.66E-05
435	2.9	52.99598024	0.545	1.092	0.222	2.6E-05	0.0001	1.1E-05	8.61E-05
438	2.92	53.65170108	0.53	1.096	0.208	2.5E-05	0.0001	9.9E-06	8.71E-05
441	2.94	53.50881739	0.53	1.096	0.217	2.5E-05	0.0001	1E-05	8.69E-05
444	2.96	53.86773914	0.535	1.106	0.227	2.5E-05	0.00011	1.1E-05	8.75E-05
447	2.98	53.800907	0.53	1.101	0.217	2.5E-05	0.0001	1E-05	8.74E-05
450	3	54.30594953	0.53	1.111	0.222	2.5E-05	0.00011	1.1E-05	8.82E-05
453	3.02	54.51904439	0.52	1.111	0.217	2.5E-05	0.00011	1E-05	8.86E-05
456	3.04	54.39768282	0.535	1.111	0.212	2.5E-05	0.00011	1E-05	8.84E-05
459	3.06	54.47711527	0.545	1.116	0.217	2.6E-05	0.00011	1E-05	8.85E-05
462	3.08	54.17229248	0.54	1.111	0.222	2.6E-05	0.00011	1.1E-05	8.8E-05
465	3.1	54.91515812	0.54	1.121	0.212	2.6E-05	0.00011	1E-05	8.92E-05

Analysis of Data between 8 and 12 Microstrain

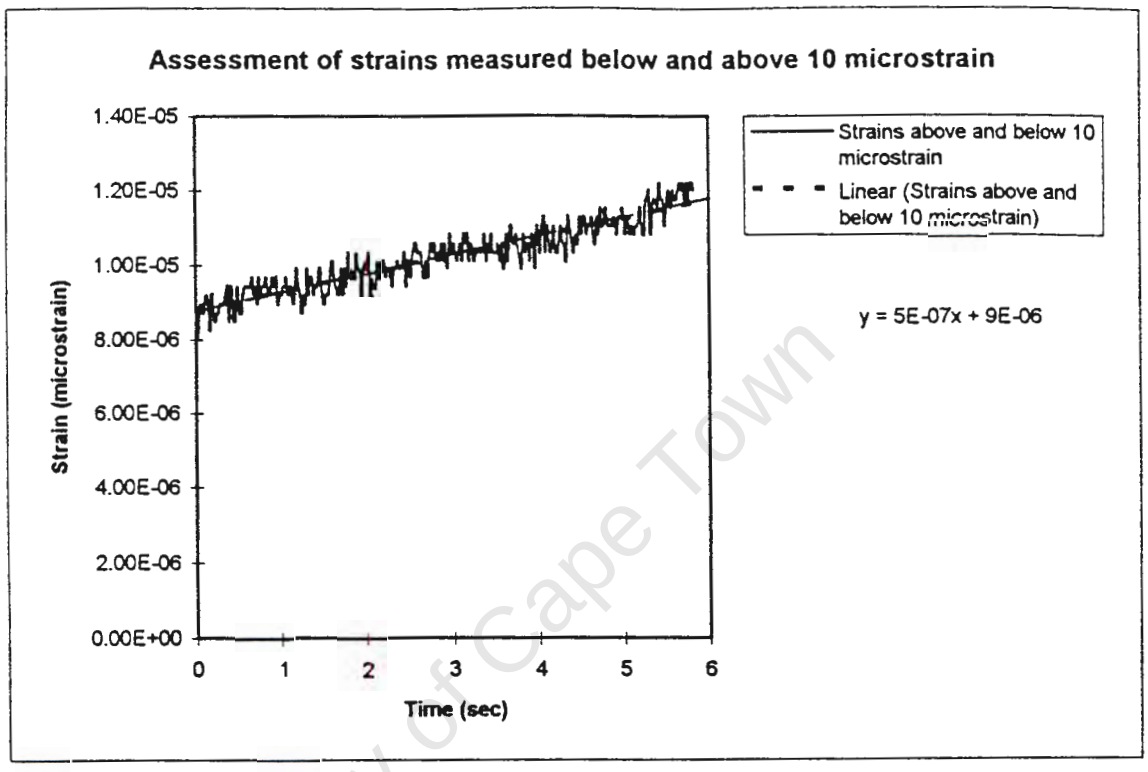

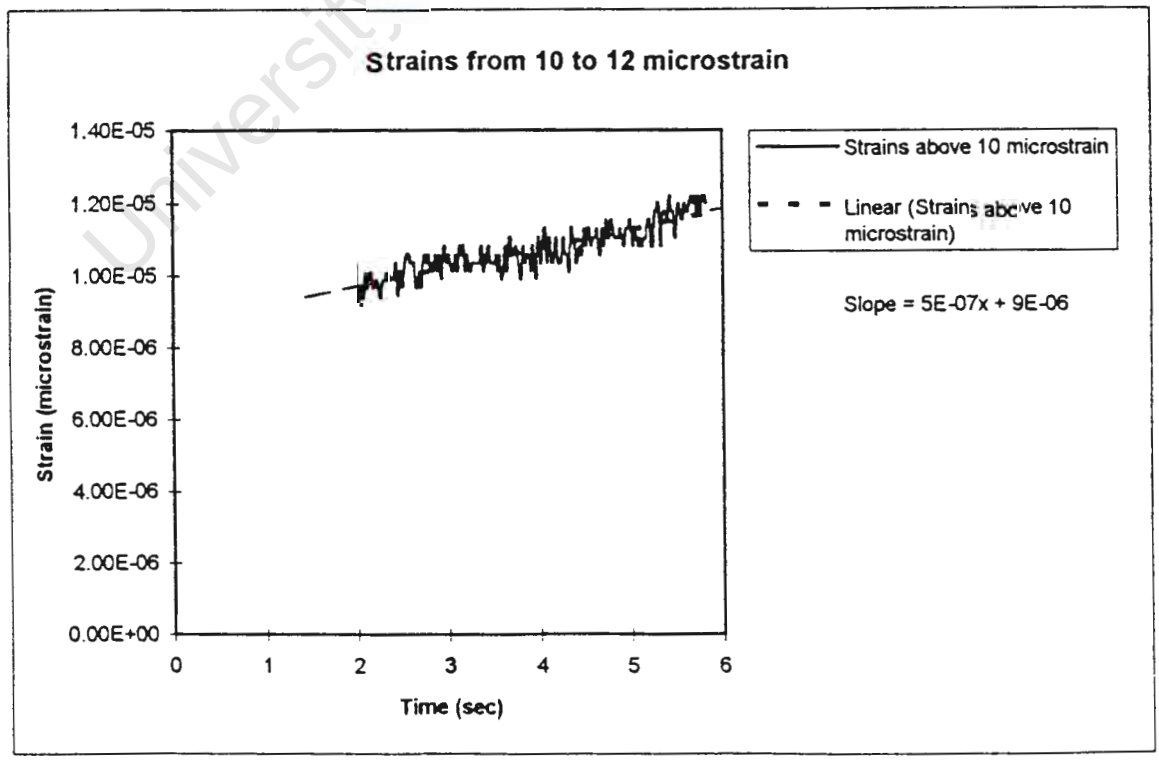

Analysis of Data between 8 and 12 Microstrain

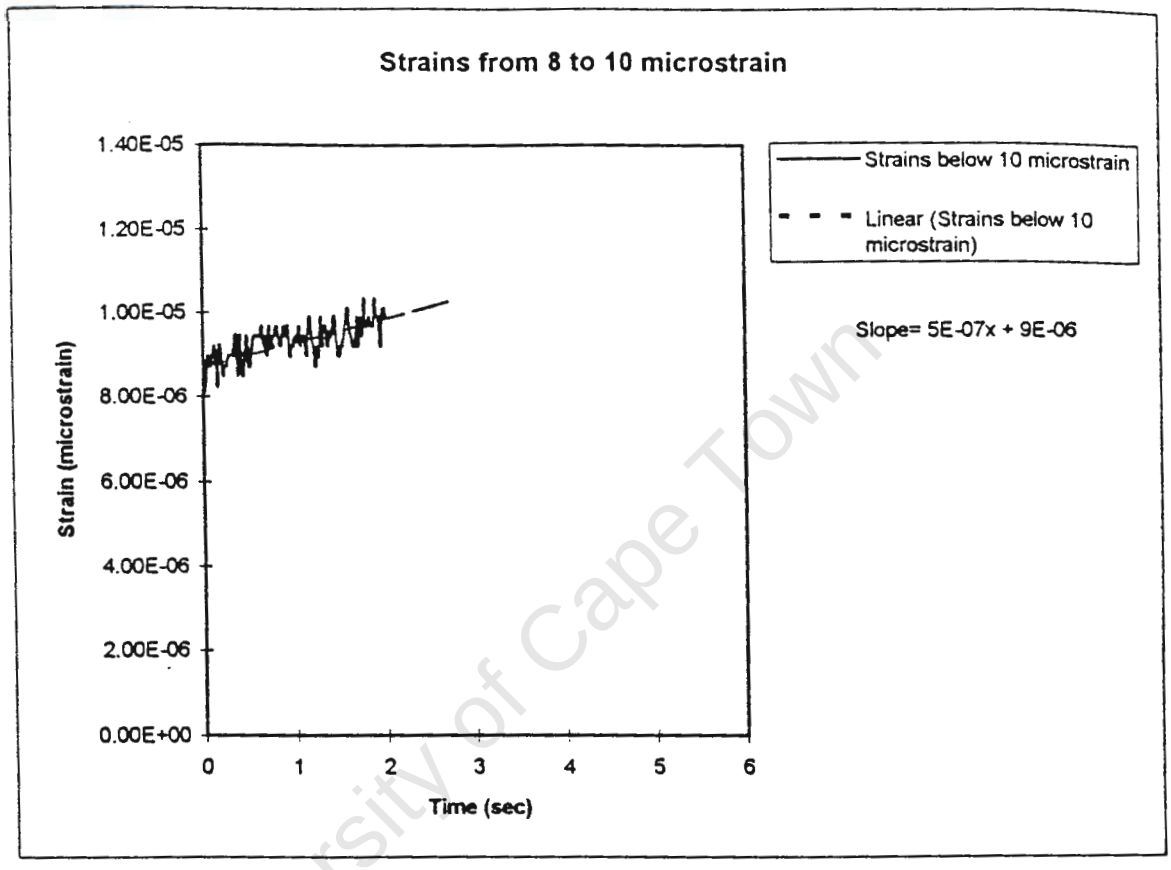

Best fit curve equations

Test No	Zwick input curve	Test No	Experimental curve
1	y=0.037x^2+6.8129x+25.77 R^2=0.9994	1	y=0.0253x^2+7.9513x+25.322 R^2=0.9996
2	y=0.0296x^2+7.5191x+18.519 R^2=0.9994	2	y=0.0209x^2+7.9126x+25.045 R^2=0.9996
3	y=0.0296x^2+7.3728x+16.545 R^2=0.9997	3	y=0.021x^2+7.7024x+26.206 R^2=0.9994
4	y=0.0291x^2+7.3499x+16.057 R^2=0.997	4	y=0.0209x^2+7.9879X+20.812 R^2=0.9994
5	y=0.0463x^2+6.7636x+31.063 R^2=0.9998	5	y=0.0535x^2+6.2499x+34.146 R^2=0.9999
6	y=0.0501x^2+6.6356x+27.481 R^2=0.9998	6	y=0.0493x^2+6.3371x+35.418 R^2=0.9999
7	y=0.0529x^2+6.585x+26.975 R^2=0.9997	7	y=0.0583x^2+5.9723x+38.95 R^2=0.9999
8	y=0.0579x^2+6.3708x+25.709 R^2=0.9996	8	y=0.0566x^2+5.8951x+37.693 R^2=0.9998
9	y=0.0614x^2+6.2746x+25.589 R^2=0.9995	9	y=0.0569x^2+6.0722x+38.373 R^2=0.9998
10	y=0.0594x^2+5.6495x+27.937 R^2=0.9999	10	y=0.0525x^2+6.0262x+26.85 R^2=0.9999

Random Error Plots

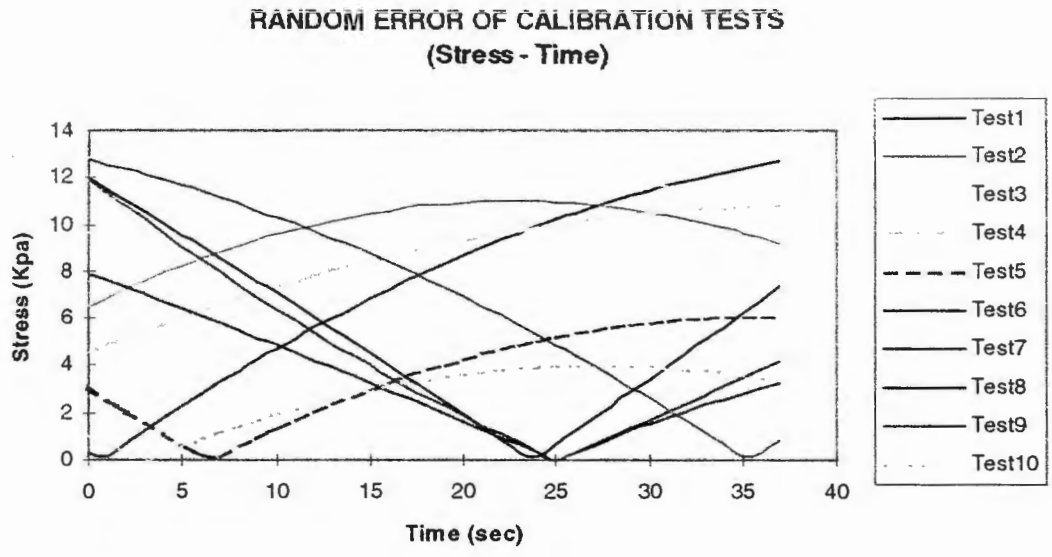

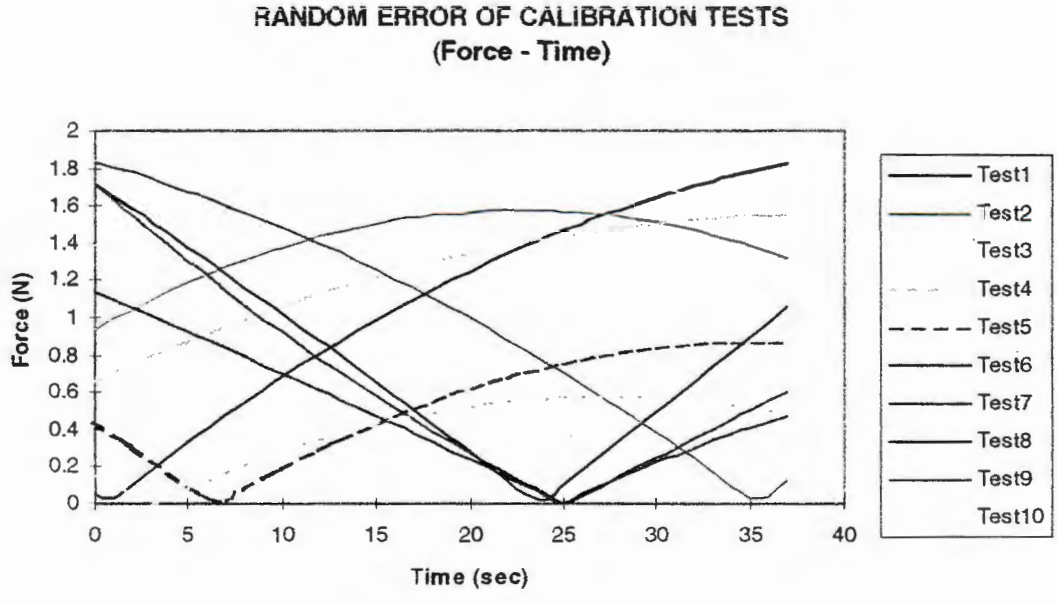

APPENDIX E

F - SCAN INSOLE

I. F-SCAN INSOLE

F-Scan Insole

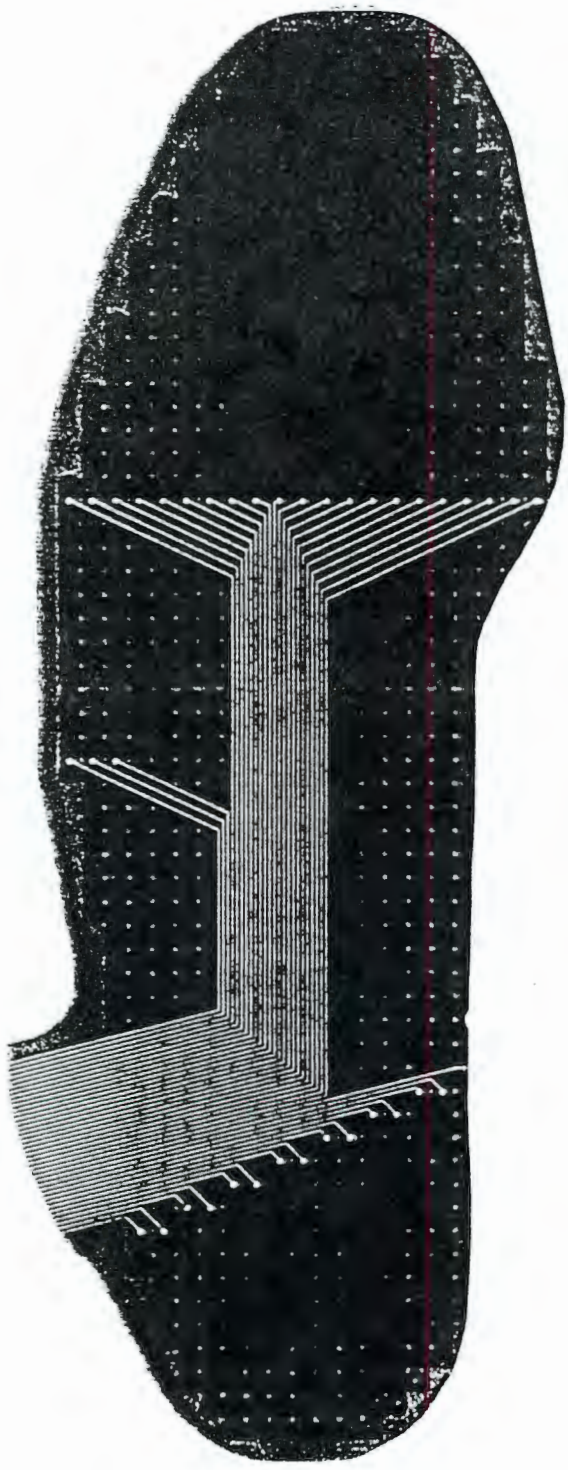

View from below

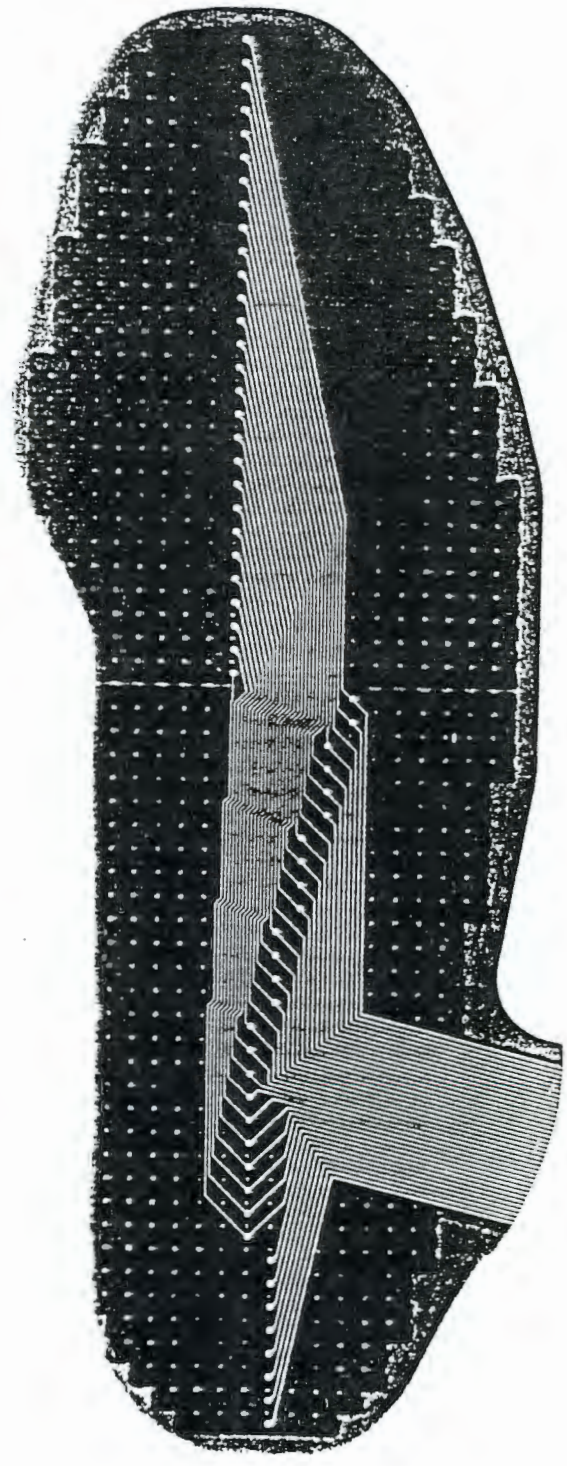

View from above

APPENDIX F

IN-SHOE TEST RESULTS

I. ILLUSTRATION OF RESULTS OBTAINED DURING THE ANALYSIS TESTS

II. ANALYSIS PERFORMED ON THE RESULTS

Illustration of results obtained during the Analysis Tests

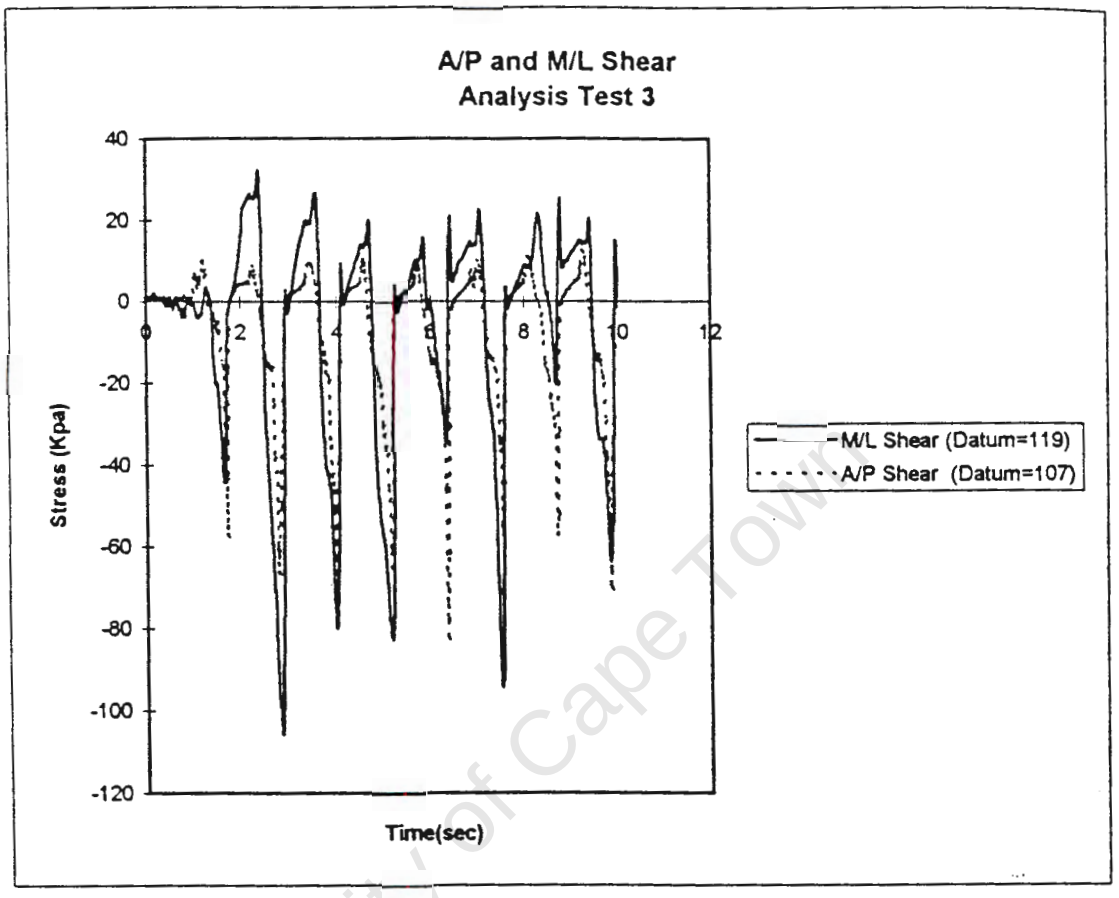

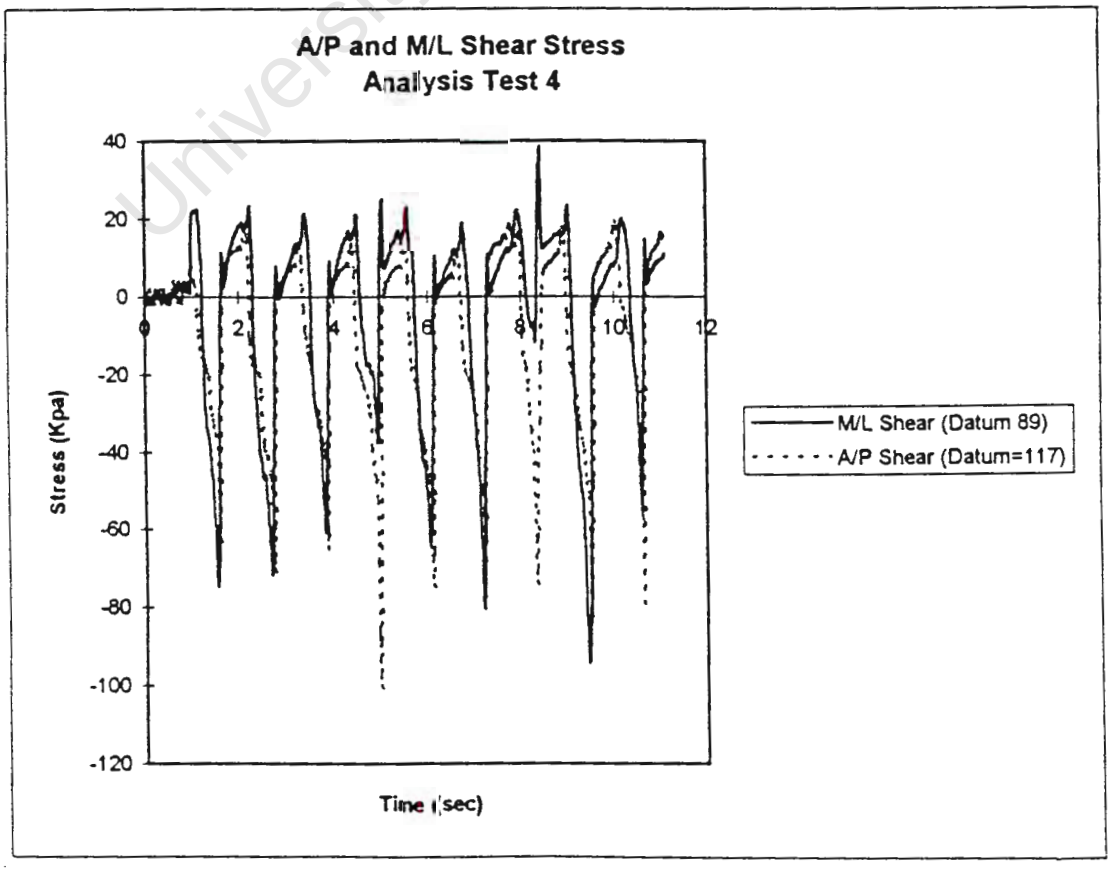

Illustration of results obtained during the Analysis Tests

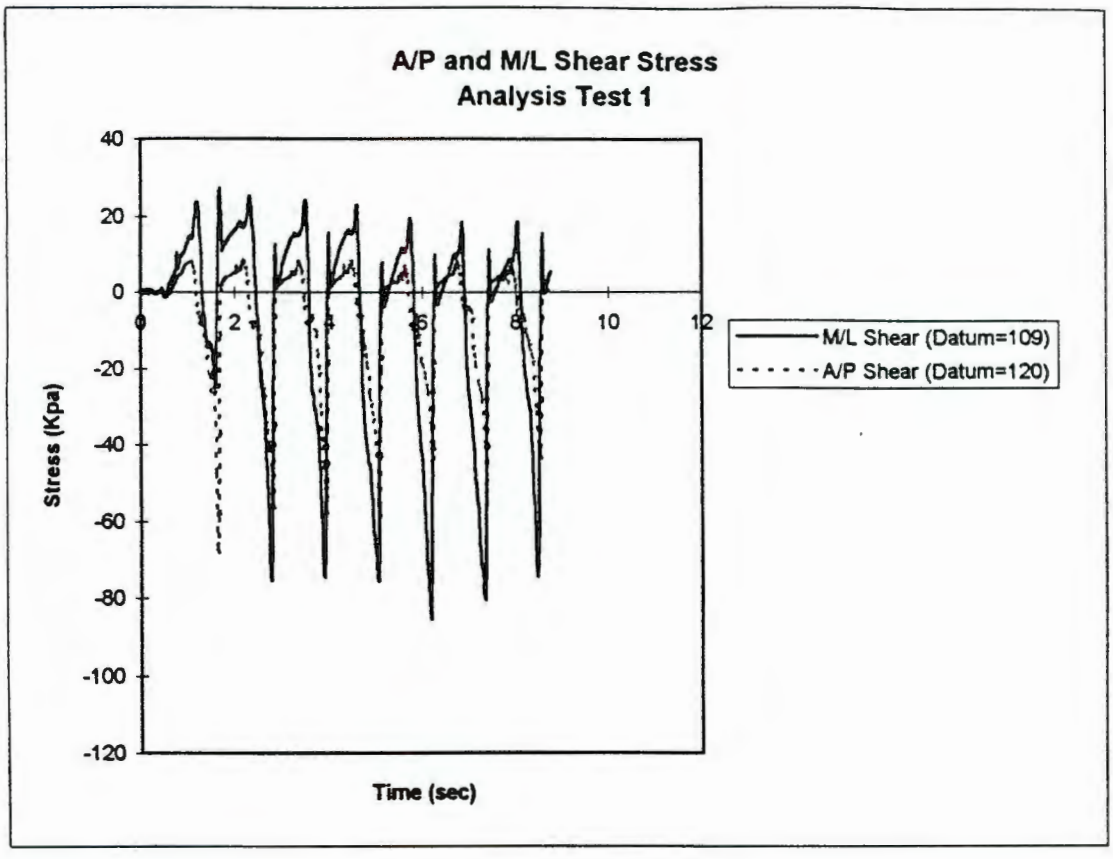

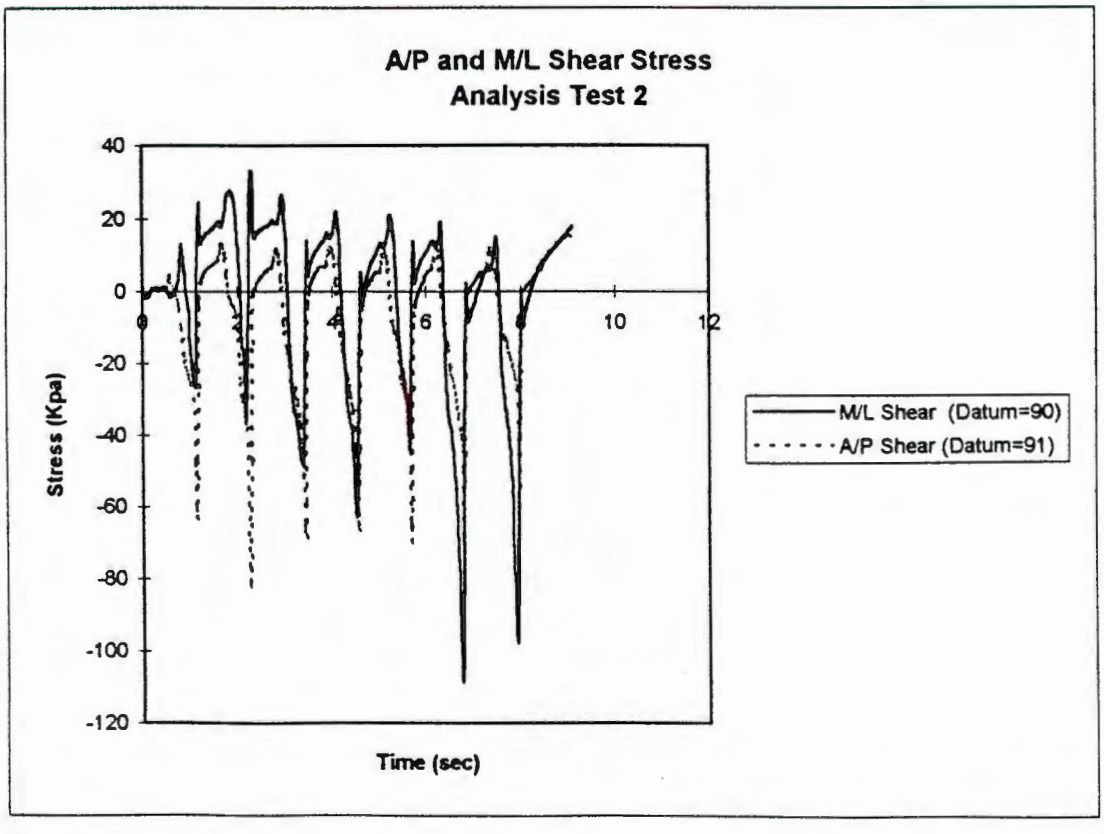

Analysis performed on the Results

		Test No	A/P		
Average Time	StDev		Gait Time		
1149.333333	43.362042	3	1143		
			1227		
			1120		
			1169		
			1109		
			1128		
1138.428571	47.077444	4	1182		
			1128		
			1166		
			1060		
			1173		
			1169		
			1091		
1149.6	38.095932	2	1144		
			1167		
			1149		
			1092		
			1196		
1146.857143	31.077476	1	1140		
			1121		
			1125		
			1137		
			1129		
			1208		
			1168		
1143.4	50.796653	5	1144		
			1136		
			1163		
			1207		
			1067		
Average Steps	6.6				
Combined	**Combined**				
Average	**StDev**				
1145.266667	39.46883				

Analysis performed on the Results

	TestNo	*M*	*L*	*A*	*P*
Magnitude Mean	*3*	20.6	-74.1	9.2	-65.2
	4	20.1	-58.4	14.6	-75.5
	2	19.7	-55.7	13.8	-68.4
	5	19.2	-64.2	13.1	-53.1
	1	20.5	-75.6	7.9	-54.8
	Average	20.02	-65.6	11.72	-63.4
	StDev	0.580517011	9.000833	2.977751	9.416740413
		M/L	*A/P*		
Datum Value	*3*	119.6	107		
	4	89.4	117.2		
	2	90.3	91.8		
	5	80.6	111.3		
	1	109.4	120.9		
	Average	97.86	109.64		
	StDev	16.06573995	11.31296		
		M	*L*	*A*	*P*
Max Values	3	20.8	-74.6	9.6	-65.7
	4	23.2	-95.7	20.3	-100.91
	2	27.5	-110.2	14.2	-83.4
	5	23.4	-88.7	13.1	-63.6
	1	25.1	-87.4	8.4	-69.3
	Average	24	-91.32	13.12	-76.582
	StDev	2.484954728	13.01372	4.674077	15.63900956